

Metal-Organofunctionalized SBA-15 catalysts for fine chemical syntheses

**Thesis Submitted to AcSIR
For the Award of the Degree of**

DOCTOR OF PHILOSOPHY

In

Chemical Sciences



By

Anish Lazar

Registration Number: 10CC15A26022

Under the guidance of

Dr. A. P. Singh (Supervisor)

Dr. C. P. Vinod (Co-Supervisor)

Catalysis & Inorganic Chemistry Division

CSIR-National Chemical Laboratory

Pune-411008, India

January 2018

CERTIFICATE

This is to certify that the work incorporated in this Ph.D. thesis entitled "*Metal-Organofunctionalized SBA-15 catalysts for fine chemical syntheses*" submitted by **Mr. Anish Lazar** to Academy of Scientific and Innovative Research (AcSIR) in fulfillment of the requirements for the award of the Degree of *Doctor of Philosophy in Chemical Sciences*, embodies original research work under our supervision. We further certify that this work has not been submitted to any other University or Institution in part or full for the award of any degree or diploma. Research material obtained from other sources has been duly acknowledged in the thesis. Any text, illustration, table etc., used in the thesis from other sources, have been duly cited and acknowledged.



Mr. Anish Lazar
Research Scholar



Dr. Anand Pal Singh
Supervisor



Dr. Vinod C. Prabhakaran
Co-supervisor

Date : 29/01/2018

Place : Pune

DECLARATION

I hereby declare that the work described in the thesis entitled "*Metal-Organofunctionalized SBA-15 catalysts for fine chemical syntheses*" submitted for the degree of *Doctor of Philosophy* in *Chemical sciences* to the Academy of Scientific and Innovative Research (AcSIR), New Delhi, has been carried out by me at the Catalysis and Inorganic Chemistry Division, CSIR-National Chemical Laboratory, Pune-411008, India under the supervision of **Dr. Anand Pal Singh** and **Dr. Vinod C. Prabhakaran**. I further declare that the material obtained from other sources has been duly acknowledged in this thesis. The work is original and has not been submitted in part or fully by me for any other degree or diploma to this or any other university.

Date: 29th January, 2018

CSIR-NCL, Pune



Mr. Anish Lazar

(Research Scholar)

Acknowledgements

My research career at CSIR-National Chemical Laboratory brings to me an enchanting and memorable experience in my life. The unconditional blessings, prayers, love, affection and support from my colleagues, teachers, family, friends and well wishers throughout my research life made me fulfill my research activities in great success. On this occasion, I would like to thank all well wishers who helped me, directly or indirectly, with their extraordinary blessings and encouragements.

My research supervisor, Dr. Anand Pal Singh, has been providing pleasant and tension free atmosphere in my research activities since my joining date. Few words of acknowledgement will not be sufficient to express my sincere gratitude to all the positive contributions he has given to my research career. His invaluable guidance and constant inspiration in modern heterogeneous catalysis directed me to focus my views in the proper perspective without any hurdles. I take this opportunity to express my sincere gratitude towards my co-supervisor, Dr. Vinod C. Prabhakaran, for his extensive scientific discussions and for giving me the freedom in research. Their strong support as friend, philosopher and guide at various stages helped in making me a true researcher and also a great human being.

I express my intense reverence to the Director of CSIR-NCL, Prof. Ashwini Kumar Nangia, Dr. V. K. Pillai and Dr. Sourav Pal (former directors) and Head of Catalysis and Inorganic Chemistry Division, Dr. D. Srinivas and Dr. A. P. Singh (former H.O.D) for providing me a golden chance to utilize infrastructural facilities for my research activities. I thank Council of Scientific and Industrial Research (CSIR), New Delhi, for my Senior Research Fellowship. I am indebted to my DAC members, Dr. C. V. Ramana, Dr. C. S. Gopinath and Dr. V. V. Bokade for their distinct suggestions, instructions and support in my PhD program.

I am thankful to all scientists and technical staffs in Catalysis and Inorganic Chemistry Division, CSIR-NCL for their significant contribution and assistance during these years. I take this opportunity to express my earnest respect to my school teachers, B.Sc. and M.Sc. professors for teaching me to climb the first step of my research career. I owe Dr. Balakrishnan Ganeshan and Dr. C. Venkatesh for directing me to CSIR-NCL for research activities. I would like to thank all seniors, colleagues, lab mates and friends in CSIR-NCL, Drs. Chidambaram, Selvakumar, Edwin, Sheetal, Priti, Sanjay, Sunil, Vysakh, Sreedhala, Surekha, Deepa, Tanmay, Laksmi

Prasad, Ashok, Lenin, Prasenjith, Anoop, Sagar, Sandip and Yogita, Sharad, Preeti, Betsy, Sumanta, Govind, Mahesh, Manisha, Mohan, Richa, Ruchi, Prabhakar Reddy, Tanusree, Pranjal, M. Prabhu, K. Prabhu and Vinod. I personally thank all postgraduate trainees, Sanjush, Silpa, Saravanan, Dharumraj, Aswathkumar, Athira, Irine, Irfana, Anju and Joona who helped me in various projects. I extend my thanks to past and present trainees in our lab, Ziyad, Yadhukiran, Mridual, Shebin, Joes, Neethu, Cygnet, Vidhya and Bonsy.

I want to express my gratitude to my best friend, Shoy George (Sr. Scientist, Halliburton, Pvt. Ltd., Pune), who motivated and directed me to dream a research life (PhD) and for being a great support for my crisis situations. Many thanks to my dear M.Sc. & B.Sc. batch mates (Dr. Ajin C.V and Dr. Anoop Thomas) and Kancor friends (Sarin, Vipin, Sreejesh, Prejeesh and Jinesh) for their valuable points to make my journey successful. I would like to thank my dear NCL Malayali friends, Drs. Hariprasad, Shijo, Suresh, Venugopal, Alson Mart, Rajesh, Eldho, Girish, Renjith, Govind, Sumesh, Anumon, Jijo, Sarath, Jijil, Bihag, Unni, Leena, Prajitha, Nishamol, Jaya, Nisha, Jayaprabha, Soumya, Anju, Suyanna and Kiran, Jithesh, Manjunath, Sabareesh, Vishal, Hari, Sreevisakh, Jishnu, Sanal, Jino, Tony, Teena, Hilda, Aswathy, Kavya, Nishina, Anupriya, Shubin, Fayis, Munvar, Emmanuel, Kayum, Sandip, Sanoop, Renjish, Rajith, Ajith, Shabeeb, Pranav, Vipin, Vidyanand, Rashid and all juniors. A special thanks to all research scholars in CSIR-NCL who provided friendly and cheerful working atmosphere throughout my stay in NCL.

I don't have words to express my feelings towards my parents for supporting me in my personal and education life. I sincerely express my deepest gratitude to them from bottom of my heart for allowing me to chase my dreams in my entire life. I am forever indebted to my elder sisters and their family for their love and encouragement.

I would like to apologize if somebody is missing in my mind whoever directly or indirectly helped me in my personal and professional life so far.

Above all, I thank almighty for all the blessings in throughout of my life.....

Dedicated to

My Beloved

Parents

CONTENTS

Table of Contents

List of Figures

List of Tables

List of Schemes

Thesis Abstract

Chapter 1: Introduction and Literature Review

1. Introduction.....	2
1.1. Catalysis.....	2
1.2. Heterogeneous catalysis.....	3
1.3. Nanoporous solids.....	4
1.4. Mesoporous materials.....	4
1.5. SBA-15 (Santa Barbara Amorphous Materials).....	7
1.6. Organofunctionalized Mesoporous Materials (OMMs).....	8
1.7. Physico-Chemical characterization techniques.....	11
1.7.1. Elemental analysis (CHN analysis).....	11
1.7.2. Inductively Coupled Plasma-Atomic Emission Spectroscopy (ICP-AES).....	12
1.7.3. Energy Dispersive Analysis of X-rays (EDAX).....	12
1.7.4. Powder X-ray Diffraction (XRD).....	13
1.7.5. N ₂ -Sorption analyses.....	14
1.7.6. Thermal analyses (TG and DTA).....	15
1.7.7. Fourier Transform Infrared Spectroscopy (FT-IR).....	15
1.7.8. Raman Spectroscopy.....	16
1.7.9. Cross Polarization Magic Angle Spinning NMR Spectroscopy (CP MAS NMR).....	16
1.7.10. Electron Paramagnetic Resonance Spectroscopy (EPR).....	17
1.7.11. Diffuse Reflectance UV-Visible Spectroscopy (DR UV-Vis).....	18
1.7.12. X-ray Photoelectron Spectroscopy (XPS).....	18

1.7.13. Scanning Electron Microscopy (SEM).....	19
1.7.14. Transmission Electron Microscopy (TEM).....	19
1.7.15. Gas Chromatography (GC).....	20
1.8. Catalytic applications.....	20
1.8.1. Asymmetric sulfoxidation reactions.....	20
1.8.2. Epoxidation reactions.....	21
1.8.3. Hydrogenation reactions.....	21
1.8.4. Coupling reactions (-C-C- and -C-N- Coupling reactions).....	22
1.8.5. Acetalization reactions of aldehydes.....	22
1.9. Scope and objectives of the thesis.....	23
1.10. References.....	24

Chapter 2: V(IV)O-Organofunctionalized SBA-15 for asymmetric sulfoxidation reactions

2.1. Introduction.....	29
2.2. Experimental.....	30
2.2.1. Materials.....	30
2.2.2. Synthesis of parent SBA-15.....	30
2.2.3. Synthesis of -OH protected PrNH ₂ SBA-15.....	30
2.2.4. Synthesis of 5-chloromethyl-3-tertbutyl-2-hydroxybenzaldehyde.....	31
2.2.5. Synthesis of V(IV)O-Sal-Indanol complex.....	31
2.2.6. Synthesis of V(IV)O-Sal-Ind-SBA-15.....	32
2.2.7. General procedure for enantioselective sulfoxidation reactions.....	32
2.3. Results and discussions.....	34
2.3.1. Characterizations.....	34
2.3.1.1. X-ray Diffraction (XRD).....	34
2.3.1.2. N ₂ -Sorption analyses.....	35
2.3.1.3. Thermal analyses (TG and DTA).....	36
2.3.1.4. Fourier Transform Infrared Spectroscopy (FT-IR).....	37
2.3.1.5. Solid state ¹³ C and ²⁹ Si NMR spectroscopy.....	38

2.3.1.6. Vanadium (^{51}V) NMR spectroscopy.....	40
2.3.1.7. Electron Paramagnetic Resonance spectroscopy (EPR).....	40
2.3.1.8. DR UV-Visible spectroscopy (UV-Vis).....	41
2.3.1.9. X-ray Photoelectron Spectroscopy (XPS).....	42
2.3.1.10. Scanning Electron Microscopy (SEM).....	43
2.3.1.11. Transmission Electron Microscopy (TEM).....	43
2.3.2. Activity of catalysts.....	44
2.3.3. Recyclability of catalysts.....	46
2.4. Conclusions.....	46
2.5. References.....	47

Chapter 3: Mo(VI)O₂-Organofunctionalized SBA-15 for epoxidation and sulfoxidation reactions

3.1. Introduction.....	51
3.2. Experimental.....	52
3.2.1. Materials.....	52
3.2.2. Synthesis of -OH protected PrClSBA-15.....	52
3.2.3. Synthesis of neat (L)Mo(VI)O ₂ complex.....	53
3.2.4. Synthesis of (L)Mo(VI)O ₂ @SBA-15.....	53
3.2.5. Procedure for catalytic reactions.....	54
3.3. Results and discussions.....	55
3.3.1. Characterizations.....	55
3.3.1.1. X-ray Diffraction (XRD).....	55
3.3.1.2. N ₂ -Sorption analyses.....	56
3.3.1.3. Thermal analyses (TG and DTA).....	57
3.3.1.4. Fourier Transform Infrared Spectroscopy (FT-IR).....	59
3.3.1.5. Raman spectroscopy.....	60
3.3.1.6. Solid state ^{13}C NMR spectroscopy (^{13}C CP MAS NMR).....	61
3.3.1.7. Solid state ^{29}Si NMR spectroscopy (^{29}Si CP MAS NMR).....	62
3.3.1.8. X-ray Photoelectron Spectroscopy (XPS).....	64

3.3.1.9. DR UV-Visible spectroscopy (UV-Vis).....	64
3.3.1.10. Scanning Electron Microscopy (SEM).....	65
3.3.1.11. Transmission Electron Microscopy (TEM).....	66
3.3.2. Catalytic activity.....	67
3.3.3. Heterogeneity tests.....	68
3.4. Conclusions.....	70
3.5. References.....	71

Chapter 4: Pd(II)-Organofunctionalized SBA-15 catalysts for coupling and hydrogenation reactions

4A: Pd(II)-2,2'-Dihydroxybenzophenone(DHBP)-NH₂@SBA-15

4B: Pd(II)-3-Allylsalicyaldiminophenol(ASIP)-SH@SBA-15

4A.1. Introduction.....	74
4A.2. Experimental.....	75
4A.2.1. Materials.....	75
4A.2.2. Synthesis of aminofunctionalized SBA-15.....	75
4A.2.3. Synthesis of Pd(II)-2,2'-Dihydroxybenzophenone (DHBP)-NH ₂ @SBA-15.....	76
4A.2.4. Procedure for catalytic reactions.....	77
4A.3. Results and discussions.....	77
4A.3.1. Characterizations.....	77
4A.3.1.1. X-ray Diffraction (XRD).....	77
4A.3.1.2. N ₂ -Sorptions analyses.....	78
4A.3.1.3. Thermal analyses (TG and DTA).....	80
4A.3.1.4. Fourier Transform Infrared Spectroscopy (FT-IR).....	81
4A.3.1.5. Solid state ¹³ C NMR spectroscopy (¹³ C CP MAS NMR).....	82
4A.3.1.6. Solid state ²⁹ Si NMR spectroscopy (²⁹ Si CP MAS NMR).....	83
4A.3.1.7. X-ray Photoelectron Spectroscopy (XPS).....	84
4A.3.1.8. DR UV-Visible spectroscopy (UV-Vis).....	85
4A.3.1.9. Scanning Electron Microscopy (SEM).....	85

4A.3.1.10. Transmission Electron Microscopy (TEM).....	86
4A.3.2. Catalytic activity.....	86
4A.3.3. Heterogeneity tests.....	90
4A.4. Conclusions.....	90
4B.1. Introduction.....	92
4B.2. Experimental.....	94
4B.2.1. Materials.....	94
4B.2.2. Synthesis of thiofunctionalized SBA-15 (SHSBA-15).....	94
4B.2.3. Synthesis of neat Pd(II)ASIP complex.....	94
4B.2.4. Synthesis of Pd(II)-3-Allylsalicyaldiminophenol(ASIP)-SH@SBA-15...95	
4B.2.5. Amination reactions of aryl halides (>C-N Coupling reactions).....	96
4B.3. Results and discussions.....	96
4B.3.1. Characterizations.....	96
4B.3.1.1. X-ray Diffraction (XRD).....	96
4B.3.1.2. N ₂ -Sorption analyses.....	97
4B.3.1.3. Thermal analyses (TG and DTA).....	98
4B.3.1.4. Fourier Transform Infrared Spectroscopy (FT-IR).....	99
4B.3.1.5. Solid state ¹³ C NMR spectroscopy (¹³ C CP MAS NMR).....	100
4B.3.1.6. Solid state ²⁹ Si NMR spectroscopy (²⁹ Si CP MAS NMR).....	101
4B.3.1.7. X-ray Photoelectron Spectroscopy (XPS).....	102
4B.3.1.8. DR UV-Visible spectroscopy (UV-Vis).....	103
4B.3.1.9. Scanning Electron Microscopy (SEM).....	103
4B.3.1.10. Transmission Electron Microscopy (TEM).....	104
4B.3.2. Catalytic activity.....	104
4B.3.3. Recyclability and Sheldon hot filtration test.....	106
4B.4. Conclusions.....	108
4A&B. References.....	108

Chapter 5: Ru(III)-Organofunctionalized SBA-15 for acetalization of aldehydes and ketones

5.1. Introduction.....	113
5.2. Experimental.....	114
5.2.1. Synthesis of (L)Ru(III)@SBA-15.....	114
5.2.2. Procedure for catalytic reactions.....	115
5.3. Results and discussions.....	115
5.3.1. Characterizations.....	115
5.3.2. Chemo-selective acetalization reactions.....	120
5.4. Conclusions.....	125
5.5. References.....	126

Chapter 6: Summary and Conclusions

6.1. Summary.....	129
6.2. Conclusions.....	132

Publications/ Symposia/ Conferences

Publications

Symposia and Conferences

LIST OF FIGURES

Figures	Descriptions	Page
Fig. 1.1	Pictorial representation of a catalytic reaction and its energy diagram.....	2
Fig. 1.2	Heterogeneous catalytic cycle.....	3
Fig. 1.3	Schematic diagram for the classification of nanoporous solids.....	4
Fig. 1.4	Designing of mesoporous material by Liquid Crystal Templating Mechanism (LCT).....	6
Fig. 1.5	Shapes of different M41S materials (a) hexagonal (MCM-41) (b) Cubic (MCM-48) and (c) Lamellar (MCM-50).....	7
Fig. 1.6	Surface modification by post-grafting (first) and co-condensation methods (second).....	9
Fig. 1.7	Sequential and convergent approaches in post-grafting methods.....	9
Fig. 2.1	XRD pattern of (a) as-synthesized SBA-15 (b) calcined SBA-15 (c) –OH protected PrNH ₂ SBA-15 and (d) V(IV)O-Sal-Ind- SBA-15.....	34
Fig. 2.2	N ₂ -isotherm and pore-size (inset) of (A) SBA-15 and (B) V(IV)O-Sal-Ind-SBA-15.....	36
Fig. 2.3	TG and DTA analyses of SBA-15 and V(IV)O-Sal-Ind-SBA-15.....	36
Fig. 2.4	FT-IR spectra of (a) as-synthesized SBA-15 (b) calcined SBA-15 (c) –OH protected PrNH ₂ SBA-15 (d) neat V(IV)O-Sal-Indanol complex and (e) V(IV)O-Sal-Ind-SBA-15.....	37
Fig. 2.5	Solid state ¹³ C (A) and ²⁹ Si (B) NMR spectra of V(IV)O-Sal-Ind-SBA-15...	39
Fig. 2.6	Liquid state ⁵¹ V NMR spectra of neat V(IV)O-Sal-Indanol complex for sulfoxidation reaction (a) after 4 h (b) after completion of the reaction 10 h.	40
Fig. 2.7	EPR spectra of V(IV)O-Sal-Ind-SBA-15.....	41
Fig. 2.8	DR UV-Vis spectra of (a) SBA-15 (b) Capped PrNH ₂ SBA-15 (c) V(IV)O-Sal-Ind-SBA-15.....	42
Fig. 2.9	XPS spectra of V2p core level of V(IV)O-Sal-Ind-SBA-15.....	42
Fig. 2.10	SEM images of (A) SBA-15 and (B) V(IV)O-Sal-Ind-SBA-15.....	43
Fig. 2.11	TEM images of (A) SBA-15 and (B) V(IV)O-Sal-Ind-SBA-15.....	43
Fig. 2.12	Recycling Studies of V(IV)O-Sal-Ind-SBA-15 catalyst.....	46

Fig. 3.1	XRD pattern of (a) as-synthesized SBA-15 (b) calcined SBA-15 (c) –OH protected PrCl@SBA-15 and (d) (L)Mo(VI)O ₂ @SBA-15.....	56
Fig. 3.2	N ₂ -isotherm and pore-size (inset) of (A) SBA-15 and (B) (L)Mo(VI)O ₂ @SBA-15.....	57
Fig. 3.3	TGA (A) and DTA (B) pattern of (a) as-synthesized SBA-15 (b) calcined SBA-15 (c) -OH protected PrCl@SBA-15 and (d) (L)Mo(VI)O ₂ @SBA-15.	58
Fig. 3.4	FT-IR spectra of (A) [(a) as-synthesized SBA-15, (b) calcined SBA-15, (c) protected PrCl@SBA-15] and (B) [(a) the neat (L)Mo(VI)O ₂ complex (b) (L)Mo(VI)O ₂ @SBA-15].....	60
Fig. 3.5	Raman spectra of (a) the neat (L)Mo(VI)O ₂ complex (b) (L)Mo(VI)O ₂ @SBA-15.....	60
Fig. 3.6	Solid state ¹³ C CP MAS NMR spectra of (A) PrCl@SBA-15, (B)-OH protected PrCl@SBA-15 (C) (L)Mo(VI)O ₂ @SBA-15.....	61
Fig. 3.7	Solid state ²⁹ Si CP MAS NMR spectra of (A) calcined SBA-15 (B) PrCl@SBA-15, (C) -OH protected PrCl@SBA-15 and (D) (L)Mo(VI)O ₂ @SBA-15.....	63
Fig. 3.8	XPS spectra of (a) the neat (L)Mo(VI)O ₂ complex (b) (L)Mo(VI)O ₂ @SBA-15.....	64
Fig. 3.9	DR-UV-Visible spectra of (a) calcined SBA-15 (b) the neat (L)Mo(VI)O ₂ complex and (c) (L)Mo(VI)O ₂ @SBA-15.....	65
Fig. 3.10	SEM images of (A) calcined SBA-15 and (B) (L)Mo(VI)O ₂ @SBA-15.....	66
Fig. 3.11	TEM images of (A) calcined SBA-15 and (B) (L)Mo(VI)O ₂ @SBA-15.....	66
Fig. 3.12	Sheldon’s hot filtration tests in (A) Epoxidation and (B) Sulfoxidation reactions.....	70
Fig. 4A.1	XRD pattern of (a) as-synthesized SBA-15 (b) calcined SBA-15 (c) NH ₂ @SBA-15 and (d) Pd(II)DHBP@SBA-15.....	78
Fig. 4A.2	N ₂ -isotherm and pore-size (inset) of (a) SBA-15 and (b) Pd(II)DHBP@SBA-15.....	79
Fig. 4A.3	TGA (A) and DTA (B) pattern of (a) as-synthesized SBA-15 (b) calcined SBA-15 (c) NH ₂ @SBA-15 and (d) Pd(II)DHBP@SBA-15.....	80
Fig. 4A.4	FT-IR Spectra of (a) as-synthesized SBA-15 (b) calcined SBA-15 (c)	

	NH ₂ @SBA-15 and (d) Pd(II)DHBP@SBA-15.....	81
Fig. 4A.5	Solid state ¹³ C NMR spectra of (a) NH ₂ @SBA-15 and (b) Pd(II)DHBP @SBA-15.....	82
Fig. 4A.6	Solid state ²⁹ Si NMR spectra of (a) calcined SBA-15 (b) NH ₂ @SBA-15 and (c) Pd(II)DHBP@SBA-15.....	83
Fig. 4A.7	XPS spectroscopy of 3d _{5/2} and 3d _{3/2} core levels of Pd(II)DHBP@SBA-15....	84
Fig. 4A.8	DR UV-Vis spectra of (a) calcined SBA-15 (b) NH ₂ @SBA-15 and (c) Pd(II)DHBP@SBA-15.....	85
Fig. 4A.9	SEM images of (A) calcined SBA-15 and (B) Pd(II)DHBP@SBA-15.....	86
Fig.4A.10	TEM images of (A) calcined SBA-15 and (B) Pd(II)DHBP@SBA-15.....	86
Fig. 4B.1	The XRD pattern of (a) as-synthesized SBA-15 (b) calcined SBA-15 (c) SHSBA-15 and (d) Pd(II)ASIP@SBA-15.....	97
Fig. 4B.2	N ₂ adsorption-desorption isotherm and pore size distribution curves (inset) of (a) calcined SBA-15 (b) SHSBA-15 and (d) Pd(II)ASIP@SBA-15.....	98
Fig. 4B.3	TGA (A) and DTA (B) pattern of (a) as-synthesized SBA-15 (b) calcined SBA-15 (c) SHSBA-15 and (d) Pd(II)ASIP@SBA-15.....	99
Fig. 4B.4	FTIR spectra of (a) as-synthesized SBA-15 (b) calcined SBA-15 (c) SHSBA-15 (d) the neat Pd(II)ASIP complex and (e) Pd(II)ASIP@SBA-15.	100
Fig. 4B.5	Solid state ¹³ C NMR spectra-(a) SHSBA-15 and (b) Pd(II)ASIP@SBA-15.	101
Fig. 4B.6	²⁹ Si NMR spectra-(a) SBA-15 (b) SHSBA-15 and (c) Pd(II)ASIP@SBA-15	102
Fig. 4B.7	XPS spectra-(a) the neat Pd(II)ASIP complex and (b) Pd(II)ASIP@SBA-15	102
Fig. 4B.8	UV-Vis spectra of (a) calcined SBA-15 (b) SHSBA-15 and (c) Pd(II)ASIP @SBA-15.....	103
Fig. 4B.9	SEM images of (A) calcined SBA-15 and (B) Pd(II)ASIP@SBA-15.....	104
Fig. 4B.10	TEM images of (A) calcined SBA-15 and (B) Pd(II)ASIP@SBA-15.....	104
Fig. 4B.11	Recycling study of Pd(II)ASIP@SBA-15 in amination reactions of aryl halides.....	106
Fig. 4B.12	Sheldon hot filtration test in amination of aryl halides.....	107
Fig. 5.1	XRD pattern of (a) SBA-15 and (b) (L)Ru(III)@SBA-15.....	115
Fig. 5.2	N ₂ -sorption isotherm and pore size (inset) of (a) SBA-15 and (L)Ru(III) @SBA-15.....	116

Fig. 5.3	TG (A) and DTA (B) of (a) SBA-15 and (b) (L)Ru(III)@SBA-15.....	117
Fig. 5.4	Solid state ^{13}C (A) and ^{29}Si (B) NMR of (L)Ru(III)@SBA-15.....	118
Fig. 5.5	FT-IR spectra of (a) SBA-15 and (b) (L)Ru(III)@SBA-15.....	118
Fig. 5.6	XPS spectra of Ru3d core levels of (L)Ru(III)@SBA-15.....	119
Fig. 5.7	DR UV-Visible spectra of (a) SBA-15 and (b) (L)Ru(III)@SBA-15.....	119
Fig. 5.8	SEM images of (A) SBA-15 and (B) (L)Ru(III)@SBA-15.....	120
Fig. 5.9	TEM images of (A) SBA-15 and (B) (L)Ru(III)@SBA-15.....	120
Fig. 5.10	The influence of the amount of methanol in acetalization reactions.....	124
Fig. 5.11	Sheldon's hot filtration test (A) and Recycling studies (B) of (L)Ru(III)@SBA-15.....	125

LIST OF TABLES

Tables	Descriptions	Page
Table 2.1	Textural properties of SBA-15 and V(IV)O-Sal-Ind-SBA-15.....	35
Table 2.2	Effect of different catalysts & substrates for asymmetric sulfoxidation reaction.....	44
Table 2.3	Influence of solvents & temperatures for asymmetric sulfoxidation reaction.....	45
Table 3.1	Textural properties of calcined SBA-15 and (L)Mo(VI)O ₂ @SBA-15.....	56
Table 3.2	Epoxidation of cycloalkenes.....	67
Table 3.3	Sulfoxidation of various sulfides.....	68
Table 3.4	Recycling Study in epoxidation and sulfoxidation reaction.....	69
Table 4A.1	Textural properties of calcined SBA-15 and Pd(II)DHBP@SBA-15.....	79
Table 4A.2	Arylation of alkenes (Heck reaction).....	87
Table 4A.3	Hydrogenation of alkenes.....	89
Table 4A.4	Recycling Study of Pd(II)DHBP@SBA-15 in arylation and hydrogenation reactions of alkenes.....	90
Table 4B.1	Textural properties of calcined SBA-15, SHSBA-15 and Pd(II)ASIP @SBA-15.....	97
Table 4B.2	Amination of arylhalides (>C-N coupling reactions) using Pd(II)ASIP @SBA-15.....	105
Table 5.1	Textural properties of calcined SBA-15 and (L)Ru(III)@SBA-15.....	117
Table 5.2	Synthesis of acetals from aldehydes.....	121
Table 5.3	Chemo-selective synthesis of acetals from aldehydes and ketones.....	122
Table 5.4	Influence of organic protective groups in acetalization reactions.....	123

LIST OF SCHEMES

Tables	Descriptions	Page
Scheme 1.1	Organo-linker on mesoporous silica.....	10
Scheme 1.2	Metal precursor anchored over functionalized silica.....	10
Scheme 1.3	Metal-ligand complex immobilized over organomodified support.....	10
Scheme 1.4	Asymmetric Sulfoxidation reactions.....	21
Scheme 1.5	Epoxidation reactions.....	21
Scheme 1.6	Hydrogenation reactions.....	22
Scheme 1.7	Arylation of alkenes (-C-C coupling) and amination of aryl halides (C-N-Coupling).....	22
Scheme 1.8	Acetalization reactions of aldehydes.....	22
Scheme 2.1	Synthesis of V(IV)O-Organofunctionalized SBA-15 [V(IV)O-Sal-Ind-SBA-15].....	33
Scheme 3.1	Preparation of Mo(VI)O ₂ -Organofunctionalized SBA-15 [(L)Mo(VI)O ₂ @SBA-15].....	54
Scheme 4A.1	Synthesis of Pd(II)-2,2'-Dihydroxybenzophenone(DHBP)-NH ₂ @SBA-15 [Pd(II)DHBP@SBA-15].....	76
Scheme 4B.1	Preparation of Pd(II)-3-Allylsalicylaldiminophenol(ASIP)-SH@SBA-15 [Pd(II)ASIP@SBA-15].....	95
Scheme 5.1	Synthesis of ruthenium based organofunctionalized SBA-15 catalyst [(L)Ru(III)@SBA-15].....	117
Scheme 5.2	Chemo-selective synthesis of acetal from aldehydes and ketones.....	120
Scheme 5.3	Tentative mechanism for the acetalization of aldehydes by (L)Ru(III)@SBA-15.....	124

LIST OF ABBREVIATIONS

IUPAC	: International Union of Pure and Applied Chemistry
OMM	: Organofunctionalized Mesoporous Materials
MCM	: Mobil's Crystalline Material
SBA	: Santa Barbara Amorphous
XRD	: X-ray Diffraction
SEM	: Scanning Electron Microscopy
TEM	: Transmission Electron Microscopy
FT-IR	: Fourier Transform Infrared Spectroscopy
XPS	: X-ray Photoelectron Spectroscopy
EDAX	: Energy Dispersive Analysis of X-rays
ESCA	: Electron Spectroscopy for Chemical Analysis
EPR	: Electron Paramagnetic Resonance spectroscopy
ICP-AES	: Inductively Coupled Polarized-Atomic Emission Spectroscopy
DR UV-Vis	: Diffuse Reflectance Ultraviolet-Visible spectroscopy
TGA	: Thermal Gravimetric Analysis
DTA	: Differential Thermal Analysis
Salpr	: 3-[N, N'-bis-3-(salicylidenamino)ethyl]triamine
acac	: Acetylacetonate
DHBP	: Dihydroxybenzophenone
ASIP	: Allylsalicyaldiminophenol
LCT	: Liquid Crystal Templating
CMC	: Critical Micelle Concentration
P123	: Pluronic 123
TEOS	: Tetraethylorthosilicate
TON	: Turn Over Number
TOF	: Turn Over Frequency
BET	: Brunauer-Emmett-Teller
BJH	: Barrett-Joyner-Halenda

MAS	: Magic Angle Spinning
CP	: Cross Polarization
LMCT	: Ligand to Metal Charge Transition
MLCT	: Metal to Ligand Charge Transition
FID	: Flame Ionization Detector
GC	: Gas Chromatography
APTMS	: 3-Aminopropyltrimethoxysilane
CPTMS	: 3-Chloropropyltrimethoxysilane
MPTMS	: 3-Mercaptopropyltrimethoxysilane
TBHP	: Tert-butyl hydrogen peroxide
H ₂ O ₂	: Hydrogen peroxide
AIBN	: Azobisisobutyronitrile
NHC	: N-Heterocyclic Carbene
EDG	: Electron Donating Group
EWG	: Electron Withdrawing Group
DMF	: Dimethylformamide
Et ₃ N	: Triethylamine
DCM	: Dichloromethane
CHCl ₃	: Chloroform
a _o	: Unitcell parameter
D _p	: Pore diameter
V _p	: Pore Volume
ω _t	: Wall thickness

THESIS ABSTRACT

The discoveries of MCM-41 and SBA-15 materials, in 1990's by Mobil and Santa Barbara research groups, were historic milestones in the evolution of mesoporous materials. These discoveries overcame the existing shortcomings at that time, such as diffusional constraints in microporous channels and low surface area of macroporous materials, leading way to inspire and engineer hierarchical mesoporous materials in synthetic material chemistry. Even though the mesoporous material exhibit excellent textural properties, their utilization and application in catalysis are hindered due to its lower number of active sites. To extend the applicability of mesoporous materials, especially these based on silica, it is necessary to modify the surface by organic functional groups for anchoring metals and metal complexes.

Organofunctionalized Mesoporous Materials (OMMs), where organomoities are functionalized over the surface of silica by using high density of silanol groups, are consider as a class of promising catalyst in producing chemical commodities. In the past, the metal free organofunctionalized mesoporous materials were mainly applied for physical adsorption of metal and antibiotics from the solutions and during solid base reactions. To widen the applicability of organofunctionalized materials, in fields like catalysis, generation of metal-based organofunctionalized mesoporous materials are necessary and inevitable in present era.

Metal-Organofunctionalized SBA-15 heterogeneous catalysts are fantastic alternative for the synthesis of the commodity chemicals via. organotransformation reactions. These materials compensate the disadvantages of homogeneous and metal-free organofunctionalized catalysts, such as difficulties in separation and reusability, corrosion, high metal waste and deficiency in active sites. The scope of this work is, (i) to heterogenize sustainable homogeneous complexes over functionalized SBA-15, (ii) to design novel homogeneous complexes from organic ligands to use as linkers for modified SBA-15 which can act as competitive catalysts in view of sustainable catalysis, (iii) optimization of reaction parameters and heterogeneity tests were carried out to attain high catalytic activities and stability, and (iv) overall, to design different types of metal (V, Mo, Pd and Ru) based organofunctionalized SBA-15 heterogeneous catalysts for oxidation, hydrogenation, coupling and acetalization reactions.

Chapter 1 sets the motivation and objectives for the study and also reports the literature background and introductory remarks on inherent properties of mesoporous,

organofunctionalized materials. A brief description of different techniques which has been used for the characterization of synthesized catalysts is also included.

Chapter 2 explains the synthesis of reusable, mesoporous, heterogeneous vanadium complex, V(IV)O-Sal-Ind-SBA-15, from (1R,2S)-(+)-Cis-1-amino-2-indanol for enantioselective sulfoxidation reaction. The physico-chemical properties of the functionalized catalyst were analyzed by a series of characterization techniques like XRD, N₂ sorption measurement isotherm, TG & DTA, TEM, FT-IR, XPS, EPR, DR UV-Visible, ICP-OES and solid & liquid state ¹³C, ²⁹Si and ⁵¹V NMR spectroscopy. Catalytic evaluation in asymmetric sulfoxidation reaction of sulfides indicate that V(IV)O-Sal-Ind-SBA-15 to show higher catalytic activity, stability, reusability and comparable enantioselectivity than SBA-15, PrNH₂-SBA-15 and neat V(IV)O-Sal-Indanol complex. The effects of different catalysts, temperature, solvents and substrates on sulfoxidation reaction were examined in order to optimize the conversion and enantioselectivity of thioanisoles to sulfoxides.

Chapter 3 describes an efficient and reusable oxidation catalyst 3-[N,N'-bis-3-(salicylidenamino)ethyltriamine]Mo(VI)O₂@SBA-15 which has been synthesized by the anchoring of the 3-[N,N'-bis-3-(salicylidenamino)ethyltriamine] ligand (L or Salpr) on the inner surfaces of organofunctionalized SBA-15 followed by subsequent complexation with Mo(VI)O₂(acac)₂. The physico-chemical properties of the functionalized catalysts were analyzed by elemental analysis, ICP-OES, XRD, N₂-sorption measurements, TG & DTA, solid state ¹³C, ²⁹Si NMR spectroscopy, FT-IR, Raman spectroscopy, XPS, DRS UV-Vis spectroscopy, SEM and TEM. The synthesized catalysts were evaluated in epoxidation and sulfoxidation reactions, and the results show that (L)Mo(VI)O₂@SBA-15 exhibits high conversion and selectivity towards epoxidation and sulfoxidation reactions in combination with high stability. The anchored solid catalysts can be recycled effectively and reused several times without major loss in activity. In addition, Sheldon's hot filtration test was also carried out.

Fourth chapter mainly focus on the Pd(II)-Organofunctionalized SBA-15 catalysts for hydrogenation, C-C- and -C-N- coupling reactions. This chapter is further sub-divided into two; 4A and 4B.

Chapter 4A deals with the synthesis of an efficient, simple, phosphine and co-catalyst free C-C coupling heterogeneous catalyst via a post grafting method. The synthesized catalysts were characterized by elemental analysis, XRD, N₂ sorption analyses, TG, DTA, FT-IR, solid state

^{13}C and ^{29}Si NMR spectra, XPS, UV-Visible, SEM, EDAX and TEM. Further, catalysts were screened in arylation (Heck reactions) and hydrogenation reactions of alkenes, and the results show that Pd(II)DHBP@SBA-15 exhibits high conversion and selectivity towards arylation and hydrogenation reactions of alkenes with high stability. The anchored solid catalysts can be recycled effectively and reused several times without major loss in activity.

Chapter 4B reports an effective and impressive heterogeneous catalyst, Pd(II)-3-allylsalicylaldiminophenol-SBA-15, dubbed as Pd(II)ASIP@SBA-15, for amination reactions of aryl halides to synthesize secondary amines (2^0). The synthesized catalyst were characterized by CHN analysis, PXRD, Nitrogen sorption analyses, TG & DTA, FTIR, ^{13}C and ^{29}Si CPMAS NMR spectra, XPS, UV-Visible, SEM, EDAX and TEM. Pd(II)ASIP@SBA-15 catalyst was screened in heterogeneous amination reactions of aryl halides to produce N-aryl derivatives or secondary amines with high catalytic activity as revealed by turn over frequency (TOF) calculations. To explore the heterogeneous nature of catalysts, amination reactions were carried with neat Pd(II)ASIP complex and Pd(II)(OAc) $_2$ catalysts. The catalyst was recycled several times without much loss of activity and Sheldon hot filtration test has been performed.

Chapter 5 explains a combining effect of electron deficient Ru(III) coordination sites with organofunctionalized SBA-15, (L)Ru(III)@SBA-15, which result in a mild, neutral, water scavenger free and chemo-selective acetalization catalyst for cyclic/acyclic acetals. Synthesized (L)Ru(III)@SBA-15 catalyst has been thoroughly characterized and act as competitive catalyst compared to conventional acid catalysts. (L)Ru(III)@SBA-15 performs high catalytic activity as well as selectivity within 20 min with high TOF. The catalyst can be recycled and reaction parameters are optimized.

Sixth chapter deals with the summary and conclusions of the entire work which is related with synthesis, characterization and catalytic evaluation of metal based organofunctionalized SBA-15 heterogeneous catalysts in various organotransformation reactions.

Chapter 1

Introduction and Literature Review

1. Introduction

1.1. Catalysis

Catalysis is a prime technology and processes that impact on various fields like solid state chemistry, ceramics, metallurgy, surface chemistry, thermodynamics, chemical kinetics and organic chemistry etc. and its name derived from two Greek words; ‘Kata’ and ‘lyein’.¹ According to definition, catalysis is a phenomenon in which a stoichiometric amount of material (catalyst) speeds up chemical reaction rate with intact chemical nature up to the end of the reaction. In a chemical point of view, a catalyst is a substance which decreases the activation energy of reaction pathway via. the formation of stable and feasible intermediates followed by the evolution of products with regenerated catalyst.

A Swedish chemist, J. J. Berzelius, coined the term ‘Catalysis’ in 1835 and explained the necessity of certain substances (catalysts) in industrial processes and chemical reactions without undergoing any chemical change.² Further, in 1909, W. Ostwald, Nobel Laureate, states a thermodynamic definition of catalysis is that all chemical reactions going through more/less stable intermediates and reveals the novelty of chemical equilibrium and reaction kinetics on the aspect of catalysis.³ After that, Sebatier and Taylor in 1925 expressed the importance of distinct sites in catalytic surface which itself act as catalyst in various reactions. Catalysts are providing an alternative mechanism compared to non-catalyzed reactions with lower activation energy thereby to enable reaction occurring at lower temperatures.⁴

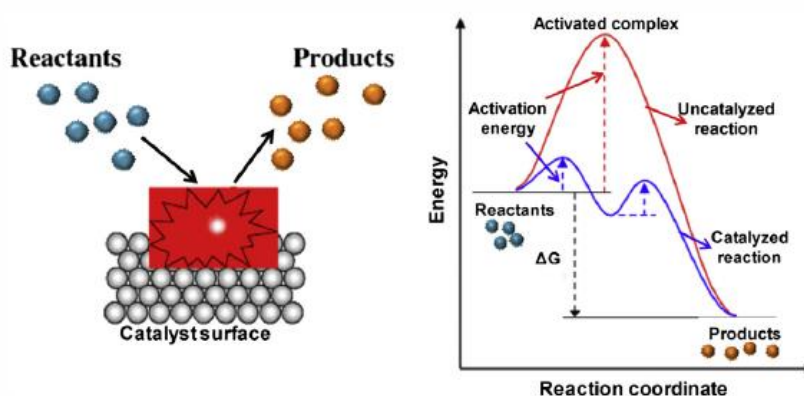


Fig. 1.1: Pictorial representation of a catalytic reaction and its energy diagram⁴

The overall output and thermodynamics are same which is illustrated by energy profile diagram or potential energy diagram (Figure. 1.1). In a catalyzed reaction, the interaction between catalyst and reactants results in overcoming the activation energy or energy barrier with the formation of intermediate complex which break down to give the final products and regenerating the catalyst. The regenerated catalyst again interacts with remaining reactants to favor further reactions. Presently, 90 % of industrial processes and >20 % of all industrial products involve catalytic steps which provide faster reaction rate and overall energy efficiency.

1.2. Heterogeneous catalysis

In heterogeneous catalysis, the phase of catalyst is different from the reactants and hence called as heterogeneous catalyst. Heterogeneity is the common feature of such type of catalysts and most of them exist as solids, eg: metal oxides and supported metal particles, compared to liquids and gases. Heterogeneous catalysts exhibit unprecedented characteristics such as easy handling, easy separation, high recyclability, minimization of metal content in products during reactions and good mechanical and thermal stability compared to its homogeneous analogues where both phases are same.⁵ The overall advantages of heterogeneous catalysts can provide cost effective and a feasible pathway for chemical reactions. In short, support and active sites are considered as main components in an efficient heterogeneous catalyst.

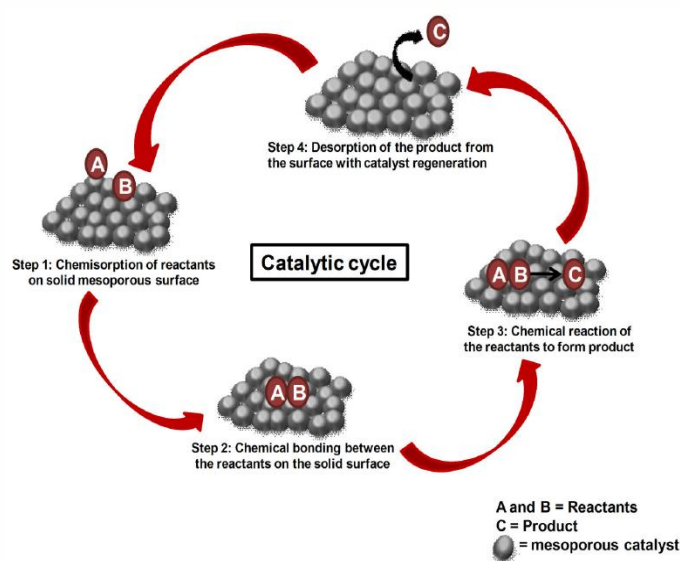


Fig. 1.2: Heterogeneous catalytic cycle⁴

The action of heterogeneous catalysts on catalytic reactions are plotted in Figure 1.2 and explained as, (i) diffusion and adsorption of reactants on solid surface, (ii) chemical interaction of reactants on the surface, (iii) the formation of products after chemical reactions and (iv) desorption of products from surface with regenerated catalyst.

1.3. Nanoporous Solids

Nanoporous solids act as a promising candidate and support or host for the synthesis of sustainable catalysts in heterogeneous catalysis. Nanoporous solids are mainly classified into two according to their pore size and the nature of species present in the framework (Figure 1.3). On the basis of IUPAC, porous materials are divided into micro (<2 nm), meso (2-50 nm) and macro (>50 nm) porous materials.⁶ Further, porous materials can be divided into purely inorganic, inorganic-organic hybrid and purely organic etc.

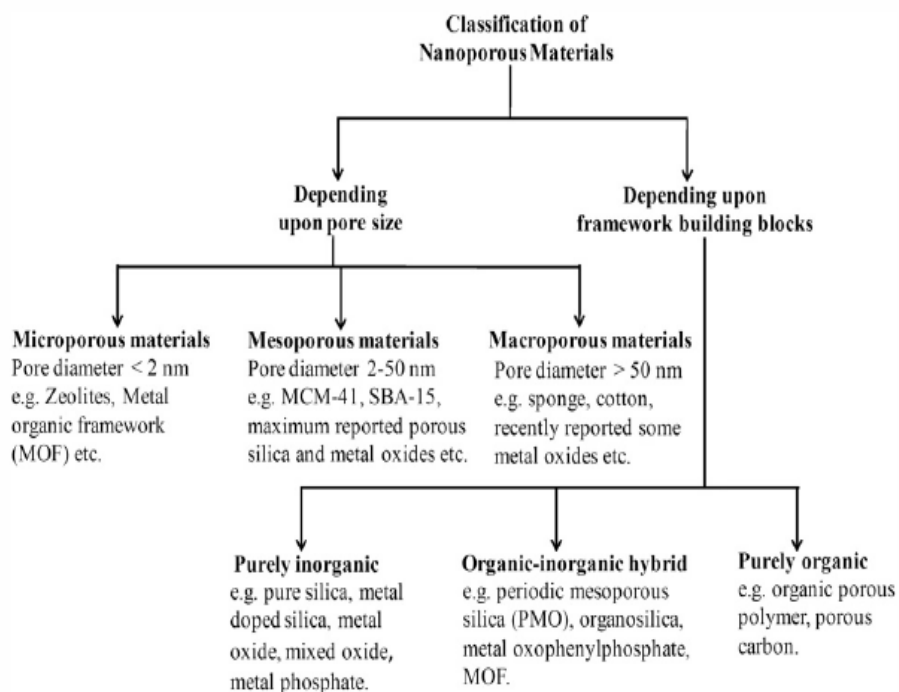


Fig. 1.3: Schematic diagram for the classification of nanoporous solids⁴

1.4. Mesoporous Materials

The introduction of microporous solids like zeolites in shape selective catalysis resulted in the evolution of porous materials in solid state chemistry. However, their small size has a

disadvantage in liquid phase reactions warranted the engineering of hierarchical material in nanoscale regime with larger pore diameters. To improve the applications of porous materials, the catalytic activity over macroporous materials have been performed, however; owing to low surface area and wide range pores of this category is not suitable candidate for the liquid phase heterogeneous catalysis. These shortcomings observed in above mentioned porous solids have ultimately lead to the discovery of ordered mesoporous silicas⁷ through co-operative self-assembly of surfactant molecules. By this way, generated mesoporous materials were shown less diffusional strain of molecules inside channels of supports.

A mesoporous material, is a substance having pore size between 2 to 50 nm, which can be ordered or disordered structure and show unprecedented intrinsic textural properties,⁸ such as (i) high surface area and narrow pore size distribution, (ii) high thermal stability and high density of silanols, (iii) tunable pore diameter (2-50 nm), (iv) good adsorption capacity, (v) flexibility to accommodate functional groups and metals and (vi) environmentally benign (non-toxic, non-corrosive and non-air sensitive).⁹ The discovery of periodic mesoporous ordered materials, like MCM-41¹⁰ and SBA-15,¹¹ in eighteenth century (1992-1998), using surfactant template mechanism, was a milestone breakthrough in material chemistry, especially in the field of porous materials, due to its unprecedented intrinsic textural properties compared to other porous materials.

In 1992, Mobil researchers proposed a mechanism, dubbed as “Liquid Crystal Templating Mechanism” (LCT) (Figure 1.4), for the synthesis of highly ordered mesoporous materials by using tetraethyl orthosilicate (TEOS) as silica precursor and long chain ammonium surfactants, amines or triblock copolymers as templating agents.¹² According to LCT mechanism, at lower concentration, surfactant behave as mono molecules and thereafter it is reaching a minimum concentration known as Critical Micelle Concentration (CMC) to form spherical isotropic micelles. With the increase of surfactant concentrations, spherical micelles get converted to cylindrical or rod like micelles followed by the interaction between silicate anions and surfactant cationic head groups. Thereafter, the condensation between silicate species results leading to the formation of an inorganic polymeric species. After removing the template by calcinations¹³ or solvent extraction,¹⁴ hexagonally arranged inorganic hollow cylinders will be produced. Among these extraction methods, calcinations method is efficient due to the high purity of mesoporous material compared to solvent extraction methods. However, solvent extraction method¹⁵ is also

applicable in the extraction of organic-inorganic hybrid material to obtain high density of surface silanol groups which play a crucial role in surface modification process.

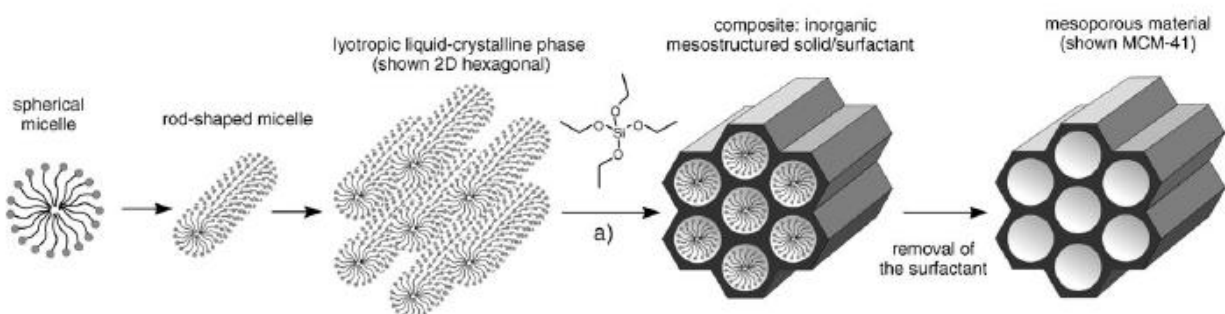


Fig. 1.4: Designing of mesoporous material by Liquid Crystal Templating Mechanism (LCT)¹²

Generally, mesoporous structures have been formed by different type of interactions, like electrostatic, hydrogen-bonding and covalent interactions, which occurs between surfactant (S) and inorganic silica precursor (I). Among these, electrostatic interaction happens through four approaches,¹² represented as S^+I^- , S^-I^+ , $S^+X^-I^+$ and $S^-X^+I^-$, which is based on with or without counter ions. The first two interactions is based on the ionic interaction between corresponding cations and anions of surfactant (S) and inorganic silica precursor (I), respectively and vice versa. The latter two occur through counter ion mediated pathways by using halide ions (X^-) and alkali metal ions (X^+) with the assembly of cations and anions, respectively.

Recently, designing hierarchical mesoporous materials with different pore size, crystalline size and shape are challenging and attractive in various fields such as catalysis, adsorption, separation and drug delivery systems. Mesoporosity or poresize of the materials depends on the chain length of surfactants (C_8 - C_{20}),¹⁰ addition of organic swelling agents (1, 3, 5-trimethylbenzene)¹⁰ and reaction parameters.¹⁶ The crystallite size of mesoporous material is important for catalytic processes where diffusion of molecules in inside channels depends on its length. Shorter pore length or smaller crystallite size in mesostructures favors higher catalytic activity by avoiding diffusional constraints of molecules during chemical reactions. The variation in the amount of surfactant concentration can greatly influenced the formation of three liquid crystalline phases or shapes (Figure 1.5); hexagonal (MCM-41), cubic (MCM-48)¹⁷ and lamellar (MCM-50).¹⁸

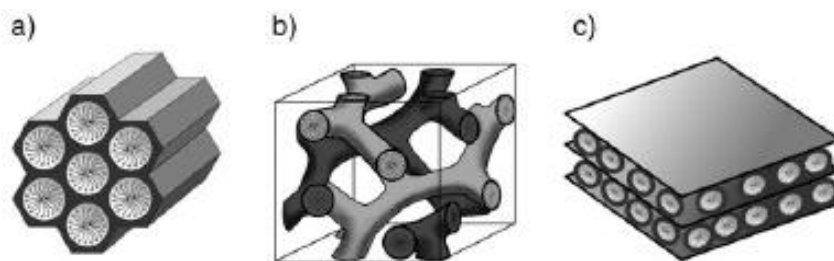


Fig. 1.5: Shapes of different M41S materials (a) hexagonal (MCM-41) (b) Cubic (MCM-48) and (c) Lamellar (MCM-50)¹²

1.5. SBA-15 (Santa Barbara Amorphous Material)

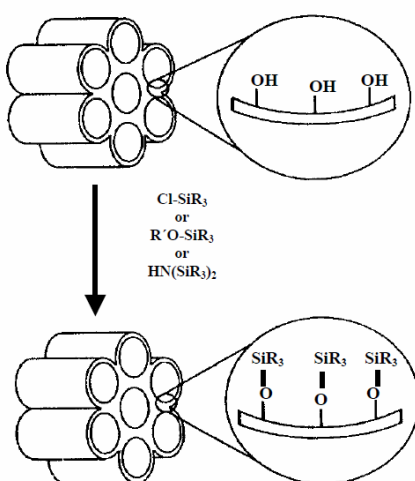
Since the discovery of MCM-41 material in 1992, researchers in material chemistry have started to design vivid type of mesoporous material. Even though M41S material shows potential applications in material chemistry, their limitations like lower thermal stability and complicated synthesis procedures led to the search of a candidate for heterogeneous catalysis. SBA-15¹¹ is a mesoporous material reported by Santa Barbara group in 1998 having good textural properties such as thicker pore walls, higher thermal stability, smaller crystalline sizes and higher mesoporous integrity compared to M41S materials.

To engineer SBA-15 materials, poly(alkeneoxide)triblock polymer are used as surface directing agent (P123) with TEOS as silica precursor were used in acidic conditions. Non-ionic neutral surfactant, P123, made up of three polymeric block units like polyethylene oxide-polypropylene oxide-polyethylene oxide (EOn-POM-EOn), respectively. Herein, long and less hydrophilic nature of polypropylene oxide (POM units) located at the centre or core compared to higher hydrophilic nature of polyethylene oxide (EOn units) which is situated at head portion in water medium during micelle formation. At lower pH, head EOn units are protonated followed by the hydrogen bonding interaction with cationic silicate oligomers where Cl^- ions act as counter ions. The weak interaction (S^+Cl^-) between protonated surfactant (S^+) and cationic silicates (I^+) with mediator Cl^- ions helps to tune and stabilize the wall thickness of material. Otherwise, the higher wall thickness provides greater thermal stability of the materials. Overall, SBA-15 offers rigid framework, insoluble, unswelling and inert nature in catalytic processes and provides better thermal and mechanical stability towards the chemical reactions.

1.6. Organofunctionalized Mesoporous Materials (OMMs)

To explore the characteristics of mesoporous materials and to extend their potential applications in catalysis, surface modification of mesoporous materials has been carried out by post-grafting method¹⁹⁻²¹ or co-condensation methods,²²⁻²⁴ to develop novel heterogeneous catalysts. Moreover, to improve the surface properties of mesoporous materials, Isomorphous substitution of metals (Ti, Al, V and Sn) in silicon framework of mesoporous materials^{25, 26} has been performed. Among these strategies, surface modification of mesoporous material is more popular than isomorphous substitution method due to its limitation towards some specific metals.

Organofunctionalized mesoporous materials (OMMs) are a novel class of materials in which organofunctional groups from siloxane linker or precursor are successfully anchored over surface of mesoporous supports by consuming active surface silanol groups. Generally, designing of OMMs were carried out by Post-grafting or co-condensation method (Figure 1.6). Post-grafting refers to inner modification of pre-synthesized mesostructured silica in anhydrous conditions, to avoid self coupling of silane-organic tethering groups, by using active silanol groups. But, in the case of co-condensation or in-situ or one-pot method, surface modification was achieved by the reaction of siloxane organic precursor or linker with surfactant and inorganic silica precursors in one-pot or via. in-situ manner. Among these methods, Post-grafting method is efficient due to its uniform arrangements of functional groups on surface, hydrolytically stable and well defined structure compared to latter method.



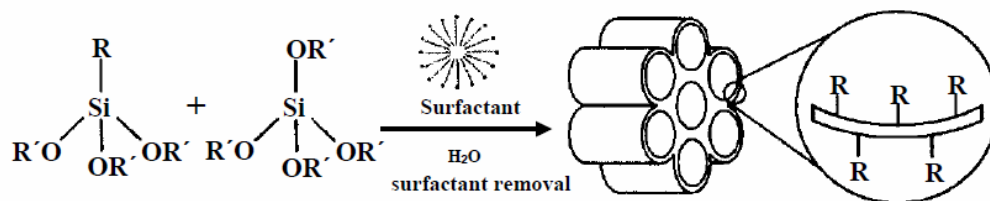


Fig. 1.6: Surface modification by post-grafting (first)¹⁹ and co-condensation methods (second)²³

Post-grafting method was achieved in two ways, sequential and convergent modes (Figure 1.7).²⁷ In sequential approach, catalysts were synthesized by the following order of (i) linker on support, (ii) ligand on modified support and (iii) metal precursor on heterogenized ligand. But, in convergent approach, homogeneous complexes, derived from ligand and metal precursors, was grafted over modified mesoporous silica. Sequential grafting method is efficient compared to convergent method because of its high purity.²⁸ There are four methods adopted for the immobilization processes²⁹ like covalent binding,³⁰ electrostatic interaction,³¹ adsorption³² and encapsulation³³ which is based on the interaction between the catalyst and the solid support. For example, silica materials like MCM-41 and SBA-15 have been functionalized with amino or aminopropyl groups,³⁴⁻³⁷ chloropropyl,^{38, 39} malonamide, carboxy, thiol, as well as saccharides.

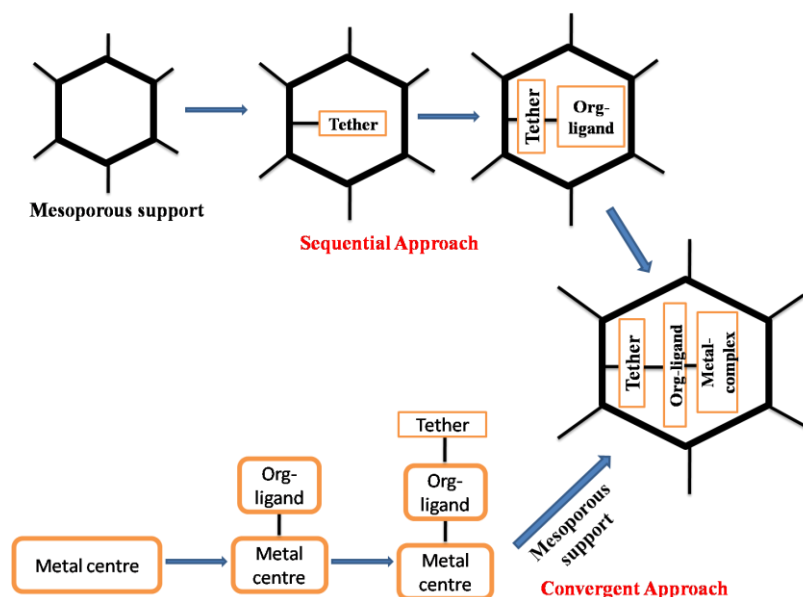
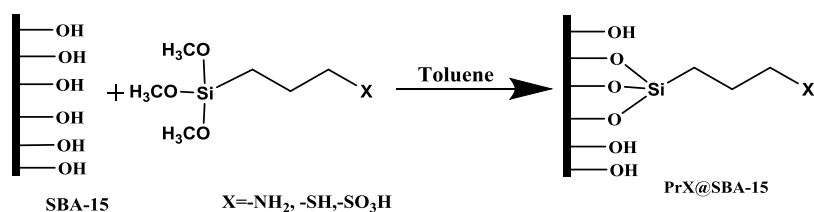


Fig. 1.7: Sequential and convergent approaches in post-grafting methods

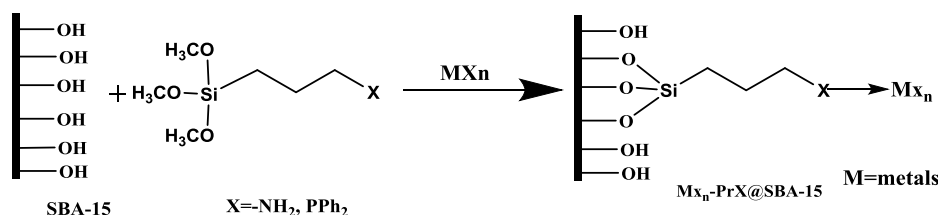
Efficient grafting process mainly depends on reactivity, counting, accessibility of silanol groups,⁴⁰ the nature of grafting agent and reaction parameters. The importance of silanol

groups⁴¹ in heterogeneous catalysis are, (i) act as reaction sites for functionalization,⁴² (ii) offers tunable surface properties,⁴³ (iii) to precise control of position and density of immobilized catalyst⁴⁴ and (iv) act as mild acid in bifunctional cooperativity effects of solid base-acidic reactions.⁴⁵ The isolated Si-OH and vicinal Si-OH groups are successfully utilized for the organofunctionalization instead of H-bonded silanol groups where they can make hydrophilic networks.

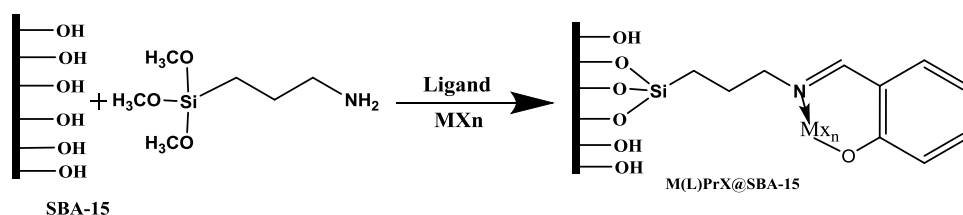
Functionalized materials are generally classified into three groups which are (i) organo-linker on mesoporous silica, (Scheme 1.1) (ii) metal precursor anchored over functionalized silica (Scheme 1.2) and (iii) metal-ligand complex anchored over modified support (Scheme 1.3).



Scheme 1.1: Organo-linker on mesoporous silica



Scheme 1.2: Metal precursor anchored over functionalized silica



Scheme 1.3: Metal-ligand complex immobilized over organomodified support.

In first case, silane precursor or organic linker has been used for the surface modification on mesoporous support to attain organofunctionalized silica catalysts in which solid base or acidic catalysts were applied in acid-base reactions and rest of them were used in adsorption of metals

and antibiotics from reaction mixtures. But, their applications are restricted to certain extent due to the absence of metal. To alleviate this problem, metal-organofunctionalized catalysts (second case) have been synthesized and applied for organo-transformation reactions. However, metal leaching from such type of heterogeneous catalysts creates a huge metal waste in industrial scale. To overcome these limitations, a lot of ligands were applied, which provides a higher coordination environment or chelation effect for metal complexes. By this way, an efficient and highly reusable metal-organofunctionalized catalyst were generated and screened in wide applications of fine chemical synthesis. Catalytic activity of metal-organofunctionalized complexes depends on (i) the nature of metal active sites, (ii) the nature of supports, (iii) spacer effect and (iv) steric effect.

Among various organic ligands, imine based ligands or salicyaldimines⁴⁶ act as better choice or cost effective in hereogeneous catalysis. Schiff base ligand or salicylaldimine, one of the most widely utilized organic ligand due to its good coordination capacity, has been synthesized by simple condensation reaction between carbonyl compounds and amine compounds. In addition, salicylaldimines show good chelating ability with metal due to the number of coordination sites and their vacant sites is available for coordination of substrates in reaction medium. Due to its high potential, OMMs were screened in:

- Physical adsorption of metals and bio-molecules
- Used in controlled drug delivery systems
- Fine chemical synthesis via. Organic reactions
- Asymmetric catalysis
- Tandem catalysis
- Bifunctional catalysis
- Valorization of Biomass
- Used in Sensors, Optics and Electrochemistry
- A good specimen to detect dynamic motion of molecules via. hierarchical NMR

1.7. Physico-Chemical Characterization Techniques

1.7.1. Elemental analysis or CHN analysis

The percentage of elements, especially C, H and N, and degree of surface modification over mesoporous silica were determined by CHN analysis. Moreover, this technique has been used to

predict the structure of unknown compound as well as to ascertain the purity of synthesized materials. In experimental part, samples or materials are subjected to combustion by an excess of oxygen to attain oxides of C, H and N as combustion products which is efficiently collected by various traps. Further, masses of these oxides or combustion products have been used to calculate the percentage and composition of synthesized materials. Generally, CHN analyzer are mainly divided into four zones like; (i) combustion zone, occurring combustion, (ii) Gas control zone, homogenization of combustion products or gaseous products, (iii) Separation zone, collection of gaseous by various traps and (iv) Detector zone, identification and quantitative determination of oxides of elements like CO₂, H₂O and N₂O etc. Elemental analysis (C, H and N) were performed on a Carlo Erba (Model EA 1108) elemental analyzer.

1.7.2. Inductively Coupled Plasma-Atomic Emission Spectroscopy (ICP-AES)

The weight percentage of metals or elements is quantitatively determined by Inductively Coupled Plasma-Optical Emission Spectrometry. These results can be used to calculate the Turn Over Number/ Frequency (TON/F) of a catalytic system thereby to optimize the reaction parameters in organo-transformation reactions. In this technique, plasma source ionizes the sample into its constituent ions or atoms and excite them into higher levels. After the relaxation of excited electrons, it will be return back to ground state level with emission of radiations. Identification and measurement of intensity of radiations reveal the nature or type and concentration of elements in the sample. Generally, experiment set up was performed by the dissolution of calculated amount of sample in HF solutions and this solution subjected to ionization and excitation by inductively coupled plasma source. ICP-AES offers advantages like; (i) detection of almost all cations and anions except alkali and light metals, (ii) performance level down to parts per million in some elements and (iii) highly selective and quantitative determination of elements. The element content in the material was determined by inductively coupled plasma-optical emission spectrometer (ICP-OES) on a Therm IRIS Intrepid II XSP.

1.7.3. Energy Dispersive Analysis of X-rays (EDAX)

EDAX is complementary technique to find out the nature and average weight percentage of metal in synthesized materials. EDAX analysis⁴⁷ was performed by quantitative measurement of X-rays of corresponding elements which is produced due to the electronic transitions between

shells during electron microscope analyses. It measures the number of emitted X-rays against its energy to find out the relative abundance of element. EDAX analysis was determined by model Quanta 200 3D, FEI Company, using a dual beam scanning electron microscope which is working at 30 kV.

1.7.4. Powder X-ray Diffraction (XRD)

XRD technique has been applied to identify the purity, composition and distribution of phases in solids,^{48, 49} to calculate crystalline size (D), wall thickness (ω) and unit cell parameters (a) of materials and to distinguish the amorphous and crystalline nature of silica samples from the width of lattice reflections.^{50, 51} Overall, it is a primary tool based on the scattering of X-rays owing to lattice planes to identify structural integrity and mesoporosity of solid particles. The number, intensity and broadening of peaks or Bragg reflections in XRD pattern indicate the purity and composition of materials. In XRD method, X-rays from Cu K α source interacts with atoms in a lattice plane at Bragg's angle and scattering of X-rays occurs in constructive manner to produce X-ray pattern, which is based on Bragg's equation, $n\lambda=2d\sin\theta$; where n is order of reflection (1), λ is X-ray wavelength, d is lattice distance and θ is glancing angle.⁵² Even though XRD is a primary technique, its application is restricted in small amount of samples, short-range, amorphous and smaller particles.

Crystalline size of particles can be determined by Debye-Scherrer equation, $D=k\lambda/\beta\cos\theta$; where D, k, λ , β and θ corresponds to average particle diameter, a constant ~ 1 , wavelength of X-rays, full width at half maximum (FWHM) and glancing angle, respectively.⁵² The reflection in XRD pattern allows phase identification and the calculation of lattice distance between the planes and width of peaks are providing an information related to dimension of Bragg reflecting planes. The unit cell parameters of hexagonal and cubic phases have been calculated by $a_0=2d_{100}/\sqrt{3}$ and $a_0=2d_{211}/\sqrt{6}$, respectively, where 'a' unit cell parameter and 'd' distance between two planes.⁵² The wall thickness of mesoporous material can be calculated by the subtraction between unit cell parameter and pore diameter of substances. Powder X-ray diffraction (XRD) patterns were measured on a PAN analytical X'pert Pro dual goniometer diffractometer using Ni-filtered Cu K α radiation ($\lambda=1.5404 \text{ \AA}$) over the 2θ range of $0.5-10^\circ$, with a scan speed of 1° min^{-1} .

1.7.5. N₂ sorption analysis

The porosity, structural integrity and textural properties of silica materials have been calculated from N₂-adsorption and desorption analysis via. BET isotherm and BJH pore size distribution curves. Even though a lots of shortcomings in Brunauer-Emmett-Teller (BET) theory, it can be used as multilayer adsorption analysis and the evaluation of surface area, pore volume and pore diameter. The BET equation is,

$$\frac{p}{v(p_0 - p)} = \frac{1}{v_m c} + \frac{c - 1}{v_m c} \frac{p}{p_0}$$

Where p and p₀ are denote the equilibrium and saturation pressures at same temperature and V and V_m are indicated to volume adsorbed at pressure p and volume of gas required to uniform monolayer adsorption, respectively, c is a constant related to energy of adsorption.⁵³ Barrett-Joyner-Halenda (BJH) model⁵⁴ has been used to derive the pore size distribution curves of material from N₂-physisorption isotherm. The mesoporosity of silica materials can be calculated by assuming the shape of pores like a cylindrical nature with Kelvin equation which is given as,

$$r_k = \frac{-2\gamma V_m}{RT \ln(p/p_0)}$$

Where r_k=Kelvin pore radius, γ=surface tension of N₂, V_m= Molar volume of N₂, p/p₀=relative pressure, T= boiling point of N₂ and R=gas constant.

Type IV isotherm with H1 hysteresis loop indicate the formation of mesoporous material and this isotherm is mainly divided into three portions like; (i) multilayer adsorption in mesopores (first linear region), (ii) capillary condensation within mesopores (steep region) and (iii) multilayer formation on external surfaces (last linear region). Moreover, N₂-sorption isotherm provides informations like; (i) a increased sharpness at inflection point indicate to the uniformity of mesostructured material, (ii) width of hysteresis loop represent to the retaining of mesopore structure and (iii) fluctuations in p/p₀ value to minor structural damage of material during synthetic procedures. N₂ adsorption–desorption isotherms, pore size distributions as well as the textural properties of the hybrid materials were determined by using an Autosorb 1C Quantachrome USA. The program consist of both an adsorption and desorption branch and typically run at -196 °C after the samples were degassed at 150 °C for 4 h. The BET method was

applied to calculate the total surface area at relative pressures of $P/P_0 = 0.65-0.45$ and the BJH model was applied to the adsorption branch of the isotherm to determine the total pore volume and average pore diameter at a relative pressure of $P/P_0 = 0.99$.

1.7.6. Thermal Analyses (TG and DTA)

The thermal stability and decomposition or weight loss of materials were determined by thermogravimetric analysis (TGA) or Differential Thermal analysis (DTA). In principle, both techniques have been performed by the measuring of variation in weight loss of sample occurring at elevated temperatures under controlled atmosphere. Moreover, these techniques provide information regarding the phase transformations and endo- and exo-thermic reactions. In material chemistry, especially mesoporous silica materials, the physisorbed moisture in pores, oxidative decomposition of inside organic templates and dehydroxylation of surface silanol groups were identified.⁵⁵ The gravimetric analyses technique depend on (i) heating rate, (ii) furnace atmosphere and (iii) shape of sample holder. Thermal analysis (TG-DTA) of the samples was conducted using a Pyris Diamond TGA analyzer with a heating rate of $10\text{ }^\circ\text{C min}^{-1}$ under an air atmosphere.

1.7.7. Fourier Transform Infrared Spectroscopy (FT-IR)

The nature of surface silanol groups and organic moieties in materials were found out by IR technique, a vibrational spectroscopy, where molecules undergo vibrations according to their variation in dipole moment, from ground state to excited state, via. the absorption of infrared radiations from the region of $4000-400\text{ cm}^{-1}$. Moreover, IR spectroscopy which is based on Hooke's law, given by equation, $\lambda=1/2\pi\sqrt{k/\mu}$, where, λ =wavelength of infrared radiations, k =force constant and μ =reduced mass, which indicates that vibrational frequency of molecules depends on force constant and reduced mass of materials. Experimentally, IR regions are mainly divided into four regions, (i) $400-1500\text{ cm}^{-1}$, single bonded molecules, finger print region and metallic materials, (ii) $1500-1900\text{ cm}^{-1}$, double bond region, (iii) $1900-2300\text{ cm}^{-1}$, triple bond region and (iv) $>2500\text{ cm}^{-1}$, electronegative element bonds (-OH and -NH bonds) and different Bronsted and Lewis acid sites.⁵⁶ In the case of silica material, $3000-3600\text{ cm}^{-1}$ region corresponds to vibrations of surface silanol groups and 1100 cm^{-1} assigned to the stretching

vibrations of Si-O-Si bonds in its framework. FTIR spectra of the solid samples were recorded in the range of 4000–400 cm^{-1} on a Bruker alpha T FTIR spectrophotometer at room temperatures.

1.7.8. Raman Spectroscopy

Raman spectroscopy is a complementary technique to infrared spectroscopy in which scattering of light occurs by the rotations and vibrations of molecules which depend on change in polarizability. In experimental setup, when the monochromatic visible light of frequency ν_0 falls on the investigated sample, the path of most of the lights are unaffected; however, some extend is affected by scattering of light in all directions. Among these scatterings, elastic scattering (Rayleigh scattering) where frequency of incident light ν_0 and scattered light ν_1 are equal and inelastic scattering in which the frequency of incident light and scattered light are unequal due to the addition of some other frequencies. These lines of frequencies known as Stokes and Anti-stokes lines where the intensity of Stokes line are higher than Antistokes lines due to a certain amount of unstable excited state at initial state. In instrumentation part, Raman spectrometer contains four components such as visible source, sample holder, monochromator and detector.⁵⁷

⁵⁸ Raman spectra of the complexes were recorded with a Horiba Jobin YVON Lab Ram HR spectrometer at 633 nm with a He–Ne laser.

1.7.9. Cross Polarization Magic Angle Spinning NMR Spectroscopy (CP MAS NMR)

In earlier decades, liquid phase NMR spectroscopy regarded as a prime technique is used to elucidate the structure and to check the purity of samples with respect to the number and intensity of NMR peaks. In principle, atomic nuclei having odd number of protons or neutrons with nuclear spin (I) greater than zero produces a nuclear magnetic moment (μ) in the presence of an applied magnetic field (B_0). The chemical shift of peaks originates from the secondary magnetic fields generated by the interaction between surrounding electrons with nucleus. This secondary magnetic field opposes applied magnetic field thereby shielding the nucleus.⁵⁹ In recent decades, NMR spectra of solid material are challenging and difficult to interpret the structure of molecules (wider line width) due to its dipolar and quadrupolar interaction with nucleus. However, high-resolution NMR spectroscopy overcomes the shortcomings observed in solid matrix, especially porous materials, and applied for the structural elucidation of several atoms like ^{13}C , ^{27}Al , ^{29}Si , ^{31}P , ^{51}V etc.⁶⁰

A popular technique, Magic Angle Spinning (MAS),⁶¹ where samples are rotated fast in an axis at a magic angle $\theta=54^{\circ}.44'$ towards the direction of applied magnetic field, lift up the solid state NMR spectroscopy to higher resolution mode with narrow line width of peaks instead of broader line width. Moreover, Cross Polarization (CP) technique⁶¹ is applied to obtain better sensitivity (signal to noise ratio) of spectra of nuclei with lower natural abundance elements. For this purpose, a highly abundant ^1H spin system can be used to transfer its magnetization power towards the lower abundant system for excitation process and thereby to attain good sensitive spectra in porous materials. Magic angle spinning (MAS) NMR spectra for ^{29}Si and ^{13}C nuclei were recorded on BRUKER DSX300 spectrometer at 7.05 T (resonance frequencies: ^{29}Si , 59.595 MHz, rotor speed 10000 Hz; ^{13}C , 75.43 MHz, rotor speed 10000 Hz; contact time: 1.5 ms; pulse delay: 5 μs).

1.7.10. Electron Paramagnetic Resonance Spectroscopy (EPR)

Electron Paramagnetic Resonance Spectroscopy has been used to find out the nature of catalytic active sites and its chemical environment in heterogeneous as well as homogeneous catalysis. Due to its high sensitivity, it can be applied in lower concentration of metallic sites and paramagnetic materials, which is inactive in NMR spectroscopy. Moreover, this powerful tool provides information like elemental composition, electronic structure of a paramagnetic state, g-factor, A-factor, hyperfine and super hyperfine interactions of molecules.⁶² An EPR spectrum is mainly based on interactions, called as Zeeman interactions, where electron magnetic moment (β) interacts with applied external magnetic field (H). During analysis, a paramagnetic sample is irradiated by microwave radiations with a particular frequency ν perpendicular to a external magnetic field, which permit a electronic transitions between two spin states with emission of energy of photons $E=h\nu$. The energy gap between two Zeeman levels called as g-factor or energy factor which is used to assess the spin state and to identify the number of nuclei associated with EPR transitions. Moreover, A-factor, hyperfine coupling constant, which is raised due to the interactions between generated electronic spin states with nuclear spin, is used to predict the type and number of ligands in equatorial plane and its value depends on substituent and steric effect of molecules. Even though it is a sensitive technique, its application is limited to paramagnetic systems.

1.7.11. Diffuse Reflectance UV-Visible Spectroscopy (DR UV-Vis)

UV-Visible spectroscopy can be used to identify the nature of organic moieties and to find out the oxidation state and chemical environment of metals in metal-organofunctionalized heterogeneous catalysts via. the monitoring of electronic transitions between orbitals or bands. DRS spectra is based on the reflection of light by a solid samples in the region of UV, Visible and near IR regions and it is measured as the ratio between scattered light from sample and scattered light from reference as function of wavelength (λ). Generally, UV-Visible spectroscopy based on the Beer-Lamberts Law and is expressed as, $\log I_0/I = \epsilon cl$, where I_0 and I are corresponds to intensity of incident light and scattered light, respectively, ϵ =molar extinction coefficient, c =concentration of sample in path length l . The broadening and merging of UV signals owing to the interaction of electronic transitions with their chemical environment of samples influence the interpretation and isolation of UV peaks difficult compared to other spectroscopic techniques. DRS UV-Vis spectra analysis helps to find out the Ligand to Metal Charge Transitions (LMCT) or vice versa (MLCT) and d-d transitions of molecules.⁶³ A Shimadzu UV-Vis spectrophotometer with a dual beam was used for UV-Vis spectra analysis.

1.7.12. X-ray Photoelectron Spectroscopy (XPS)

XPS, referred to another acronym as Electron Spectroscopy for Chemical Analysis (ESCA), is based on photoelectric effect⁶⁴ in which X-rays from $AlK\alpha$ or $MgK\alpha$ as source are irradiated on sample with the energy of $h\nu$ and after that photoelectrons having binding energy (E_b) are ejected from core or valence shell with a set of kinetic energy (E_k). The photo electric effect equated as; $E_k = h\nu - E_b - \phi$, where ϕ , ν and h are indicated as work function of instrument, frequency of radiation and Planck's constant, respectively. XPS spectrum, is a plot of photoelectron intensity verses binding energy and reveals the information about the identification of element, composition, empirical formulae, oxidation state and coordination environment etc. of molecules. A set of binding energies in XPS spectra consider as a characteristic for a specific element and composition of material and are evaluated according to their peak area and cross section of samples for photo emission.⁵⁰ The kinetic energies of ejected photoelectrons from solid samples depend on the electronic level and the nature of atoms which is involved in this process. Core level chemical shifts is an elegant way to identify different type of atoms and depend on certain factors such as; (i) formal oxidation state, (ii) overall charge on atom and (iii)

number and electro negativity of substituent groups. Even though XPS is a non-destructive surface technique, it exhibits certain short comings like ultra high vacuum for the avoiding of surface reactions and contaminations.⁶⁵ Near Ambient Pressure X-ray photoelectron spectrometer (AP-XPS) from Prevaic, Polland, has been used to determine XPS measurements of all samples recorded at ultra high vaccum conditions.

1.7.13. Scanning Electron Microscopy (SEM)

SEM is an electron probe technique which has been used to determine the surface structure, morphology, chemical composition and crystallographic information of solid materials. When a high energy beam of electrons are falls on investigated sample, electron beam interacts with nucleus or its core or valence shell electrons resulting to produce variety of signals via. elastic and inelastic scattering which contains backscattered electrons, secondary electrons, characteristic X-rays, light, current and transmitted electrons.⁶⁶ Herein, secondary electrons and backscattered electrons are important for surface analysis; in which, former one are emitted due to the interaction of electron beam with surface electrons and latter one are originated owing to the reflection of electron beam by its nucleus. The yield of secondary electrons mainly depends on (i) higher atomic number targets and (ii) higher angle of incidence. The drawback of SEM analysis is that it is an efficient method towards the conductive samples than non-conducting samples and non-detectable in lower atomic number elements. Scanning electron micrographs of the samples were obtained in a dual beam scanning electron microscope (FEI company, model Quanta 200 3D) operating at 30 kV.

1.7.14. Transmission Electron Microscopy (TEM)

Transmission Electron Microscopy provides information related to electronic structure details of mesoporous materials.⁶⁷ In TEM analysis, irradiation of dilute sample drop cast on holy carbon grid by high energy beam of electrons are diffracted by lattices of powdered or crystalline materials and propagated in different directions. These scattered radiations or transmitted electrons are magnified by the electron optics to attain a bright field image on a photographic plate or fluorescent screen. Three different interactions are mainly occurring between specimen and electron beam, which are given as, (i) Unscattered electrons (transmitted beam), (ii) elastic scattered electrons and (iii) inelastic scattered electrons. A modified technique, High Resolution

Transmission Electron Microscopy (HR-TEM), can be used to line mapping of elements present in metal based heterogeneous catalysts, in which a transmitted beam and a diffracted beam joined together to create an image compared to conventional TEM where transmitted beam is applied. A JEOL JEM-3010 and Tecnai (Model F30) both operating at 300 kV were used for HRTEM samples imaging.

1.7.15. Gas Chromatography (GC)

Gas chromatography (GC) has been used to analyze and interpret the products obtained from reaction mixtures. The principle of chromatography is based on the partial distribution of components between two phases, namely, stationary phase and mobile phase. In GC, silica coated capillary column act as stationary phase and inert gases such as nitrogen, argon and helium consider as mobile phase. The sample used for analysis are vaporized, and is transported through capillary column by carrier gas where partial distribution of components are occur and eventually, these components are identified by efficient detectors like Flame Ionization Detector (FID). A gas chromatograph (Agilent 6890) equipped with a flame ionization detector (FID) and a capillary column (HP-5) is used for analysis purpose.

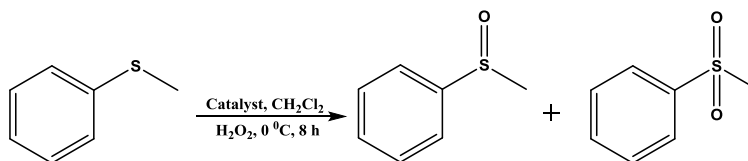
1.8. Catalytic Applications

Since the evolution of commercial industries by using variety of catalysts, researcher's great attention is that to provide cleaner, eco-friendly and economical pathway for fine chemical syntheses, thereby to create an unpolluted nature or universe for all sustainable organisms, by excluding the harmful and toxic metal wastes. In this thesis, metal-organofunctionalized SBA-15 catalysts have been studied by asymmetric sulfoxidation, epoxidation, hydrogenation, coupling reactions and acetalization of aldehydes.

1.8.1. Asymmetric sulfoxidation reactions

Asymmetric sulfoxidation reactions can be used to synthesize chiral sulfoxides, a main ingredient of medicines in pharmaceutical chemistry, from prochiral sulfides using a homo- or heterogeneous complexes with efficient oxidizing agents. In the perspective of metal-organofunctionalized catalysts, enantioselective sulfoxidation reaction by different organic chiral

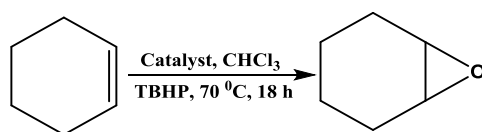
ligands such as Schiff base, Salen and aminoalcohol with metals like V, Mn and Mo etc. are challenging and admirable.



Scheme 1.4: Asymmetric Sulfoxidation reactions

1.8.2. Epoxidation reactions

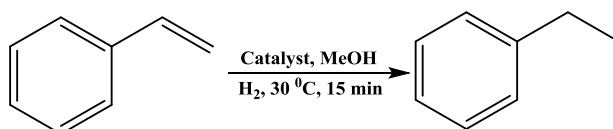
The synthesis of epoxides from olefins is challenging due to its instability and formation of by products during the liquid phase reactions. Earlier decades, metal incorporated mesoporous solids were used as catalysts for epoxidation reactions with oxygen or hydrogen peroxides as oxidizing agents. But, the lack of active sites and leaching of metal from previously mentioned catalysts prompt new promising scaffolds like organic-inorganic hybrid material catalysts and have been reported in present study.



Scheme 1.5: Epoxidation reactions

1.8.3. Hydrogenation reactions

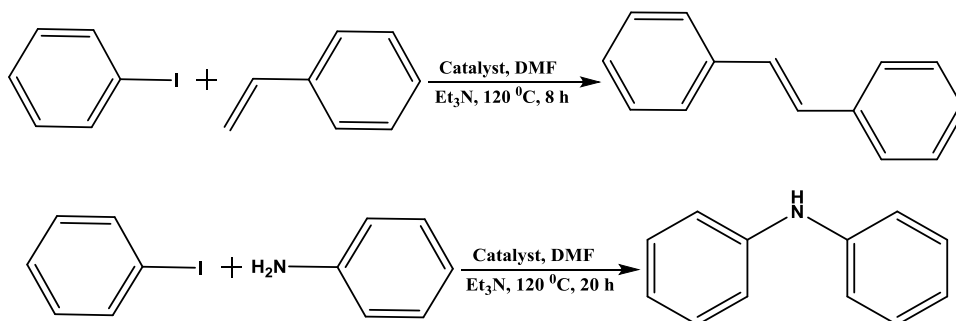
Hydrogenation reactions, a process of reduction of unsaturated compounds to saturated compounds by molecular hydrogen, provide valuable alkane compounds for fine chemical synthesis in commercial industries. Earlier, transition metal (Ni, Pd and Pt) based homogenous catalysts were used for this same and further, metal-organofunctionalized catalysts, especially N based ligands, have been used as an efficient and more sustainable catalysts where it is stable at harsh reaction conditions. During hydrogenation reactions, all reactants are adsorbed on metal surface followed by the decomposition of molecular hydrogen. Further, one by one hydrogen atom reacts with double bonded C atoms to attain a saturated product which is finally desorbed from catalyst surface.



Scheme 1.6: Hydrogenation reactions

1.8.4. Coupling reactions (-C-C- and -C-N coupling reactions)

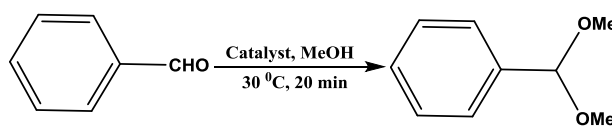
Coupling reactions, like arylation of alkenes and amination of aryl halides, are considered as prominent reaction in organic chemistry whereby providing stilbene derivatives and secondary amine compounds as products. Due to the importance of such type reactions, Richard F. Heck, Ei-ichi Negishi and Akira Suzuki were awarded Nobel Prize in 2010. After that, a lot of works have been carried out by different type of catalysts, especially phosphine or phosphine free catalysts, for the improvement and sustainable strategies for these reactions.



Scheme 1.7: Arylation of alkenes (-C-C coupling) and amination of aryl halides (C-N-Coupling)

1.8.5. Acetalization reactions of aldehydes

Acetalization reactions of aldehydes is one of the prime reactions in organic chemistry to protect aldehydes by alcohols, diols and thiols to form masked carbonyl compounds or cyclic/acyclic acetals. Electron deficient metal-organofunctionalized heterogeneous catalysts provide a cleaner, easiest and eco-friendly pathway for this reaction via. mild, acid and water scavenger free chemo-selective reactions.



Scheme 1.8: Acetalization reactions of aldehydes

1.9. Scope and Objectives of the thesis

The prime goal of this thesis is to design metal-organofunctionalized SBA-15 catalysts by the immobilization of organic ligand over functionalized SBA-15 via. Grafting method followed by the metallation using corresponding metal complexes. These organic-inorganic hybrid catalysts were evaluated in asymmetric sulfoxidation, epoxidation, hydrogenation, coupling reactions and acetalization of aldehydes. The engineering of organofunctionalized catalysts by tuning their chemical environment (spacer and steric effects) are of significant interest in sustainable catalysis due to its superficial advantages like higher stability, lower metal leaching and higher exposure of active sites thereby to enable higher catalytic activities and selectivity in fine chemical syntheses. Moreover, synthesized transition metal complexes over functionalized SBA-15 behave as heterogeneous catalysts which are confirmed by heterogeneity tests thereby to alleviate shortcomings raised from homogenous analogues. Systematic characterization of synthesized materials is directed towards the correct and efficient designing of organic-inorganic material for organo-transformation reactions. Following are the salient objectives of the thesis,

- Engineering of vanadyl oxide [V(IV)O] based aminoindanol Schiff base complex over functionalized SBA-15 for efficient catalytic and enantioselective sulfoxidation reactions [V(IV)O-Sal-Ind-SBA-15].
- Designing of an efficient epoxidation and sulfoxidation catalyst by the anchoring of 3-[N,N'-bis-3-(salicylidenamino)ethyltriamine]-Mo(IV)O₂ complex over modified SBA-15 [(L)Mo(VI)O₂@SBA-15].
- An efficient synthesis of simple, reusable, phosphine free 2,2'-dihydroxybenzophenone ligand based Pd catalyst for arylation and hydrogenation of alkenes.
- Immobilization of highly flexible and long 3-Allylsalicylaldiminophenol(ASIP) palladium complex over thiofunctionalized SBA-15 [Pd(II)ASIP@SBA-15] for the preparation of secondary amines through amination of aryl halides.
- Investigation of heterogeneous nature of ruthenium based 2,2'-dihydroxybenzophenone complex over aminofunctionalized SBA-15 for the protection of aldehydes as cyclic/acyclic acetals in synthetic organic chemistry via. acetalization reactions by alcohols, diols and thiols. It act as neutral and water scavenger free competitive catalyst in conventional catalysis.

- Characterization of all synthesized materials by physical, spectroscopic and microscopic techniques where GC, elemental analysis, ICP-OES, EDAX, XRD, N₂-Sorption analysis, TG and DTA, FT-IR, Raman spectroscopy, solid state ¹³C and ²⁹Si NMR, DR UV-Vis, EPR, XPS, SEM and TEM were performed.
- Heterogeneous nature of all catalysts is proved by Sheldon's hot filtration test and recycling studies.

1.10. References

1. G. Ertl, H. Knozinger, J. Weitkamp, "Handbook of Heterogeneous Catalysis", Willey-VCH, Weinheim, 1997, **1**, 64.
2. J. J. Berzelius, P. A. Reseanteckningar, Norstedt & Soner, Stockholm, 1903.
3. B. Lindstroma, L. J. Pettersson, "A Brief History of Catalysis", 2003, **7**, 4.
4. N. Pal, A. Bhaumik, RSC Adv., 2015, **5**, 24363.
5. W. A. Herrmann, B. Cornils, Angew. Chem. Intl. Ed., 1997, **36**, 1048.
6. K. S. W. Singh, D. H. Everett, R. A. W. Haul, L. Moscou, R. A. Pierotti, J. Rouquerol, T. Siemieniewska, Pure Appl. Chem., 1985, **57**, 603.
7. J. S. Beck, J. C. Vartuli, W. J. Roth, M. E. Leonowicz, C. T. Kresge, K. D. Schmitt, J. Am. Chem. Soc., 1992, **114**, 10834.
8. J. Rouquerol, D. Avair, C. W. Fairbridge, D. H. Everett, J. M. Hayness, N. Pernicone, J. D. F. Ramsay, K. S. W. Sing, K. K. Unger, Pure Appl. Chem., 1994, **66**, 1739.
9. A. Taguchi, F. Schuth, Micropor. Mesopor. Mater., 2005, **77**, 1.
10. C. T. Kresge, M. E. Leonowicz, W. J. Roth, J. C. Vartuli, J. S. Beck, Nature, 1992, **359**, 710.
11. D. Zhao, Q. Huo, J. Feng, B. F. Chmelka, G. D. Stucky, J. Am. Chem. Soc., 1998, **120**, 6024.
12. F. Hoffmann, M. Cornelius, J. Morell, M. Froba, Angew. Chem. Intl. Ed., 2006, **45**, 3216.
13. F. Kleitz, W. Schmidt, F. Schuth, Micropor. Mesopor. Mater., 2003, **65**, 1.
14. A. Doyle, B. K. Hodnett, Micropor. Mesopor. Mater., 2003, **58**, 251.
15. W. J. Hunks, G. A. Ozin, Adv. Fun. Mater., 2005, **15**, 259.

16. D. Khushalani, A. Kupermann, G. A. Ozin, K. Tanaka, J. Garces, M. M. Olken, N. Coombs, *Adv. Mater.*, 1996, **7**, 842.
17. A. Corma, *Chem. Rev.*, 1997, **97**, 2373.
18. T. Linssen, K. Cassiers, P. Cool, E. F. Vansant, *Adv. Colloid. Interface Sci.*, 2003, **103**, 121.
19. A. Stein, B. J. Melde, R. C. Schroden, *Adv. Mater.*, 2000, **12**, 1403.
20. P. M. Price, J. H. Clarck, D. J. Macquarrie, *J. Chem. Soc. Dalton. Trans.*, 2000, 101.
21. K. Moller, T. Bein, *Stud. Surf. Sci. Catal.*, 1998, **117**, 53.
22. C. Sanchez, F. Ribot, B. Lebeau, *J. Mater. Chem.*, 1999, **9**, 35.
23. A. P. Wight, M. E. Davis, *Chem. Rev.*, 2002, **102**, 3589.
24. C. Sanchez, F. Ribot, *New J. Chem.*, 1994, **18**, 1007.
25. J. Y. Ying, C. P. Mehnert, M. S. Wong, *Angew. Chem. Intl. Ed.*, 1999, **38**, 56.
26. P. T. Tanev, M. Chibwe, T. J. Pinnavaia, *Nature*, 1994, **368**, 321.
27. X. S. Zhao, X. Y. Bao, W. Guo, F. Y. Lee, *Materials Today*, 2006, **9**, 32.
28. J. M. Thomas, R. Raja, D. W. Lewis, *Angew. Chem. Intl. Ed.*, 2005, **44**, 6456.
29. P. McMorn, G. J. Hutchings, *Chem. Soc. Rev.*, 2004, **33**, 108.
30. C. Li, *Catal. Rev.*, 2004, 46, 419.
31. H. H. Wagner, H. Hausmann, W. F. Holderich, *J. Catal.*, 2001, **203**, 150.
32. J. Jamis, J. R. Anderson, R. S. Dickson, E. M. Campi, W. R. Jackson, *J. Organomet. Chem.*, 2000, **603**, 80.
33. S. B. Ogunwami, T. Bein, *Chem. Commun.*, 1997, 1285.
34. A. Walcarius, M. Etienne, B. Lebeau, *Chem. Mater.*, 2003, **15**, 2161.
35. A. Matsumoto, K. Tsutsumi, K. Schumacher, K.K. Unger, *Langmuir*, 2002, **18**, 4014.
36. K.Y. Ho, G. McKay, K.L. Yeung, *Langmuir*, 2003, **19**, 3019.
37. H. Yoshitake, T. Yokoi, T. Tatsumi, *Chemistry of Materials*, 2002, **14**, 4603.
38. M. Masteri-Farahani, F. Farzaneh, M. Ghandi, *J. Mole. Catal. A: Chem.*, 2006, **243**, 170.
39. S. Shylesh, P.P. Samuel, A.P. Singh, *Catal. Commun.*, 2007, **8**, 894.
40. X. S. Zhao, G. Q. Lu, A. K. Whittaker, G. J. Millar, H. Y. Zhu, *J. Phys. Chem. B.*, 1997, **101**, 6525.
41. X. S. Zhao, G. Q. Lu, *J. Phys. Chem. B.*, 1998, **102**, 1556.
42. X. S. Zhao, G. Q. Lu, L. J. Hu, *Chem. Commun.*, 1999, 1391.

43. J. M. Thomas, B. F. G, Johnson, R. Raja, G. Sankar, P. Midgley, *Acc. Chem. Res.*, 2003, **36**, 20
44. S. A. Raynor, J. Thomas, R. Raja, B. Johnson, R. Bell, M. Mantle, *Chem. Commun.*, 2000, 1925.
45. J. Lauwaert, E. G. Moschetta, P. V. D. Voort, J. W. Thybaut, C. W. Jones, G. B. Marin, *J. Catal.*, 2015, **325**, 19.
46. A. Lazar, C. P. Vinod, A. P. Singh, *Micropor. Mesopor. Mater.*, 2017, **242**, 173.
47. J. R. Fryer, *Chemical Applications of Transmission Electron Microscopy*, Academic Press, San Diego, 1979.
48. G. Bergeret, *Handbook of Heterogeneous Catalysis*, Vol. 2, Eds: G. Ertl, H. Knozinger, J. Weitkamp, Wiley-VCH, Weinheim, 1997, 464.
49. R. C. Rau, *Advances in X-Ray Analysis*, Vol. 5, Ed: W. M. Mueller, Sir Isaac Pitman and Sons, Ltd., London, 1962, 104.
50. J. W. Niemantsverdriet, *Spectroscopic Methods in Heterogeneous Catalysis*, VCH, Weinheim, 1993.
51. S. Biz, M. Occelli, *Catal. Rev-Sci. Eng.*, 1998, **40**, 329.
52. W. H. Bragg, W. L. Bragg, *The Crystalline State*, Vol. 1, McMillan, New York, 1949.
53. S. Brunauer, P. H. Emmett, E. Teller, *J. Am. Chem. Soc.* 1938, **60**, 309.
54. E. P. Barrett, L. G. Joyner, P. P. Halenda, *J. Am. Chem. Soc.* 1951, **73**, 373.
55. C-Y. Chen, H-X. Li, M. E. Davis, *Microporous Mater.*, 1993, **2**, 17.
56. C. C. Freyhardt, M. Tsapatsis, Jr. Balkus, M. E. Balkus, M. E. Davis, *Nature*, 1996, **381**, 295.
57. B. P. Straughan, S. Walker, *Spectroscopy*, Chapman and Hall, London, Vol.2, 1976.
58. F. A. Rushworth, D. P. Tunstall, *Nuclear Magnetic Resonance*, Gordon and Breach Science, Publishers Ltd., London, 1973.
59. M. Mehring, *High Resolution NMR Spectroscopy in Solids*, Springer-Verlag, Berlin, 1976.
60. G. Engelhardt, in: *Handbook of Heterogeneous Catalysis*, Vol. 2, Eds: G. Ertl, H. Knozinger, J. Weitkamp, Wiley-VCH, Weinheim, 1997, 525.
61. J. W. Robinson, *Atomic Absorption Spectroscopy*, Marcel Dekker, New York, 1975.

62. J. C. Vedrine, Electron Spin Resonance, Chapter 5 in: Characterization of Heterogeneous Catalysts, F. Delannay (Ed.) Marcel Dekker, New York, 1984.
63. X. T. Gao, I. E. Wachs, *J. Catal.* 1999, **188**, 325.
64. T. A. Carlson, X-Ray Photoelectron Spectroscopy, Dowden, Hutchinson & Ross: Stroudsburg, PA, 1978.
65. B. M. Weckhuysen, D. M. Keller, *Catal. Today*, 2003, **78**, 25.
66. J. I. Goldstein, H. Yakowitz (Eds.), *Practical Scanning Electron Microscopy*, Plenum Press, New York, 1975.
67. J. M. Thomas, O. Terasaki, P. L. Gai, W. Zhou, J. Gonzalez-Calbet, *Acc. Chem. Res.* 2001, **34**, 583.

Chapter 2

V(IV)O-Organofunctionalized SBA-15 for Asymmetric Sulfoxidation reactions

[Anish Lazar](#), P. Sharma and A. P. Singh*

Microporous and Mesoporous Materials 170 (2013) 331-339

2.1. Introduction

Asymmetric sulfoxidation is one of the most challenging approaches in synthetic organic chemistry to attain chiral sulfoxides.^{1,2} Asymmetric sulfoxides are useful as chiral auxiliaries and chiral ligands in pharmaceutical industry. Asymmetric sulfoxidation can be performed by catalysis with the use of nonmetal oxidation systems and chiral ligand complexes.³ Recently, the enantioselective oxidation of sulfides catalyzed by active chiral ligands such as bidentate diethyl tartrate, diol, BINOL, tridentate Schiff base ligands⁴ and tetradentate Salen type ligands⁵ with transition metal such as Ti, V, Fe, Mn, Cu, W, Pt, Mg, Nb, Os, Zr, Mo and Al⁶⁻¹⁸ has been reported. In 1986, Fujita¹⁹ and coworkers carried out first vanadium based asymmetric oxidation of alkyl aryl sulfides with V(salen) complexes to get 40% ee. In 1995, Bolm and Bienewald⁴ found that a robust vanadium complex obtained from the substituted salicylaldehydes and chiral tert-leucinol to achieve high yield (94%) and good enantioselectivity (ee, 70%). After that, Berkessel, Katsuki, Anson and Ahn²⁰⁻²³ improved the Bolm's protocol by applying additional elements of chirality.

Chiral β -amino alcohols and their derivatives are important ligands in enantioselective oxidation of sulfides and other asymmetric reactions. In these chiral β -amino alcohols,²⁴ rigid (1R,2S)-(+)-Cis-1-amino-2-indanol²² act as good chiral ligand in several asymmetric synthetic processes because of their availability, ease of recovery, the high degree of asymmetric induction and highly defined chiral environment in rigid amino indanol backbone. Mesoporous SBA-15²⁵ shows significant attraction due to its high surface area, uniform pore size, high wall thickness and high hydrothermal stability than other mesoporous materials. To extend the applicability of SBA-15 materials, it is necessary to modify the surface by organic functional groups for anchoring metals and metal complexes. Synthesis of heterogeneous vanadium complexes from β -amino alcohol, especially cis-1-amino-2-indanol, for sulfoxidation has been rarely reported. In these heterogeneous vanadium complexes, Barbarini et al.²⁶ investigated the use of polymer supported vanadium Schiff base complexes with V(IV)O(acac)₂ for the oxidation of thioanisole and reported highest enantiopurity was 61% ee.

To the best of our knowledge this is the first time report on the synthesis, characterization and catalytic applications of V(IV)O-Sal-Ind-SBA-15 complex for asymmetric sulfoxidation of thioanisole which exhibits moderate enantioselectivities, high catalytic and recyclic activities.

2.2. Experimental

2.2.1. Materials

Tetraethylorthosilicate (TEOS), Pluronic 123 (P123, Average Mol Wt = 5800), 3-tertbutyl-2-hydroxybenzaldehyde, (3-aminopropyl)trimethoxy silane (3-APTMS), dimethoxydimethylsilane [(MeO)₂SiMe₂], (1R,2S)-(+)-Cis-1-amino-2-indanol, thioanisole (methyl phenyl sulfide) were purchased from Aldrich. Paraformaldehyde and HCl (36.5%) were purchased from Thomas baker (India). 5-chloromethyl-3-tertbutyl-2-hydroxybenzaldehyde was synthesized according to the modified literature procedure.²⁷ The dry reagent grade solvents were obtained from Merck (India) and dried before use according to standard methods.

2.2.2. Synthesis of parent SBA-15

The synthesis of mesoporous SBA-15²⁸ was carried out hydrothermally under the autogeneous pressure in an autoclave. The polymer surfactant P123 was used as a template and hydrochloric acid served as a mineralizer. The following was the gel composition.

0.043 TEOS: 4.4 g P123 $M_{avg} = 5800 = [EO_{20}-PO_{70}-EO_{20}]$: 8.33 H₂O : 0.24 HCl

Typically, 4.4 g of tri block co-polymer was dispersed in 30 g of distilled water and stirred for 1.5 h. To the resultant solution, 120 g of 2 M HCl was added with constant stirring and the stirring was continued for next 2 h. Finally, 9 g of TEOS was added drop wise and the mixture was maintained at 40 °C for 24 h with continuous stirring. The mass was submitted to a hydrothermal treatment (100 °C, 48 h) under static condition. The precipitate was filtered, washed with distilled water, dried in an oven (90 °C, 12 h) and then calcined in air (500 °C, 6 h) to remove the template completely.

2.2.3. Synthesis of –OH protected PrNH₂SBA-15

Surface modification of SBA-15 was achieved by a post synthesis grafting method mentioned in Scheme 2.1. One gram of SBA-15 was suspended in a 50 ml of dry toluene and refluxed with 3.7 mmol of organosilane as 3-aminopropyltrimethoxysilane (3-APTMS) for 8 h under N₂ atmosphere. The material was filtered after cooling to ambient temperature, washed with dry toluene followed dichloromethane. Soxhlet extraction was carried out for 24 h in dichloromethane (CH₂Cl₂) to remove occluded organosilane. The sample was dried in vacuum for 10 h and designated as PrNH₂SBA-15. It is evident from elemental analysis (C, H, N

analysis) 3.3 wt% N being in aminofunctionalized materials. The free –OH groups being in PrNH₂SBA-15 were protected by the addition of 1.5 mmol of dimethoxydimethylsilane to a stirred suspension of 1 g of PrNH₂SBA-15 in dry toluene (50 ml) followed by the stirring of 12 h at reflux temperature under inert atmosphere. Resulting Material was filtered, washed with toluene and soxhlet extracted with CH₂Cl₂ for 24 h, named as –OH protected PrNH₂SBA-15 [Scheme 2.1(d)].

2.2.4. Synthesis of 5-chloromethyl-3-tertbutyl-2-hydroxybenzaldehyde

2 g of 3-tertbutyl-2-hydroxybenzaldehyde (11 mmol) were treated with 10.09 g of para-formaldehyde (336 mmol) in 25 ml of conc. HCl and refluxed for 48 h. The resulting solution was extracted with CH₂Cl₂ and carefully washed with saturated aqueous sodium bicarbonate followed by brine solution, dried over MgSO₄. Resultant residue was further concentrated using vacuum to give 5-chloromethyl-3-tertbutyl-2-hydroxybenzaldehyde in the form of viscous oil [Scheme 2.1(a)]. (80 % yield, 1.6 gm, 7 mmol). ¹³C NMR (50 MHz, [D₁] CDCl₃, 25 °C, TMS) 29.12 (s, 3C; –C(CH₃)₃); 34.98 (s, 1C; –C(CH₃)₃); 45.92 (s, 1C; –CH₂Cl); 120–140 (s, 1C; Ph); 161.28 (s, 1C; –C(OH) in Ph); 196.74 (s, 1C; –CHO). ¹H NMR (200 MHz, [D₁] CDCl₃, 25 °C, TMS) 1.43 (s, 9H; –C(CH₃)₃); 4.59 (s, 2H; –CH₂Cl); 5.34 (s, 1H; –C(OH) in Ph); 7.45–7.52 (s, 1H; Ph); 9.88 (s, 1H; –CHO); 11.86 (s, 1H; –CHO).

2.2.5. Synthesis of V(IV)O-Sal-Indanol complex

A mixture of (1R,2S)-(+)-cis-1-amino-2-indanol (0.50 g, 3.35 mmol) and 5-chloromethyl-3-tertbutyl-2-hydroxybenzaldehyde (0.76 g, 3.35 mmol) in 25 ml of dry toluene with anhydrous MgSO₄ (1.69 g) was refluxed for 10 h. The solution was filtered, the solvent was evaporated under reduced pressure giving as a yellow solid {(1R,2S)-(+)-1-[N-(3-tertbutyl-5-chloromethyl salicylidene)amino]-2-indanol ligand} (71.5% yield, 0.85 g, 2.38 mmol) [Scheme 2.1(b)]. For complexation, a mixture of yellow organic ligand and calculated amount of V(IV)O(acac)₂ in dichloromethane was stirred at 25 °C for 6 h to get neat V(IV)O-Sal-Indanol complex [Scheme 2.1(c)]. ²⁹ ¹³C NMR (50 MHz, [D₁] CDCl₃, 25 °C, TMS) 29.12 (s, 3C; –C(CH₃)₃); 34.98 (s, 1C; –C(CH₃)₃); 39 (s, 1C, –CH₂ in indanol); 46 (s, 1C; –CH₂Cl); 78, 80 (s, 1C, –CH in indanol); 120–140 (s, 1C; Ph); 161.28 (s, 1C; –C(OH) in Ph); 165.57 (s, 1C, –CH@N). ¹H NMR (200 MHz,

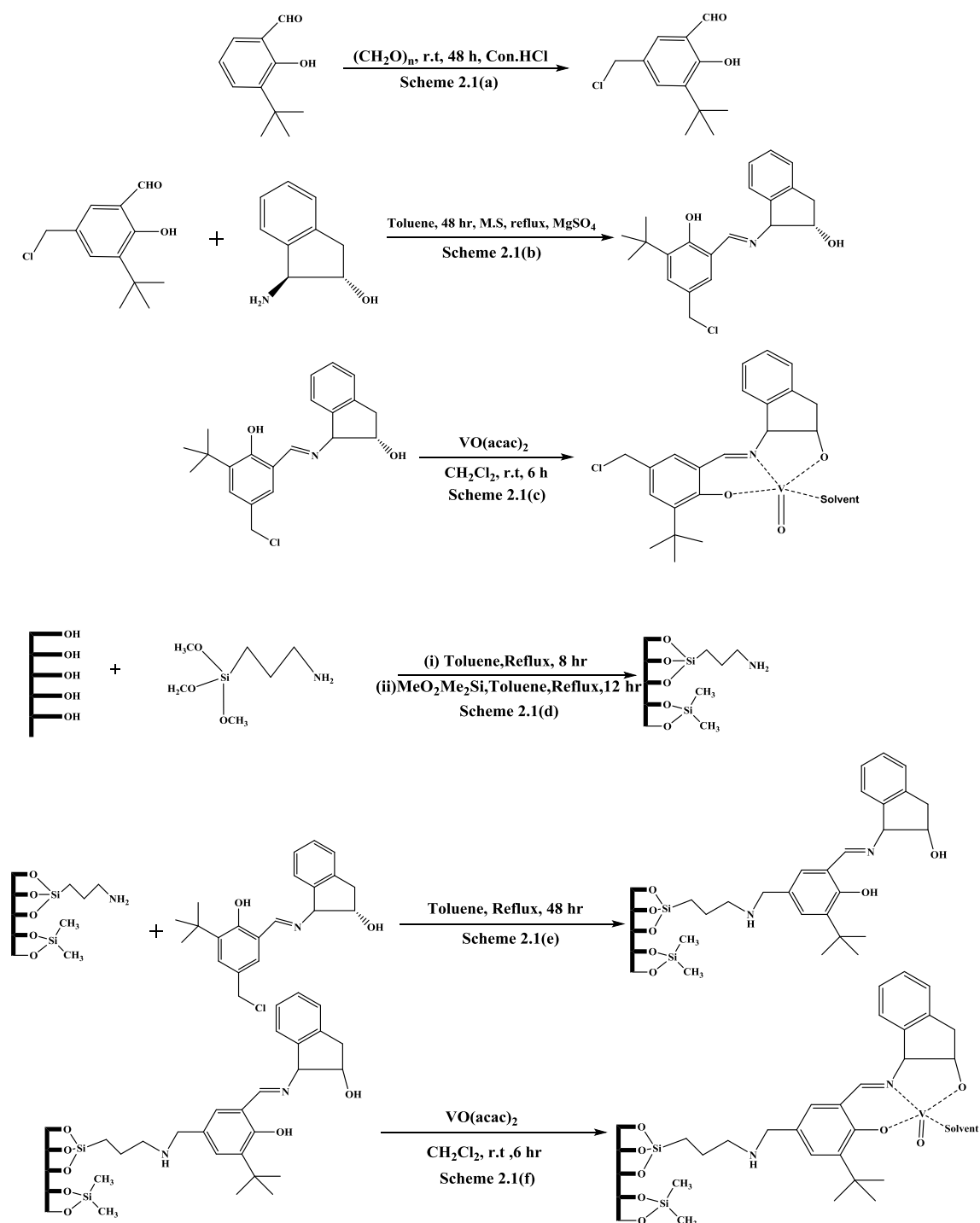
[D₁] CDCl₃, 25 °C, TMS) 1.40 (s, 9H; –C(CH₃)₃); 2.99–3.17 (s, 2H; –CH₂ in indanol); 3.49, 3.77 (s, 1H; –CH in indanol); 4.57 (s, 2H; –CH₂Cl); 7.45–7.52 (s, 1H; Ph); 8.59 (s, 1H; –CH=N).

2.2.6. Synthesis of V(IV)O-Sal-Ind-SBA-15

Schiff base ligand like (1R,2S)-(+)-1-[N-(3-tertbutyl-5-chloromethylsalicylidene)amino]-2-indanol (0.99 g, 2.77 mmol) in dry toluene (20 ml) was refluxed with PrNH₂SBA-15 for 48 h under an inert atmosphere. The immobilized catalyst was filtered, washed thoroughly with dry toluene, diethyl ether and extracted repeatedly with methanol and dichloromethane using a soxhlet extractor until the washing become colorless to get a solid compound [Scheme 2.1(e)]. To a stirred solution of (1R, 2S)-1-(N-Salicylideneamino)-2-indanol on PrNH₂SBA-15 (300 mg) in 5 ml dichloromethane, V(IV)O(acac)₂ (222 mg, 0.08 mmol) was added. The resulting solution was stirred for 6 h at room temperature. After 6 h, the solution was filtered and washed with dichloromethane to remove extra vanadium salt [Scheme 2.1(f)]. The vanadium loading in heterogeneous catalyst [V(IV)O-Sal-Ind-SBA-15] was found to be 3 wt.% as estimated by ICP-OES analysis.

2.2.7. General procedure for enantioselective sulfoxidation reactions

The catalytic activity and enantioselectivity of without catalyst, SBA-15, -OH protected PrNH₂ SBA-15, neat V(IV)O-Sal-Indanol complex and V(IV)O-Sal-Ind-SBA-15 were tested in enantioselective sulfoxidation reaction of sulfides.³⁰ The 25 ml of R.B flask was loaded with 5 ml solution of various catalysts (50 mg of SBA-15 or –OH protected PrNH₂SBA-15 or V(IV)O-Sal-Ind-SBA-15 or 25 mg of neat V(IV)O-Sal-Indanol complex) in CH₂Cl₂. To this reaction mixture, 2 mmol of sulfides (thioanisoles) and 2.2 mmol of 30% H₂O₂ were added at 0 °C for 10 h with continuous stirring. Samples were periodically withdrawn from the reaction mixture, filtered off, and analyzed with GC. Sulfide conversion (wt.%) and selectivity (%) were determined by gas chromatography (GC) (HP 6890) equipped with a flame ionization detector (FID) and a capillary column (Cyclodex-B, 30 m length, 0.250 diameter, 0.25 μm film thickness). Before GC analysis, the samples were centrifuged for 5 min at 4000 rpm. The crude product was purified by flash column chromatography.



Scheme 2.1: Synthesis of V(IV)O-Organofunctionalized SBA-15 [V(IV)O-Sal-Ind-SBA-15]; Syntheses of 2.1(a) 5-chloromethyl-3-tertbutyl-2-hydroxybenzaldehyde, 2.1(b) {(1R,2S)-(+)-1-[N-(3-tertbutyl-5-chloromethylsalicylidene)amino]-2-indanol ligand}, 2.1(c) neat V(IV)O-Sal-Indanol complex, 2.1(d) Capped PrNH_2 SBA-15, 2.1(e) Heterogenized ligand and 2.1(f) V(IV)O-Sal-Ind-SBA-15.

2.3. Results and discussions

2.3.1. Characterizations

2.3.1.1. X-ray Diffraction (PXRD)

Characterization results from XRD (Figure 2.1) analysis for V(IV)O-Sal-Ind-SBA-15 catalyst show that the ordered mesoporous channel structure was preserved upon functionalization and immobilization of neat V(IV)O-Sal-Indanol complex occurred within the pores. XRD pattern of (a) as-synthesized SBA-15 (b) calcined SBA-15 (c) –OH protected PrNH₂SBA-15 (d) V(IV)O-Sal-Ind- SBA-15 are depicted in Fig. 2.1. The pristine SBA-15 shows three (hkl) reflections of (100), (110) and (200) in the range 2θ of $0.8\text{--}2^\circ$ indexed to two-dimensional (2D) hexagonal $p6mm$ symmetry, indicating a highly ordered hexagonal structure.³¹ The existence of the (100), (110) and (200) reflections (Fig. 2.1) provides good structural stability, existence of long range order and high pore wall thickness even after a number of treatments with organic molecules in solvents under radical conditions.

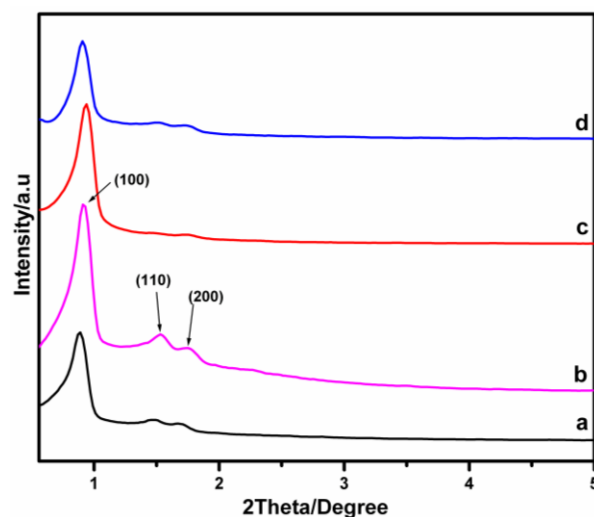


Fig. 2.1: XRD pattern of (a) as-synthesized SBA-15 (b) calcined SBA-15 (c) –OH protected PrNH₂SBA-15 (d) V(IV)O-Sal-Ind- SBA-15.

The calcined SBA-15 shows larger peak intensities than the as-synthesized sample and these differences arise due to the enhanced contrast in electron density after the removal of the surfactant from the pore channels than the surfactant-silicate samples.³² From the XRD pattern of –OH protected PrNH₂SBA-15 and V(IV)O-Sal-Ind-SBA-15, intensities of peaks decreased

without changing the peak positions due to the proper loading of organic modifier and neat V(IV)O-Sal-Indanol complex on calcined SBA-15. The decrease in signal intensity may be due to the loss of some regularity in the 2D hexagonal structural ordering or due to reduction of the scattering contrast between the SBA-15 silica walls and filled pores with propyl amine and neat V(IV)O-Sal-Indanol complex. After functionalization of propylamine and subsequent anchoring of neat complex, the width of the d100 reflections became narrow. This is an evidence for the homogeneous distribution of the pore structure brought about by the attachment of propylamine groups inside the mesopore channels. Structural stability and ordered mesoporosity of the samples have retained after incorporation of V(IV)O-Sal- Indanol complex over SBA-15.

2.3.1.2. N₂-Sorptions analyses

The N₂ adsorption–desorption isotherm and pore size distribution of (A) SBA-15 and (B) V(IV)O-Sal-Ind-SBA-15 complex are shown in Fig. 2.2. V(IV)O-Sal-Ind-SBA-15 shows type-IV isotherms with H1 hysteresis relates to capillary condensation steps, a characteristic feature of the highly ordered mesoporous materials (2–50 nm).³³ Textural properties such as BET surface area, pore volume (BJH) and the pore diameter (BJH) of calcined SBA-15 and V(IV)O-Sal-Ind-SBA-15 samples are summarized in Table 2.1. The mesoporous calcined SBA-15 shows BET surface area 605 m²/g, pore volume of 1.00 cc/g and pore diameter of 65 Å. As shown in Table 2.1, compared to calcined SBA-15, a further reduction in the surface area from 605 to 201 m²/g and pore size from 65 to 48 Å was observed for V(IV)O-Sal-Ind-SBA-15. The significant decrease in surface area, pore diameter and the pore volume of V(IV)O-Sal-Ind-SBA-15 complex indicates the successful anchoring of organic modifier group and neat V(IV)O-Sal-Indanol complex on SBA-15 and thereby reduces a large extent of their textural qualities.

Table 2.1: Textural properties of SBA-15 and V(IV)O-Sal-Ind-SBA-15

Sample	$a_0[\text{Å}]^a$	S.A [m ² /g]	$D_p[\text{Å}]$	$V_p[\text{cc/g}]$	$\omega_t(\text{Å})^b$
SBA-15	106	605	65	1.00	41
V(IV)O-Sal-Ind-SBA-15	105	201	48	0.30	57

a_0 =Unit cell parameter, S.A= BET Surface area, D_p = Pore diameter, V_p = Pore volume, ω_t = Wall Thickness; From ICP-OES analysis $V \sim 3$ wt%; ^a $a_0 = 2d_{100}/1.73$; ^b $\omega_t = a_0 - D_p$.

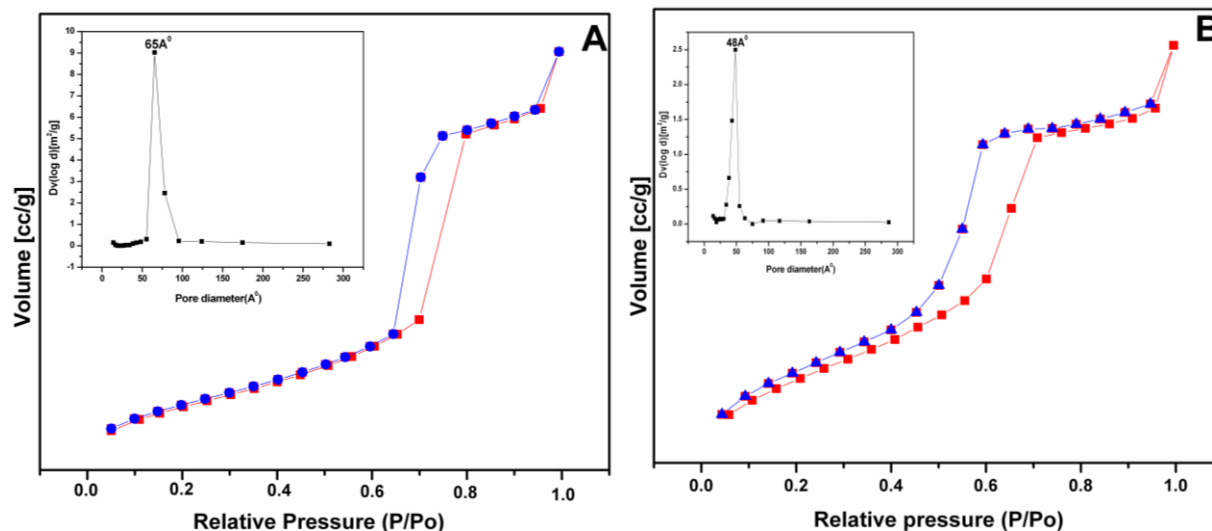


Fig. 2.2: N₂-isotherm and pore-size (inset) of (A) SBA-15 and (B) V(IV)O-Sal-Ind-SBA-15

2.3.1.3. Thermal analyses (TG and DTA)

The thermal stability and the amount of organomoieties functionalized in V(IV)O-Sal-Ind-SBA-15 catalyst were determined by gravimetric analyses such as TG and DTA which is plotted in Figure 2.3. In TG, 13 wt % losses was measured in SBA-15 materials due to the exclusion of physisorbed water molecules and this result correlated with DTA analysis where no peaks are observed. Three peaks at 236 °C, 290 °C and 490 °C in DTA analysis, indicated the decomposition of aminopropyl groups, capping agent and aminoindanol ligand moieties, respectively, in V(IV)O-Sal-Ind-SBA-15, also supported by TG analysis where ~30 wt% loss was observed compared to its support, SBA-15.

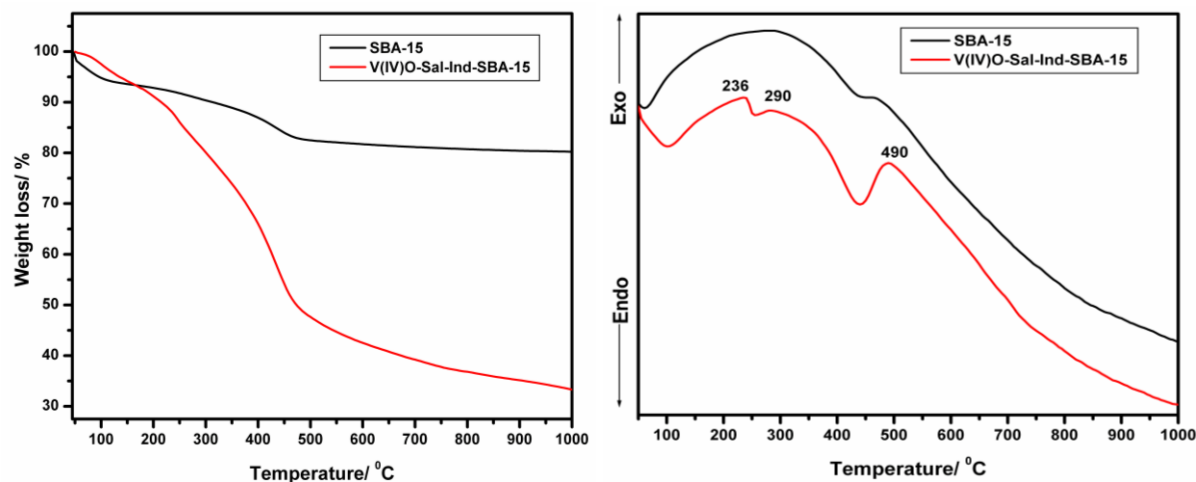


Fig. 2.3: TG and DTA analyses of SBA-15 and V(IV)O-Sal-Ind-SBA-15

2.3.1.4. Fourier Transform Infrared Spectroscopy (FT-IR)

FT-IR spectra of (a) as-synthesized SBA-15 (b) calcined SBA-15 (c) –OH protected PrNH₂SBA-15 (d) neat V(IV)O-Sal-Indanol complex and (e) V(IV)O-Sal-Ind-SBA-15 are shown in Fig. 2.4. FTIR spectroscopy has been extensively used to study different type of silanol groups present in silica samples. In the spectrum of calcined SAB-15 (Fig. 2.4b), a broad band at 3600–3200 cm⁻¹ and a weak band at 3738 cm⁻¹ indicate the ν -OH stretching vibrations of hydrogen bonded and isolated surface silanol groups in host materials. Further, sharp band at 1628 cm⁻¹ reveals –OH bending frequency of silanol groups. The bands observed at 798 cm⁻¹ and 1080 cm⁻¹ are assigned to the asymmetric and symmetric stretching vibrations of Si–O bond in Si–O–Si framework (Fig. 2.4a–c and e). A strong band is observed in the mid-infrared region at 960 cm⁻¹ which is attributed to ν (Si–OH) vibrations. The above stretching vibrations reveal the formation of siliceous materials. Generally, the free and geminal silanol sites are the active silanol sites participating in the condensation reactions with the silylating agents, whereas the hydrogen-bonded silanol groups do not participate due to the efficient hydrophilic networks formed among them.³⁴ But in present case, hydrogen-bonded silanol groups are also available for the condensation of 3-APTMS.

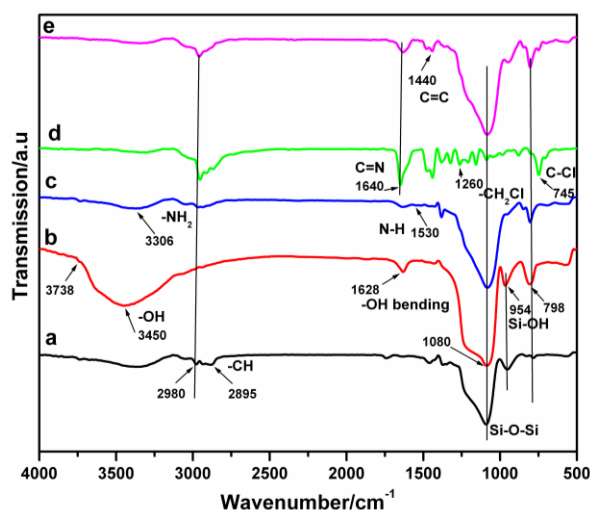


Fig. 2.4: FT-IR spectra of (a) as-synthesized SBA-15 (b) calcined SBA-15 (c) –OH protected PrNH₂SBA-15 (d) neat V(IV)O-Sal-Indanol complex and (e) V(IV)O-Sal-Ind-SBA-15.

The removal of surfactants from the pore channels of mesoporous materials and the attachment of aminopropyl groups over the silica surfaces was also examined by IR

spectroscopy. The absence of strong absorptions in calcined SBA-15 (Fig. 2.4b) at 3000–2700 cm^{-1} indicates the complete removal of surfactants. After amino functionalisation of SBA-15 (Fig. 2.4c), peaks at 3738 cm^{-1} and 3600–3400 cm^{-1} disappeared which indicates transformation of silanol groups on the surface of SBA-15 into Si–O–Si. The peaks at 3306 cm^{-1} and 1530 cm^{-1} correspond to stretching and bending vibrations of N–H bond in –OH protected PrNH₂SBA-15 (Fig. 2.4c). Further, peaks at 2980 cm^{-1} and 2895 cm^{-1} indicate the stretching vibrations of –CH₂ group in propyl chain of organic modifiers. These results support the attachment of amino propyl groups to the solid support. In Sal-Indnol ligand (Fig. 2.4d), peaks at 1260 cm^{-1} and a medium band at 745 cm^{-1} represent to –CH vibrations of –CH₂Cl group and C–Cl band, respectively. After V(IV)O-Sal-Indanol complex immobilization (Fig. 2.4e) peaks at 703 cm^{-1} and 1440 cm^{-1} are assigned to the C–H bending and the C=C stretching vibrations of benzene framework. Moreover, a strong band at 1640 cm^{-1} is assigned to –C=N stretching vibrations of azomethylene group and a characteristic band due to the V=O stretching frequency appear as a weak band between 900 cm^{-1} and 1000 cm^{-1} . The above mode of vibrations clearly indicate that V(IV)O-Sal-Indanol complex and organic modifiers were incorporated over the modified SBA-15 successfully.

2.3.1.5. Solid state ¹³C and ²⁹Si NMR spectroscopy

The organic moieties anchored over the surface of SBA-15 was further demonstrated by NMR techniques. The ¹³C solid state NMR spectra of V(IV)O-Sal-Ind-SBA-15 are depicted in Fig. 2.5A. The presence of peaks at 10, 22 and 43 ppm are assigned to the carbon atoms (C₁–C₃) of the propyl chain in organic modifier which indicates the successful amino functionalization of SBA-15. Additionally a sharp peak at -1.7 ppm (C₄) is evidence to the presence of –CH₃ group owing to the capping of hydroxyl groups by dimethoxydimethylsilane. The grafting of the Sal-Indanol ligand is confirmed by the presence of new resonances in the ¹³C CP/MAS NMR spectrum of V(IV)O-Sal-Ind-SBA-15. First, distinct peaks observed in the region of 110–150 ppm correspond to aromatic region of Sal-Indanol ligand. Further, a set of peaks in the range of 65–85 ppm are assigned to cyclic –CH₂ groups in immobilized Sal-Indanol molecule. Moreover, two extra resonances at 28 ppm and 34 ppm (in the region of 0–50 ppm) are representative of the methyl carbon of tert-butyl group. The small peak at 165 ppm is ascribed to the carbon atom of imine group in V(IV)O-Sal-Ind-SBA-15, whereas one shoulder peak at 50 ppm correspond to

carbon which is directly attached to NH₂ groups of organic linker. All the resonance peaks are supporting the successful anchoring of V(IV)O-Sal-Indanol complex into SBA-15.

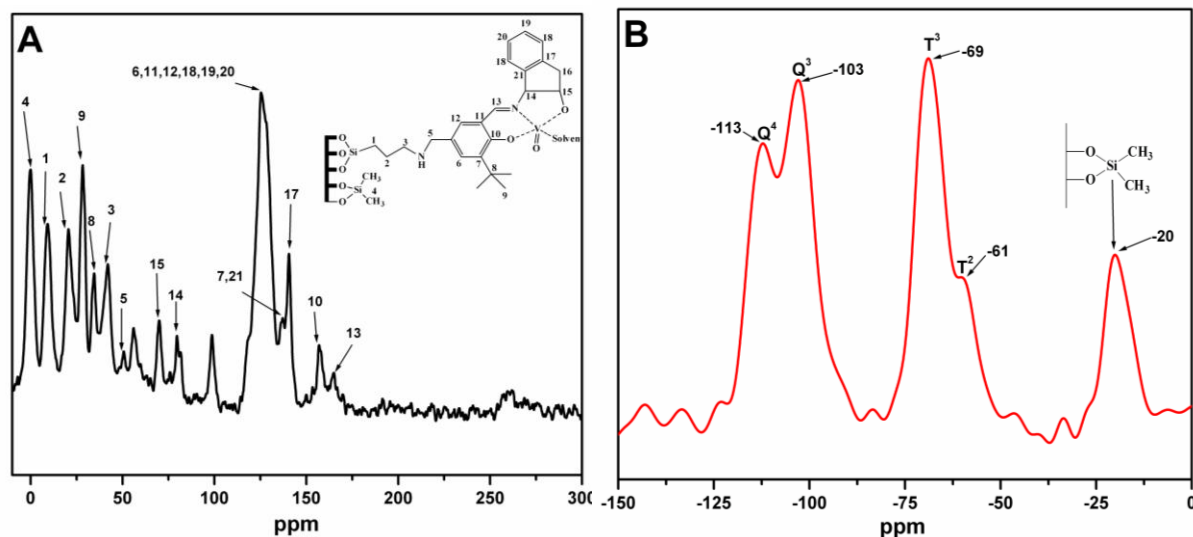


Fig. 2.5: Solid state ¹³C (A) and ²⁹Si (B) NMR spectra of V(IV)O-Sal-Ind-SBA-15

The degree of functionalization of surface silanol groups with organic moiety on the mesostructured materials can be monitored by means of ²⁹Si CP MAS NMR spectroscopy. ²⁹Si CP MAS NMR spectra of V(IV)O-Sal-Ind-SBA-15 are depicted in Fig. 2.5B. The spectrum of V(IV)O-Sal-Ind-SBA-15 shows broad resonance peaks from -90 to -115 ppm indicating a range of Si–O–Si bond angles and the bands are centered at -93 ppm, -103 ppm and -113 ppm assigned to Q² [germinal silanol, (SiO)₂Si(OH)₂], Q³ [single silanol, (SiO)₃Si(OH)] and Q⁴ [siloxane, (SiO)₄Si] sites of the silica framework, respectively. In general, the Q³ sites are associated with isolated Si–OH groups, which may be free or hydrogen bonded, while the Q² sites correspond to geminal silandiols. After aminofunctionalization, two additional peaks at -69 ppm and at -61 ppm are assigned to T³ [SiR(OSi)₃] and T² [Si(OH)R(OSi)₂] respectively, with T³ as the major system. The existence T³ confirms that SBA-15 has been modified by organic moieties. Further, a sharp peak at -20 ppm indicates Si atoms of dimethoxydimethylsilane which used for capping agent. ²⁹Si CPMAS NMR spectra provide direct evidence for the formation of a highly condensed siloxane network with organic group covalently bonded to the mesoporous silica and also revealed that both synthesis process and surfactant-extraction treatment did not cause cleavage of the Si–C bonds.

2.3.1.6. Vanadium (^{51}V) NMR spectroscopy

The catalytic activity of neat V(IV)O-Sal-Indanol complex was monitored by using liquid state ^{51}V NMR spectroscopy (Fig. 2.6), recorded at $-10\text{ }^\circ\text{C}$, by withdrawing aliquots of sample at suitable intervals. In liquid state ^{51}V NMR spectroscopy, the sample at 4 h (Fig. 2.6a), showed peaks in the range of -500 to -600 ppm, attributed to the peroxo complexes of vanadium (V) containing chiral ligand (Sal-Indanol ligand), which is the active species for asymmetric sulfoxidation reaction. After the completion of reaction (Fig. 2.6b), at 10 h, the peaks in the range of -500 to -600 ppm disappeared due to the colloidal precipitation of V(V) species which can either be NMR-silent or produce broad/weak NMR signals.³⁵ Further, oxidation state of heterogeneous complex, V(IV)O-Sal-Ind-SBA-15, was determined by using solid state ^{51}V NMR spectroscopy. V(IV)O-Sal-Ind-SBA-15 does not show solid state ^{51}V NMR spectroscopy due to the presence of paramagnetic nature of V(IV)O complexes.

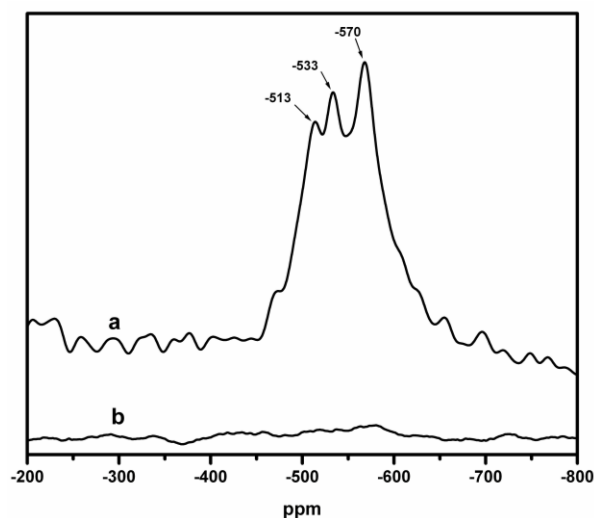


Fig. 2.6: Liquid state ^{51}V NMR spectra of neat V(IV)O-Sal-Indanol complex for sulfoxidation reaction (a) after 4 h (b) after completion of the reaction, i.e 10 h.

2.3.1.7. Electron Paramagnetic Resonance spectroscopy (EPR)

The EPR spectra of V(IV)O-Sal-Ind-SBA-15 (Fig. 2.7) is recorded at room temperature with frequency (9.716 GHz) and it provides the information about the oxidation state and coordination environment of metal in complexes. The V(IV)O-Sal-Ind-SBA-15 exhibits eight-line hyperfine patterns due to the interaction of the unpaired electron (V^{4+} , $3d^1$) with the nuclear spin of

vanadium nuclei ($I = 7/2$).³⁶ The EPR parameters, g and A values,³⁷ are sensitive to the vanadium coordination environment and it may be used to distinguish species with different ligation. V(IV)O-Sal-Ind-SBA-15 displays well resolved axial spectra with ^{51}V hyperfine structure having $g_{\parallel} \sim 1.929$ ($A_{\parallel} \sim 181\text{G}$) and $g_{\perp} \sim 1.966$ ($A_{\perp} \sim 80\text{G}$). The A_{\parallel} value (181G) helps to assume the donor group set like a phenolate oxygen, an imine nitrogen, an indanol oxygen of a tridentate ligand and an oxygen of solvent which are coordinated to an oxovanadium (IV) species in V(IV)O-Sal-Ind-SBA-15 complex.³⁸ The $g_{\parallel} < g_{\perp}$ and $A_{\parallel} > A_{\perp}$ relationships for the V(IV)O-Sal-Ind-SBA-15 are consistent with suitable coordination environment (mentioned in above) around the vanadium (IV) centre with unpaired electron in the d_{xy} orbital.³⁹

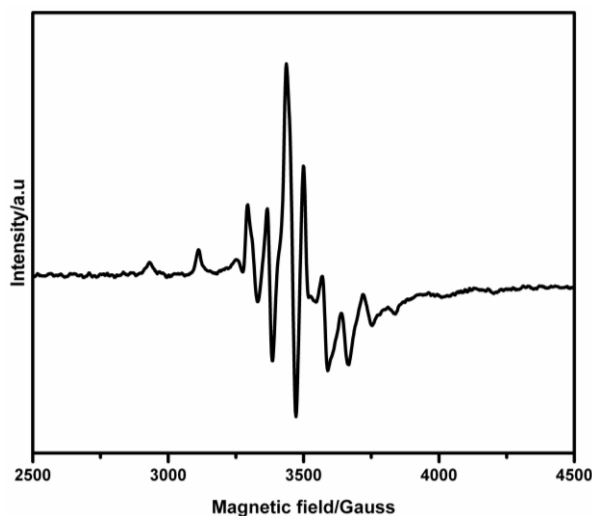


Fig. 2.7: EPR spectra of V(IV)O-Sal-Ind-SBA-15

2.3.1.8. DR UV-Visible spectroscopy (UV-Vis)

The DRS UV-Visible spectra of (a) SBA-15 (b) PrNH₂SBA-15 and (c) V(IV)O-Sal-Ind-SBA-15 are represented in Fig. 2.8. All the samples exhibit a particular peak at 220 nm, typical for siliceous materials. In V(IV)O-Sal-Ind-SBA-15, the broad band between 250–330 nm (Fig. 2.8c) is assigned to a ligand to metal charge transfer (LMCT) transition for V(IV) species. Further, a sensitive weak band at 690 nm (Fig. 2.8c) is attributed to d-d transition of V(IV) species which occurred in visible region.⁴⁰

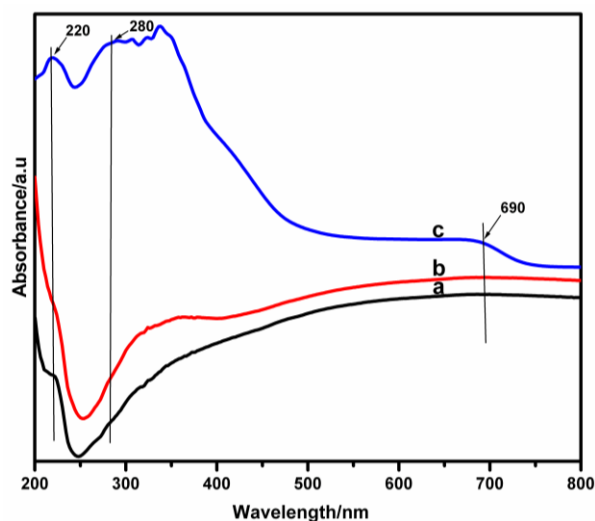


Fig. 2.8: DR UV-Vis spectra of (a) SBA-15 (b) Capped PrNH₂SBA-15 (c) V(IV)O-Sal-Ind-SBA-15.

2.3.1.9. X-ray Photoelectron spectroscopy (XPS)

The XPS Spectra of V2p core level of V(IV)O-Sal-Ind-SBA-15 are represented in Fig. 2.9. V(IV)O-Sal-Ind-SBA-15 shows peaks at 517.5 and 523.4 eV correspond to V2p_{3/2} and V2p_{1/2} spin orbit component. These binding energies correspond to a V(IV) species and showed the unchanged oxidation state of the metal ion even after anchoring with the heterogenized Sal-Indanol ligand. The correction of binding energy was performed by using the C1s peak of carbon at 284.9 eV as reference. The results confirm the successful anchoring of V(IV)O-Sal-Indanol complex over SBA-15.

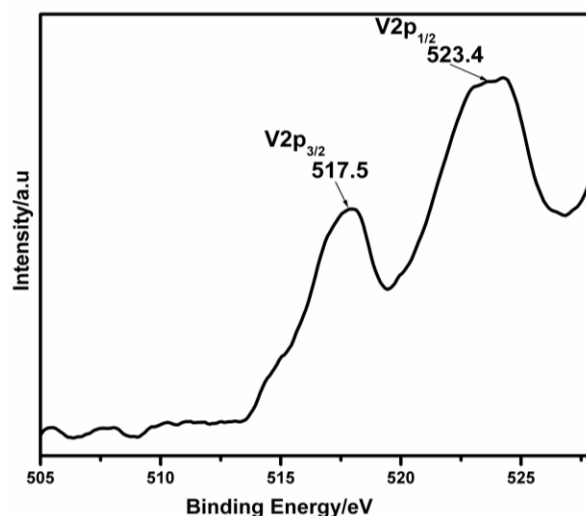


Fig. 2.9: XPS spectra of V2p core level of V(IV)O-Sal-Ind-SBA-15.

2.3.1.10. Scanning Electron Microscopy (SEM)

The SEM Images of A) SBA-15 and B) V(IV)O-Sal-Ind-SBA-15 are shown in Fig. 2.10. Both materials exhibit hexagonal type plate like structure which is retained in V(IV)O-Sal-Ind-SBA-15 catalyst even after heterogenization process.

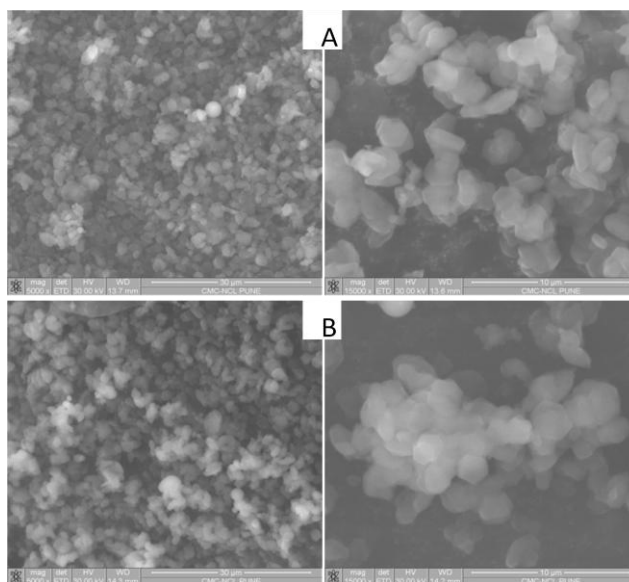


Fig. 2.10: SEM images of (A) SBA-15 and (B) V(IV)O-Sal-Ind-SBA-15

2.3.1.11. Transmission Electron Microscopy (TEM)

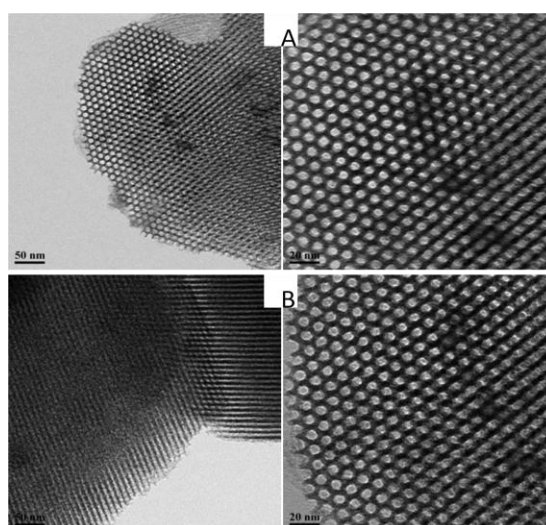


Fig. 2.11: TEM images of (A) SBA-15 and (B) V(IV)O-Sal-Ind-SBA-15

The TEM images (Fig. 2.11) of A) SBA-15 and B) V(IV)O-Sal-Ind-SBA-15 reveals the formation of a regular hexagonal array of uniform channels having long-range order and the formation of well defined 1-D channels.

2.3.2. Activity of catalysts

In order to elucidate the catalytic activity and enantioselectivity of the synthesized catalysts, the asymmetric sulfoxidation reaction of sulfides (thioanisole, 4-chloro-, 4-bromo thioanisole) have been performed using H₂O₂ as an oxidant at 0 °C. The results obtained from the sulfoxidation reaction of thioanisole, 4-chloro-, 4-bromo thioanisole over SBA-15, -OH protected PrNH₂SBA-15, neat V(IV)O-Sal-Indanol complex as well as V(IV)O-Sal-Ind-SBA-15 are presented in Table 2.2 and compared with uncatalysed reaction.

Table 2.2: Effect of different catalysts & substrates for asymmetric sulfoxidation^a reaction

Sample	Thioanisole			4-Chlorothioanisole			4-Bromothioanisole		
	Con ^b %	Sele. ^b %	e.e ^c %(R)	Con ^b %	Sele. ^b %	e.e ^c %(R)	Con ^b %	Sele. ^b %	e.e ^c %(R)
Without Catalyst	10.3	90	–	10.0	89	–	10.5	90	–
SBA-15	11.5	89	–	11.3	90	–	11.7	91	–
PrNH ₂ SBA-15	12.5	90	–	12.3	90	–	12.8	90	–
Neat V ^{IV} O-Sal-Indanol complex	84.0	94	34	85.0	96	33	86.0	95	32
V ^{IV} O-Sal-Ind-SBA-15	86.0	93	33	87.7	95	32	87.4	94	30

a) Reaction conditions: SBA-15 or PrNH₂SBA-15 or V(IV)O-Sal-Ind-SBA-15: 50 mg; Neat V(IV)O-Sal-Indanol complex: 25 mg; Thioanisoles: 2 mmol ; 30% H₂O₂ : 2.2 mmol ; CH₂Cl₂ : 5 ml; Reaction temperature: 0 °C; Reaction time: 8 h; b) Conversion (Con.) of sulfides and Selectivity (Sele.) of sulfoxides monitored by GC method; c) Optical rotation determined by Polarimeter and comparing with literature values.⁴²

As it can be observed in Table 2.2, V(IV)O-Sal-Ind-SBA-15 complex gives better conversion of all substrates (86 %–88 %) and comparative enantioselectivity [e.e, 30–33% (R)] than the neat V(IV)O-Sal-Indanol complex [84–86%, 32–34% e.e (R)]. V(IV)O-Sal-Ind-SBA-15 and neat V(IV)O-Sal-Indanol complex exhibit sulfoxide selectivity between 92% and 96% which is

greater than SBA-15, –OH protected PrNH₂SBA-15 and uncatalysed reaction (~90%). Further, the catalytic activity of without catalyst, SBA-15 and –OH protected PrNH₂SBA-15 were negligible (10–13 %) and shows no enantioselectivity. Hence, the catalytic activity is entirely attributed to the complex immobilized on SBA-15.

The conversion and enantioselectivity of thioanisole (model substrate) as a function of reaction temperature and polar solvents (CH₂Cl₂, CH₃COCH₃, EtOAc) over V(IV)O-Sal-Ind-SBA-15 are given in Table 2.3. The effect of reaction temperature on asymmetric sulfoxidation reaction in the temperature range -10 °C to 20°C using H₂O₂ as an oxidant and CH₂Cl₂ as a solvent were studied. In the case of V(IV)O-Sal-Ind-SBA-15, asymmetric sulfoxidation of thioanisole at -10 °C, 0 °C and 20 °C showed 70%, 79% and 89% conversion and corresponding e.e was found to be 25%, 31% and 28%, respectively, at 6 h.⁴¹ However, the selectivity for phenyl methyl sulfoxide remains nearly unchanged with the increase in reaction temperature. Further, the influence of solvents on thioanisole oxidation is depicted in Table 2.3.

Table 2.3: Influence of solvents & temperatures for asymmetric sulfoxidation^a reaction

Temp. (°C)	Solvents	Con. ^b (%)	Sele. ^b (%)	e.e ^c (%) (R)
0	EtOAc	85	87	17
0	CH ₃ COCH ₃	84	88	21
0	CH ₂ Cl ₂	79	91	31
20	CH ₂ Cl ₂	89	92	28
-10	CH ₂ Cl ₂	70	92	25

a) Reaction conditions: V(IV)O-Sal-Ind-SBA-15: 50 mg; Thioanisole: 2 mmol, 248.4 mg; 30% H₂O₂ : 2.2 mmol, 248.9 mg; CH₂Cl₂ : 5 ml, Reaction time : 6 h; b) Conversion (Con.) of sulfides and Selectivity (Sele.) of sulfoxides monitored by GC method.; c) Optical rotation determined by Polarimeter and comparing with literature values.⁴²

The oxidation of thioanisole in CH₃COCH₃ and EtOAc exhibited 84% and 85% conversion and corresponding e.e was found to be 21% and 17%, respectively. The weak polar solvent (CH₂Cl₂) only afforded relatively lower conversion (79%) than other polar solvents (CH₃COCH₃, EtOAc) with moderate enantioselectivity (31% R). In general, among all solvents, CH₂Cl₂ act as an efficient solvent for asymmetric sulfoxidation reaction. The higher catalytic activity observed in V(IV)O-Sal-Ind-SBA-15 may be due to easy access of the substrate molecules to the active sites of the complex in mesoporous channels.

2.3.3. Recyclability of catalysts

The stability and activity of V(IV)O-Sal-Ind-SBA-15 complex was tested four times (fresh + three cycles) in asymmetric sulfoxidation reaction (Fig. 2.12). The results show that the conversion of sulfide get slightly decreased after first recycle (2 %) and selectivity of products (including enantioselectivity) remained nearly the same (~90%). The ICP-OES analysis of the used catalyst after second recycle showed comparative loss of conversion (5 %) than first recycle which is attributed to the stability of the catalysts even after recycling. But, after third cycle, 9% loss of conversion was occurred from second cycle that may be due to the higher leaching of vanadium metal from V(IV)O-Sal-Ind-SBA-15 complex.

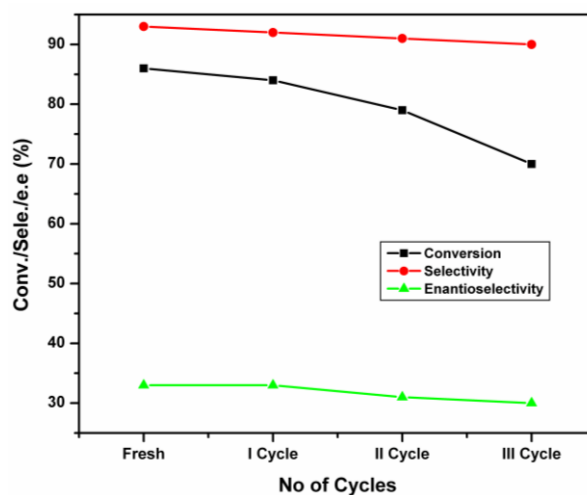


Fig. 2.12: Recycling Studies of V(IV)O-Sal-Ind-SBA-15 catalyst

2.4. Conclusions

A highly reactive and recyclable heterogeneous catalytic system was developed by immobilizing asymmetric (1R,2S)-(+)-1-[N-(3-tertbutyl-5-chloromethylsalicylidene)amino]-2-indanol (Sal-Indanol) ligand over mesoporous -OH protected amino functionalized SBA-15 with further complexation of V(IV)O(acac)₂ to attain V(IV)O-Sal-Ind-SBA-15. The powder X-ray diffraction, TEM and N₂-adsorption desorption analysis of the catalyst confirmed the structural integrity of the mesoporous hosts and the spectroscopic characterization techniques (FTIR, ¹³C & ²⁹Si MAS-NMR) proved the successful anchoring of the metal complex over the modified mesoporous support. In addition, the oxidation state and coordination environment of vanadium metal in V(IV)O-Sal-Ind-SBA-15 complex were confirmed by XPS, EPR, ⁵¹V NMR and DR

UV–Visible techniques. In order to deduce the optimum reaction conditions for asymmetric sulfoxidation reaction, the influence of different temperatures (-10 °C, 0 °C & 20 °C) and solvents (CH₂Cl₂, CH₃COCH₃ and EtOAc) were examined. The results show that CH₂Cl₂ act as an efficient solvent and the temperature at 0 °C provides slightly higher e.e than other temperatures. V(IV)O-Sal-Ind-SBA-15 showed comparative enantioselectivity [30–33% (R)], selectivity (>93%) and slightly higher catalytic conversion of thioanisoles (86–88 %) compared with SBA-15, PrNH₂SBA-15, neat V(IV)O-Sal-Indanol complex and without catalyst. Moreover, recycling study of V(IV)O-Sal-Ind-SBA-15 shows no major deactivation of the catalyst.

2.5. References

1. M. Beller, C. Bolm, *Transition metals for organic synthesis*, Wiley-VCH, Weinheim, 1998, 1.
2. C. Bolm, *Coord. Chem. Rev.*, 2003, **237**, 245.
3. a) T. Katsuki, *Coord. Chem. Rev.*, 1995, **140**, 189; b) K. Matsumoto, T. Yamaguchi, T. Katsuki, *Chem. Commun.*, 2008, 1704.
4. C. Bolm, F. Bienewald, *Angew. Chem. Int. Ed.*, 1995, **34**, 2640.
5. C. Kokubo, T. Katuski, *Tetrahedron*, 1996, **52**, 13895.
6. M. De Rosa, M. Lamberti, C. Pellecchia, A. Scettri, R. Villano, A. Soriente, *Tetrahedron Lett.*, 2006, **47**, 7233.
7. a) M. Al-Hashimi, E. Fisset, A. C. Sullivan, J. R. H. Wilson, *Tetrahedron Lett.*, 2006, **47**, 8017; b) M. R. Maurya, A. K. Chandrakar, S. Chand, *J. Mol. Catal. A: Chem.*, 2007, **263**, 227.
8. a) J. Legros, C. Bolm, *Chem. Eur. J.*, 2005, **11**, 1086; b) J. Legros, C. Bolm, *Angew. Chem. Int. Ed.*, 2004, **43**, 4225.
9. a) F. Hosseinpoor, H. Golchoubian, *Tetrahedron Lett.*, 2006, **47**, 5195; b) J. Brinksma, R. La Crois, B. L. Feringa, M. I. Donnoli, C. Rosini, *Tetrahedron Lett.*, 2001, **42**, 4049.
10. R. Liu, L.-Z. Wu, X.-M. Feng, Z. Zhang, Y.-Z. Li, Z.-l. Wang, *Inorg. Chim. Acta.*, 2007, **360**, 656.
11. a) N. N. Mahamuni, P. R. Gogate, A. B. Pandit, *Ultrasonics Sonochem.*, 2007, **14**, 135; b) B. Karimi, M. Ghoreishi-Nezhad, J. H. Clark, *Org. Lett.*, 2005, **7**, 625.

12. A. Scarso, G. Strukul, *Adv. Synth. Catal.*, 2005, **347**, 1227.
13. M.-Y. Chen, L. N. Patkar, C-L. Lin, *J. Org. Chem.*, 2004, **69**, 2884.
14. T. Miyazaki, T. Katsuki, *Synlett*, 2003, 1046.
15. M. L. Kantam, B. V. Prakash, B. Bharathi, , C. V. Reddy, *J. Mol. Catal. A: Chem.*, 2005, **226**, 119.
16. a) M. Bonchio, G. Licini, F. Di Furia, S. Mantovani, G. Modena, W. A. Nugent, *J. Org. Chem.*, 1999, **64**, 1326; b) G. Licini, M. Bonchio, G. Modena, W. A. Nugent, *Pure Appl. Chem.*, 1999, **71**, 463.
17. a) M. Bonchio, T. Carofiglio, F. Di Furia, R. Fornasier, *J. Org. Chem.*, 1995, **60**, 5986; b) A. Basak, A. U. Barlan, H. Yamamoto, *Tetrahedron: Asymmetry*, 2006, **17**, 508.
18. K. Matsumoto, T. Yamaguchi, J. Fujisaki, B. Saito, T. Katsuki, *Chem. Asian J.*, 2008, **3**, 351.
19. K. Nakajima, M. Kojima, J. Fujita, *Chem. Lett.*, 1986, 1483.
20. H. Vetter, A. Berkessel, *Tetrahedron Lett.*, 1998, **39**, 1741.
21. C. Ohta, H. Shimizu, A. Kondo, T. Katsuki, *Synlett*, 2002, 161.
22. R. Pelotier, M. S. Anson, I. B. Campbell, S. J. F. Macdonald, G. Priem, R. F. W. Jackson, *Synlett*, 2002, 1055.
23. Y. C. Jeong, S. Choi, Y. D. Hwang, K. H. Ahn, *Tetrahedron Lett.*, 2004, **45**, 9249.
24. D. A. Cogan, G. Liu, K. Kim, B. J. Backes, J. A. Ellman *J. Am. Chem. Soc.*, 1998, **120**, 8011.
25. D. Zhao, J. Feng, Q. Huo, N. Melosh, G. H. Fredrickson, B. F. Chmelka, G. D. Stucky, *Science*, 1998, **279**, 548.
26. A. Barbarini, R. Maggi, M. Muratori, G. Sartori, R. Sartorio, *Tetrahedron Asymmetry*, 2004, **15**, 2467.
27. Minutolo, F. Pini, D. A. Petri, P. Salvadori, *Tetrahedron Asymmetry*, 1996, **7**, 2293.
28. M. Jia, A. Seifert, W. R. Thiel, *Chem. Mater.*, 2003, **15**, 2174.
29. a) C. J. Carrano, C. M. Nunn, R. Quen, J. A. Bonadies, V. L. Pecoraro, *Inorg. Chem.*, 1990, **29**, 944; b) P. Adão, M. L. Kuznetsov, S. Barroso, A. M. Martins, F. Avecilla, J. C. Pessoa, *Inorg. Chem.*, 2012, **51**, 11430.
30. Y. C. Jeong, S. Choi, Y. D. Hwang, K. H. Ahn, *Tetrahedron: Asymmetry*, 2005, **16**, 3497.

31. D. Zhao, Q. Huo, J. Feng, B. F. Chmelka, G. D. Stucky, *J. Am. Chem. Soc.*, 1998, **120**, 6024.
32. S. Shylesh, S. P. Mirajkar, A. P. Singh, *J. Mol. Catal. A. Chem.*, 2005, **239**, 57.
33. R. Ryoo, I.-S. Park, S. Jun, C. W. Lee, M. Kruk, M. Jaroniec, *J. Am. Chem. Soc.*, 2001, **123**, 1650.
34. X. S. Zhao, G. Q. Lu, *J. Phys. Chem. B.*, 1998, **102**, 1556.
35. a) N. N. Karpyshev, O. D. Yakovleva, E. P. Talsi, K. P. Bryliakov, O. V. Tolstikova, A. G. Tolstikov, *J. Mol. Catal. A: Chem.*, 2000, **157**, 91; b) X. Lu, *Electrochimica Acta*, 2001, **46**, 4281.
36. C. Yuan, L. Lu, X. Gao, Y. Wu, M. Guo, Y. Li, X. Fu, M. Zhu., *J. Biol. Inorg. Chem.*, 2009, **14**, 841.
37. R. Ando, T. Yagyu, M. Maeda, *Inorg. Chim. Acta*, 2004, **357**, 2237
38. T. S. Smith, R. LoBrutto, V. L. Pecoraro, *Coord. Chem. Rev.*, 2002, **228**, 1-18.
39. T. Ghosh, C. Bandyopadhyay, *Transition Metal Chemistry*, 2004, **29**, 444.
40. M. R. Maurya, S. Khurana, W. Zhang, D. Rehder, *Eur. J. Inorg. Chem.*, 2002, 1749.
41. C. Ohta, H. Shimizu, A. Kondu, T. Katsuki, *Synlett*, 2002, 161.
42. J. M. Brunel, P. Diter, M. Duetsch, H. B. Kangan, *J. Org. Chem.*, 1995, **60**, 8086.

Chapter 3

Mo(VI)O₂-Organofunctionalized SBA-15 for Epoxidation and Sulfoxidation Reactions

[Anish Lazar](#), W. R.Thiel and A. P. Singh*
RSC Advances 4 (27) (2014) 14063-14073

3.1. Introduction

Catalytic oxidations, especially olefin epoxidation¹ and sulfoxidation² reactions, using transition metal complexes,^{3,4} are considered to be among the most eco-friendly, most important reactions in industrial chemistry. Oxidation catalysis has played a leading role in this era due to the production of huge quantities of intermediates and monomers for industrial chemistry. Epoxides are versatile precursors in the synthesis of a variety of compounds such as resins, cosmetics, surface coatings, sweeteners, perfumes, drugs, etc. and sulfoxides are well known valuable building blocks to produce biologically important compounds.^{5,6} Schiff-bases^{7,8} represent one of the most widely utilized classes of ligands in inorganic chemistry, which are capable to bind various metal ions to give complexes with tunable properties. They are also used as ligands in industrial chemistry due to the following facts: (i) there are simple synthetic methods for preparation in large scale (ii) they provide several binding sites for metals and can be designed to leave vacant sites for coordination of substrates (iii) the substitution on the aromatic ring allows a fine-tuning of their properties.

In recent years, the design and synthesis of catalytically active supported metal complexes has received increasing attention due to the some disadvantages of homogeneous systems compared to heterogeneous catalysts. In the case of molybdenum based catalysts⁹⁻¹¹ derived from Schiff-base ligands, cis-dioxomolybdenum species have been particularly investigated because of their good catalytic activity for the selective oxidation of cycloalkenes and sulfides. A variety of Schiff-base ligands such as bidentate-N-donor ligands (bipyridines,¹² diazabutadienes¹³ and pyrazolylpyridines¹⁴) and tetradentate-N-ligands^{15,16} (Salpr) have been used to improve the catalytic activity of these reactions with suitable peroxides. Environmentally benign, safer and economically favorable oxidants such as tert-butyl hydroperoxide (TBHP) and hydrogen peroxide (H₂O₂)¹⁷⁻¹⁹ have been used for epoxidation and sulfoxidation reaction with such systems. Out of these ligands, the tetradentate-N-donor ligand, ‘Salpr’ {3-[N,N-bis-3-(salicylidenamino)ethyl]triamine} was used as the ligand for epoxidation and sulfoxidation reactions due to its high chelating ability with molybdenum complexes.²⁰ To avoid the well known limitations from the homogeneous complexes such as poor recyclability, catalyst contamination in the products, etc., supported complexes of catalytically active metals have been synthesized during the recent years. Mesoporous SBA-15²¹ shows significant attraction in this context due to its high surface area, its uniform pore sizes, its high wall thickness and its high

hydrothermal stability compared to other mesoporous materials like MCM-41, MCM-48. To extend the applicability of SBA-15 materials, it is necessary to modify the surface by organic functional groups for anchoring metals and metal complexes.

The stability and selectivity of catalysts in epoxidation and sulfoxidation reactions were challenging tasks in the last decades. To overcome this limitations, SBA-15 was used as the support to immobilize of neat (L)Mo(VI)O₂ complex than other mesoporous materials, due to its higher wall thickness.^{22,23} Further, chelation of molybdenum with Schiff base ligand, Mo(VI)O₂-3-[N,N-bis-3(salicylidenamino)ethyltriamine] complex, over SBA-15 provides extra stability to the homogeneous complexes. In this work, we report, the synthesis, characterization and catalytic applications of highly stable (L)Mo(VI)O₂@SBA-15 for efficient heterogeneous epoxidation and sulfoxidation reactions. The catalyst is recyclable and exhibits high catalytic activities.

3.2. Experimental

3.2.1. Materials

Tetraethylorthosilicate (TEOS), Pluronic 123 (P123, average molecular weight: 5800), 3,5-di-tertbutyl-2-hydroxybenzaldehyde, 3-chloropropyltrimethoxysilane (3-CPTMS), dimethoxy dimethylsilane [(MeO)₂Me₂Si], cyclohexene, cyclooctene, cyclohexene oxide, cyclooctene oxide and sulfides were purchased from Aldrich. Diethylene triamine and HCl (36.5%) were purchased from Merck and Thomas Baker (India), respectively. Dry reagent grade solvents were obtained from Merck (India) and further dried before use according to standard methods.

3.2.2. Synthesis of –OH protected PrCl@SBA-15

The highly stable and reusable heterogeneous complex, (L)Mo(VI)O₂@SBA-15 was synthesized under a nitrogen atmosphere in a step-by-step manner (Scheme 3.1). The synthesis of mesoporous SBA-15²⁴ was carried out hydrothermally under the autogeneous pressure in an autoclave and detailed procedure mentioned in experimental part of Chapter 2 (Page No: 30). Surface modification of SBA-15 was achieved by a post synthesis grafting method [Scheme 3.1(b)]. One gram of SBA-15 was suspended in 50 ml of dry toluene and then heated to reflux together with 3.7 mmol of 3-chloropropyltrimethoxysilane (3-CPTMS) for 8 h under a N₂ atmosphere. The material was filtered after cooling to ambient temperature, washed with dry

toluene and then with dichloromethane. Soxhlet extraction was carried out for 24 h with dichloromethane (CH₂Cl₂) as the solvent to remove occluded organosilane. The sample was then dried in vacuum for 10 h. The material obtained is designated as PrCl@SBA-15 [Scheme 3.1(b)]. The free –OH groups still present in PrCl@SBA-15 were protected by adding 1.5 mmol of dimethoxydimethylsilane to a stirred suspension of 1 g of PrCl@SBA-15 in dry toluene (50 ml), followed by stirring for 12 h at reflux temperature under an inert atmosphere. The resulting material was filtered off, washed with toluene and was extracted in a Soxhlet with CH₂Cl₂ for 24 h. The obtained material was named as –OH protected PrCl@SBA-15 [Scheme 3.1(c)].

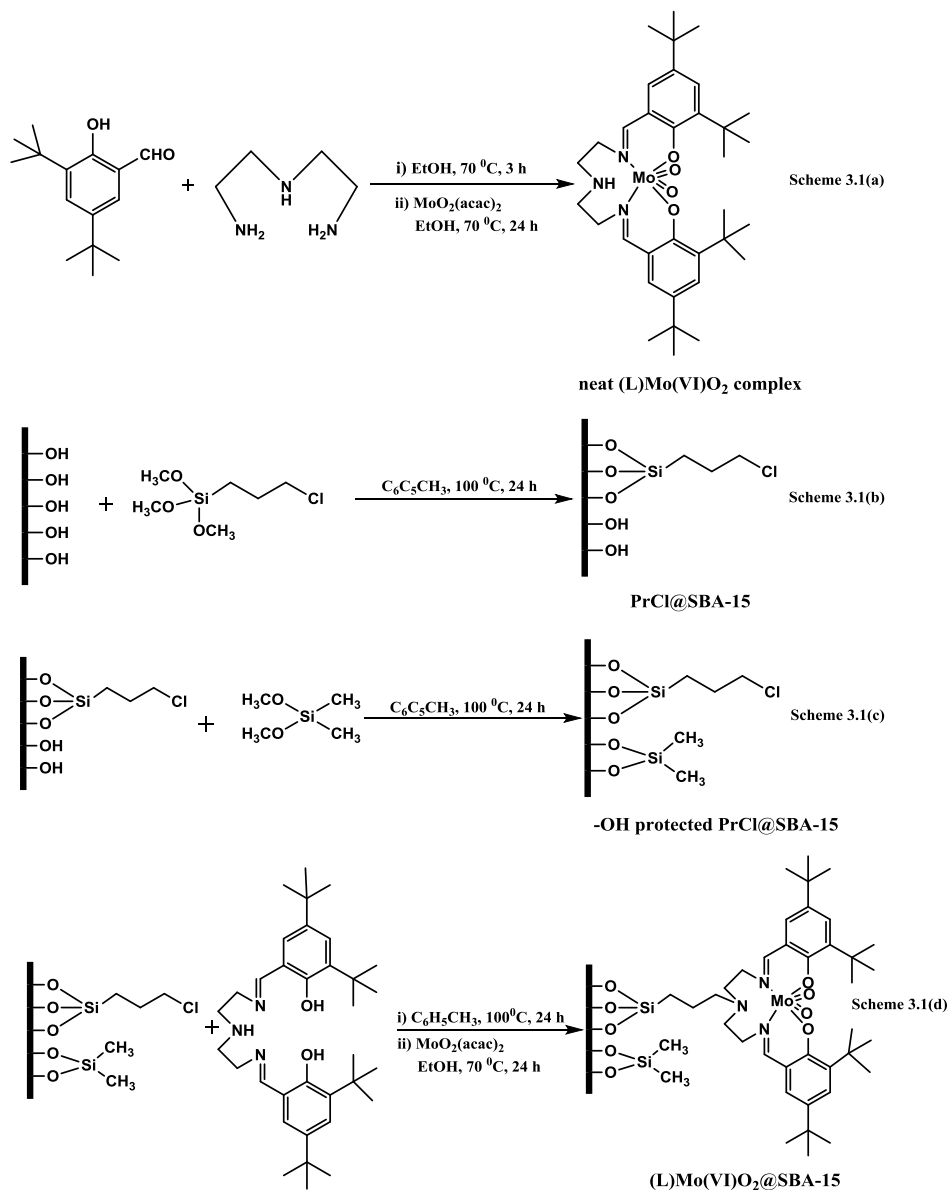
3.2.3. Synthesis of neat (L)Mo(VI)O₂ complex

The Salpr ligand, 3-[N,N'-bis-3(salicylidenamino)ethyltriamine], was prepared according to a reported procedure²⁵ [Scheme 3.1(a)]. Diethylenetriamine (0.5158 g, 5 mmol) was added into an ethanolic solution of 3,5-di-tertbutyl-2-hydroxybenzaldehyde (2.3433 g, 10 mmol) and the resulting yellow colored solution was heated to reflux for 3 h. After that, the excess of solvent was removed under vacuum and a dark yellow oily product was obtained after purification by column chromatography [silica column, hexane–ethyl acetate (9 : 1)]. 2 g (0.3732 mmol) of the Salpr ligand were dissolved in 30 ml of ethanol. This solution was added dropwise into an ethanolic solution of Mo(VI)O₂(acac)₂ (1.384 g in 120 ml) in a 250 ml two neck round bottom flask and the mixture was heated to reflux for 24 h. After filtration, the product was dried and then extracted in a Soxhlet apparatus with a mixture of dichloromethane and ethanol (1 : 1) to remove unreacted Mo(VI)O₂(acac)₂.

3.2.4. Synthesis of (L)Mo(VI)O₂@SBA-15

To a suspension of –OH protected PrCl@SBA-15 (1 g) in 30 ml of toluene, a solution of the Salpr ligand (L) (1.28 g, 0.0024 mol) in 10 ml of toluene was added, and then the mixture was heated to reflux for 24 h under an inert atmosphere. The resulting suspension was filtered, the residue was washed with toluene and CH₂Cl₂, and further purified extraction in a Soxhlet apparatus with a mixture of CH₂Cl₂ and diethylether (1 : 1) for 24 h. The final material was designated as 3-[N,N'-bis-3(salicylidenamino)ethyltriamine]@SBA-15 or (L)PrCl@SBA-15. For complexation, an excess of Mo(VI)O₂(acac)₂ (1 g, 3 mmol) in 100 ml ethanol was added into 2 g of dried (L)PrCl@SBA-15 and heated to reflux for 24 h to get (L)Mo(VI)O₂@SBA-15

[Scheme 3.1(d)]. After filtration, the product was dried and then extracted in a Soxhlet apparatus with a mixture of dichloromethane and ethanol (1 : 1) to remove unreacted Mo(VI)O₂(acac)₂.



Scheme 3.1: Preparation of Mo(VI)O₂-Organofunctionalized SBA-15 [(L)Mo(VI)O₂@SBA-15]; Synthesis of 3.1(a) neat [(L)Mo(VI)O₂ complex, 3.1(b) PrCl@SBA-15, 3.1(c) -OH protected PrCl@SBA-15 and 3.1(d) [(L)Mo(VI)O₂@SBA-15].

3.2.5. Procedure for catalytic reactions

The epoxidation of cycloalkenes such as cyclohexene and cyclooctene were carried out in a 50 ml double necked round bottom flask fitted with a water-cooled condenser and a magnetic stirrer

by using anhydrous TBHP as the oxidant. In a typical procedure, anhydrous TBHP (5.0–6.0 M in decane, 1.6 ml, 14.4 mmol) was added into a mixture of (L)Mo(VI)O₂@SBA-15 (150mg) or the neat (L)Mo(VI)O₂ complex (75 mg, 0.113 mmol) and 8 mmol of the appropriate cycloalkene in 25 ml of chloroform under a nitrogen atmosphere. The mixture was heated to reflux for 18 h.²⁵ Samples were withdrawn periodically and analyzed by using a Gas chromatograph (Agilent 6890) equipped with a capillary column (HP-5) and a flame ionization detector (FID).

A 25 ml of round bottom flask was loaded with 5 ml of a suspension responding solution of the appropriate catalysts [25 mg of (L)Mo(VI)O₂@SBA-15 or 10 mg (0.015 mmol) of the neat (L)Mo(VI)O₂ complex] in CH₃CN. To this reaction mixture, 1 mmol of the sulfides (thioanisoles) and 1.1 mmol of 30 % H₂O₂ were added at room temperature and stirring was continued for 3 h.²⁶ Samples were periodically withdrawn from the reaction mixture and filtered off, and analyzed with GC. Sulfide conversion (wt%) and selectivity (%) were determined by using a gas chromatograph (Agilent 6890) equipped with a flame ionization detector (FID) and a capillary column (HP-5).

3.3. Results and discussions

3.3.1. Characterizations

3.3.1.1. X-ray Diffraction (PXRD)

Figure 3.1 exhibits the XRD spectra of (a) as-synthesized SBA-15 (b) calcined SBA-15 (c) –OH protected PrCl@SBA-15 and (d) (L)Mo(VI)O₂@SBA-15. The parent SBA-15 shows three reflections at $2\theta = 0.9^\circ$, 1.5° and 1.7° , which are assigned to the (100), (110) and (200) Miller indices, respectively, indicating the formation of a highly ordered hexagonal structure.²⁷ In all synthesized samples, the (110) reflections are more intense than the (200) reflection, which favors a more complete condensation of the wall structure due to the high temperatures selected for the hydrothermal synthesis and the further calcination. The existence of the (100), (110) and (200) reflections (Fig. 3.1) provides a hint for a high structural stability of the material, the existence of a long range ordering and a large pore wall thickness even after a number of treatments with organic molecules. The peak intensities of the (100) reflections are decreasing with broadening from calcined SBA-15 to (L) Mo(VI)O₂@SBA-15 due to the proper loading of the organic modifier and the neat (L)Mo(VI)O₂ complex in the calcined SBA-15. Moreover, the decrease in signal intensity may be due to loss of regularity in the 2D hexagonal structure of

mesoporous SBA-15. The structural stability and ordered mesoporosity of the samples have retained after incorporation of (L)Mo(VI)O₂ complex in the SBA-15 support.

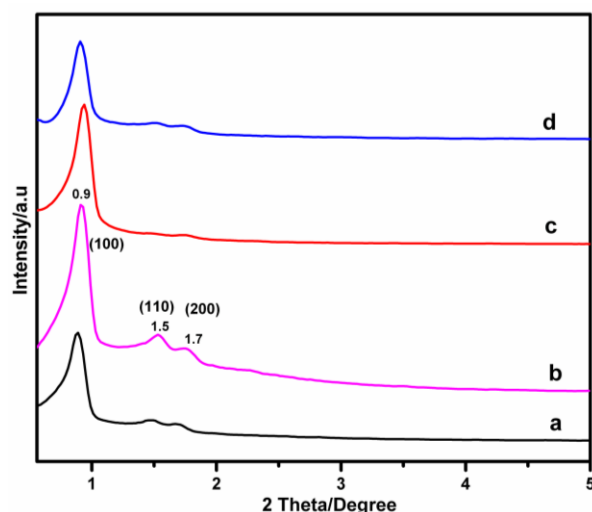


Fig. 3.1: XRD pattern of (a) as-synthesized SBA-15 (b) calcined SBA-15 (c) –OH protected PrCl@SBA-15 and (d) (L)Mo(VI)O₂@SBA-15.

3.3.1.2. N₂-Sorption analyses

The N₂ adsorption–desorption isotherms and pore size distributions (inset) of calcined SBA-15 and (L)Mo(VI)O₂@SBA-15 are shown in Fig. 3.2A and B, respectively. (L)Mo(VI)O₂@SBA-15 shows type-IV isotherms with a H1 hysteresis related to capillary condensation steps, a characteristic feature of the highly ordered mesoporous materials (pore size: 2–50 nm).²⁸ Textural properties of calcined SBA-15 and (L)Mo(VI)O₂@SBA-15 samples are summarized in Table 3.1. The mesoporous SBA-15 exhibits a BET surface area (601 m² g⁻¹), a pore volume (1.02 cm³ g⁻¹) and a mean pore diameter (66 Å°).

Table 3.1: Textural properties of calcined SBA-15 and (L)Mo(VI)O₂@SBA-15.

Sample	a ₀ [Å] ^a	S.A [m ² /g]	D _p [Å]	V _p [cc/g]	ω _t (Å) ^b
SBA-15	106	601	66	1.02	40
(L)Mo(VI)O ₂ @SBA-15	105	252	56	0.37	49

a₀=Unit cell parameter, S.A= BET Surface area, D_p= Pore diameter, V_p= Pore volume, ω_t= Wall Thickness; From ICP-OES analysis Mo≈0.18 mmol/g; ^a a₀=2d₁₀₀/1.73; ^b ω_t= a₀- D_p.

As shown in Table 3.1, compared to SBA-15, a further reduction of the surface area from 601 to 252 m² g⁻¹ and of the mean pore size from 66 to 56 Å was observed for (L)Mo(VI)O₂@SBA-15. The SBA-15 samples exhibit a sharp increase in the N₂ adsorption at a higher P/Po value (~0.65) indicating the uniformity of the mesoporous structure. In the case of (L)Mo(VI)O₂@SBA-15, the P/Po value changed to a lower value of ~0.6, indicative of a minor structural damage of the material after the modifications and being consistent with the XRD results. The significant decrease in surface area, in pore diameter and in pore volume of (L)Mo(VI)O₂@SBA-15 indicates the successful anchoring of organic modifier group and the further complexation with the molybdenum site occurring on SBA-15.

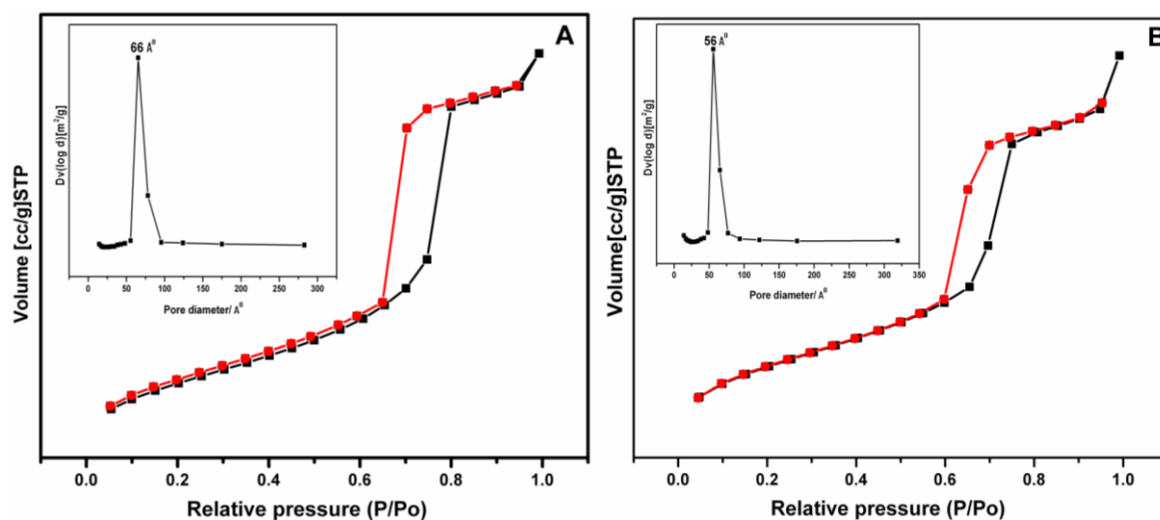


Fig. 3.2: N₂-isotherm and pore-size (inset) of (A) SBA-15 and (B) (L)Mo(VI)O₂@SBA-15

3.3.1.3. Thermal analyses (TG and DTA)

Thermal analysis is a technique for measuring changes in the physico-chemical properties of substances as a function of temperature. The thermal stability of (a) as-synthesized SBA-15 (b) calcined SBA-15 (c) –OH protected PrCl@SBA-15 (d) (L)Mo(VI)O₂@SBA-15 was determined by TGA (Fig. 3.3A) and DTA (Fig. 3.3B) in an atmosphere of air from 30 to 1000 °C with a temperature ramp of 10 °C min⁻¹. The TGA curve of the as-synthesized SBA-15 [Fig. 3.3A(a)] exhibits a 48% weight loss with a corresponding exothermic peak observed in the DTA analysis [Fig. 3.3B(a)] in the region of 170–220 °C which is assigned to the removal of surfactant from as-synthesized sample. Calcined SBA-15 [Fig. 3.3A(b)] shows only 13% weight loss from TG

curve with no other peak observed in DTA analysis [Fig. 3.3B(b)]. These evidences support the complete removal of the surfactants from the calcined SBA-15 and the successful formation of a pure siliceous SBA-15 material.

The TGA plot of $-OH$ protected $PrCl@SBA-15$ [Fig. 3.3A(c)] shows three distinct weight losses corresponding to exothermic peaks in the DTA [Fig. 3.3B(c)] (i) between 70 and 150 °C corresponding to physisorbed water molecules (ii) between 230 and 310 °C indicating the decomposition of the chloropropyl moiety from $PrCl@SBA-15$ (iii) between 330 and 450 °C representing the combustion of dimethoxydimethylsilane acting as the capping agent. In the case of $(L)Mo(VI)O_2@SBA-15$ [Fig. 3.3B(d)], one extra peak along with two peaks already observed in the $-OH$ protected $PrCl@SBA-15$, in the region of 450–510 °C is observed.²⁹ It confirms the high thermal stability of $(L)Mo(VI)O_2$ sites on SBA-15.

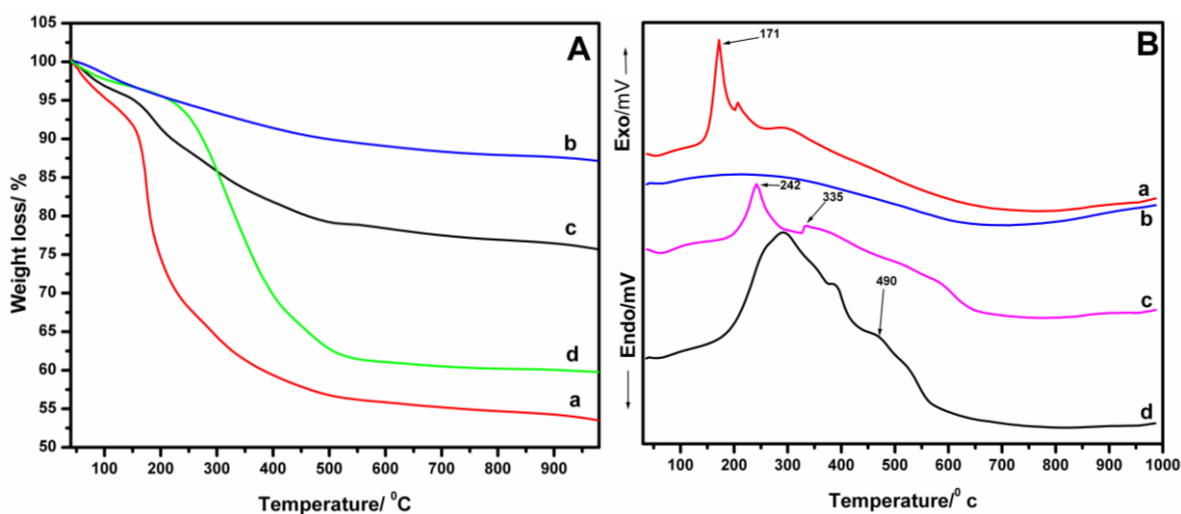


Fig. 3.3: TGA (A) and DTA (B) pattern of (a) as-synthesized SBA-15 (b) calcined SBA-15 (c) $-OH$ protected $PrCl@SBA-15$ and (d) $(L)Mo(VI)O_2@SBA-15$.

In some cases the weight loss between 530 and 570 °C arises due to an additional water loss by an ongoing condensation of residual silanol groups.³⁰ The TGA result of the $-OH$ protected $PrCl@SBA-15$ quantitatively shows 26% of weight loss, being greater than in the case of calcined SBA-15. This strongly supports the successful anchoring of 3-CPTMS on the calcined SBA-15. Further, $(L)Mo(VI)O_2@SBA-15$ shows 42% of weight loss, which is greater than the loss observed for the $-OH$ protected $PrCl@SBA-15$, strongly supporting a 16% loading of neat

(L)Mo(VI)O₂ sites in the calcined SBA-15. All these results support that the material was synthesized and the (L)Mo(VI)O₂ sites are directly anchored over the modified SBA-15.

3.3.1.4. Fourier Transform Infrared Spectroscopy (FT-IR)

Infrared spectroscopy helped to find out the nature of the surface functional groups being present in the materials and it is furthermore used for monitoring of the multistep assembly of the catalyst inside the mesoporous SBA-15 material. FT-IR spectra of (a) as-synthesized SBA-15 (b) calcined SBA-15 (c) –OH protected PrCl@SBA-15, (a) the neat (L)Mo(VI)O₂ complex and (b) (L)Mo(VI)O₂@SBA-15 are shown in Fig. 3.4A and B, respectively. In the spectrum of the as-synthesized SBA-15 [Fig. 3.4A(a)], peaks at 2980 cm⁻¹ and 2895 cm⁻¹ indicate the stretching vibrations of the –CH₂ groups being present in the surfactant molecules. In calcined SAB-15 [Fig. 3.4A(b)], a broad band at 3600–3200 cm⁻¹ and a weak band at 3738 cm⁻¹ are attributed to the ν-OH stretching vibrations of hydrogen bonded and isolated surface silanol groups being present in the host materials.^{31,32} Further, a sharp band at 1628 cm⁻¹ is corresponding to the –OH bending vibration of the silanol groups. Moreover, the absence of strong absorptions in calcined SBA-15 at 3000–2700 cm⁻¹ indicates the complete removal of surfactants.

After the chlorofunctionalization of the SBA-15 [Fig. 3.4A(c)], the peaks at 3738 cm⁻¹ and 3600–3400 cm⁻¹ had disappeared, indicating that the silanol groups on the surface of SBA-15 are transferred into a Si–O–Si framework. Further, peaks at 2980 cm⁻¹ and 2895 cm⁻¹ appeared being assigned to the stretching vibrations of the –CH₂ groups in propyl chain of the organic modifiers which evidently supports that the chloropropyl group is attached to the SBA-15. In both compounds, the neat (L)Mo(VI)O₂ complex [Fig. 3.4B(a)] and in (L)Mo(VI)O₂@SBA-15 [Fig. 3.4B(b)], peaks at 755 cm⁻¹ and 1420 cm⁻¹ are assigned to C–H bending and C=C stretching vibrations, respectively, of the arene groups. Moreover, a strong band at 1640 cm⁻¹ is assigned to the –C=N stretching vibration of the azomethylene group. Characteristic peaks at 940 cm⁻¹ and 910 cm⁻¹ are assigned to the symmetric and asymmetric vibrational modes of the *cis*-coordinated MoO₂ moiety of the neat (L)Mo(VI)O₂ complex, which are not observed for (L)Mo(VI)O₂@SBA-15 due to a overlapping of these peaks with ν(Si–OH) vibrations. The MoO₂ species prefers to form a *cis* configuration due to a maximized utilization of the dπ groups at molybdenum centre.³³ In all these samples, except the neat (L)Mo(VI)O₂ complex, the asymmetric and symmetric stretching vibrations of Si–O bonds in the Si–O–Si framework are

observed at 798 cm⁻¹ and 1080 cm⁻¹, respectively [Fig. 4A(a-c) and B(b)]. A strong band at 954 cm⁻¹ is attributed to the $\nu(\text{Si-OH})$ vibration,^{34,35} indicating the effective formation of siliceous materials.

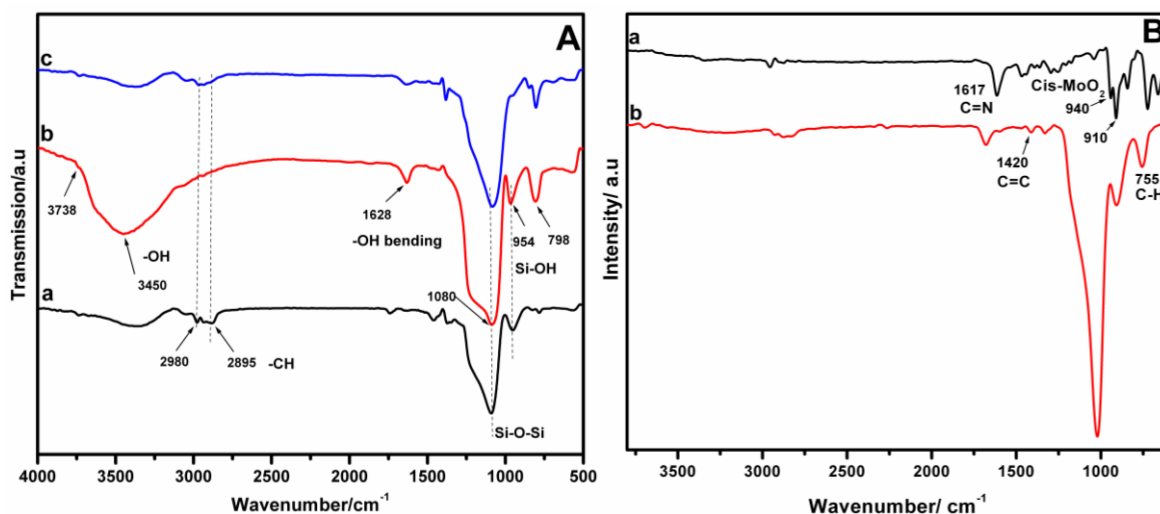


Fig. 3.4: FT-IR spectra of (A) [(a) as-synthesized SBA-15, (b) calcined SBA-15, (c) protected PrCl@SBA-15] and (B) [(a) the neat (L)Mo(VI)O₂ complex (b) (L)Mo(VI)O₂@SBA-15].

3.3.1.5. Raman Spectroscopy

In addition to this, the results of Raman spectroscopic investigations, being technique complementary to IR spectroscopy, of (a) the neat (L)Mo(VI)O₂ complex (b) (L)Mo(VI)O₂@SBA-15 are plotted in Fig. 3.5.

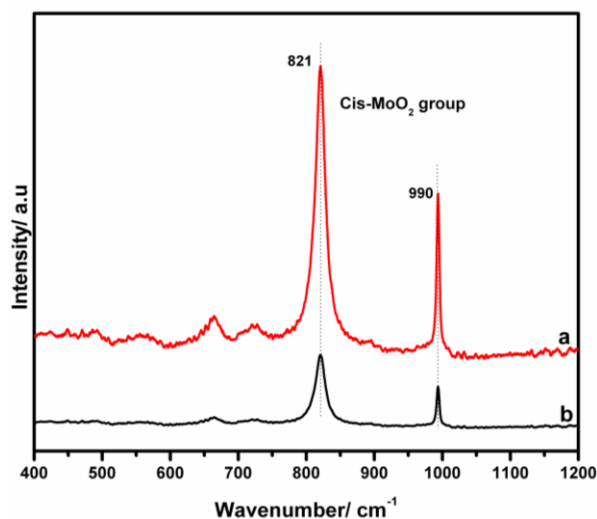


Fig. 3.5: Raman spectra of (a) the neat (L)Mo(VI)O₂ complex (b) (L)Mo(VI)O₂@SBA-15.

The characteristic peaks at 821 and 990 cm⁻¹, corresponds to asymmetric and symmetric stretching vibrations of the *cis*-coordinated MoO₂ moiety.³⁶ This indicates that the oxidation state of molybdenum is VI, which is though retained even after immobilization over SBA-15. Further, results obtained from the Raman spectra are in good agreement with the results of the IR spectroscopic investigations.

3.3.1.6. Solid state ¹³C NMR Spectroscopy (¹³C CP MAS NMR)

The ¹³C solid state NMR spectra of (A) PrCl@SBA-15 (B) –OH protected PrCl@SBA-15 and (C) (L)Mo(VI)O₂@SBA-15 are depicted in Fig. 3.6.

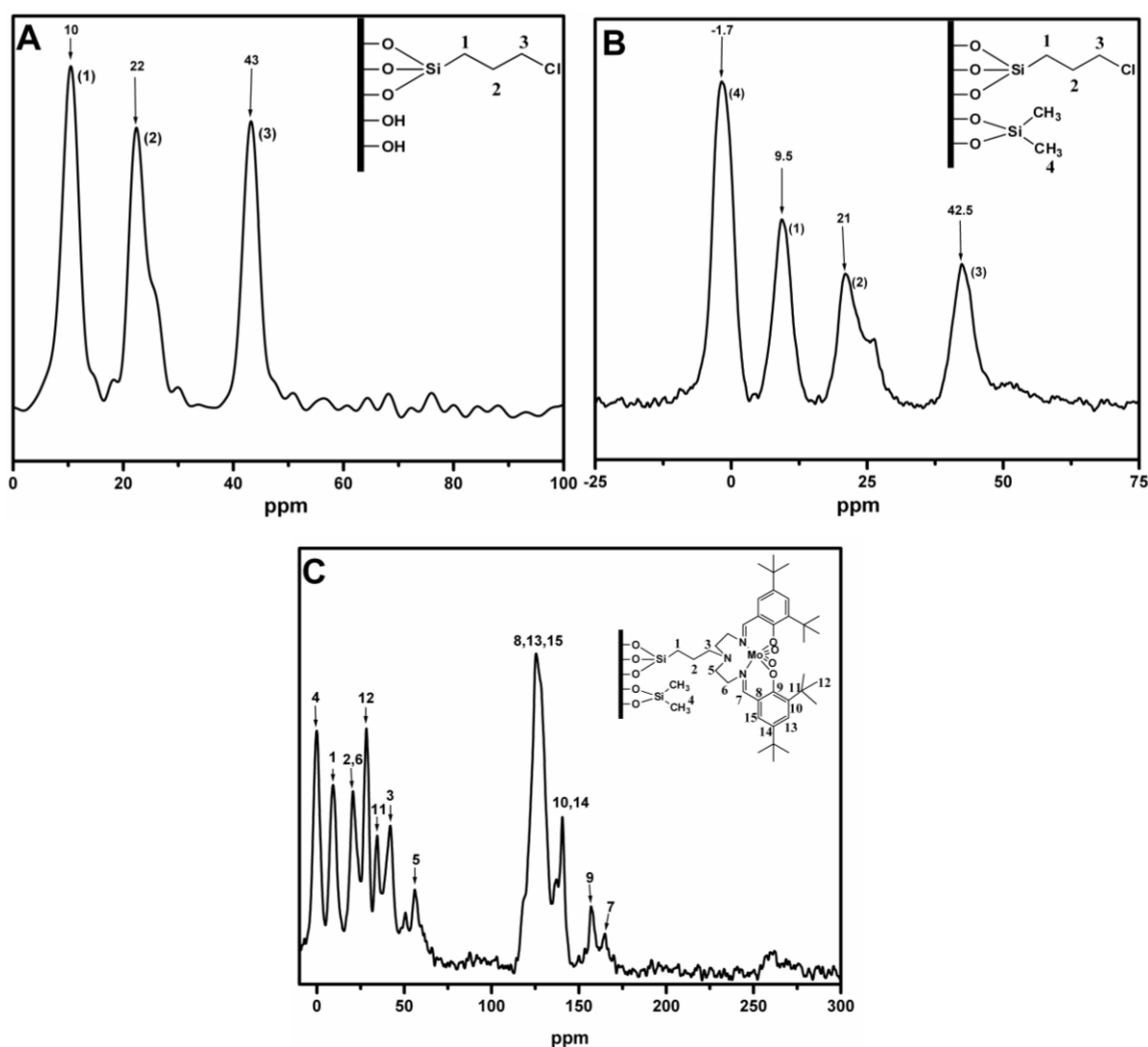


Fig. 3.6: Solid state ¹³C CP MAS NMR spectra of (A) PrCl@SBA-15, (B)-OH protected PrCl@SBA-15 (C) (L)Mo(VI)O₂@SBA-15.

The presence of peaks at 10, 22 and 43 ppm, assigned to the carbon atoms (C₁– C₃) of the propyl chain in organic modifier, indicates the successful chlorofunctionalization of SBA-15 (Fig. 3.6A). Additionally a sharp peak at -1.7 ppm (C₄) evidences the presence of –CH₃ groups as result of the capping of residual hydroxyl groups by dimethoxydimethylsilane in –OH protected SBA-15 (Fig. 3.6B). In the case of (L)Mo(VI)O₂@SBA-15 (Fig. 3.6C), resonances in the region between 110 and 150 ppm correspond to the aromatic moieties of the Salpr ligand. Moreover, in the region between 0 and 50 ppm, two extra resonances at 28 ppm and 34 ppm (Fig. 3.6C), represent the methyl carbon atoms of the tert-butyl groups. The small peak at 165 ppm is ascribed to the carbon atoms of the imine groups in (L)Mo(VI)O₂@SBA-15. Furthermore, one shoulder peak at 56 ppm is assigned to –CH₂ groups of diethylenetriamine being present in (L)Mo(VI)O₂@SBA-15. All the resonance peaks support the successful anchoring of the (L)Mo(VI)O₂ sites on SBA-15.

3.3.1.7. Solid state ²⁹Si NMR Spectroscopy (²⁹Si CP MAS NMR)

The degree of functionalization of surface silanol groups with organic moieties on the mesostructured materials can be monitored by means of ²⁹Si CP-MAS NMR spectroscopy. ²⁹Si CPMAS NMR spectra of (A) calcined SBA-15 (B) PrCl@SBA-15 (C) –OH protected PrCl@SBA-15 and (D) (L)Mo(VI)O₂@SBA-15 are depicted in Fig. 3.7. The spectrum of calcined SBA-15 (Fig. 3.7A) shows broad resonance peaks from -90 to -115 ppm, indicative for a range of Si–O–Si and Si–OH bonds. The bands centered at -93 ppm, -103 ppm and -113 ppm can be assigned to the Q² [geminal silanol, (SiO)₂Si(OH)₂], Q³ [single silanol, (SiO)₃Si(OH)] and Q⁴ [siloxane, (SiO)₄Si] sites of the silica framework, respectively.^{31,32} Compared to the parent SBA-15, PrCl@SBA-15 (Fig. 3.7B) shows a decrease in the Q³ and Q² intensities with a corresponding increase in the percentage of Q⁴ sites showing that the 3-CPTMS effectively consumes the geminal as well as the single silanol sites. The appearance of the Q³ signal indicates the presence of some residual non-condensed OH groups attached to the silicon atoms. After chlorofunctionalization (Fig. 3.7C), two additional peaks at -69 ppm and at -61 ppm were observed and assigned to T³ [SiR(OSi)₃] and T² [Si(OH)R(OSi)₂] units, respectively. The existence of the T³ signal confirms that SBA-15 has been modified by organic moieties. Further, a sharp peak at -22 ppm in the –OH protected PrCl@SBA-15 material indicates the Si atoms of the methoxydimethylsilyl units which are present as capping sites (Fig. 3.7C).

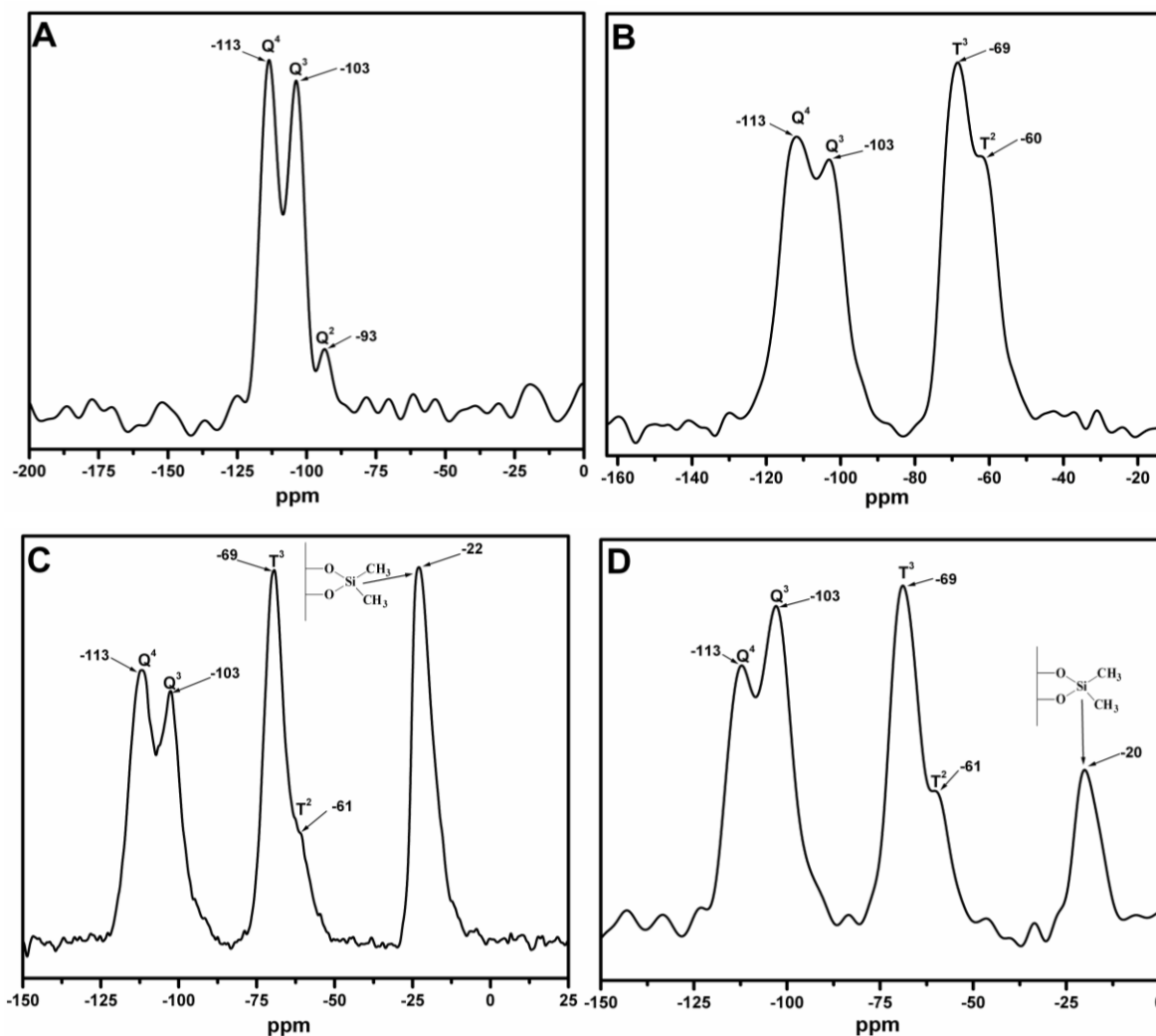


Fig. 3.7: Solid state ²⁹Si CP MAS NMR spectra of (A) calcined SBA-15 (B) PrCl@SBA-15, (C) -OH protected PrCl@SBA-15 and (D) (L)Mo(VI)O₂@SBA-15.

The $(Q^3 + Q^2)/Q^4$ ratio indicates the presence of silanol groups residing on the support surface, and a lower $(Q^3 + Q^2)/Q^4$ value for chlorofunctionalized samples suggests that the material contains fewer residual silanols. Changes in the relative intensities of the Q^4 , Q^3 and Q^2 signals can be explained by the redistribution of the silicon sites during the surface silylation. In the spectrum of (L)Mo(VI)O₂@SBA-15 (Fig. 7D), peak at -20 ppm decreases with an increase of the Q^3 sites compared to Q^4 indicating the removal of some capping units ongoing with a formation of free silanol groups under the drastic synthetic conditions (Fig. 3.7D). ²⁹Si CP-MAS NMR spectra provide direct evidence for the formation of a highly condensed siloxane network with

organic group covalently bound to the mesoporous silica and also revealed that both the synthesis process and surfactant extraction treatment did not cause cleavage of the Si–C bonds.

3.3.1.8. X-ray Photoelectron Spectroscopy (XPS)

XPS is a surface technique which helps us to find out the oxidation state and chemical environment of atoms due to the shift in binding energies. The XPS spectra of the Mo3d core level of (a) the neat (L)Mo(VI)O₂ complex and (b) (L)Mo(VI)O₂@SBA-15 are depicted in Fig. 3.8. The correction of the binding energies was performed by using the C1s peak of carbon at 284.9 eV as the reference. In the neat (L)Mo(VI)O₂ complex (Fig. 3.8a), peaks at 233 and 236 eV correspond to the 3d_{5/2} and 3d_{3/2} spin-orbit component, which are shifted to higher binding energy values (234 and 237, respectively) in the case of (L)Mo(VI)O₂@SBA-15 (Fig. 3.8b). These binding energies correspond to Mo(VI) species and prove the unchanged oxidation state of the metal ion even after heterogenization of the (L)Mo(VI)O₂ sites over SBA-15.

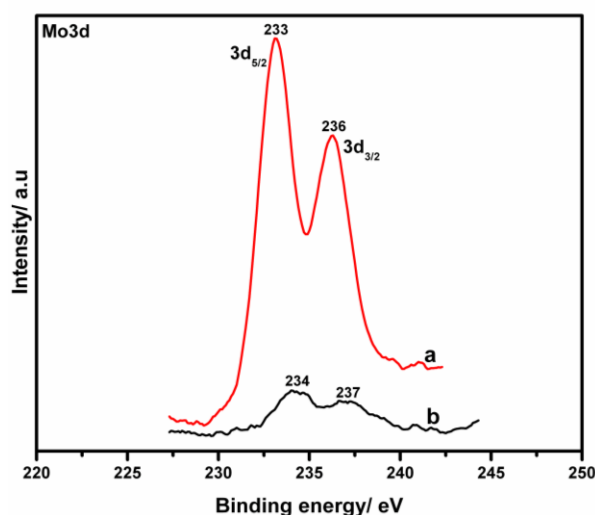


Fig. 3.8: XPS spectra of (a) the neat (L)Mo(VI)O₂ complex (b) (L)Mo(VI)O₂@SBA-15.

3.3.1.9. DR UV-Visible Spectroscopy (DR UV-Vis)

The DRS UV-Vis spectra of (a) calcined SBA-15 (b) the neat (L)Mo(VI)O₂ complex and (c) (L)Mo(VI)O₂@SBA-15 are presented in Fig. 3.9 to get further information about the coordination environment and the oxidation state of molybdenum in the neat (L)Mo(VI)O₂ complex as well as (L)Mo(VI)O₂@SBA-15. The spectra of calcined SBA-15 (Fig. 3.9a) and

(L)Mo(VI)O₂@SBA-15 (Fig. 3.9c) exhibit a peak at 225 nm, typical for siliceous materials.³⁷ In both compounds, namely, the neat (L)Mo(VI)O₂ complex (Fig. 3.9b) and (L)Mo(VI)O₂@SBA-15, two bands at 240 and 280 nm are attributed to $\pi \rightarrow \pi^*$ transitions of the aromatic ring and the azomethine group, respectively. Further, a broad peak at 330 nm is assigned to $n \rightarrow \pi^*$ transitions of the azomethine group.³⁸ Moreover, a broad band at 440 nm is attributed to $N \rightarrow Mo(VI)$ and $O \rightarrow Mo(VI)$ ligand to metal charge-transfer transitions (LMCT) due to the promotion of an electron from the ligand centered highest occupied molecular orbital (HOMO) to the molybdenum centered lowest unoccupied molecular orbital (LUMO).³⁹ The absence of a d-d transition in the visible region (400 nm to 800 nm) confirms the 4d⁰ electron configuration of the molybdenum sites.⁴⁰

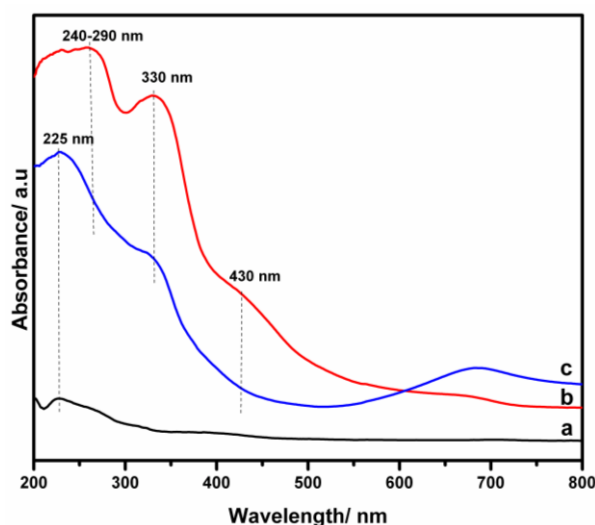


Fig. 3.9: DR-UV-Visible spectra of (a) calcined SBA-15 (b) the neat (L)Mo(VI)O₂ complex and (c) (L)Mo(VI)O₂@SBA-15.

3.3.1.10. Scanning Electron Microscopy (SEM)

Scanning electron microscopy (SEM) is an important tool for the morphological characterization of mesoporous molecular sieve materials. Fig. 3.10 (A and B) shows the SEM images of calcined SBA-15 and (L)Mo(VI)O₂@SBA-15 with a 2D *p6mm* hexagonal type structure. The particle size of both materials was found to be in the range between 1.15 and 1.25 μm . Furthermore, the morphology of (L)Mo(VI)O₂@SBA-15 was retained after anchoring of the (L)Mo(VI)O₂ sites over the functionalized SBA-15 support.

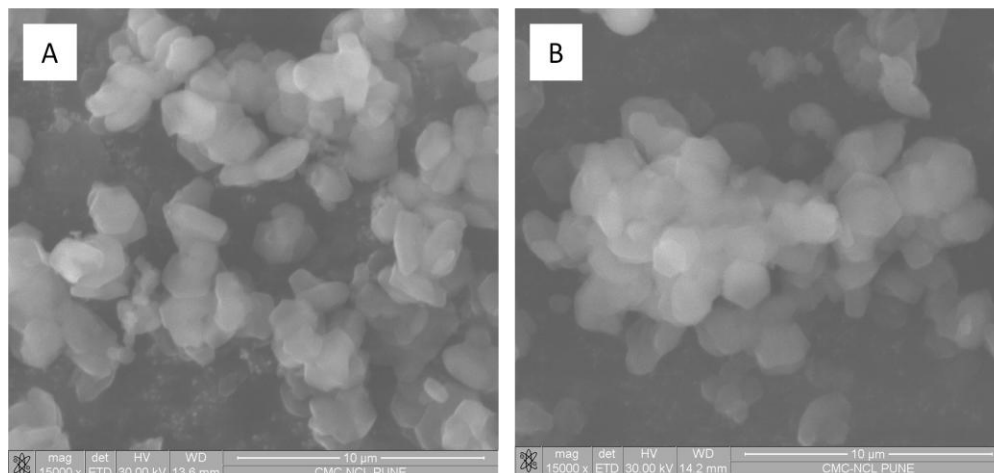


Fig. 3.10: SEM images of (A) calcined SBA-15 and (B) (L)Mo(VI)O₂@SBA-15.

3.3.1.11. Transmission Electron Microscopy (TEM)

Transmission electron microscopy (TEM) is typically used for high resolution imaging of thin films of solid samples for microstructural and compositional analysis. It has been used to obtain topographic information about the mesoporous matrices at nearly atomic resolution. The TEM images of calcined SBA-15 and (L)Mo(VI)O₂@SBA-15 shown in Fig. 3.11 (A and B) revealed the formation of a regular hexagonal array of uniform channels having a long-range ordering and well defined 1-D channels. These results are further supported by XRD results presented earlier.

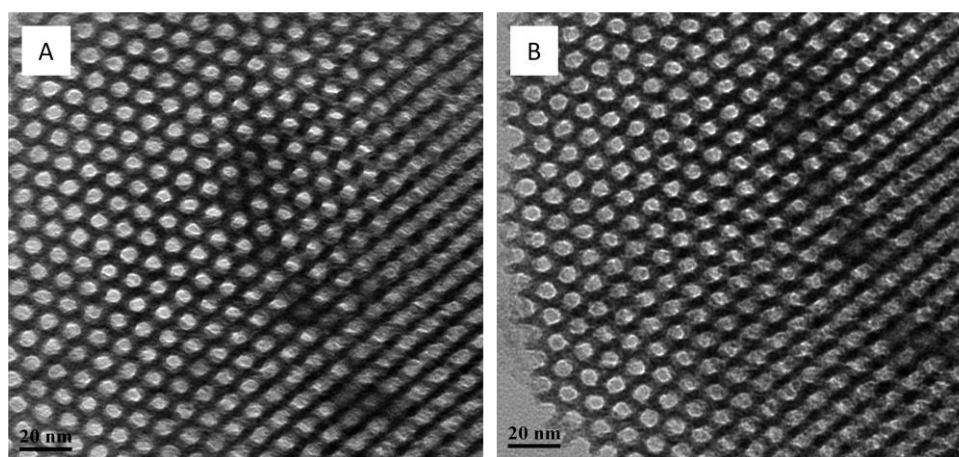


Fig. 3.11: TEM images of (A) calcined SBA-15 and (B) (L)Mo(VI)O₂@SBA-15.

3.3.2. Catalytic activity

The catalytic activity and selectivity of the synthesized catalysts were evaluated in the epoxidation cycloalkenes and in the oxidation of sulfides. The results of the epoxidation reactions catalysed by (L)Mo(VI)O₂@SBA-15 and the neat (L)Mo(VI)O₂ complex together with a blank experiment (absence of catalyst) are depicted in Table 3.2. In the epoxidation reaction, cyclooctene and cyclohexene were used as substrates together with anhydrous TBHP (5.0–6.0 M in decane) as the oxidizing agent and CHCl₃ as the solvent. In the case of (L)Mo(VI)O₂@SBA-15, results in Table 3.2 reveal that cyclooctene exhibits higher conversion (93%) and selectivity (97%) than cyclohexene (86% of conversion and 95% of selectivity), due to the presence of a more electron rich C=C double bond.⁴¹ The neat (L)Mo(VI)O₂ complex gave 88% and 78% conversion for cyclooctene and cyclohexene, respectively. The corresponding selectivities for both epoxides were found to be 96%. The blank experiment showed a very low cycloalkene conversion with poor epoxide selectivity even after 18 h of reaction time.

Table 3.2: Epoxidation of cycloalkenes

No	Catalyst	Cyclooctene			Cyclohexene		
		Con. (%)	-oxide	others	Con. (%)	-oxide	others
1	No catalyst	6	88	12	5	86	14
2	(L)Mo(VI)O ₂ complex	88	96	4	78	96	4
3	(L)Mo(VI)O ₂ @SBA-15	93	97	3	86	95	5

Reaction conditions: (L)Mo(VI)O₂@SBA-15: 150 mg or (L)Mo(VI)O₂ complex: 75 mg, Substrate: 8 mmol, TBHP (5.0-6.0 M in decane): 14.4 mmol, CHCl₃: 25 ml, Reaction temperature: 70 °C, Reaction time: 18 h.

To find out the widespread application of the heterogeneous catalyst, (L)Mo(VI)O₂@SBA-15, sulfoxidation reactions of various sulfides such as thioanisole, 4-chlorothioanisole, 4-bromothioanisole, ethyl methyl sulfide and diethyl sulfide were carried out with H₂O₂ as the oxidizing agent and CH₃CN as the solvent (Table 3.3). Normally, sulfides like methyl phenyl sulfide (thioanisole), ethyl phenyl sulfide and diethyl sulfide exhibit slightly higher conversions and comparative selectivities than substituted thioanisoles (–Cl & –Br) due to the electronic effects of –chloro and –bromo substituents in the substrates. As can be seen in Table 3.3,

(L)Mo(VI)O₂@SBA-15 catalyst gives slightly better conversions (80% to 100%) and selectivities (85% to 91%) for various alkyl aryl sulfides than the neat (L)Mo(VI)O₂ complex (conversion, 75% to 100% and selectivity, 84% to 88%). In the absence of the catalyst, lower conversion (10% to 15%) and selectivities (82% to 88%) for various alkyl aryl sulfides were obtained.

Table 3.3: Sulfoxidation of various sulfides

No	Substrate	No catalyst			(L)Mo(VI)O ₂ complex			(L)Mo(VI)O ₂ @SBA-15		
		Con. (%)	-oxide	-one	Con. (%)	-oxide	-one	Con. (%)	-oxide	-one
1	Thioanisole	14	87	13	100	85	15	100	89	11
2	4-chlorothioanisole	10	82	18	75	84	16	80	90	10
3	4-bromothioanisole	15	88	12	84	87	13	92	90	10
4	Ethyl methyl sulfide	13	87	13	90	88	12	95	91	9
5	Diethylsulfide	12	85	15	92	86	14	96	85	15

Reaction conditions: (L)Mo(VI)O₂@SBA-15: 25 mg or (L)Mo(VI)O₂ complex: 10 mg, Substrate: 1 mmol, H₂O₂: 1 mmol, CH₃CN: 5 ml, Reaction temperature: r.t, Reaction time: 3 h.

3.3.3. Heterogeneity tests

To check the stability and recyclability of the catalyst, (L)Mo(VI)O₂@SBA-15 was recycled four times (fresh + three cycles) in the epoxidation of cyclooctene and five times (fresh + four cycles) in the sulfoxidation of thioanisole (Table 3.4). After each cycle, the catalyst was removed by simple centrifugation, washed several times with a suitable solvent like CHCl₃ or CH₃CN (each time in 5 ml at 26 °C) and dried under vacuum. In every cycle, it can be seen that there is no considerable change in the conversion of the cyclooctene or the thioanisole and for the selectivity of the products. Finally, after the last cycle, the ICP-OES analysis of the used catalyst showed 0.04 mmol g⁻¹ molybdenum metal lost from the fresh catalyst, which confirms that the stability of the (L)Mo(VI)O₂@SBA-15 was largely retained upto the third (in the epoxidation) or the fourth (in the sulfoxidation) cycle.

Table 3. 4: Recycling Study in Epoxidation^a and sulfoxidation reaction^b

No of Cycles	Epoxidation (Cyclooctene)		Sulfoxidation (Thioanisole)	
	Conv.	Sele.	Conv.	Sele.
Fresh	93	97	100	89
I cycle	92	96	99	87
II cycle	88	95	97	86
III cycle	80	93	92	85
IV cycle	-	-	85	85

^a Reaction conditions: (L)Mo(VI)O₂@SBA-15: 150 mg; Cyclooctene: 8 mmol, 0.8816 g; TBHP (5.0-6.0 M in decane) : 14.4 mmol, 1.6 ml; CHCl₃: 25 ml; Reaction temperature: 70 °C; Reaction time: 18 h; ^b Reaction conditions: (L)Mo(VI)O₂@SBA-15: 25 mg; Thioanisole: 1 mmol, 0.1242 g; H₂O₂: 1.1 mmol, 0.1245 g; CH₃CN: 5 ml; Reaction temperature: 30 °C; Reaction time: 3 h.

In addition, to confirm the heterogeneity and stability of (L)Mo(VI)O₂@SBA-15 complex, Sheldon's hot filtration test was carried out, indicating that there is virtually no molybdenum content leaching into the reaction solution under the applied reaction conditions. At first, epoxidation reaction of cyclooctene (Fig. 3.12A) and sulfoxidation reaction of thioanisole (Fig. 3.12B) were performed over (L)Mo(VI)O₂@SBA-15 complex under appropriate reaction conditions (fresh cycle), which are already mentioned in the bottom of the Table 3.4. To perform the Sheldon's hot filtration test in epoxidation of cyclooctene at 70 °C for 18 h, heterogeneous catalyst like (L)Mo(VI)O₂@SBA-15 was filtered out from the reaction mixture after 6 h during the reaction, and the filtrate was again charged into round bottom flask for the continuation of the reaction in the absence of catalyst upto 18 h. The results show that 53% cyclooctane oxide was formed after 6 h and there is no changes in the conversion of cyclooctene were observed after 18 h. For the hot filtration test in sulfoxidation reaction of thioanisole (Fig. 3.12B) at 30 °C for 3 h, (L)Mo(VI)O₂@SBA-15 catalyst was filtered from the reaction mixture after 1 h during the reaction and the reaction continued uninterrupted in the absence of catalyst upto 3 h. It was observed that 65% methyl phenyl sulfide was converted after 1 h and the conversion of methyl

phenyl sulfide remained similar upto 3 h. In both reactions, results show that leaching of the molybdenum atoms was not occurred.

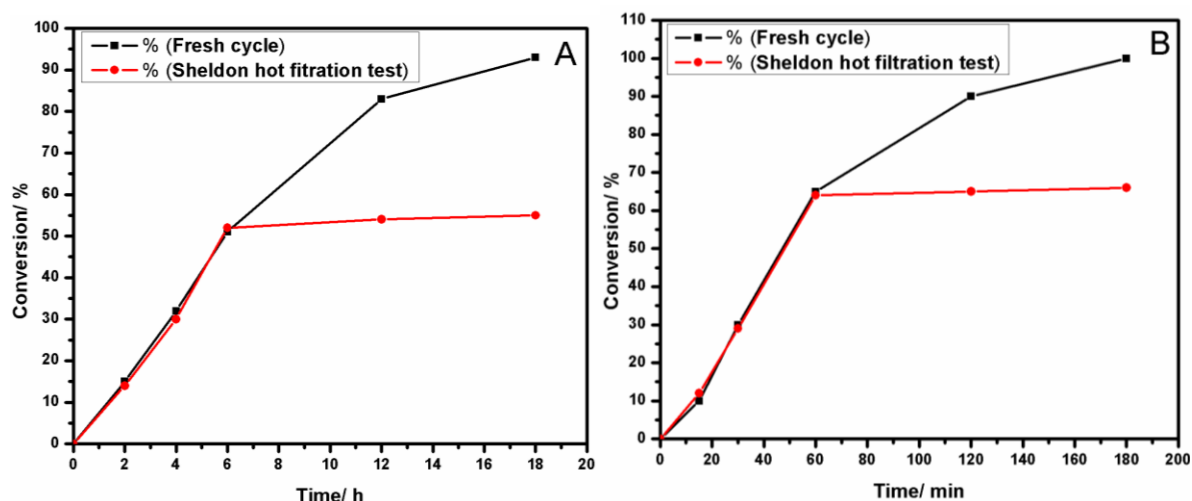


Fig. 3.12: Sheldon's hot filtration tests in (A) Epoxidation and (B) Sulfoxidation reactions

3.4. Conclusions

In this chapter, the heterogenization of the (L)Mo(VI)O₂ complex over SBA-15 is reported by a multistep synthetic procedure, using the 3-[N,N-bis-3(salicylidenamino)ethyltriamine] ligand (L) and Mo(VI)O₂(acac)₂. The physico-chemical properties of the functionalized catalyst were analyzed by a series of characterization techniques like elemental analysis, ICP-OES, XRD, N₂ sorption measurements, TG & DTA, solid state ¹³C, ²⁹Si NMR spectroscopy, FT-IR, Raman spectroscopy, XPS, DRS UV-Vis spectroscopy, SEM and TEM. The integrity and textural properties of mesoporous support and synthesized catalysts were obtained from the XRD and N₂ adsorption-desorption analysis. Thermal stabilities of the complexes were confirmed by thermal analyses like TG and DTA. The organic moieties anchored over the surface of SBA-15 were investigated by solid state ¹³C NMR and FT-IR spectroscopy. The degree of functionalization of surface silanol groups with organic moieties on the mesostructured materials can be monitored by means of ²⁹Si CP MAS NMR spectroscopy. The oxidation state and the chemical environment of molybdenum atoms were determined by Raman spectroscopy, XPS and DRS UV-Vis spectroscopy and the morphology and topographic information of the synthesized catalysts were confirmed by SEM and TEM imaging. (L)Mo(VI)O₂@SBA-15 complex was found to be highly active, selective and recyclable in the epoxidation and sulfoxidation reactions

of various cycloolefins and alkyl aryl sulfides, respectively, compared to the neat (L)Mo(VI)O₂ sites and the blank reaction. Further, to confirm the heterogeneity of (L)Mo(VI)O₂@SBA-15 complex, Sheldon's hot filtration test was carried out, and the results show that molybdenum metal does not leach out from the (L)Mo(VI)O₂@SBA-15 complex.

3.5. References

1. M. Beller, C. Bolm, *Transition Metals for Fine Chemicals and Organic Synthesis*, Vol. 2, Wiley-VCH, Weinheim, 1998, 261.
2. S. Patai, Z. Rappoport, *Synthesis of Sulfones, Sulfoxides and Cyclic Sulfides*, John Wiley, Chichester, UK, 1994.
3. K. A. Jorgensen, *Chem. Rev.*, 1989, **89**, 431.
4. E. M. Mc Garrigle, D. G. Gilheany, *Chem. Rev.*, 2005, **105**, 1563.
5. W. Zhang, J. L. Loebach, S. R. Wilson, E. N. Jacobsen, *J. Am. Chem. Soc.*, 1990, **112**, 2801.
6. W. Yang, F. Diederich, J. S. Valentine, *J. Am. Chem. Soc.*, 1991, **113**, 7195.
7. R. Atkins, G. Brfwer, E. Kokto, G. M. Mockler, E. Sinn, *Inorg.Chem.*, 1985, **24**, 128.
8. B. De Clereq, F. Verpoort, *Macromolecules*, 2002, **35**, 8943.
9. W. R. Thiel, T. Priermeier, *Angew. Chem. Int. Ed. Engl.*, 1995, **34**, 1737.
10. R. M. Calvante, J. M. Campos-Martin, J. L. G. Fierro, *Catal. Commun.*, 2002, **3**, 247.
11. F. E. Kühn, A. D. Lopes, A. M. Santos, E. Herdtweck, J. J. Haider, C. C. Romao, A. M. Santos, *J. Mol. Catal. A: Chem.*, 2000, **151**, 147.
12. A. Gunyar, D. Betz, M. Dress, E. Herdtweck, F. E. Kühn, *J. Mol. Catal. A: Chem.*, 1010, **331**, 117.
13. F. E. Kühn, A. M. Santos, A. D. Lopes, I. S. Goncalves, E. Herdtweck, J. J. Haider, C. C. Romao, A. G. Santos, *J. Mol. Catal. A: Chem.*, 2000, **164**, 25.
14. S. M. Bruno, C. C. L. Pereira, M. S. Balula, M. Nolasco, A. A. Valente, A. Hazell, M. Pilligner, P. Ribeiro-Claro, I. S. Goncalves, *J. Mol. Catal. A: Chem.*, 2007, **261**, 79.
15. P. Sutra, D. Brunel, *Chem. Commun.*, 1996, 2485.
16. S. Singha, K. M. Parida, *Catal. Sci. Technol.*, 2011, **1**, 1496.
17. M. D. Rosa, M. Lamberti, C. Pellicchia, A. Scettri, R. Villano, A. Soriente, *Tetrahedron Lett.*, 2006, **47**, 7233.

18. A. Massa, E. M. Lorenzo, A. Scettri, *J. Mol. Catal. A: Chem.*, 2006, **250**, 27.
19. C. Aprile, A. Corma, M. E. Domine, H. Garcia, C. Mitchell, *J. Catal.*, 2009, **264**, 44.
20. M. Masteri-Farahani, N. Tayyebi, *J. Mol. Catal. A: Chem.*, 2011, **348**, 83.
21. D. Zhao, J. Feng, Q. Huo, N. Melosh, G. H. Fredrickson, B. F. Chmelka, G. D. Stucky, *Science*, 1998, **279**, 548.
22. X. Feng, G. E. Fryxell, L. Q. Wang, A. Y. Kim, J. Liu, K. M. Kemner, *Science*, 1997, **276**, 500.
23. L. Mercier, T. J. Pinnavia, *Adv. Mater.*, 1997, **9**, 500.
24. M. Jia, A. Seifert, W. R. Thiel, *Chem. Mater.*, 2003, **152**, 174.
25. M. M. Farahani, F. Farzaneh, M. Ghandi, *J. Mole. Cat. A: Chem.*, 2006, **243**, 170.
26. Y. C. Jeong, S. Choi, Y. D. Hwang, K. H. Ahn, *Tetrahedron: Asymmetry*, 2005, **16**, 3497.
27. D. Zhao, Q. Huo, J. Feng, B. F. Chmelka, G. D. Stucky, *J. Am. Chem. Soc.*, 1998, **120**, 6024.
28. R. Ryoo, I-S. Park, S. Jun, C.W. Lee, M. Kruk, M. Jaroniec, *J. Am. Chem. Soc.*, 2001, **123**, 1650.
29. T. Soundiressane, S. Selvakumar, S. Menage, O. Hamelin, M. Fontecave, A. P. Singh, *J. Mol. Catal. A: Chem.*, 2007, **270**, 132.
30. S. C. Laha, P. Mukherjee, S. R. Sainkar, R. Kumar, *J. Catal.*, 2002, **207**, 1.
31. A. Lazar, P. Sharma and A. P. Singh, *Micropore. Mesopore. Mater.*, 2013, **170**, 331.
32. P. Sharma, A. Lazar and A. P. Singh, *Appl. Catal., A*, 2012, **439–440**, 101.
33. A. Syamal, M. M. Singh, D. Kumar. *React. Funct. Polym.*, 1999, **39**, 27.
34. A. G. S. Prado, C. Airoidi, *J. Colloid Interface Sci.*, 2001, **236**, 161.
35. M. D. Alba, Z. Luan, J. Klinowski, *J. Phys. Chem.*, 1996, 100, 2178.
36. C. Fickert, V. Nagel, W. Kiefer, G. Wahl, J. Sundermeyer, *J. Mol. Structure*, 1999, **482-483**, 59.
37. S. Shylesh, A. P. Singh, *J. Catal.*, 2004, **228**, 333.
38. B. İ. Ceylan, Y. D. Kurt, B. Ülküseven, *J. Coord. Chem.*, 2009, **62**, 757.
39. J. H. Enemark, C. G. Young, *Adv. Inorg. Chem.* 1993, **40**, 1.
40. C. S. J. Chang, J. H. Enemark, *Inorg. Chem.*, 1991, **30**, 683.
41. M. M. Farahani, *J. Mole. Cat. A: Chem.*, 2010, **316**, 45.

Chapter 4

Pd(II)-Organofunctionalized SBA-15 Catalysts for Coupling and Hydrogenation Reactions

4A: Pd(II)-2,2'-Dihydroxybenzophenone(DHBP)-NH₂@SBA-15

4B: Pd(II)-3-Allylsalicylaldiminophenol(ASIP)-SH@SBA-15

[Anish Lazar](#), C. P. Vinod and A. P. Singh*
New Journal of Chemistry 40 (3) (2016) 2423-2432.

[Anish Lazar](#), C. P. Vinod and A. P. Singh*
Microporous and Mesoporous Materials 242 (2017) 173-181.

4A: Pd(II)-2,2'-Dihydroxybenzophenone(DHBP)-NH₂@SBA-15 catalyst for arylation and hydrogenation of alkenes

4A.1. Introduction

The discovery of C–C coupling reactions in 19th century has opened up several alternative challenges for the production of fine chemicals. A lot of materials such as ionic liquids,¹ silica supported² and polymer supported³ catalysts, pure Pd/C⁴ etc. were used for the carbon–carbon coupling reactions. The phosphine supported catalysts⁵ for C–C coupling reactions are the well established method in the past decades. However, several drawbacks of phosphine ligands such as cost, toxicity and recovery from the reaction mixture are challenging and have resulted in the process being less preferred. In addition, phosphine undergoes oxidation in the catalytic cycle to get phosphine oxide, and thereby causing the cleavage of a P–C bond and degradation of the catalytic cycle. Due to these reasons, there is a growing interest in the development of a phosphine free heterogeneous catalyst.⁶ Such a catalyst should be stable under ambient conditions and should afford coupling products in high yields at short reaction times. Out of carbon–carbon cross-coupling reactions, the arylation of alkenes⁷ in the presence of a base (Heck reaction) is an excellent method for the synthesis of fine chemicals.

In the past decades, complexes of palladium such as palladium acetate, palladium chloride or triarylphosphine palladium complexes are used⁸ in the arylation reactions of alkenes with aryl halides. However, as with all homogeneous catalysts, its separation and reusability are difficult, thereby increasing the production cost with liberation of large volumes of hazardous wastes. To mitigate the above mentioned serious problems, palladium based organofunctionalized mesoporous catalysts,^{9–11} which shows high periodicity in the pore arrangement as well as high surface area and pore sizes, have been synthesized via a post grafting method and used for coupling reactions.¹² Further, liquid phase hydrogenation of alkenes^{13,14} using heterogeneous catalysts is a relevant industrial process to obtain alkanes. An appropriate, cheap and simple ligand is necessary for the synthesis of highly active palladium based organofunctionalized complexes. For this purpose, a number of ligands such as -C–N- and N, N' based ligands¹⁵ have been reported for coupling reactions. Due to the instability and tedious synthesis procedure of previously said ligands, a robust and stable 2, 2'-dihydroxybenzophenone ligand derivative is used in the present study.

To heterogenize the palladium based organofunctionalized complexes with better stability and to avoid the diffusional strain of reactants in the channels of other mesoporous or microporous materials, a solid support like SBA-15 is synthesized by using a neutral triblock polyether as templates and TEOS as a silica precursor. In addition, SBA-15¹⁶ has the advantage due to its special characteristics such as high surface area, uniform pore sizes, high wall thickness and high hydrothermal stability compared to other mesoporous materials like MCM-41 and MCM-48. To explore the utility of SBA-15 materials, especially in catalysis, the surface of SBA-15 was modified by organic functional groups for anchoring of metals and metal complexes.¹⁷

In this work, we tried to synthesize and characterize a highly efficient, phosphine and co-catalyst free, reusable heterogeneous catalyst, Pd(II)DHBP@SBA-15, for arylation and hydrogenation reactions of alkenes. The synthesis of the Pd(II)DHBP@SBA-15 catalyst is mainly divided into four steps and it is described as (i) synthesis of parent solid support like SBA-15, (ii) aminofunctionalization of SBA-15, (iii) anchoring of 2, 2'-dihydroxybenzophenone (DHBP) ligand over amino-functionalized SBA-15 (NH₂@SBA-15) and (iv) metallation of a heterogenized ligand (DHBP@SBA-15) with Pd(II)(OAc)₂.

4A.2. Experimental

4A.2.1. Materials

Pluronic 123 (P123, average Mol Wt = 5800), tetraethylorthosilicate (TEOS), 3-aminopropyl trimethoxysilane (3-APTMS), 2,2'-dihydroxybenzophenone (DHBP) and Pd(II)(OAc)₂ were purchased from Aldrich. In addition, aryl halides and alkenes as organic reagents used for the coupling and hydrogenation reactions were purchased from Aldrich. Further, hydrochloric acid (HCl) and solvents like dichloromethane (DCM), acetonitrile (CH₃CN) and toluene were purchased from Merck. All chemicals were used as received without further purification.

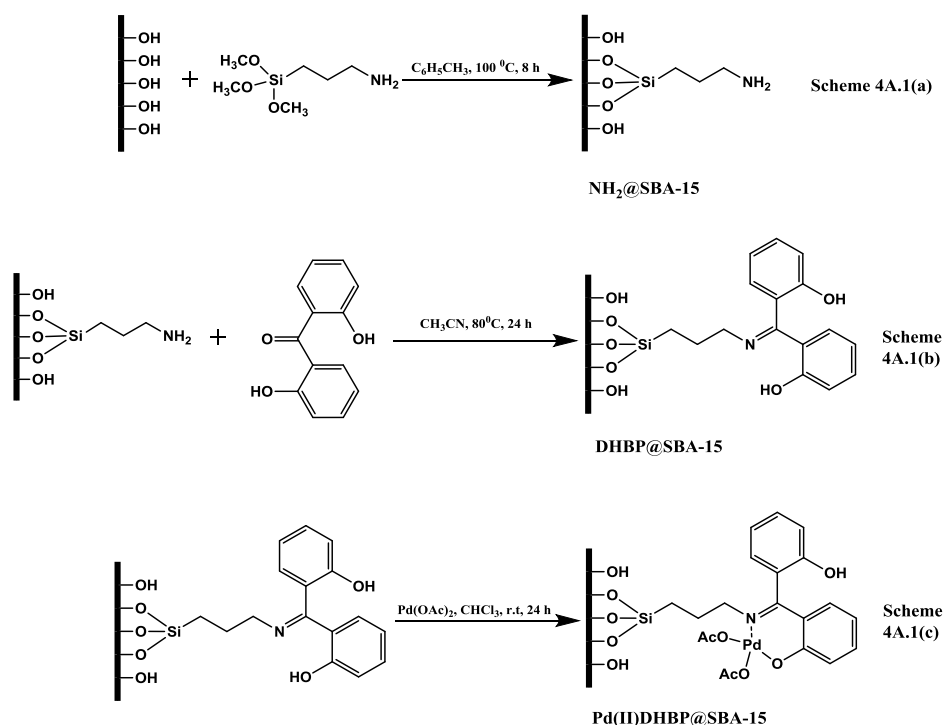
4A.2.2. Synthesis of aminofunctionalized SBA-15

The synthesis of mesoporous SBA-15¹⁸ was carried out hydrothermally under the autogeneous pressure in an autoclave and detailed procedure mentioned in experimental part of Chapter 2. The amino-functionalized SBA-15 (NH₂@SBA-15) was synthesized by using 3-aminopropyl trimethoxysilane (3-APTMS) as an organic linker via the post-grafting method [Scheme 4A.1(a)]. The reaction procedure is briefly explained as: 3 g of calcined SBA-15 was dispersed in 60

ml dry toluene followed by 1.5 g of 3-APTMS added into this solution under a N₂ atmosphere and the reaction mixture was refluxed at 100 °C for 8 h. The solid material was filtered, washed with toluene and dichloromethane, and dried in oven at 70 °C for 12 h. The dried material was extracted using a Soxhlet apparatus with dichloromethane as a solvent to remove the unreacted silylating agent like 3-APTMS and was vacuum dried to get NH₂@SBA-15.

4A.2.3. Synthesis of Pd(II)-2,2'-Dihydroxybenzophenone(DHBP)-NH₂@SBA-15

The synthesis of Pd(II)DHBP@SBA-15 is mainly divided into two steps as shortly described as (i) anchoring of a 2,2'-dihydroxybenzophenone ligand (DHBP) over aminofunctionalized SBA-15 (NH₂@SBA-15) [Scheme 4A.1(b)] to get DHBP@SBA-15 and (ii) complexation of a heterogenized ligand (DHBP@SBA-15) with Pd(II)(OAc)₂ to achieve Pd(II)DHBP@SBA-15 [Scheme 4A.1(c)].



Scheme 4A.1: Synthesis of Pd(II)-2,2'-Dihydroxybenzophenone(DHBP)-NH₂@SBA-15 [Pd(II)DHBP@SBA-15]; Synthesis of 4A.1(a) NH₂@SBA-15, 4A.1(b) DHBP@SBA-15, 4A.1(c) Pd(II)DHBP@SBA-15.

In brief, the first step involves the addition of 2,2'-dihydroxybenzophenone (0.52 g, 2.41 mmol) which is dissolved in 35 ml of dry acetonitrile into the dispersed solutions of NH₂@SBA-

15 (1 g) in 15 ml of dry acetonitrile. The reaction mixture was refluxed at 80 °C for 24 h with constant stirring, and then filtered, washed thoroughly with acetonitrile and dried in oven at 50 °C for 16 h to get DHBP@SBA-15. In the second step, called as the metallation process, 0.2 g of Pd(II)(OAc)₂ (0.89 mmol) in 20 ml of CHCl₃ was added into the solution of heterogenized ligand, DHBP@SBA-15 (1 g) in 10 ml of CHCl₃. The dispersed solution was stirred at room temperature for 24 h, and then filtered, washed with CHCl₃ and dried in oven at 50 °C for 12 h. The dried material was Soxhlet extracted to remove unreacted Pd(II)(OAc)₂ to attain Pd(II)DHBP@SBA-15.

4A.2.4. Procedure for catalytic reactions

The arylation of alkenes with palladium catalysts is one of the important organic reactions, referred to as the Heck reaction, which is helpful for the synthesis of various types of coupling compounds. Arylations of alkenes were carried out in a 50 ml double necked RB flask fitted with a water-cooled condenser and magnetic stirrer by using Et₃N as a base. In a typical Heck reaction procedure, a mixture of 0.015 g of Pd(II)DHBP@SBA-15, aryl halide (1 mmol), alkenes (1.2 mmol), Et₃N (3.5 mmol) and 3.5 ml of DMF was refluxed at 120 °C for 12 h. The samples were withdrawn periodically and the cooled sample was analyzed using a Gas chromatography (HP, Agilent 68909 N) equipped with a capillary column (HP-5) and a FID detector.

Hydrogenation reactions of alkenes, especially aromatic olefins, cycloolefins, aliphatic olefins and bicyclo olefins, are used to synthesize various hydrocarbons, which can be applied in industrial chemistry. In a typical procedure, a mixture of 0.015 g of Pd(II)DHBP@SBA-15 and olefins (5 mmol) in 50 ml methanol were taken in a 100 ml Parr autoclave reactor and stirred with H₂ Pressure (5 bar) at room temperature for 15 minutes. The samples were withdrawn periodically and the cooled sample was analyzed using a Gas chromatography (HP, Agilent 68909 N) equipped with a capillary column (HP-5) and a FID detector.

4A.3. Results and discussions

4A.3.1. Characterizations

4A.3.1.1. X-ray Diffraction (XRD)

The synthesized catalysts were characterized by different physicochemical characterization techniques and the results are discussed below. The XRD pattern of (a) as-synthesized SBA-15,

(b) calcined SBA-15 (c) NH_2 @SBA-15 and (d) Pd(II)DHBP@SBA-15 are represented in Fig. 4A.1. The uniqueness of the mesoporous structure, phase purity, degree of orderedness and unit cell parameters of all synthesized catalysts were determined by powder X-ray diffraction. The typical hexagonal phase (p6mm) of SBA-15 showing three reflections, mainly (100) peak with weak (110) and (200) peaks are clearly visible in all samples at $2\theta = 0.901$, 1.501 and 1.741, respectively. This indicates high degree of orderedness of the two dimensional hexagonal mesophase.¹⁹ In all the synthesized catalysts [Fig. 4A.1(a–d)], (110) reflection is more intense than (200) reflection, which occurs due to the complete condensation of the wall structure owing to the higher hydrothermal synthesis temperature at calcinations. Further, the XRD pattern of calcined SBA-15 [Fig. 4A.1(b)] shows an intense peak compared with the as-synthesized SBA-15 which reveals that the surfactant present in as-synthesized sample was completely removed from calcined SBA-15. The peak intensities of (100) reflections in NH_2 @SBA-15 and Pd(II)DHBP@SBA-15 [Fig. 4A.1(c and d)] were gradually decreasing from calcined SBA-15 due to the proper loading of an organic modifier and homogeneous complexes, respectively, on calcined SBA-15.

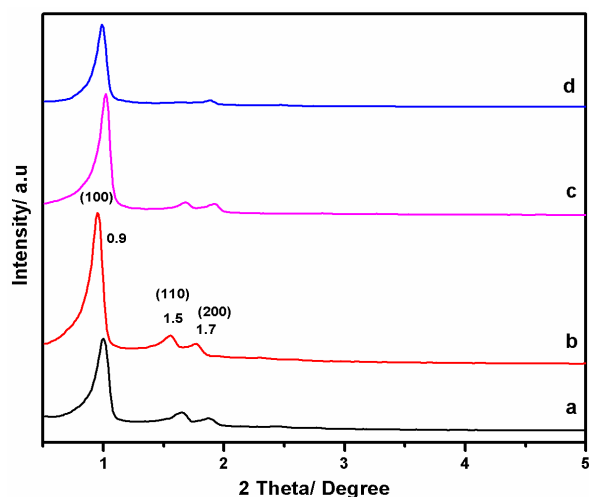


Fig. 4A.1: XRD pattern of (a) as-synthesized SBA-15 (b) calcined SBA-15 (c) NH_2 @SBA-15 and (d) Pd(II)DHBP@SBA-15.

4A.3.1.2. N_2 -Sorptions analyses

The physical properties of calcined SBA-15 and Pd(II)DHBP@SBA-15 are summarized in Table 4A.1. The BET surface area, pore volume, pore diameter, unit cell parameter and pore wall

thickness of calcined SBA-15 and Pd(II)DHBP@SBA-15 are found to be $550 \text{ m}^2 \text{ g}^{-1}$, 1.02 cc g^{-1} , 65.00 \AA , 102 \AA , 36 \AA and $220 \text{ m}^2 \text{ g}^{-1}$, 0.51 cc g^{-1} , 47.00 \AA , 103 \AA , 55 \AA , respectively. As shown in Table 4A.1, compared to SBA-15, a further reduction of surface area, pore volume and pore diameter were observed in the Pd(II)DHBP@SBA-15 catalyst, indicating the successful anchoring of homogeneous complex on the channels of SBA-15.

Table 4A.1: Textural properties of calcined SBA-15 and Pd(II)DHBP@SBA-15

Sample	$a_0[\text{\AA}]^a$	S.A [m^2/g]	$D_p[\text{\AA}]$	$V_p[\text{cc/g}]$	$\omega_t(\text{\AA})^b$
SBA-15	102	550	65	1.02	36
Pd(II)DHBP@SBA-15	103	220	47	0.51	55

a_0 =Unit cell parameter, S.A= BET Surface area, D_p = Pore diameter, V_p = Pore volume, ω_t = Wall Thickness; From EDAX analysis Pd= $\sim 6.88 \text{ wt}\%$; $^a a_0=2d_{100}/1.73$; $^b \omega_t= a_0- D_p$.

The N_2 adsorption–desorption isotherm and pore size distribution curves (inset) of (a) calcined SBA-15 and (b) Pd(II)DHBP@SBA-15 are plotted in Fig. 4A.2. In both materials, calcined SBA-15 and Pd(II)DHBP@SBA-15 exhibit type IV type isotherm with a H1 hysteresis loop related to the capillary condensation step, a characteristic feature of the highly ordered mesoporous materials (2–50 nm).²⁰

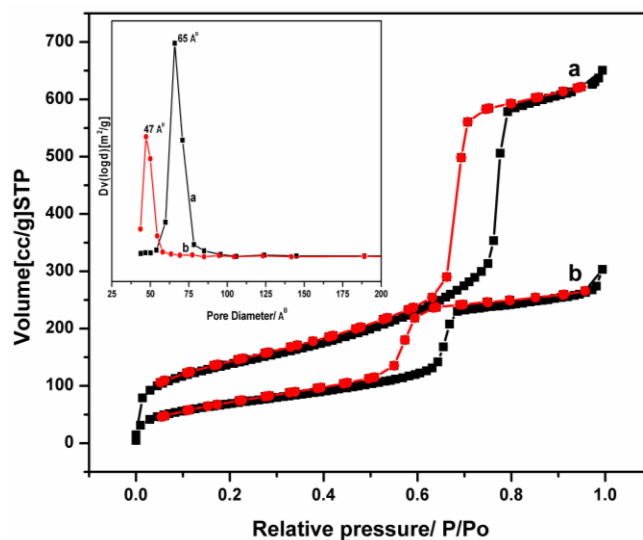


Fig. 4A.2: N_2 -isotherm and pore-size (inset) of (a) SBA-15 and (b) Pd(II)DHBP@SBA-15

4A.3.1.3. Thermal analyses (TG and DTA)

The weight percentage of organomoieties on SBA-15 and the thermal stability of (a) as-synthesized SBA-15, (b) calcined SBA-15, (c) NH₂@SBA-15 and (d) Pd(II)DHBP@SBA-15 were determined by TGA (Fig. 4A.3 A) and DTA (Fig. 4A.3 B) in an atmosphere of air from 30 to 1000 °C with a temperature ramp of 10 °C min⁻¹. As-synthesized SBA-15 [Fig. 4A.3 A(a)] exhibits a 50% weight loss in TG analysis with observation of an exothermic peak in DTA analysis [Fig. 4A.3 B(a)], in the range of 175 °C to 230 °C. Thus it can be inferred that the decomposition of surfactants is present in as-synthesized SBA-15. In calcined SBA-15 [Fig. 4A.3 A(b)], a 11% weight loss was observed in TGA due to the physisorbed water molecules, and no peak was observed in DTA analysis [Fig. 4A.3 B(b)]. This indicates a complete removal of surfactants from parent SBA-15 with the generation of pure siliceous material.

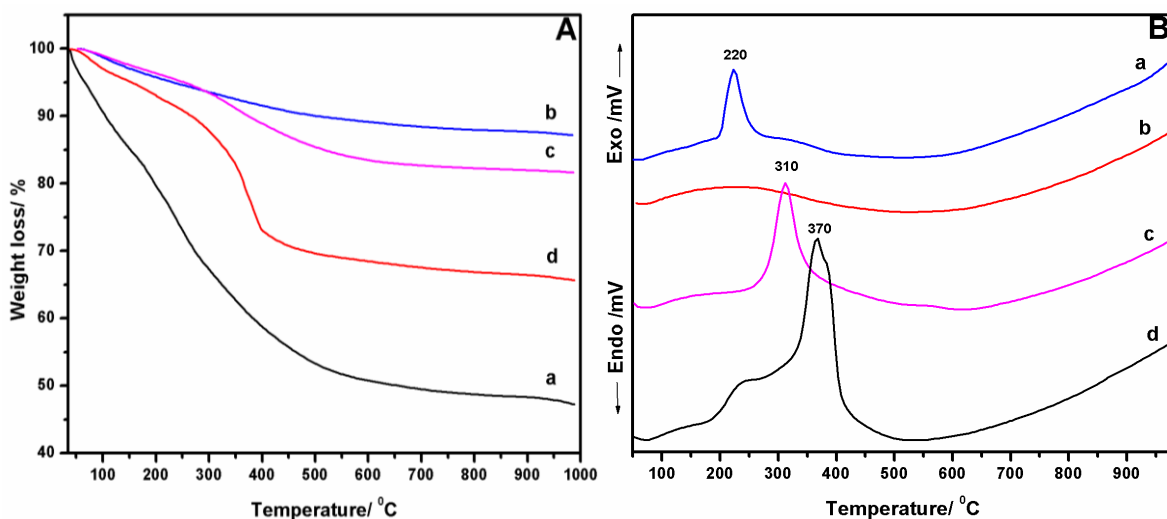


Fig. 4A.3: TGA (A) and DTA (B) pattern of (a) as-synthesized SBA-15 (b) calcined SBA-15 (c) NH₂@SBA-15 and (d) Pd(II)DHBP@SBA-15.

The TG and DTA analyses of NH₂@SBA-15 [Fig. 4A.3 A and B(c)] shows two distinct weight loss regions; first one, corresponds to the adsorbed moisture molecule in the region of 75 °C to 150 °C and second one, indicates the decomposition of an aminopropyl moiety from NH₂@SBA-15 in the range of 250 °C to 320 °C. In the case of Pd(II)DHBP@SBA-15 [Fig. 4A.3 A and B(d)], an extra peak was observed between 350 °C and 420 °C along with the peaks of the aminopropyl group in NH₂@SBA-15. The combustion of the Pd(II)-2,2'-dihydroxy benzophenone (DHBP) complex can be confirmed along with the high thermal stability of

organomoiety on SBA-15. The TGA results of $\text{NH}_2\text{@SBA-15}$ [Fig. 4A.3 A(c)] exhibits 18% weight loss which is greater than calcined SBA-15 (11%) [Fig. 4A.3 A(b)] indicating the successful anchoring of 3-APTMS on the calcined SBA-15. Further, Pd(II)DHBP@SBA-15 [Fig. 4A.3 A(d)] shows 31% of weight loss, being greater than the loss observed for the $\text{NH}_2\text{@SBA-15}$, strongly supporting a 13% loading of a neat Pd(II)-2,2'-dihydroxy benzophenone (DHBP) complex on calcined SBA-15. All decomposition results of synthesized materials from TG and DTA analyses confirm the successful anchoring of the organomodifier and neat homogeneous complex over SBA-15.

4A.3.1.4. Fourier Transform Infrared Spectroscopy (FT-IR)

FT-IR was employed to find out the nature of surface silanol groups and organomoiety attached on SBA-15. The FT-IR spectra of (a) as-synthesized SBA-15, (b) calcined SBA-15, (c) $\text{NH}_2\text{@SBA-15}$ and (d) Pd(II)DHBP@SBA-15 are depicted in Fig. 4A.4. The peaks at 2940 and 2867 cm^{-1} in the as-synthesized SBA-15 [Fig. 4A.4(a)] are attributed to the $-\text{CH}_2$ asymmetrical and symmetrical stretching vibrations of surfactant molecules present in host materials. After calcination [Fig. 4A.4(b)], the above mentioned peaks disappeared due to the complete removal of surfactants, and a broad band at $3800\text{--}3000\text{ cm}^{-1}$ and a medium sharp band at 1630 cm^{-1} were observed, which corresponds to $-\text{OH}$ stretching and bending vibrations of isolated surface silanol groups in calcined SBA-15.^{21,22}

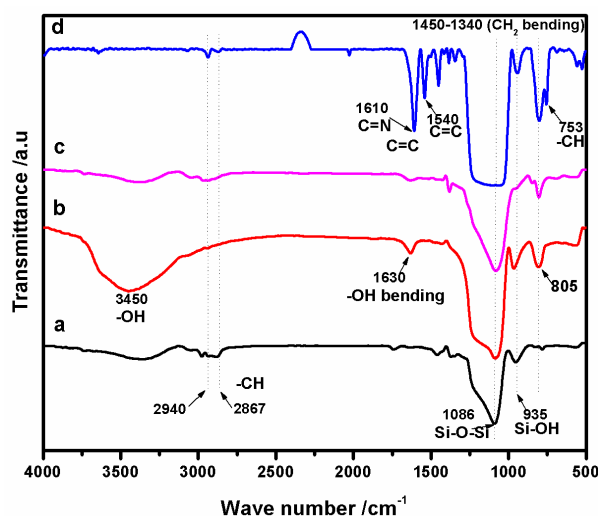


Fig. 4A.4: FT-IR Spectra of (a) as-synthesized SBA-15 (b) calcined SBA-15 (c) $\text{NH}_2\text{@SBA-15}$ and (d) Pd(II)DHBP@SBA-15 .

After aminofunctionalization, NH₂@SBA-15 [Fig. 4A.4(c)], the peaks at 2940 and 2867 cm⁻¹ due to the stretching vibrations of -CH₂ groups¹⁷ in the propyl chain of 3-APTMS indicate the successful anchoring of the organic linker on parent SBA-15. Further, the peaks at 3300 cm⁻¹ and ~1500 cm⁻¹ correspond to stretching and bending vibrations of a N-H bond¹⁵ in NH₂@SBA-15 [Fig. 4A.4(c)]. In the case of Pd(II)DHBP@SBA-15 [Fig. 4A.4(d)], additional peaks at 753 cm⁻¹ and 1540 cm⁻¹ are assigned to C-H bending and C=C stretching vibrations,¹⁸ respectively, of the arene groups. Moreover, a strong band at 1610 cm⁻¹ is assigned to the -C=N stretching vibration of the azomethylene group.¹⁸ In addition, a well pronounced band at 1450 to 1340 cm⁻¹ correspond to the -CH₂ bending vibrations¹⁷ of the propyl chain in Pd(II)DHBP@SBA-15. The spectrum of as-synthesized SBA-15, calcined SBA-15, NH₂@SBA-15 and Pd(II)DHBP@SBA-15 [Fig. 4A.4(a-d)] exhibit the bands at 1086 cm⁻¹ and 805 cm⁻¹ assigned to the asymmetric and symmetric stretching vibrations of a Si-O bond in Si-O-Si and a strong band at 935 cm⁻¹ is attributed to $\nu(\text{Si-OH})$ vibrations in the silica framework.^{23,24} The results from FT-IR spectra indicates successfully anchoring of a neat Pd(II)-2,2-dihydroxy benzophenone (DHBP) complex into parent SBA-15.

4A.3.1.5. Solid state ¹³C NMR Spectroscopy (¹³C CP MAS NMR)

The ¹³C solid state NMR spectra of (a) NH₂@SBA-15 and (b) Pd(II)DHBP@SBA-15 are plotted in Fig. 4A.5.

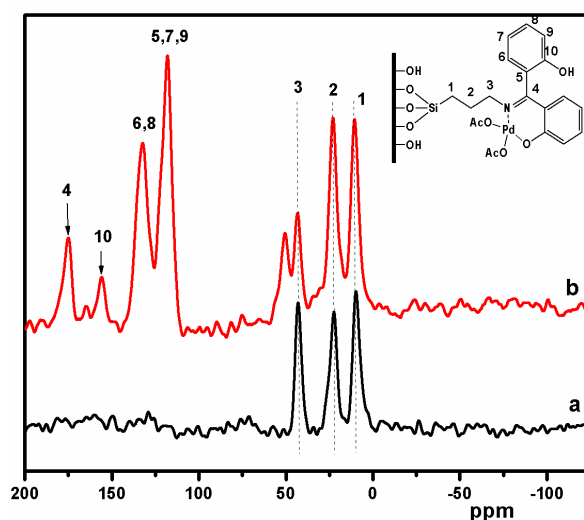


Fig. 4A.5: Solid state ¹³C NMR spectra of (a) NH₂@SBA-15 and (b) Pd(II)DHBP@SBA-15.

In aminofunctionalized SBA-15 [Fig. 4A.5(a)], peaks at 10, 23 and 43 ppm correspond to the carbon atoms of the propyl chain in the organic modifier, indicating successful aminofunctionalization of SBA-15. In the case of the Pd(II)DHBP@SBA-15 catalyst [Fig. 4A.5(b)], peaks in the range of 110–145 ppm, assigned to aromatic carbon atoms of the 2,2'-dihydroxybenzophenone (DHBP) ligand, are anchored over aminofunctionalized SBA-15. In addition, peaks at 156 ppm and 176 ppm are ascribed to the $-\text{CH}(\text{OH})$ group in the aromatic ring and the azomethine ($-\text{C}=\text{N}$) group in the Pd(II)DHBP@SBA-15 catalyst, respectively. All resonance peaks related with organomoieties confirm the anchoring of Pd(II)-2,2'-dihydroxybenzophenone (DHBP) sites on SBA-15.

4A.3.1.6. Solid state ^{29}Si NMR Spectroscopy (^{29}Si CP MAS NMR)

The ^{29}Si CP-MAS NMR spectroscopy has been employed to find out the degree of functionalization of surface silanol groups with organic moieties on the mesostructured materials. ^{29}Si solid state NMR spectra of (a) calcined SBA-15, (b) NH_2 @SBA-15 and (c) Pd(II)DHBP@SBA-15 are represented in Fig. 4A.6.

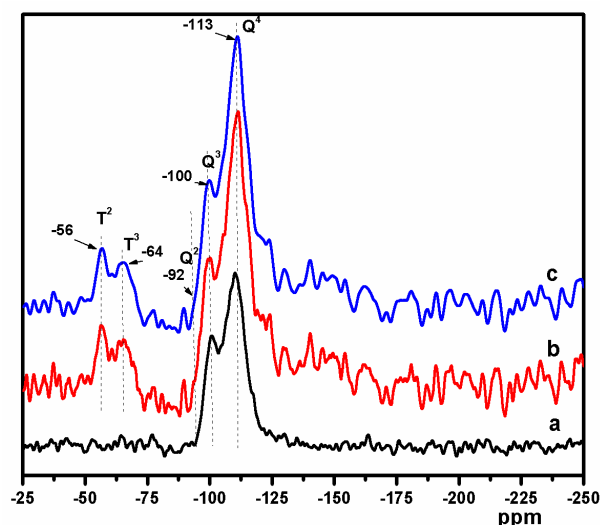


Fig. 4A.6: Solid state ^{29}Si NMR spectra of (a) calcined SBA-15 (b) NH_2 @SBA-15 and (c) Pd(II)DHBP@SBA-15.

Broad resonance peaks from -90 to -110 ppm are assigned to Si–O–Si and Si–OH bonds in all synthesized catalysts [Fig. 4A.6(a–c)]. The peaks at -92 ppm, -100 ppm and -110 ppm correspond

to the Q² [geminal silanol, (SiO)₂Si(OH)₂], Q³ [single silanol, (SiO)₃Si(OH)] and Q⁴ [siloxane, (SiO)₄Si] sites of the silica framework, respectively.^{21,22} The spectra of NH₂@SBA-15 [Fig. 4A. 6(b)] and Pd(II)DHBP@SBA-15 [Fig. 4A. 6(c)] exhibit two additional peaks at -64 ppm and -56 ppm assigned to T³ [SiR(OSi)₃] and T² [Si(OH)R(OSi)₂] units, respectively, which is conspicuously absent in parent SBA-15. The presence of T³ and T² signals confirm that SBA-15 has been modified by organomoieties. In addition, aminofunctionalized SBA-15 shows a decrease in Q² and Q³ sites with the increase of Q⁴ site, compared to calcined SBA-15, indicating the effective consumption of the silanol sites by using 3-APTMS as an organic modifier. The results from ²⁹Si NMR spectra confirm a highly condensed siloxane network with the organic group covalently bound to the mesoporous silica and the stability of the Si–C bond in the Pd(II)DHBP@SBA-15 catalyst.

4A.3.1.7. X-ray Photoelectron Spectroscopy (XPS)

X-ray Photoelectron Spectroscopy can be used to find out the oxidation state and chemical environment of synthesized catalysts. The XPS spectra of Pd3d core levels of Pd(II)DHBP@SBA-15 are plotted in Fig. 4A.7. All the spectra were calibrated and charge corrected to the C1s peak of carbon at 284.6 eV as standard reference. The peaks at 337.5 eV and 343 eV in the Pd(II)DHBP@SBA-15 catalyst correspond to Pd3d_{5/2} and Pd3d_{3/2} spin orbit components, indicating that palladium exists in the ⁺² oxidation state.

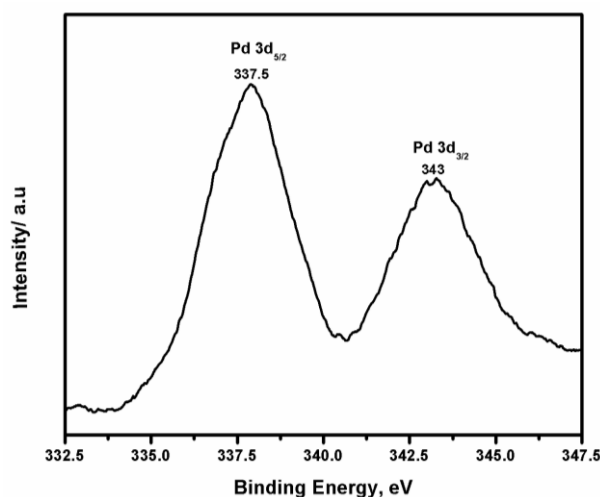


Fig. 4A.7: XPS spectroscopy of 3d_{5/2} and 3d_{3/2} core levels of Pd(II)DHBP@SBA-15

4A.3.1.8. DR UV-Visible Spectroscopy (DR UV-Vis)

The DR UV-Visible spectra of (a) calcined SBA-15, (b) NH_2 @SBA-15 and (c) Pd(II)DHBP@SBA-15 are presented in Fig. 4A.8. A peak at 230 nm,²⁵ typical for a siliceous material, is observed in all synthesized catalysts [Fig. 4A.8(a-c)]. The spectra of Pd(II)DHBP@SBA-15 [Fig. 4A.8c] exhibits two peaks at 256 nm and 295 nm are attributed to $\pi \rightarrow \pi^*$ transitions of the aromatic ring and the azomethine group, respectively.²⁶ Further, a broad peak at 367 nm is assigned to $n \rightarrow \pi^*$ transitions of the azomethine group. Two broad bands at 560 nm and 686 nm are assigned to the $\text{N} \rightarrow \text{Pd(II)}$ & $\text{O} \rightarrow \text{Pd(II)}$ ligand to metal charge-transfer transitions (LMCT) and d-d transitions of Pd(II) species, respectively.²⁷ The above results also confirm the successful anchoring of the Pd(II)-2,2'-dihydroxybenzophenone (DHBP) complex over SBA-15 with intact $+2$ oxidation state.

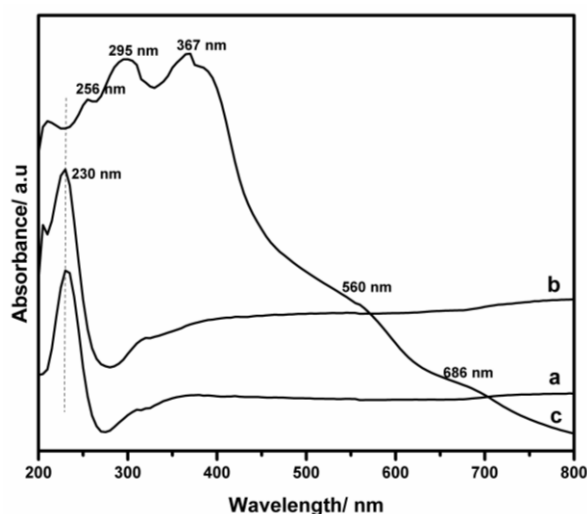


Fig. 4A.8: DR UV-Vis spectra of (a) calcined SBA-15 (b) NH_2 @SBA-15 and (c) Pd(II)DHBP@SBA-15.

4A.3.1.9. Scanning Electron Microscopy (SEM)

Scanning Electron Microscopy (SEM) analysis was used to attain nanometric and morphological details of the mesoporous materials. The SEM images of (A) calcined SBA-15 and (B) Pd(II)DHBP@SBA-15 are shown in Fig. 4A.9. The particle size of calcined SBA-15 and Pd(II)DHBP@SBA-15 was found to be in the range of 1.10 to 1.31 μm with a hexagonal plate type structure. The morphology of Pd(II)DHBP@SBA-15 [Fig. 4A.9 B] was retained with the

parent SBA-15 [Fig. 4A.9 A] after the anchoring of Pd(II)DHBP sites on aminofunctionalized SBA-15.

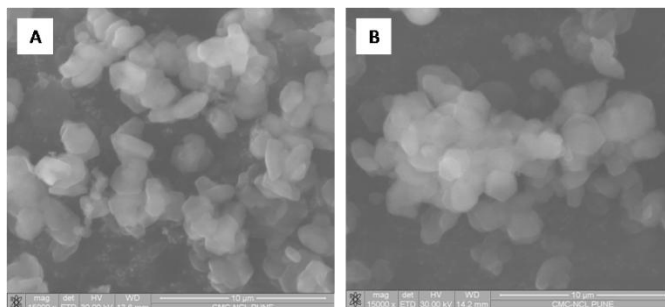


Fig. 4A.9: SEM images of (A) calcined SBA-15 and (B) Pd(II)DHBP@SBA-15

4A.3.1.10. Transmission Electron Microscopy (TEM)

The TEM images of (A) calcined SBA-15 and (B) Pd(II)DHBP@SBA-15 are shown in Fig. 4A.10 and its images show regular hexagonal array of uniform channels having a long-range order and well defined 1-D channels. The nanometric sized pore channels are in confirmation with SA and XRD analysis.

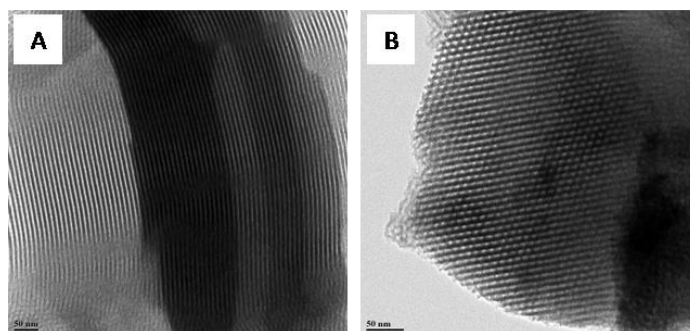


Fig. 4A.10: TEM images of (A) calcined SBA-15 and (B) Pd(II)DHBP@SBA-15

4A.3.2. Catalytic activity

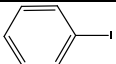
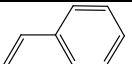
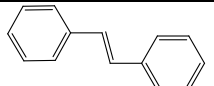
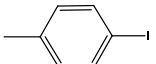
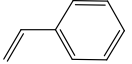
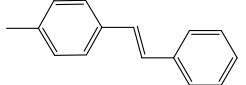
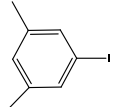
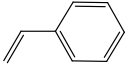
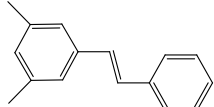
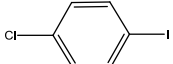
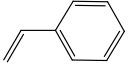
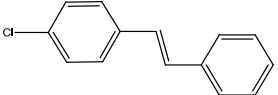
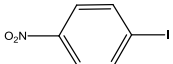
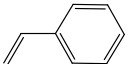
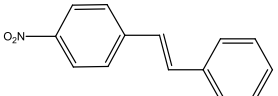
The catalytic activity of the Pd(II)DHBP@SBA-15 complex was evaluated in arylation and hydrogenation reaction of alkenes. Arylation of alkenes (Heck reaction), in which various aryl halides couple with alkenes to give trans-stillbene derivatives, using Et_3N as a base and dimethylformamide (DMF) as a solvent. The reaction progress (conversion in percentage) of the Pd(II)DHBP@SBA-15 catalyst for Heck reaction are is in Table 4A.2 (entries 1–20). To evaluate the influence of substrates, aryl halides like iodobenzene, 1-iodotoluene, 3, 5-dimethyliodo benzene, 1-iodo-4-chlorobenzene, 1-iodo-4-nitrobenzene and alkenes like styrene, α -methyl

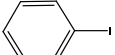
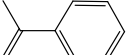
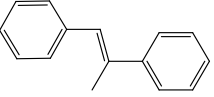
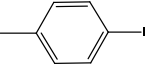
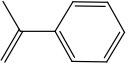
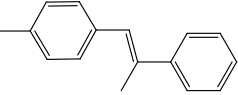
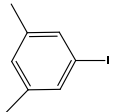
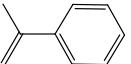
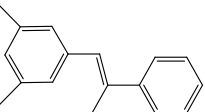

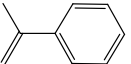
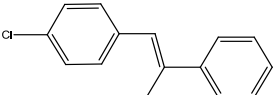
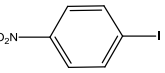
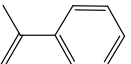
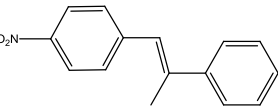
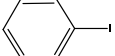
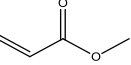
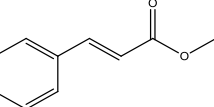
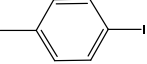
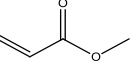
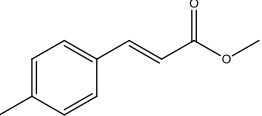
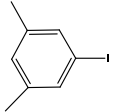
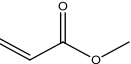
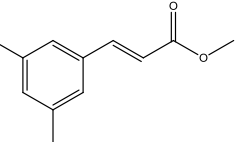

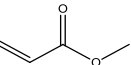
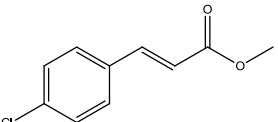
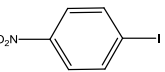
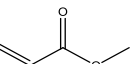
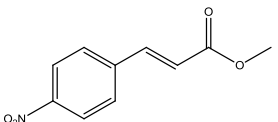
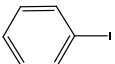
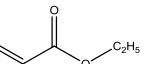
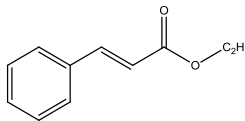
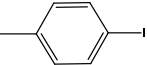
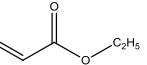
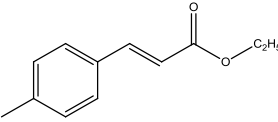
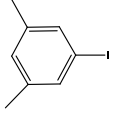
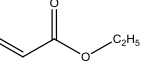
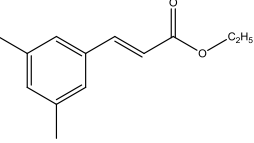

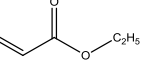
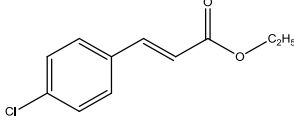
styrene, methyl acrylate, ethyl acrylate were screened, to produce coupling products. The *trans* or E isomer was formed as the dominant coupling product in all cases than *cis* or Z isomer.

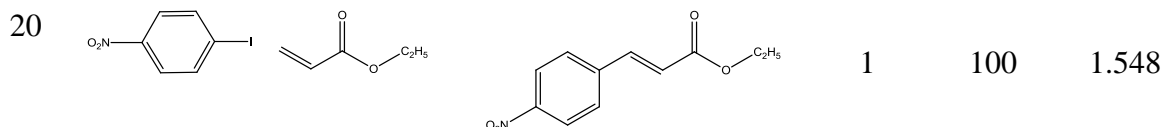
As shown in Table 4A.2, aromatic halides with an electron withdrawing group (EWG) were more imprudent than that of electron donating groups (EDG). In both cases, electronic effects at the *para* position are more predominant than the *meta* position. Thus, the electron withdrawing group containing aryl halides (entries 4 and 5) show higher and sudden conversion [95 to 100%] than electron donating groups [75 to 80%] (entries 1–3), whereas the conversion of halides constantly decreases with increasing number of electron donating groups. This result reveals that the presence of a strong electron withdrawing group in aryl halides makes the substrate more susceptible for further oxidative-addition reactions during catalytic cycle.

Likewise, EDG present in alkenes like α -methyl styrene (entries 6–10) exhibits higher conversion towards the coupling products [87 to 100%] than a model substrate like styrene [75 to 100%] (entries 1–5). In the case of acrylates as alkenes in Heck reactions (entries 11–20), ethyl acrylate (entries 16–20) shows higher conversion [90 to 100%] than methyl acrylate [90 to 95%] (entries 11–15), due to the EDG effects. The decreasing order of reactivity of aryl halides and alkenes in Heck reactions are: 1-iodo-4-nitrobenzene > 1-iodo-4-chloro benzene > iodobenzene > 1-iodotoluene > 3, 5-dimethyliodo benzene and ethyl acrylate > methyl acrylate > α -methyl styrene > styrene, respectively.

Table 4A.2: Arylation^a of alkenes (Heck reaction)

No.	Aryl halide	Alkenes	Coupling products	Time (h)	Conv. (%)	TOF ^b (h ⁻¹)
1				8	80	0.155
2				10	78	0.121
3				12	76	0.098
4				6	95	0.245
5				2	100	0.774

6				8	85	0.164
7				10	82	0.126
8				12	78	0.101
9				4	92	0.356
10				2	100	0.774
11				2	94	0.726
12				4	90	0.348
13				8	90	0.174
14				2	95	0.735
15				1	95	1.470
16				2	95	0.735
17				4	92	0.359
18				6	90	0.232
19				2	95	0.735



^a Reaction conditions: Pd(II)DHBP@SBA-15: 0.015 g; aryl halide: 1 mmol; alkenes : 1.2 mmol; Et₃N: 3.5 mmol; DMF: 3.5 ml; reaction temperature: 120 °C. ^b TOF [h⁻¹] = [the number of moles of reactant converted/the number of moles of metal active sites]/time in hours.

To test the efficiency of the Pd(II)DHBP@SBA-15 complex as a catalyst for hydrogenation reactions, aromatic olefins (styrene, α -methyl styrene), cyclic olefins (cyclohexene, cyclooctene, and 1, 4-cyclohexadiene), aliphatic olefins (1-undecene, 1-nonene) and bicycloolefin (bicyclo[2.2.1]-hepta-2,5-diene) were used as substrates (Table 4A.3, entries 1–8). All olefins showed 100% conversion under 15 minutes to give alkanes, under ambient reaction conditions (room temperature, H₂-pressure (5 bar) and MeOH as a solvent).

Table 4A.3: Hydrogenation^a of alkenes

No.	alkenes	alkanes	Conv. (%)	TOF ^b (min ⁻¹)
1			100	0.103
2			100	0.103
3			92	0.095
4			100	0.103
5			100	0.103
6	CH ₃ (CH ₂) ₈ CH=CH ₂	CH ₃ (CH ₂) ₈ CH ₂ CH ₃	100	0.103
7	CH ₃ (CH ₂) ₆ CH=CH ₂	CH ₃ (CH ₂) ₆ CH ₂ CH ₃	100	0.103
8			100	0.103

^aReaction conditions: Pd(II)DHBP@SBA-15: 0.015 g; olefins: 5 mmol; MeOH: 50 ml; H₂ Pressure: 5 bar; reaction temperature: 30 °C; reaction time: 15 min; ^b TOF [min⁻¹] = [the number of moles of reactant converted/the number of moles of metal active sites]/time in minutes.

4A.3.3. Heterogeneity tests

In order to check the stability and reusability of the Pd(II)DHBP@SBA-15 complex, the arylation and hydrogenation reactions of alkenes with styrene as the model substrate were performed under appropriate reaction conditions, which are presented in Table 4A.4. For the recyclability test, after each cycle, the catalyst was separated by filtration, washed with a suitable solvent and activated for 6 h at 150 °C in air before use in the next experiment. The synthesized catalyst showed good (fresh + four cycles) recyclability in arylation and hydrogenation reactions of alkenes with retention of conversion and selectivity up to three cycles. A ~14 % loss of conversion was observed from fresh cycle in hydrogenation and Heck reactions after fourth cycle due to the 1.5 wt% leaching of palladium metal from the fresh catalyst. However, all recycling studies reveal that the Pd based catalyst exhibits higher stability and heterogeneous nature in each and every step.

Table 4A.4: Recycling Study of Pd(II)DHBP@SBA-15 in arylation^a and hydrogenation^b reactions of alkenes

No of Cycles	Arylation (Styrene)		Hydrogenation (Styrene)	
	Conv.	Sele.	Conv.	Sele.
Fresh	80	100	100	100
I cycle	80	100	100	100
II cycle	78	99	97	99
III cycle	73	99	91	99
IV cycle	65	98	84	99

^a Reaction conditions: Pd(II)DHBP@SBA-15: 0.015 g; aryl halide: 1 mmol; alkenes : 1.2 mmol; Et₃N: 3.5 mmol; DMF: 3.5 ml; reaction temperature: 120 °C; reaction time: 8 h. ^b Reaction conditions: Pd(II)DHBP@SBA-15: 0.015 g; olefins: 5 mmol; MeOH: 50 ml; H₂ Pressure: 5 bar; reaction temperature: 30 °C; reaction time: 15 min.

4A.4. Conclusions

In conclusion, an efficient, simple and phosphine free Pd(II)DHBP@SBA-15 catalyst has been synthesized by tethering of the 2,2'-dihydroxybenzophenone (DHBP) ligand over amino-

functionalized SBA-15 via the post-grafting method and further metallation with Pd(II)(OAc)₂ resulted in a well-ordered mesostructure with a long range order. The synthesized catalysts were characterized by various characterization techniques like elemental analysis, XRD, N₂ sorption analyses, TG, DTA, FT-IR, solid state ¹³C and ²⁹Si NMR spectra, XPS, UV-Visible, SEM, EDAX and TEM. All characterization techniques proved that mesoporous SBA-15 and synthesized catalysts retained their structural integrity, textural properties, organic moieties, oxidation state, morphology and topographic characteristics after heterogenization. The catalytic activity of Pd(II)DHBP@SBA-15 was screened in arylation and hydrogenation reactions of alkenes, and the results show that Pd(II)DHBP@SBA-15 exhibits high conversion and selectivity towards arylation and hydrogenation reactions of alkenes in combination with high stability. The electronic (EWG & EDG effects) and steric effects (bulkier group) of groups on the substrates are also probed and the trend follows those reported in the literature. In addition, aliphatic olefins or less hindered olefins like acrylates gave better conversion and selectivity than aromatic olefins like substituted styrene. Due to these reasons, in the Heck reaction, 4-nitro-1-iodobenzene showed higher reactivity with ethyl acrylate to give the coupling products with 100% conversion and selectivity within 1 h. Moreover, in hydrogenation reactions, all olefins, except conjugated olefins, showed 100% conversion in less than 15 minutes to give alkanes, under mild conditions. The recyclability test was carried out to confirm the stability and the heterogeneous nature of the catalyst and the results concluded that Pd(II)DHBP@SBA-15 is reusable without much loss of activity for several cycles.

4B: Pd(II)-3-Allylsalicylaldiminophenol(ASIP)-SH@SBA-15 catalyst for amination reactions of aryl halides

4B.1. Introduction

The amination reactions of aryl halides,²⁸ named as C=N coupling reaction, is addressed to the most important and versatile reaction in fine chemical synthesis, in past decades.²⁹ The C=N moieties present in organic compounds are valuable in medicinal and natural products, and they exhibit some electronic and mechanical properties in certain materials. The construction of aryl carbon-aryl nitrogen bonds in organic chemistry were developed by Buchwald and Hartwig³⁰ using NHC-Pd complexes or Pd(0) catalysts and copper based classical Ullman and Goldberg³¹ coupling reactions. However, latter method going through harsh reaction conditions, long reaction time, laborious product purification and excess amount of copper catalyst make it an unfriendly process. To alleviate the shortcomings raised by the previously said catalysts or to synthesize environmentally friendlier catalysts, environmentally benign metals like iron³² and nickel³³ based NHC complexes have been developed. However, the formation of C=N bond via most feasible method is challenging one because of the involvement of harsh reaction conditions or the use of expensive catalysts.

The transition metal based amination reactions³⁴ are considered as a powerful and irreplaceable tool in last decades, for the synthesis of C=N bonds in synthetic organic chemistry, compared to other synthetic procedures. A variety of transition metal based catalysts such as Cu,³⁵ Pd,³⁶ Co,³⁷ Fe,³⁸ Rh,³⁹ Mn,⁴⁰ Ni⁴¹ and Cd⁴² have been reported for the previously said organotransformation reactions. However, out of these metal based catalysts, Pd based catalysts are efficient compared to other metal based catalysts because of high reactivity, lower metal waste and ambient reaction conditions during the reactions. In addition to Pd metal, different types of ligands are playing a crucial role in optimization of reaction conditions for the improvement of catalytic activity of the reactions. In past decades, different types of ligands were used for palladium based amination reactions of aryl halides, which include phosphine ligands⁴³ such as Josiphos, Xantphos, XPhos, Brettphos, and Ruphos, biaryl,³⁵ ferrocenyl-phosphine,⁴⁴ aryl-heteroaryl,⁴⁵ trialkylphosphine,⁴⁶ pincer,⁴⁷ Schiff base,⁴⁸ NHC,⁴⁹ amino-phosphine⁵⁰ and cyclometallated ligands.⁵¹ The phosphine based ligands exhibit several drawbacks such as cost, toxicity, recovery from the reaction mixture and thereby causing the

degradation of catalyst life. To surmount the limitations raised in the previously said ligands, the development of a simple and cost effective ligand is still a challenging area in these decades.

To compensate this, Schiff base ligand or salicylaldimine, one of the most widely utilized organic ligand due to its good coordination capacity, has been synthesized by simple condensation reaction between carbonyl compounds and amine compounds. In addition, salicylaldimines show good chelating ability with metal due to the number of coordination sites and their vacant sites is available for coordination of substrates in reaction medium. In this perspective, robust, highly stable and extendable 3-allylsalicylaldiminophenol based ligand (ASIP) has been used to tune the catalytic activity of synthesized catalysts in amination reactions. Among previously reported ligands, lengthen ASIP ligand provide more flexibility and expose more active sites from surface to channels of SBA-15 during the amination reactions. Moreover, in addition to nature of metal and ligand, length of linker group plays an important role in catalytic activity of organo-transformation reactions.⁵² To avoid the serious issues observed in homogeneous catalysis and to synthesize or heterogenize stable, robust Pd(II) based organofunctionalized catalyst, a silica support like SBA-15¹⁶ has been synthesized by P123 and TEOS. Moreover, Santha Barbara Amorphous (SBA-15) material provides higher wall thickness, hydrothermal stability with tunable textural properties than other mesoporous materials. The utility of SBA-15 in heterogeneous catalysis was explored by the surface modification of SBA-15 via. post grafting method of appropriate homogeneous ligand with metal precursor.

In this contest, our group tried to synthesize and characterize a novel, highly exposed and flexible 3-allylsalicylaldiminophenol ligand (ASIP) over modified SBA-15 with palladium metal, abbreviated as Pd(II)ASIP@SBA-15, for the synthesis of C=N bonds. The synthesized catalyst provides the free access of active Pd sites inside the channels of SBA-15, thereby increasing the catalytic activity of the reactions, due to the highly extendable organic chains from the surface of SBA-15. Hereby, we are trying to focus the monitoring of the reactions which was occurred in channels of SBA-15 rather than siloxane framework of SBA-15. The synthesis of Pd(II)ASIP@SBA-15 has been achieved by following steps; which includes SBA-15 synthesis, thiofunctionalization of SBA-15, anchoring of ASIP ligand over modified SBA-15 and finally, the complexation with Pd(II)(OAc)₂, respectively. The catalytic activity and selectivity of heterogeneous catalyst was evaluated and compared with the neat Pd(II)ASIP sites and Pd(II)(OAc)₂.

4B.2. Experimental

4B.2.1. Materials

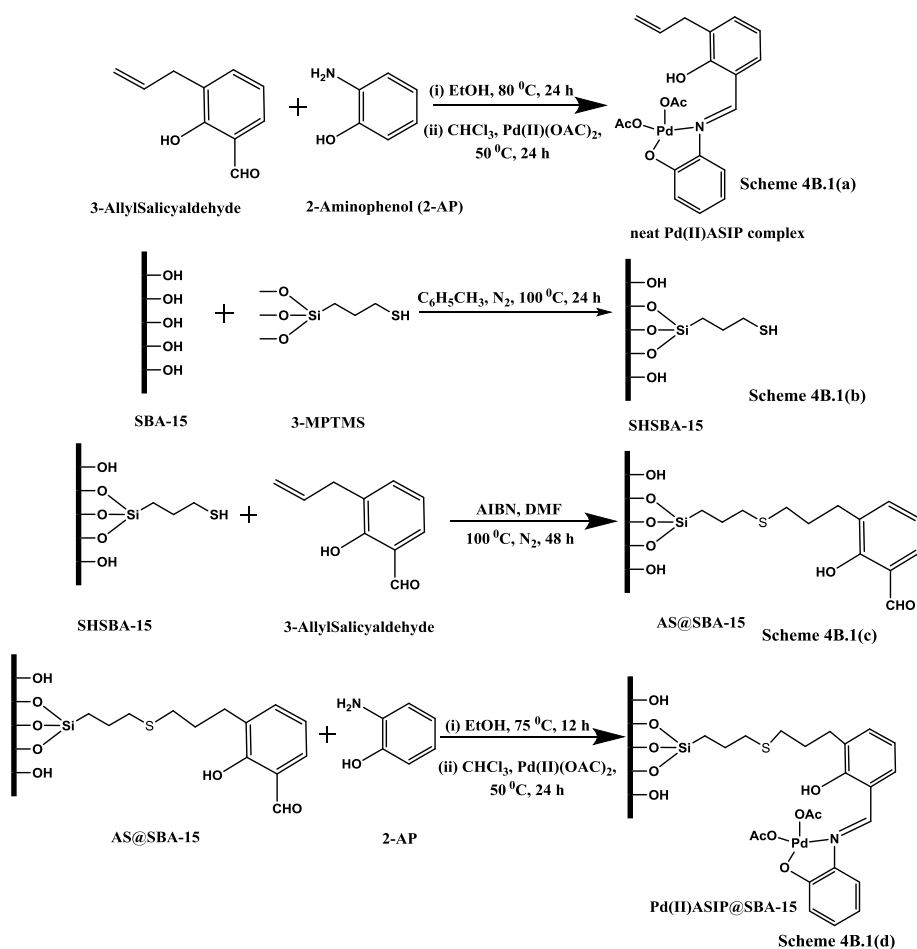
Tetraethylorthosilicate (TEOS), pluronic 123 (P123, Average Mol.Wt=5800), 3-mercaptopropyltrimethoxysilane (3-MPTMS), azobisisobutyronitrile (AIBN), 3-allylsalicylaldehyde, 2-aminophenol and palladium(II) acetate were purchased from Aldrich. In addition, substrates (reactants) such as aniline, 3-aminophenol, N-methyl aniline, hexylamine, 1-iodobenzene, 1-iodotoluene used for amination reactions of aryl halides were ordered by Aldrich. All the solvents and acids used for the synthesis and organic reactions were procured from Merck.

4B.2.2. Synthesis of thiofunctionalized SBA-15 (SHSBA-15)

The synthesis of mesoporous SBA-15⁵³ was carried out hydrothermally under the autogeneous pressure in an autoclave and detailed procedure mentioned in experimental part of Chapter 2. Thiofunctionalized SBA-15, SHSBA-15, was synthesized by the surface modification of silanol groups in SBA-15 using 3-mercaptopropyltrimethoxysilane (3-MPTMS) as organic modifier via post grafting method [Scheme 4B.1(b)]. The typical procedure for organofunctionalization of SBA-15 is following: 5 g of SBA-15 was suspended in 75 ml of dry toluene, and then, 2.0 g of 3-mercaptopropyltrimethoxysilane (3-MPTMS) was added into the solution under inert N₂ gas and refluxed for 12 h. The precipitate was filtered and washed with C₆H₅CH₃ and CH₂Cl₂. The as-synthesized material Soxhlet extracted with dichloromethane to remove any unwanted silylating reagent and was vacuum dried to attain SHSBA-15.²¹

4B.2.3. Synthesis of neat Pd(II)ASIP complex

The synthesis procedure of neat Pd(II)ASIP complex [Scheme 4B.1(a)] is following: (i) a reaction mixture of 3-allylsalicylaldehyde (4 mmol, 0.65 g) and 2-aminophenol (4 mmol, 0.44 g) in 25 ml ethanol was refluxed at 80 °C for 24 h. The solvent was evaporated and the residue was purified by recrystallization method by using ethanol. (ii) The purified salicylaldiminophenol ligand (2 mmol, 0.51 g) in 15 ml CHCl₃ was then refluxed with palladium(II)acetate (2 mmol, 0.45 g) at 75 °C for 24 h to attain the neat Pd(II)ASIP complex. ¹³C NMR (50 MHz, [D1] CDCl₃, 25 °C, TMS) 33 (C=C-CH₂); 115 (CH₂=C); 116-135 (CH in Ph); 136 (CH₂=C); 150 & 158 (C(OH) in Ph); 165 (C=N).



Scheme 4B.1: Preparation of Pd(II)-3-Allylsalicylaldiminophenol(ASIP)-SH@SBA-15 [Pd(II)ASIP@SBA-15]; synthesis of 4B.1(a) neat Pd(II)ASIP complex, 4B.1(b) SHSBA-15, 4B.1(c) AS@SBA-15 and 4B.1(d) Pd(II)ASIP@SBA-15.

4B.2.4. Synthesis of Pd(II)-3-Allylsalicylaldiminophenol(ASIP)-SH@SBA-15

Immobilization of 3-allylsalicylaldiminophenol ligand (ASIP) over thiofunctionalized SBA-15 was achieved in two steps: In the first step, a mixture of 3-allylsalicylaldehyde (0.0185 mol, 3 g) and azobisisobutyronitrile (AIBN, 0.0037 mol, 0.6 g) as radical initiator in 100 ml N,N'-dimethylformamide (DMF) were added into 6 g of SHSBA-15 which was dispersed in 20 ml of DMF at 250 ml round bottom flask. The reaction mixture was refluxed at 100 °C for 48 h under inert N₂ atmosphere, filtered, washed with DMF and then dichloromethane, and dried at vacuum to produce 3-allylsalicylaldehyde-SHSBA-15, AS@SBA-15 [Scheme 4B.1(c)] via. Thiol- Ene radical reaction.⁵⁴ In the second step, a mixture of 3 g AS@SBA-15 and 2-aminophenol (0.0061 mol, 0.6729 g) in 50 ml ethanol was refluxed at 80 °C for 24 h under N₂ inert atmosphere. The

solution was filtered, washed with ethanol and dichloromethane, and dried in vacuum to achieve 3-allylsalicylaldiminophenol-SHSBA-15, ASIP@SBA-15. Finally, to obtain Pd(II)ASIP@SBA-15 heterogenized catalyst [Scheme 4B.1(d)], 1.35 g of ASIP@SBA-15 was refluxed with the 25 ml of chloroform (CHCl_3) solution of palladium(II) acetate (0.0014 mol, 0.3112 g) at 75 °C for 24 h. The solution was filtered, washed with CHCl_3 and dried in vacuum. The whole synthetic procedure was adopted for the synthesis of Pd(II)ASIP@SiO₂ by using non-porous SiO₂ instead of porous SBA-15 material.

4B.2.5. Amination reactions of aryl halides (>C-N Coupling reactions)

Synthesis of benzonitriles or arylamines, via. amination reaction of aryl halides, are significant attention in synthetic organic chemistry. Amination of aryl halides were performed in a 25 ml RB fitted with condenser and magnetic stirrer and used as triethylamine as base. Typically, a mixture of suitable catalysts such as Pd(II)ASIP@SBA-15 (0.060 g) or neat Pd(II)ASIP complex (0.030 g) or Pd(OAc)₂ (0.015 g), aryl halide (1 mmol), amines (2 mmol), Et₃N (3.5 mmol) and DMF (3.5 ml) was heated at 120 °C for 24 h. The reaction samples were taken from R.B at appropriate intervals of time, cooled and analyzed by using Agilent 68909 N GC with HP-1 capillary column and FID.

4B.3. Results and discussions

4B.3.1. Characterizations

4B.3.1.1. X-ray Diffraction (XRD)

The synthesized catalysts were characterized by different type of physicochemical, spectroscopic and microscopic characterization techniques which confirmed the successful anchoring of organic moieties on modified SBA-15, and the results are discussed below. The XRD pattern of (a) as-synthesized SBA-15 (b) SBA-15 (c) SHSBA-15 and (d) Pd(II)ASIP@SBA-15 are represented in Fig. 4B.1. The powder X-ray diffraction (PXRD) has been used to find out the unit cell parameter, uniqueness and degree of orderedness of mesoporous catalysts. In XRD pattern, three reflections in SBA-15, (100), (110) and (200) reflections, was observed at $2\theta = 0.92^\circ$, 1.5° and 1.8° , respectively, indicating the formation of highly ordered 2-D hexagonal mesoporous materials.¹⁹ (110) reflection is more intense than (200) reflection in all synthesized materials due to the complete condensation of wall structure at higher temperatures used in

multi-synthetic procedures. Moreover, the peak intensity of (100) plane in calcined SBA-15 [Fig. 4B.1(b)] is greater than peak intensity of (100) plane in as-synthesized SBA-15 due to the complete surfactant removal from the uncalcined SBA-15 samples. In the spectrum of SHSBA-15 and Pd(II)ASIP@SBA-15 [Fig. 4B.1(c and d)], intensities of peaks decreasing due to the proper loading of organic modifier and the neat ASIP moieties on calcined SBA-15.

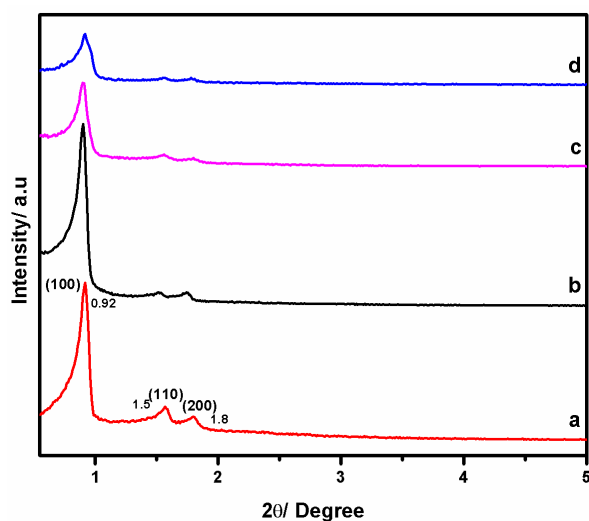


Fig. 4B.1: The XRD pattern of (a) as-synthesized SBA-15 (b) calcined SBA-15 (c) SHSBA-15 and (d) Pd(II)ASIP@SBA-15.

4B.3.1.2. N₂-Sorption analyses

Fig. 4B.2 represents the N₂ sorption isotherm and pore size distribution curves (inset) of (a) SBA-15 (b) SHSBA-15 and (c) Pd(II)ASIP@SBA-15. Isotherm exhibit type-IV with H1 hysteresis indicating the formation of highly ordered mesoporous silica materials, 2-50 nm.²⁰

Table 4B.1: Textural properties^a of calcined SBA-15, SHSBA-15 and Pd(II)ASIP@SBA-15

Sample	a_0^b [Å]	SA [m ² /g]	Dp [Å]	Vp [cc/g]	ω_t^c (Å)
SBA-15	101.73	747	60	1.14	41.73
SHSBA-15	102.25	560	58	0.82	44.25
Pd(II)ASIP@SBA-15	103.01	474	52	0.76	51.01

^a a_0 , Unit Cell parameter; SA, BET Surface Area; Dp, Pore Diameter; Vp, Pore Volume; ω_t , Wall Thickness; Pd content= ~4.75 Wt% (EDAX); b $a_0=2d_{100}/1.73$; c $\omega_t= a_0 \cdot Dp$.

The BET surface area, pore volume and pore diameter of SBA-15, SHSBA-15 and Pd(II)ASIP@SBA-15 were found to be 747 m²/g, 1.14 cc/g, 60.0 Å; 560 m²/g, 0.82 cc/g, 58.0 Å and 474 m²/g, 0.76 cc/g, 52.0 Å, respectively (Table 4B.1). The surface area, pore diameter and the pore volume of Pd(II)ASIP@SBA-15 were decreased from calcined SBA-15 due to the successful anchoring of organic modifier group and neat homogeneous complex on SBA-15.

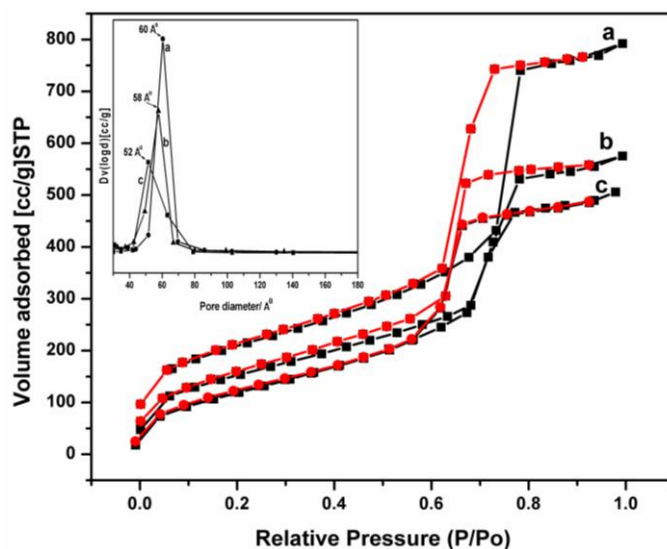


Fig. 4B.2: N₂ adsorption-desorption isotherm and pore size distribution curves (inset) of (a) calcined SBA-15 (b) SHSBA-15 and (d) Pd(II)ASIP@SBA-15.

4B.3.1.3. Thermal analyses (TG and DTA)

TGA and DTA analyses were used to find out the thermal stability, adsorbed moisture and the possible decomposition of volatile organomoieties in the nanostructured catalysts. The TG (Fig. 4B.3 A) and DTA (Fig. 4B.3 B) analyses of (a) as-synthesized SBA-15 (b) SBA-15 (c) SHSBA-15 and (d) Pd(II)ASIP@SBA-15 were carried out in the presence of air in the range of 30 °C to 1000 °C at 10 °C/min. In as-synthesized SBA-15, 45% weight loss was observed in TG analysis [Fig. 4B.3 A(a)] and an exothermic peak in DTA [Fig. 4B.3 B(a)], in the region of 169 °C to 220 °C, indicating the fully decomposition of unreacted surfactants. A 7% weight loss was observed in parent SBA-15 at TGA analysis [Fig. 4B.3 A(b)] owing to the physisorbed water molecule and the absence of any other peak in DTA [Fig. 4B.3 B(b)] confirmed the fully recovery of unreacted structure directing agents from the as-synthesized SBA-15. In the case of SHSBA-15, 12% weight loss was observed in TG analysis, being 5% greater than weight loss observed in

parent SBA-15, which indicates the successful anchoring of thiopropyl group on calcined SBA-15. In the DTA analysis, thiofunctionalized SBA-15, the decomposition of thiopropyl moieties from SHSBA-15 at 350 °C is evident. Finally, in Pd(II)ASIP@SBA-15, 20% of weight loss in TG analysis, being greater than the loss observed for the SHSBA-15, strongly support a 8% loading of neat Pd(II)ASIP sites on calcined SBA-15. Likewise in TG analysis, a number of peaks in DTA analysis in the region of 250 °C to 450 °C and 620 °C, indicates the complete decomposition of the neat Pd(II)ASIP which was anchored on SBA-15. All decomposition results shown in thermal analyses (TG and DTA) prove that organomodifier and the neat complexes were successfully anchored on SBA-15.

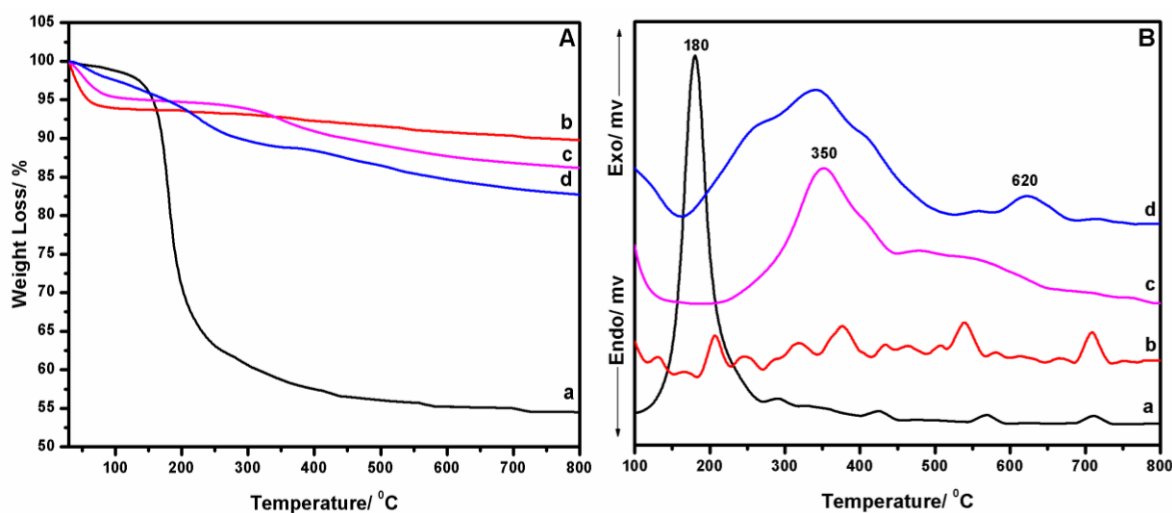


Fig. 4B.3: TGA (A) and DTA (B) pattern of (a) as-synthesized SBA-15 (b) calcined SBA-15 (c) SHSBA-15 and (d) Pd(II)ASIP@SBA-15.

4B.3.1.4. Fourier Transform Infrared Spectroscopy (FT-IR)

FT-IR spectra of (a) as-synthesized SBA-15, (b) parent SBA-15, (c) SHSBA-15, (d) the neat Pd(II)ASIP complex and (e) Pd(II)ASIP@SBA-15 are shown in Fig. 4B.4 which provides an idea regarding the nature of silanol groups and organomoieties on SBA-15. The peaks in IR spectrum corresponds to the asymmetric and symmetric -CH stretching vibrations of surfactant molecules present in as-synthesized SBA-15 [Fig. 4B.4(a)] at 2985 cm^{-1} and 2897 cm^{-1} , respectively. A broad band at 3450 cm^{-1} and sharp band at 1625 cm^{-1} , in calcined SBA-15 [Fig. 4B.4(b)], represent the -OH stretching and bending vibrations of surface silanol groups on SBA-15.²¹ In addition, after calcination, the observed peaks due to unreacted surfactants in the as-

synthesized SBA-15 were absent. The successful anchoring of organic modifier, 3-mercaptopropyltrimethoxy silane (3-MPTMS), on SBA-15 was confirmed by the observance of peaks at 2985 cm^{-1} and 2897 cm^{-1} , in SHSBA-15 [Fig. 4B.4(c)], due to the stretching vibrations of $-\text{CH}_2$ groups in 3-MPTMS.²¹ Finally, in the case of the neat Pd(II)ASIP complex [Fig. 4B.4(e)] and Pd(II)ASIP@SBA-15 [Fig. 4B.4(d)], a strong peak at 1640 cm^{-1} corresponds to the $-\text{C}=\text{N}$ stretching vibrations of the imine group. Moreover, additional peaks at 750 cm^{-1} and in the range of 1200 cm^{-1} to 1500 cm^{-1} are representative of the C-H bending and C=C stretching vibrations, respectively, of benzene groups.²² The bands at 790 cm^{-1} , 1100 cm^{-1} and 950 cm^{-1} due to the symmetric and asymmetric stretching vibrations of Si-O bond and $\nu(\text{Si-OH})$ vibrations, respectively, in silica framework were observed in all synthesized materials [Fig. 4B.4(a-d)].¹⁷ The FT-IR results analytically proves that organomoieties, which is originated from the organomodifier and the ASIP sites, were successfully immobilized on parent SBA-15.

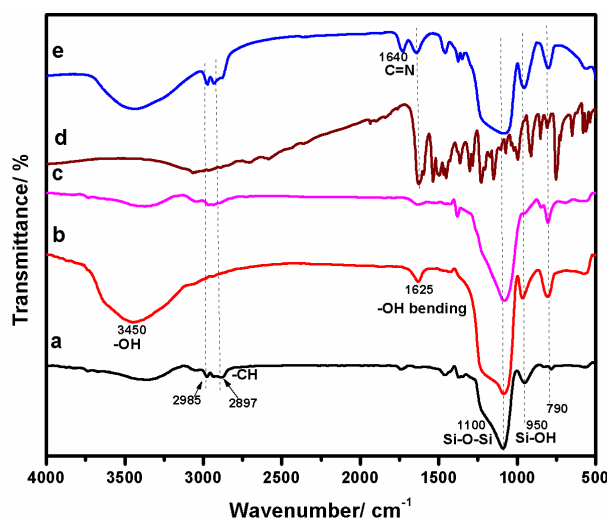


Fig. 4B.4: FTIR spectra of (a) as-synthesized SBA-15 (b) calcined SBA-15 (c) SHSBA-15 (d) the neat Pd(II)ASIP complex and (e) Pd(II)ASIP@SBA-15.

4B.3.1.5. Solid state ^{13}C NMR Spectroscopy (^{13}C CP MAS NMR)

Further, organomoieties anchored on SBA-15 were confirmed by solid state ^{13}C NMR spectra for SHSBA-15 and Pd(II)ASIP@SBA-15 and are plotted in Fig. 4B.5. The peaks at 23, 12 and 27 ppm correspond to the carbon atoms, C_1 , C_2 & C_3 , respectively, of propyl chain in 3-MPTMS, indicating the formation of thiofunctionalized SBA-15, SHSBA-15 [Fig. 4B.5(a)].²¹ After immobilization, the peaks in the range of 30-40 ppm are assigned to carbon atoms (C_4, C_5 & C_6)

which is observed between sulfur atom and aromatic ring of Pd(II)ASIP@SBA-15 catalyst. In addition, the carbon atoms of arene rings of 3-allylsalicylaldiminophenol ligand (ASIP) are ascribed to the peaks in the range of 120-140 ppm (asterisk, *). Moreover, the peaks at 160 ppm and 165 ppm (dash, #) are represented to -CH(OH) group in phenyl ring and -C=N bond in imine group, respectively. All chemical shifts observed in solid state ^{13}C NMR spectra reveal that the grafting of organomoties on SBA-15 has been done successfully.

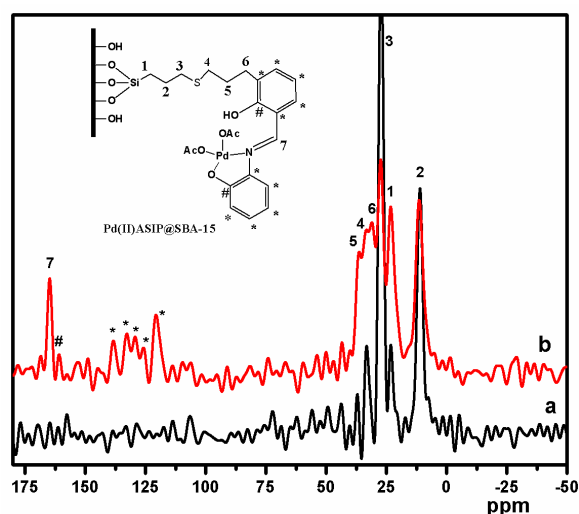


Fig. 4B.5: Solid state ^{13}C NMR spectra of (a) SHSBA-15 and (b) Pd(II)ASIP@SBA-15

4B.3.1.6. Solid state ^{29}Si NMR Spectroscopy (^{29}Si CP MAS NMR)

^{29}Si CP MAS NMR spectra, gave the degree of organofunctionalization of surface silanol groups on SBA-15, of (a) SBA-15, (b) SHSBA-15 and (c) Pd(II)ASIP@SBA-15 are depicted in Fig. 4B.6. In all synthesized catalysts [Fig. 4B.6 (a-c)], a broad peak in the region of -90 ppm to -125 ppm corresponds to the Si-O-Si and Si-OH bonds in silicon framework of SBA-15. Briefly, Q^n sites such as Q^4 , Q^3 and Q^2 corresponds to siloxane $[(\text{SiO})_4\text{Si}]$, single silanol $[(\text{SiO})_3\text{Si}(\text{OH})]$ and geminal silanol $[(\text{SiO})_2\text{Si}(\text{OH})_2]$ were centred at -112 ppm, -102 ppm and -92 ppm, respectively.¹⁸ The peaks at -63 ppm and -55 ppm, indicate T^3 $[(\text{SiO})_3\text{SiR}]$ and T^2 $[(\text{SiO})_2\text{Si}(\text{OH})\text{R}]$ signals, which represent the organofunctionalized silicon atoms in 3-MPTMS. These were observed in SHSBA-15 [Fig. 4B.6(b)] and Pd(II)ASIP@SBA-15 [Fig. 4B.6(c)]. Thus solid state ^{29}Si MAS NMR spectroscopy gave evidence for the stability of Si-C bond and the nature of highly ordered siloxane network with the grafted organomoties in Pd(II)ASIP@SBA-15.

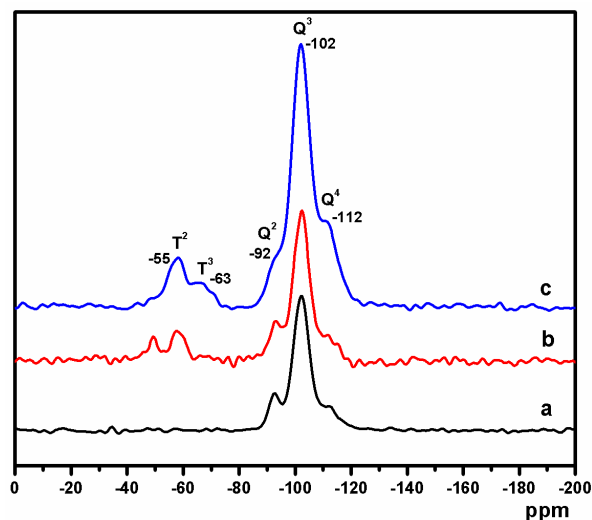


Fig. 4B.6: ^{29}Si NMR spectra of (a) SBA-15 (b) SHSBA-15 and (c) Pd(II)ASIP@SBA-15

4B.3.1.7. X-ray Photoelectron Spectroscopy (XPS)

The oxidation state and chemical environment of synthesized catalysts was determined by X-ray photoelectron spectroscopy. The XPS spectra of Pd3d core levels of (a) the neat Pd(II)ASIP complex and (b) Pd(II)ASIP@SBA-15 are plotted in Fig. 4B.7. Pd $3d_{5/2}$ and Pd $3d_{3/2}$ spin orbit component of neat Pd(II)ASIP sites [Fig. 4B.7(a)] and Pd(II)ASIP@SBA-15 [Fig. 4B.7(b)] were centred at 337.5 eV and 343.3 eV, respectively, indicating that palladium exist in $+2$ oxidation state in both catalysts.⁵³ All binding energy values were calibrated with C1s peak located at 285 eV as standard reference.

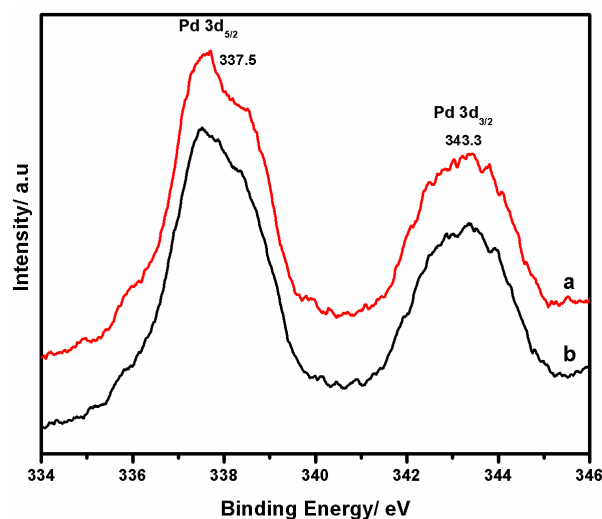


Fig. 4B.7: XPS spectra of (a) the neat Pd(II)ASIP complex and (b) Pd(II)ASIP@SBA-15.

4B.3.1.8. DR UV-Visible Spectroscopy (DR UV-Vis)

The DR UV-Visible spectra of (a) SBA-15, (b) SHSBA-15 and (c) Pd(II)ASIP@SBA-15 are shown in Fig. 4B.8. A peak at 220 nm corresponds to the siliceous nature of all synthesized materials [Fig. 4B.8 (a-c)].⁵³ The two strong peaks at 260 nm and 432 nm are assigned to $\pi \rightarrow \pi^*$ and $n \rightarrow \pi^*$ transitions of $>C=N$ group,⁵³ respectively, in Pd(II)ASIP@SBA-15 catalyst [Fig. 4B.8(c)]. Moreover, a peak at 338 nm represent $\pi \rightarrow \pi^*$ transitions of benzene ring⁵³ present in ASIP ligand [Fig. 4B.8(c)]. In addition, a weak band owing to the nitrogen to Pd(II) and oxygen to Pd(II) ligand to metal charge transfer transitions (LMCT) were observed at 522 nm. Thus, the UV-Vis spectrum indicates that 3-allylsalicylaldiminophenol (ASIP) ligand was covalently anchored on SBA-15 with sustainable $+2$ oxidation state.

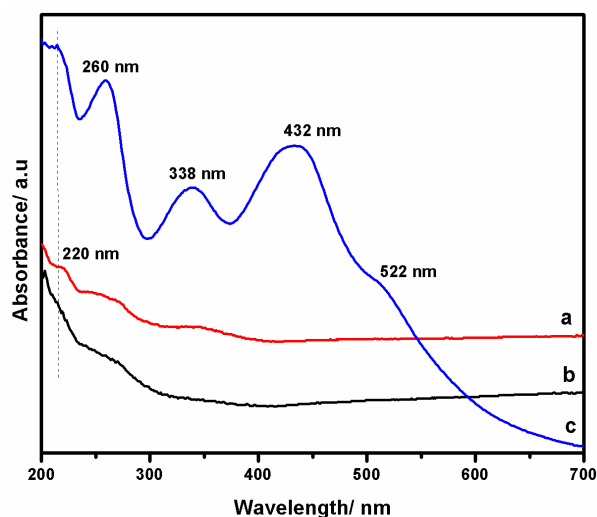


Fig. 4B.8: UV-Vis spectra of (a) calcined SBA-15 (b) SHSBA-15 and (c) Pd(II)ASIP@SBA-15

4B.3.1.9. Scanning Electron Microscopy (SEM)

The SEM images of (a) parent SBA-15 and (B) Pd(II)ASIP@SBA-15 are plotted in Fig. 4B.9. Both materials, SBA-15 and Pd(II)ASIP@SBA-15, exhibit plate type structure with hexagonal morphology and particle size in the region of 1-1.4 μm . The parallel fringes (morphology) of Pd(II)ASIP@SBA-15 was intact compared to SBA-15 even after the immobilization of Pd(II)ASIP sites on thiofunctionalized SBA-15.

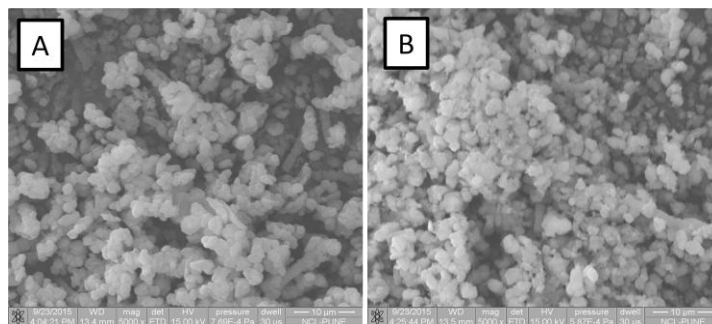


Fig. 4B.9: SEM images of (A) calcined SBA-15 and (B) Pd(II)ASIP@SBA-15.

4B.3.1.10. Transmission Electron Microscopy (TEM)

Fig. 4B.10 represents the TEM images of (a) SBA-15 and (B) Pd(II)ASIP@SBA-15 and it clearly reveals that the synthesized materials have hexagonal type uniform channels with well defined 1-D channels.

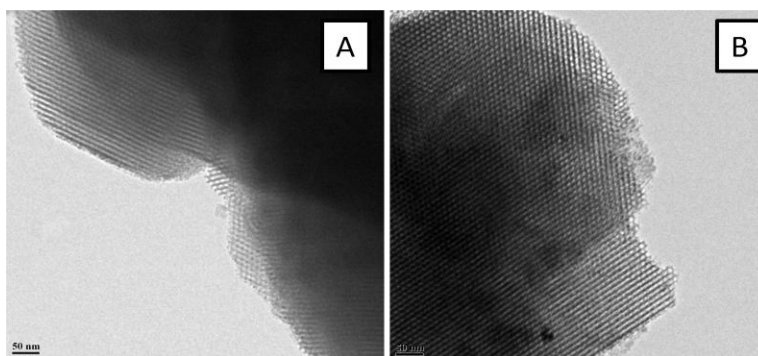


Fig. 4B.10: TEM images of (A) calcined SBA-15 and (B) Pd(II)ASIP@SBA-15

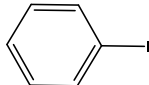
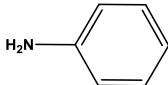
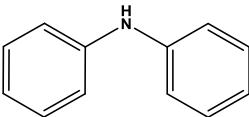
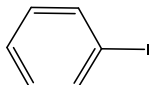
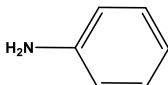
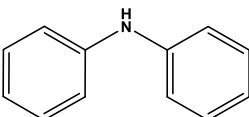
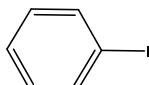
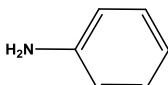
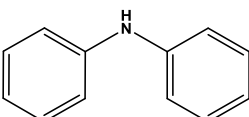
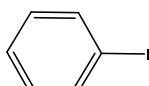
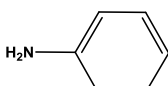
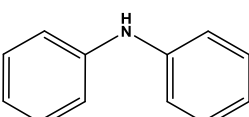
4B.3.2. Catalytic activity

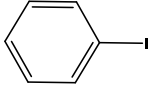
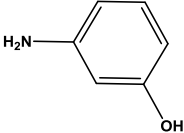
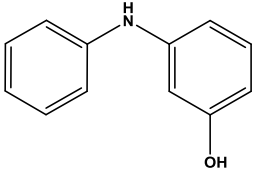
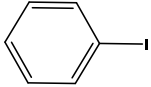
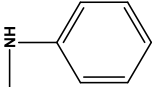
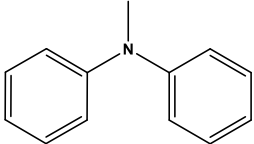
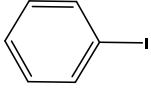
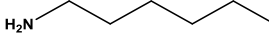
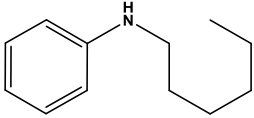
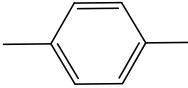
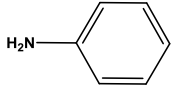
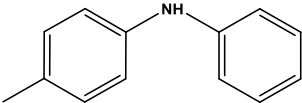
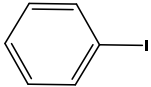
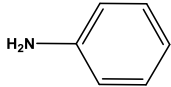
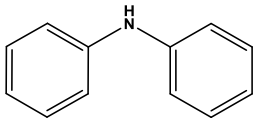
Catalytic activity of Pd(II)ASIP@SBA-15 catalyst was evaluated in heterogeneous amination reactions of aryl halides and showed that it is highly efficient, stable and reusable towards amination reactions. Amination of aryl halides, called as $>C-N$ coupling reactions, where various amines such as aromatic amines, secondary amines and aliphatic amines were coupled with aryl halides to produce benzonitrile compounds, using triethylamine as a base and DMF as a solvent. The various amines like aniline, 3-aminophenol, N-methyl aniline and n-hexyl amine and aryl halides such as iodobenzene and 1-iodotoluene were used as reactants in $>C-N$ coupling reactions. The catalytic activity results of blank reaction, Pd(OAc)₂, neat Pd(II)ASIP complex and Pd(II)ASIP@SBA-15 are included in Table 4B.2 (entries 1-8).

In the case of Pd(II)ASIP@SBA-15 (Table 4B.2), aromatic amines (entries 4, 5) and secondary amine (entry 6) show higher conversion (82%-96%) than aliphatic amine (entry 7,

conv. 78%). In addition, substituted aromatic amine like 3-aminophenol exhibits higher conversion (96%) than unsubstituted aromatic amines (82%-85%). Further, 1-iodotoluene, a substituted aryl halide, (entry 8) reacts with aniline very slowly to give 64% conversion at 24 h possibly due to the steric effect of methyl groups. However, Pd(II)ASIP@SBA-15 catalyst exhibits moderate turnover frequency (TOF) in amination reactions, in the range of 1.2-1.8 h⁻¹. In addition, this heterogeneous catalyst shows 100% selectivity towards secondary amines due to the ordered mesoporous system. Amination reactions did not show any products when the reactions were carried out in the absence of catalyst (Table 4B.2, entry 1). The neat Pd(II)ASIP complex and Pd(OAc)₂ exhibited comparatively similar conversion (Table 4B.2, entries 2 & 3) and lower selectivity (~90%) compared to the Pd(II)ASIP@SBA-15 catalyst due to the formation of tertiary amine. To check the importance of ordered and disordered catalytic system, non-porous Pd(II)ASIP@SiO₂ catalyst was synthesized and applied in amination reactions. The results shows that a mixture of secondary (90%) and tertiary amines (10%) were formed as products (Table 4B.2, entry 9), due to the concomitant overalkylation reactions⁵⁵ was occurring in amination reactions of aryl halides, compared to ordered Pd(II) ASIP@SBA-15 catalyst.

Table 4B.2: Amination of arylhalides^a (>C-N coupling reactions) using Pd(II)ASIP@SBA-15

No	Aryl halides	Amines	benzonitriles	Time (h)	Conv. (%)	TOF ^f (h ⁻¹)
1 ^b				20	0	-
2 ^c				20	80	0.61
3 ^d				20	82	2.30
4				20	82	1.53

5				20	96	1.79
6				20	85	1.59
7				20	78	1.46
8				24	64	1.20
9 ^e				20	78	1.50

(a) Reaction conditions Pd(II)ASIP@SBA-15: 0.060 g, aryl halide: 1 mmol, amines : 2 mmol, Et₃N: 3.5 mmol, DMF: 3.5 ml, reaction temperature: 120 °C; (b) without catalyst; (c) Pd(OAc)₂: 15 mg; (d) neat Pd(II)ASIP complex: 30 mg; (e) Pd(II)ASIP@SiO₂: 0.060 g; (f) TOF= [% of conversion*mmol of substrate/mmol of catalyst* time in h].

4B.3.3. Recyclability and Sheldon hot filtration test

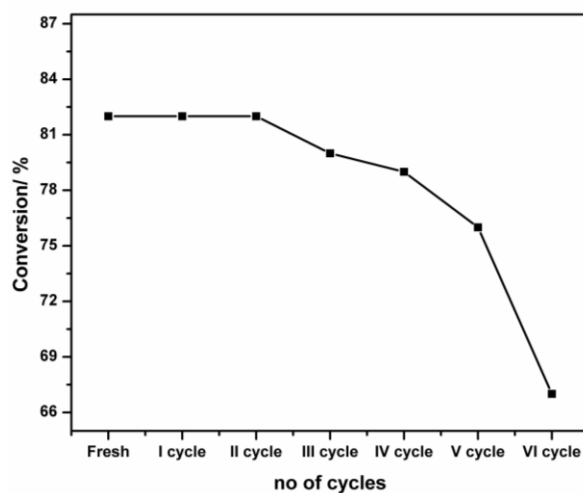


Fig. 4B.11: Recycling study of Pd(II)ASIP@SBA-15 in amination reactions of aryl halides

The recycling studies of Pd(II)ASIP@SBA-15 catalyst for amination (>C-N coupling) reactions were performed and shown in Fig. 4B.11. Pd(II)ASIP@SBA-15 could be recycled several times (fresh + six cycles) without much loss of catalytic activity. After reaction workup in fresh cycle, the catalyst was recovered by centrifugation, washed and pre-treated for 6 h at 150 °C before use in next cycle. A ~15% loss of conversion was observed in amination reactions after sixth cycles due to the loss of Pd (~1.4 wt%) from the fresh catalyst. All results confirm that Pd(II)ASIP@SBA-15 shows good stability and heterogeneous nature in organic reactions.

In addition, to check the heterogeneous nature and leaching out of palladium metal from Pd(II)ASIP@SBA-15 catalyst, Sheldon hot filtration test in amination reactions was carried out. The results shows that virtually there is no palladium leaching out from Pd(II)ASIP@SBA-15 under appropriate amination reaction conditions. At first, fresh cycle of amination reaction was carried out for comparison with Sheldon hot filtration test which is plotted in Fig. 4B.12. To perform the Sheldon hot filtration test, Pd(II)ASIP@SBA-15 catalyst in reaction medium was filtered out after 12 h during the reaction and filtrate solution again charged into round bottom flask without catalyst, reaction was continued up to 20 h. The conversion plot in Fig. 4B.12 doesn't show any drastic increase in conversion after 12 h which indicating the negligible amount of palladium metal leaching out from Pd(II)ASIP@SBA-15 catalyst.

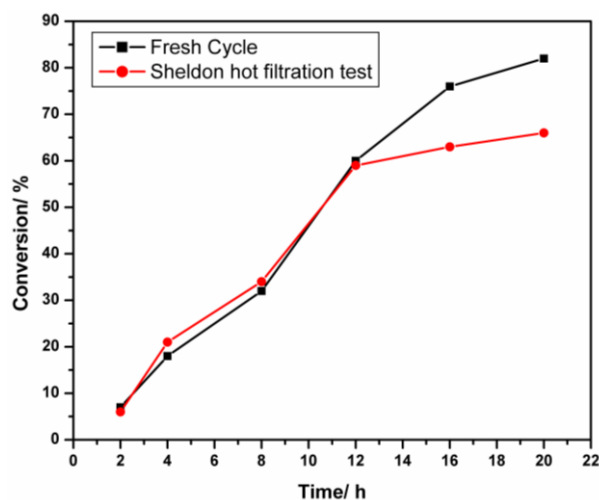


Fig. 4B.12: Sheldon hot filtration test in amination of aryl halides

4B.4. Conclusions

In conclusion, Pd(II)ASIP@SBA-15 catalyst has been synthesized by covalent anchoring of two ligands, namely, 3-allylsalicylaldehyde and 2-aminophenol, respectively, in a step by step manner, on thiofunctionalized SBA-15. This gave favourable coordination sites for metallation of Pd(II)(OAc)₂ and flexibility to lengthen the chain of organomoieties from surface to channels in SBA-15. All synthesized materials were characterized by CHN analysis, PXRD, Nitrogen sorption analyses, TG & DTA, FTIR, ¹³C and ²⁹Si CP MAS NMR spectra, XPS, UV-Visible, SEM, EDAX and TEM and gave a clear indication of mesoporosity, thermal stability, morphology, and organo-functionality of Pd(II)ASIP@SBA-15 materials. Heterogeneous amination reactions of aryl halides were catalyzed by Pd(II)ASIP@SBA-15 catalyst and compared with the neat Pd(II)ASIP complex, Pd(II)(OAc)₂ and blank reaction. The results showed that Pd(II)ASIP@SBA-15 exhibited similar conversion compared with neat Pd(II)ASIP complex and Pd(II)(OAc)₂. Eventually, the recycling studies of Pd(II)ASIP@SBA-15 was carried out for several cycles (fresh + six cycles) which showed good mechanical stability to confirm the heterogeneous nature of Pd(II)ASIP@SBA-15 catalyst.

4A&B. References

1. Y. Liu, S-S. Wang, W. Liu, Q -X. Wan, H-H. Wu, G.-H. Gao, *Curr. Org. Chem.*, 2009, **13**, 1322.
2. V. Polshettiwar, C. Len, A. Fihri, *Coord. Chem. Rev.*, 2009, **253**, 2599.
3. P. Lu, J. Lu, H. You, P. Shi, Dong, *J. Prog. Chem.*, 2009, **21**, 1434.
4. M. Seki, *Synthesis*, 2006, 2975.
5. a) C. Amatore, A. Jutand, M. Amine, M. Barki, *Organometallics*, 1992, **11**, 3009; b) H. A. Dieck and R. F. Heck, *J. Org. Chem.*, 1975, **40**, 1083;
6. a) A. Zapf, M. Beller, *Top. Catal.*, 2002, **19**, 101; b) L. X. Yin, J. Liebscher, *Chem. Rev.*, 2007, **107**, 133.
7. I. P. Beletskaya, A. V. Cheprakov, *Chem. Rev.*, 2000, **100**, 3009.
8. a) R. F. Heck, *Org. React.*, 1982, **27**, 345; b) R. F. Heck, *Palladium Reagents in Organic Synthesis*, Academic Press, Orlando, FL, 1985.

9. a) C. M. Crudden, M. Sateesh, R. Lewis, *J. Am. Chem. Soc.*, 2005, **127**, 10045; b) J. Horniakova, T. Raja, Y. Kubota, Y. Sugi, *J. mole. Cata. A: Chem.*, 2004, **217**, 73; c) P. Sharma, A. P. Singh, *Catal. Sci. & Tech.*, 2014, **4**, 2978.
10. a) A. Modak, J. Mondal, V. K. Aswal, A. Bhaumik, *J. Mater. Chem.*, 2010, **20**, 8099.
11. a) A. Modak, J. Mondal, A. Bhaumik, *Green Chemistry*, 2012, **14**, 2840.
12. a) K-I. Shimizu, S. Koizumi, T. Hatamachi, H. Yoshida, S. Komai, T. Kodama, Y. Kitayama, *J. Catalysis.*, 2004, **228**, 141; b) K. Yu, W. Sommer, J. M. Richardson, M. Weck, C. W. Jones, *Adv. Synth. Catal.*, 2005, **347**, 161.
13. a) O. Schmidt, *Chem. Rev.*, 1933, **12**, 363; b) R. A. W. Johnstone, A. H. Wilby, I. D. Entwistle, *Chem. Rev.*, 1985, **85**, 129; c) C. M. Crudden, D. Allen, M. D. Mikoluk, J. Sun, *Chem. Commun.*, 2001, 1154.
14. a) L. Wang, M. Jia, S. Shylesh, T. Philippi, A. Seifert, S. Ernst, A. P. Singh, W. R. Thiel, *ChemCatChem*, 2010, **11**, 1477; b) L. Wang, A. Reis, A. Seifert, T. Philippi, S. Ernst, M. Jia, W. R. Thiel, *Dalton Transactions*, 2009, 3315.
15. a) V. P. W. Bohm, C. W. K. Gstottmayr, T. Weskamp, W. Herrmann, *J. Organomet. Chem.*, 2000, **595**, 186; b) B. Tao, D. W. Boykin, *Tetrahedron Letters*, 2002, **43**, 4955; c) D. A. Alonso, C. Najera, M. C. Pacheco, *Org. Lett.*, 2000, **2**, 1823; d) B. Bedford, C. S. Cazin, *Chem. Commun.*, 2001, 1540; e) G. A. Grasa, A. C. Hillier, S. P. Nolan, *Org. Lett.*, 2001, **3**, 1077; f) S. R. Borhade, S. B. Waghmode, *Tetrahedron Letters*, 2008, **49**, 3423.
16. D. Zhao, J. Feng, Q. Huo, N. Melosh, G. H. Fredrickson, B. F. Chmelka, G. D. Stucky, *Science*, 1998, **279**, 548.
17. A. Lazar, P. Sharma, A. P. Singh, *Micropore. Mesopore. Mater.*, 2013, **170**, 331.
18. P. Sharma, A. Lazar, A. P. Singh, *Appl. Catal. A: Gen.*, 2012, **439–440**, 101.
19. D. Zhao, Q. Huo, J. Feng, B. F. Chmelka, G. D. Stucky, *J. Am. Chem. Soc.*, 1998, **120**, 6024.
20. R. Ryoo, I. -S. Park, S. Jun, C. W. Lee, M. Kruk, M. Jaroniec, *J. Am. Chem. Soc.*, 2001, **123**, 1650.
21. P. Sharma, A. P. Singh, *RSC Advances*, 2014, **4**, 58467.
22. A. Lazar, W. R. Thiel, A. P. Singh, *RSC Advances*, 2014, **4**, 14063.
23. A. G. S. Prado, C. Airoidi, *J. Colloid Interface Sci.*, 2001, **236**, 161.

24. M. D. Alba, Z. Luan, J. Klinowski, *J. Phys. Chem.*, 1996, **100**, 2178.
25. S. Shylesh, A. P. Singh, *J. Catal.*, 2004, **228**, 333.
26. B. I. Ceylan, Y. D. Kurt, B. Ulkuseven, *J. Coord. Chem.*, 2009, **62**, 757.
27. J. H. Enemark, C. G. Young, *Adv. Inorg. Chem.*, 1993, **40**, 1.
28. J. Bariwal, E. Van der Eycken, *Chem. Soc. Rev.*, 2013, **42**, 9283.
29. N. C. Bruno, M. T. Tudge, S. L. Buchwald, *Chem. Sci.*, 2013, **4**, 916.
30. a) D. S. Surry, S. L. Buchwald, *Chem. Sci.*, 2011, **2**, 27; b) J. F. Hartwig, *Nature* 2008, **455**, 314; c) B. P. Fors, S. L. Buchwald, *J. Am. Chem. Soc.*, 2010, **132**, 15914.
31. a) F. Ullmann, *Ber. Dtsch. Chem. Ges.*, 1903, **36**, 2382; b) I. Goldberg, *Ber. Dtsch. Chem. Ges.*, 1906, **39**, 1691.
32. a) A. Correa, C. Bolm, *Angew. Chem. Int. Ed.*, 2007, **46**, 8862; (b) A. Correa, S. Elmore, C. Bolm, *Chem. Eur. J.*, 2008, **14**, 3527.
33. a) S. Nagao, T. Matsumoto, Y. Koga, K. Matsubara, *Chem. Lett.*, 2011, **40**, 1036; b) J. P. Wolfe, S. L. Buchwald, *J. Am. Chem. Soc.*, 1997, **119**, 6054.
34. a) S. V. Lev, A. W. Thomas, *Angew. Chem. Int. Ed.*, 2003, **42**, 5400; (b) B. C. Ranu, R. Dey, T. Chatterjee, S. Ahammed, *ChemSusChem*, 2012, **5**, 22.
35. a) A. A. Kelkar, N. M. Patil, R. V. Chaudhari, *Tetrahedron Lett.*, 2002, **43**, 7143; b) F.Y. Kwong, S. L. Buchwald, *Org. Lett.*, 2003, **5**, 793; (c) L. Zhu, P. Geo, G. Li, J. Lan, R. Xie, J. You, *J. Org. Chem.*, 2007, **72**, 8535.
36. a) Sk. M. Islam, N. Salam, P. Mondal, A. S. Roy, *J. Mol. Cata. A: Chem.*, 2013, **366**, 321; b) M. J. Bhanushali, N. S. Nandurkar, M. D. Bhor, B. M. Bhanage, *J. Mol. Catal. A: Chem.*, 2006, **259**, 46-50; c) E. Rafiee, A. Ataei, M. Joshaghani, *Tetrahedron Lett.*, 2016, **57**, 219.
37. H. Ibrahim, M. D. Bala, *J. Organomet. Chem.*, 2015, **794**, 301.
38. D. Guo, H. Huang, J. Xu, H. Jiang, H. Liu, *Org. Lett.*, 2008, **10**, 4513.
39. N. Guimond, C. Gouliaras, K. Fagnou, *J. Am. Chem. Soc.*, 2010, **132**, 6908.
40. F. -F. Yong, Y.-C. Teo, *Tetrahedron Lett.*, 2010, **51**, 3910.
41. a) M. Nirmala, G. Prakash, R. Ramachandran, P. Viswanathamurthi, J. G. Malecki, W. Linert, *J. Mole. Cata. A: Chem.*, 2015, **397**, 56; b) B. H. Lipshutz, B. A. Frieman, T. Butler, V. Kogan, *Angew. Chem. Int. Ed.*, 2006, **45**, 800.
42. L. Rout, P. Saha, S. Jammi, T. Punniyamurthy, *Adv. Synth. Catal.*, 2008, **350**, 395.

43. J. L. Hawkins, C. L. Gregson, L. A. Hassall, J. L. Holmes, *Tetrahedron Lett.*, 2014, **55**, 6734.
44. a) Q. Shen, J. F. Hartwig, *Org. Lett.*, 2008, **10**, 4109; b) Q. Shelby, N. Kataoka, G. Mann, J. F. Hartwig, *J. Am. Chem. Soc.*, 2000, **122**, 10718.
45. a) F. Rataboul, A. Zapf, R. Jackstell, S. Harkal, T. Riermeier, A. Monsees, U. Dingerdissen, M. Beller, *Chem. Eur. J.*, 2004, **10**, 2983; (b) S. Harkal, F. Rataboul, A. Zapf, C. Fuhrmann, T. Riermeier, A. Monsees, M. Beller, *Adv. Synth. Catal.*, 2004, **346**, 1742.
46. C. A. Fleckenstein, H. Plenio, *Chem. Soc. Rev.*, 2010, **39**, 694.
47. A. A-Sorrosa, F. E-Negrete, S. H-Ortega, R. A. Toscano, D. M-Morales, *Inorg. Chim. Acta*, 2010, **363**, 1262.
48. Z. Jin, L.-L. Qiu, Y.-Q. Li, H.-B. Song, J.-X. Fang, *Organometallics*, 2010, **29**, 6578.
49. a) G. C. Fortman, S. P. Nolan, *Chem. Soc. Rev.*, 2011, **40**, 5151; (b) N. Marion, S. P. Nolan, *Acc. Chem. Res.*, 2008, **41**, 1440.
50. a) R. J. Lundgren, A. S-Kumankumah, M. Stradiotto, *Chem. Eur. J.*, 2010, **16**, 1983; b) C. V. Reddy, J. V. Kingston, J. G. Verkade, *J. Org. Chem.*, 2008, **73**, 3047.
51. a) A. Chartoire, M. Lesieur, A. M. Z. Slawin, S. P. Nolan, C. S. J. Cazin, *Organometallics*, 2011, **30**, 4432; b) A. Schnyder, A. F. Indolese, M. Studer, H.-U. Blaser, *Angew. Chem.*, 2002, **114**, 3820.
52. S. Rayati, Z. Sheybanifard, M. M. Amini, A. Aliakbari, *J. Mol. Catal. A: Chem.*, 2016, **423**, 105.
53. a) A. Lazar, C. P. Vinod, A. P. Singh, *New. J. Chem.*, 2016, **40**, 2423; b) B. I. Ceylen, Y. D. Kurt, B. Ulkuseven, *J. Coord. Chem.*, 2009, **62**, 757.
54. a) A. Dondoni, *Angew. Chem. Int. Ed.*, 2008, **47**, 8995; b) K. L. Killops, L. M. Campos, C. J. Hawker, *J. Am. Chem. Soc.*, 2008, **130(15)**, 5062.
55. R. N. Salvatore, C. H. Yoon, K. W. Jung, *Tetrahedron*, 2001, **57**, 7785.

Chapter 5

Ru(III)-Organofunctionalized SBA-15 for Acetalization of Aldehydes and Ketones

[Anish Lazar](#), K. J. Betsy, C. P. Vinod and A. P. Singh*
Catalysis Communications, 104 (2018) 62-66.

5.1. Introduction

Acetals have wide ranging applications from its use as protective group as well as synthetic component in fragrance, cosmetics, drugs and carbohydrate chemistry.¹ They are also used as chiral auxiliary group in enantioselective synthesis.² Some of the reagents such as alcohols,³ diols,⁴ thiols,⁵ ester⁶ and oxiranes⁷ are used for the protection of aldehydes and ketones in multistep synthesis. Among this, acetals derived from aldehydes and alcohols shows inert nature towards the different congeners such as nucleophiles, base, oxidizing and reducing agents.⁸ Generally, acetalization reactions were carried out by protonic^{9,10} and Lewis acids^{11,12} in earlier decades. But, these methodologies suffers from serious drawbacks like the corrosive nature, presence of dehydrating agents, tedious reaction set up and generation of acidic waste during reactions forcing the discovery of environmentally benign catalyst. With this intention, researchers tried developing solid acid,¹³⁻¹⁵ ionic liquid¹⁶ and MOF¹⁷ catalysts, but they also suffer from long reaction time, elevated temperature with tendency to form side products. Moreover, use of stoichiometric amount of catalyst and difficulties in recovery and recyclability due to non-volatile nature of the catalyst makes the process economically unviable.

In this regard, some groups have tried to use transition metal complexes¹⁸⁻²⁰ as homogeneous catalysts,^{21, 22} especially metal chlorides,^{23, 24} for acetalization reactions; yet, their disadvantages like separation and recovery of catalyst from products and metal wastage are serious concern in industrial field. Among various transition metal complexes, ruthenium complexes^{25, 26} have received considerable interest with its electron deficient and vacant coordination sites, which provide facile activation of reactants. To attain heterogeneity, ruthenium congeners should be grafted on organofunctionalized nanoporous silica materials. On the basis of heterogeneity, these catalysts can overcome the shortcomings in homogeneous complexes such as separation, metal impurity of products from the reaction mixture and higher economy.

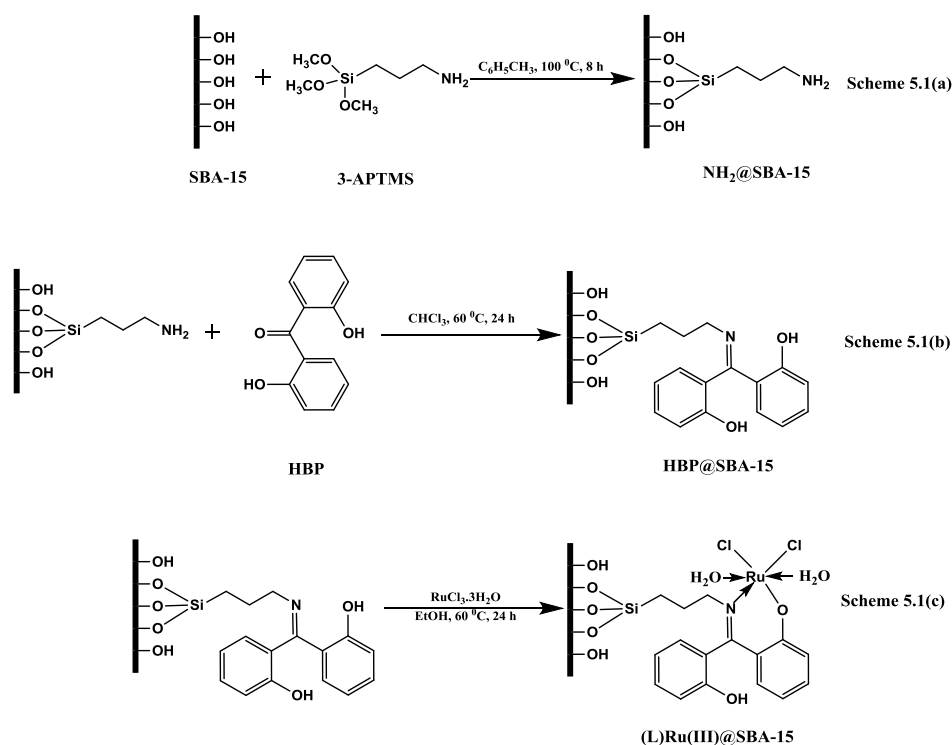
SBA-15²⁷ mesoporous material is consider as a potential candidate as support for heterogenization due to its higher wall thickness, uniform and tunable pore structure compared to zeolites, clays, silica and MCM-41. A modified benzophenone ligand is used which act as scavenger for Ru congeners and as a linker between ruthenium and SBA-15. Even with a lot of shortcomings in acetalization reactions by different catalysts, the importance of such type reactions was recently explained in tandem hydroformylation-acetalization reactions by metal based heterogeneous catalysts.^{28, 29}

In this work, we combine organofunctionalized SBA-15 and electron deficient Ru(III) sites for an efficient, acid free protection of carbonyl compounds via. Chemoselective synthesis of cyclic/acyclic acetals without any dehydrating agent at ambient reaction conditions. To increase the efficacy of grafted catalyst, (L)Ru(III)@SBA-15, reaction parameters were tuned and optimized. The ultimate goal of present work is the development of a cost-effective and simple catalyst for an efficient acetalization reaction without any by product formation.

5.2. Experimental

5.2.1. Synthesis of (L)Ru(III)@SBA-15

P123 (M. Wt = 5800), TEOS, 3-APTMS, 2,2'-dihydroxybenzophenone, aldehydes and ketones; Ru(III)Cl₃.3H₂O; all solvents were procured from Aldrich, Alfa Products and Thomas Baker, respectively. Preparation of grafted catalyst, (L)Ru(III)@SBA-15 [Scheme 5.1], was performed by three steps; (i) synthesis of host SBA-15, (ii) aminofunctionalized SBA-15, NH₂@SBA-15, (iii) grafting of 2,2'-dihydroxybenzophenone ligand over NH₂@SBA-15, HBP@SBA-15, followed by addition of Ru(III)Cl₃.3H₂O.



Scheme 5.1: Synthesis of ruthenium based organofunctionalized SBA-15 catalyst [(L)Ru(III)@SBA-15]; synthesis of 5.1(a) NH₂@SBA-15, 5.1(b) HBP@SBA-15 and 5.1(c) [(L)Ru(III)@SBA-15].

At first, SBA-15 synthesis procedure was adopted from literature reports.³⁰ In short, SBA-15 was synthesized by sol-gel hydrothermal mechanism using Pluronic 123 as surfactant and TEOS as silica precursor under acidic medium and then, as-synthesized material was calcined at 540 °C. In the second step, pretreated SBA-15 (3 g) at 110 °C for 3 h was reacted with 1.5 g of 3-APTMS in 60 ml dry toluene at 95 °C for 8 h to obtain NH₂@SBA-15 [Scheme 5.1(a)]. Finally, chelation site provided by 2,2'-dihydroxybenzophenone ligand (0.51 g, 2.41 mmol) was anchored over 1 g of functionalized SBA-15 in 50 ml CH₃CN at 70 °C for 24 h [HBP@SBA-15, Scheme 5.1(b)] and thereafter, their metallation with 1.2 mmol of Ru(III)Cl₃.3H₂O (0.1621 g) in 30 ml ethanol at 50 °C for 24 h [(L)Ru(III)@SBA-15, Scheme 5.1(c)].

5.2.2. Catalytic activity

In a typical procedure, reaction mixture of (L)Ru(III)@SBA-15 (0.010 g) and aldehyde (1 mmol) was charged into 25 ml round bottom flask with 10 ml methanol as protecting agent and stirred at room temperature for 20 min. Samples were taken periodically and injected into GC having a HP-5 column and FID detector.

5.3. Results and discussions

5.3.1 Characterizations

Ruthenium based organofunctionalized SBA-15 catalyst was thoroughly characterized by various characterization techniques, which can be divided into three portions; (i) physical methods, (ii) spectroscopic methods and (iii) microscopic methods.

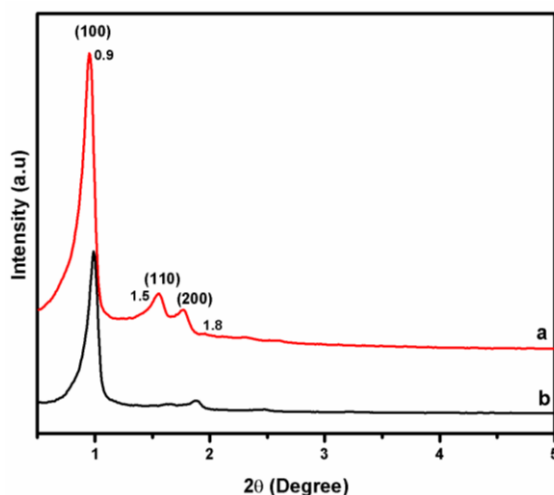


Fig. 5.1: XRD pattern of (a) SBA-15 and (b) (L)Ru(III)@SBA-15

In the physical characterization techniques, percentage of linker groups ($N = 3.3\%$) and ruthenium content ($4.35 \text{ wt}\%$) were determined by CHN and EDAX analyses. The mesoporous nature of (a) SBA-15 and (b) (L)Ru(III)@SBA-15 in Fig. 5.1 were revealed by small angle XRD, where peaks at 0.9 , 1.5 and 1.8° corresponding to (100), (110) and (200) Bragg reflections from SBA-15 type materials (Fig. 5.1a, b).³¹ Compared to SBA-15, intensity of (L)Ru(III)@SBA-15 peaks was smaller (Fig. 5.1b) due to the inside insertion of organomoieties in channels of SBA-15.

The mesoporous integrity of materials was again confirmed by N_2 -sorption analysis in Fig. 5.2, which shows type IV isotherm and pore size distribution curves (inset) of (a) SBA-15 and (b) (L)Ru(III)@SBA-15. The textural properties of³² synthesized materials are included in Table 5.1, where pore diameter, BET surface area and pore volume are mentioned. The unit cell parameter, BET surface area, pore diameter, pore volume and pore wall thickness of SBA-15 and (L)Ru(III)SBA-15 are given as: 102.54 \AA^0 , $550 \text{ m}^2/\text{g}$, 66 \AA^0 , $1.02 \text{ cm}^3/\text{g}$, 36.54 \AA^0 and 103.08 \AA^0 , $254 \text{ m}^2/\text{g}$, 47 \AA^0 , $0.49 \text{ cm}^3/\text{g}$, 56.08 \AA^0 , respectively. Similar to XRD spectra, in N_2 analysis, the intensity of isotherm curves, pore diameter, BET surface area and pore volume of (L)Ru(II)@SBA-15 from SBA-15 are decreased.

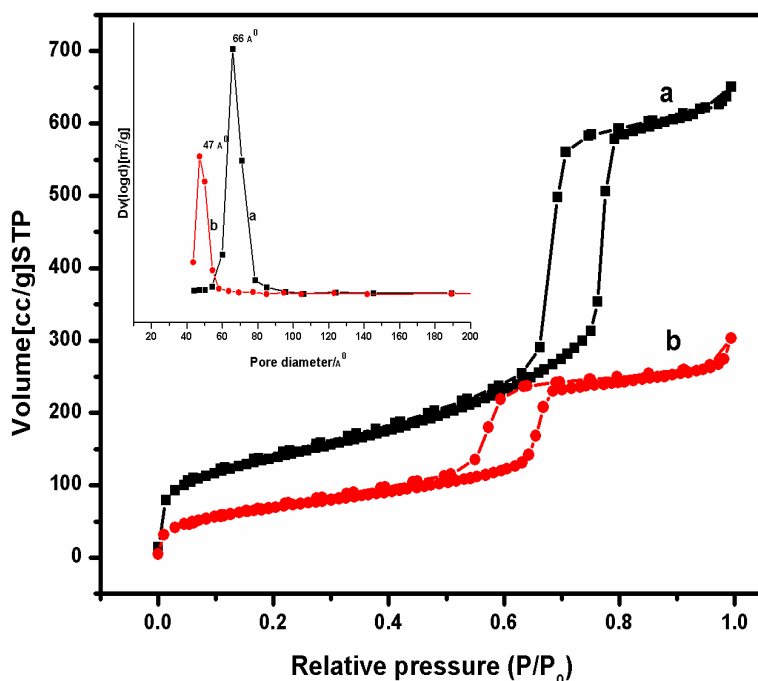


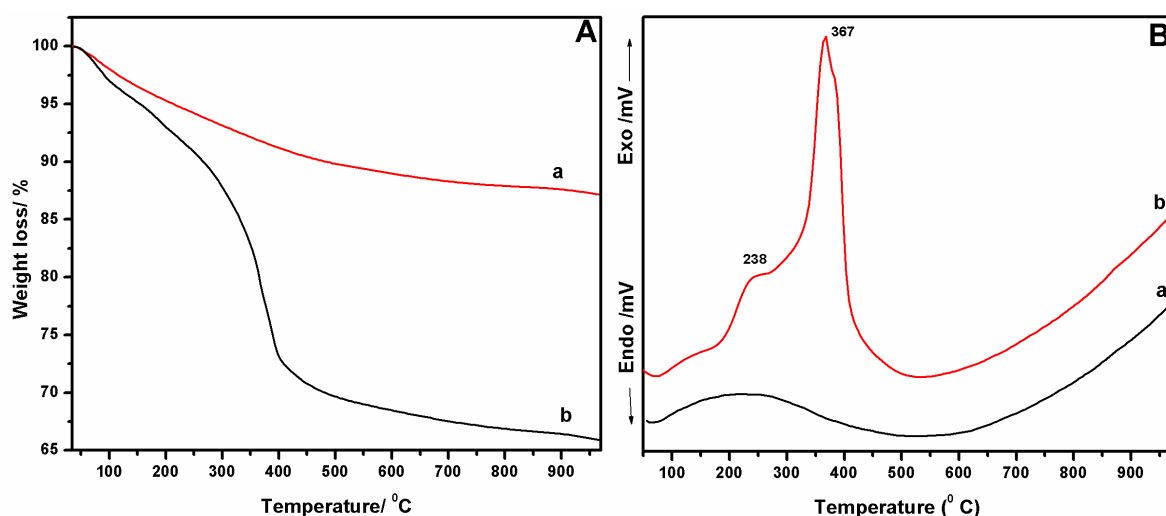
Fig. 5.2: N_2 -sorption isotherm and pore size (inset) of (a) SBA-15 and (L)Ru(III)@SBA-15

Table 5.1: Textural properties of calcined SBA-15 and (L)Ru(III)@SBA-15.

Sample	$a_0[\text{\AA}]^a$	S.A [m^2/g]	$D_p[\text{\AA}]$	$V_p[\text{cc/g}]$	$\omega_t[\text{\AA}]^b$
SBA-15	102.54	550	66	1.02	36.54
(L)Ru(III)@SBA-15	103.08	254	47	0.49	56.08

a_0 =Unit cell parameter, S.A= BET Surface area, D_p = Pore diameter, V_p = Pore volume, ω_t = Wall Thickness; From EDAX analysis Ru= \sim 4.35 wt%; ^a $a_0=2d100/1.73$; ^b $\omega_t= a_0- D_p$.

A noticeable decomposition in TGA of heterogenized catalyst (Fig. 5.3A) indicates that \sim 30% of organomoieties are incorporated in supported materials. In DTA (Fig. 5.3B), peaks at 238 and 367 corresponds to the presence of linker groups and 2,2'-dihydroxybenzophenone ligand, respectively, compared to parent SBA-15.

**Fig. 5.3:** TG (A) and DTA (B) of (a) SBA-15 and (b) (L)Ru(III)@SBA-15

The spectroscopic techniques provide an exact evidence for the anchoring of organomoieties on SBA-15. Fig. 5.4A and B show ^{13}C and ^{29}Si solid state NMR of (L)Ru(III)@SBA-15. The peaks in the region of 0–55 ppm in ^{13}C NMR corresponds to $-\text{OCH}_3$ (C_1) and $-\text{CH}_2-$ groups (C_2 - C_4) present in linker group (Fig. 5.4A). Peaks in 120–150 ppm (C_6 - C_{10}) represent the signature of carbon atoms in benzene rings. In addition to this, remaining two peaks at 155 and 175 ppm are assigned to the C-OH and C=N groups in (L)Ru(III)@SBA-15. In ^{29}Si NMR spectra (Fig. 5.4B), Q^n signals,³³ in the range of -90 to -113 ppm, corresponds to Si atoms in siloxane

framework and Tⁿ signals,³⁴ in the region of -50 to -65 ppm, assigned to Si atom in linker group which is attached to support SBA-15.

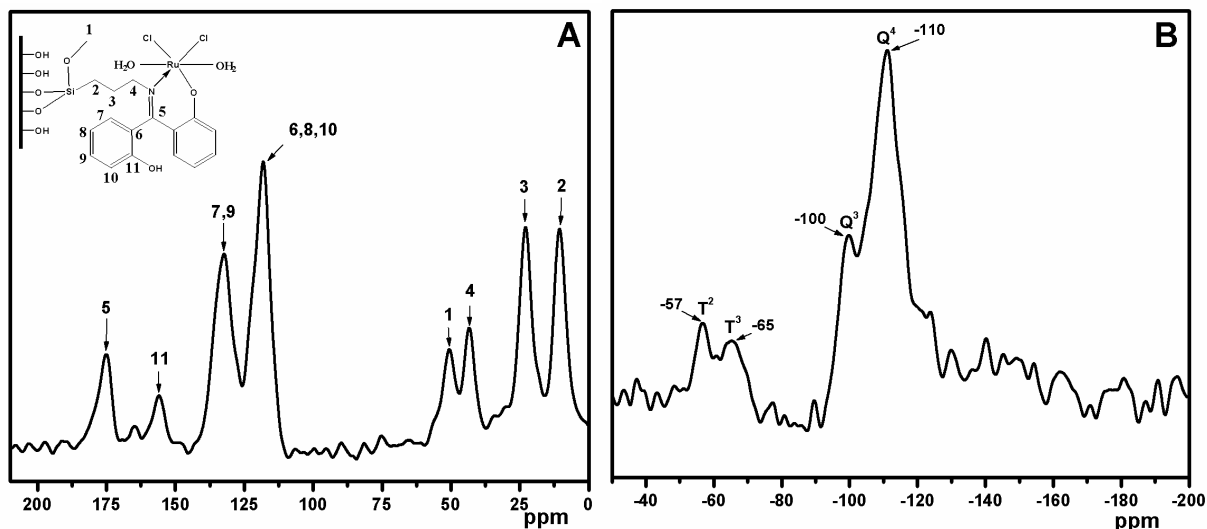


Fig. 5.4: Solid state ^{13}C (A) and ^{29}Si (B) NMR of (L)Ru(III)@SBA-15

IR spectra of (a) SBA-15 and (b) (L)Ru(III)@SBA-15 are plotted in Fig. 5.5. In both materials, characteristic peaks of Si-O bond resonances in siloxane framework were observed at 1086 , 940 and 800 cm^{-1} . Likewise, the nature of surface silanol groups (Si-OH) in material was identified in the region of 3200 – 3500 cm^{-1} and 1637 cm^{-1} . Moreover, characteristic peaks corresponding to C=N group lies at 1608 cm^{-1} and $-\text{CH}_2$ - stretching vibrations were identified at 2872 cm^{-1} and 2936 cm^{-1} .

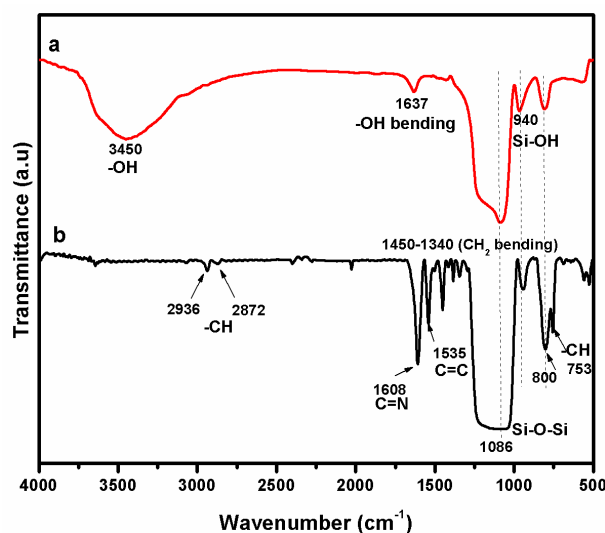


Fig. 5.5: FT-IR spectra of (a) SBA-15 and (b) (L)Ru(III)@SBA-15

XPS spectra of (L)Ru(III)@SBA-15 in Fig. 5.6 shows a peak at 281.4 eV which corresponds to Ru3d_{5/2} spin orbit component³⁵ and indicates +3 oxidation state.

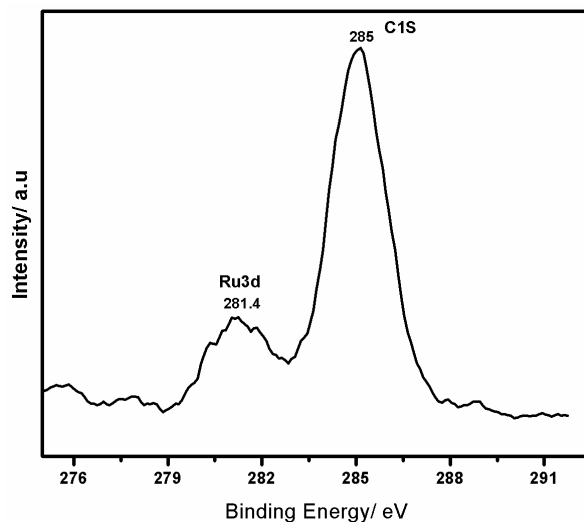


Fig. 5.6: XPS spectra of Ru3d core levels of (L)Ru(III)@SBA-15

Diffuse reflectance UV–visible spectra of (a) SBA-15 and (b) (L)Ru(III)@SBA-15 in Fig. 5.7 shows three bands centered at 220 nm, 265–365 nm and 560 nm, indicate characteristic siliceous material, electronic transitions of organic groups like >C=N and benzene ring, Ligand to Metal Charge Transition (LMCT), respectively.

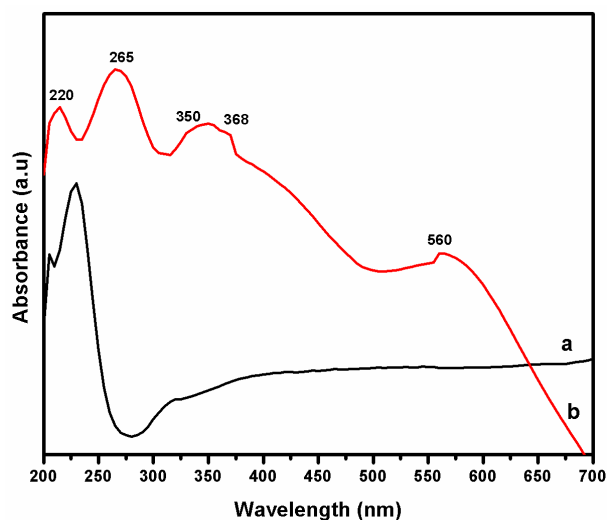


Fig. 5.7: DR UV-Visible spectra of (a) SBA-15 and (b) (L)Ru(III)@SBA-15

SEM and TEM are imaged and shown in Fig. 5.8 and Fig. 5.9. In both microscopy images, (L)Ru(III)@SBA-15 exhibits hexagonal type plate structure with uniform mesoporous channels and proves that structural stability was retained even after heterogenization.

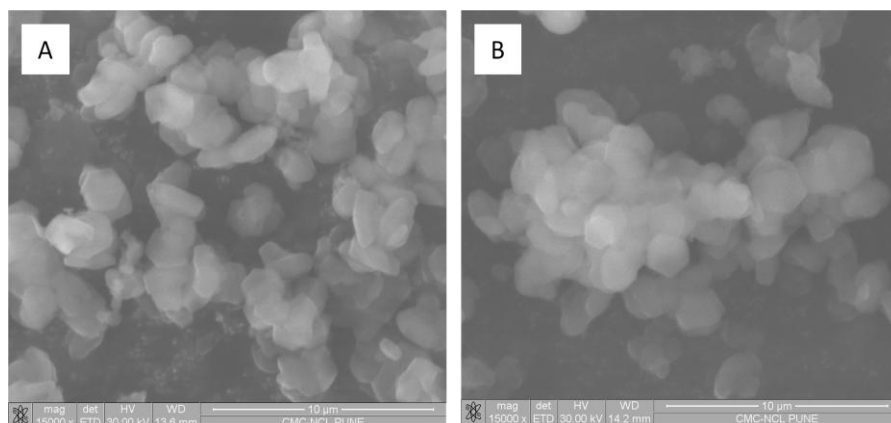


Fig. 5.8: SEM images of (A) SBA-15 and (B) (L)Ru(III)@SBA-15

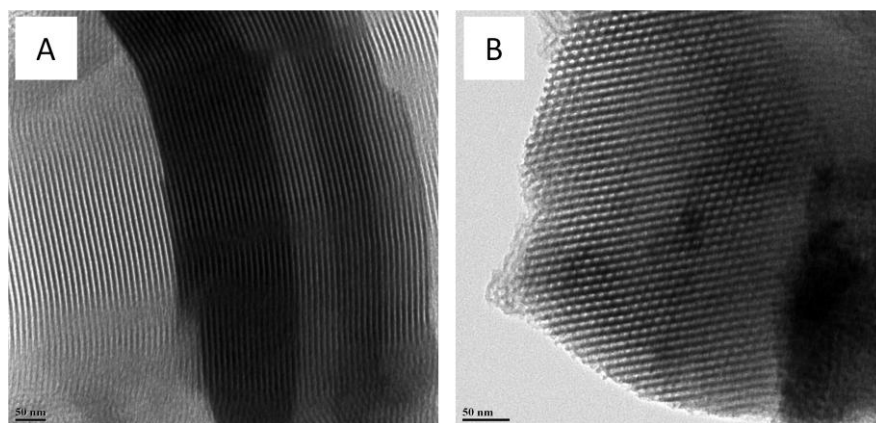
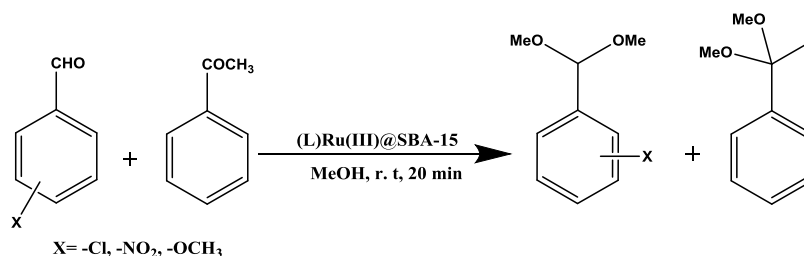


Fig. 5.9: TEM images of (A) SBA-15 and (B) (L)Ru(III)@SBA-15

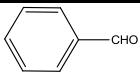
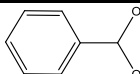
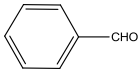
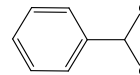
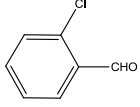
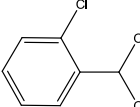
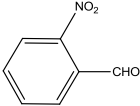
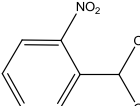
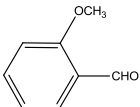
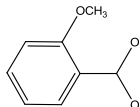
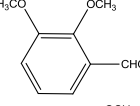
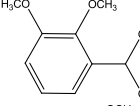
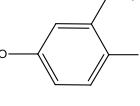
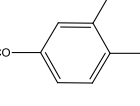
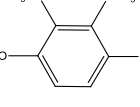
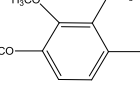
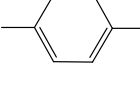
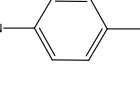
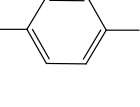
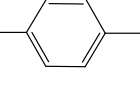
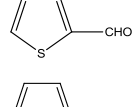
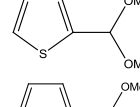
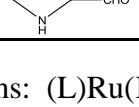
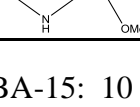
5.3.2 Chemo-selective acetalization reactions

Grafted catalyst, (L)Ru(III)@SBA-15, was applied in neutral and chemoselective acetalization reactions (Scheme 5.2), thereby to protect aldehydes as cyclic/acyclic acetals, by using methanol as model protecting group under ambient reaction conditions.



Scheme 5.2: Chemo-selective synthesis of acetal from aldehydes and ketones

Table 5.2: Synthesis of acetals^a from aldehydes.

No.	Aldehyde	Acetal	Conv. (%)	TOF ^c (h ⁻¹)
1 ^b			0	0
2			100	70.37
3			99	69.66
4			100	70.37
5			100	70.37
6			100	70.37
7			100	70.37
8			100	70.37
9			79	55.60
10			52	36.60
11			100	70.37
12			100	70.37

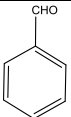
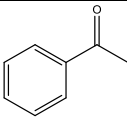
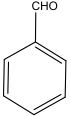
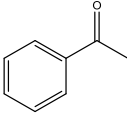
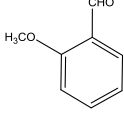
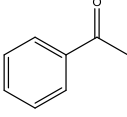
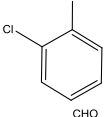
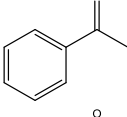
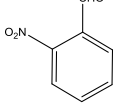
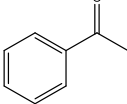
^a Reaction conditions: (L)Ru(III)@SBA-15: 10 mg; aldehyde: 1 mmol; MeOH: 250 mmol; Reaction temperature: Room Temperature, Time: 20 mins; ^b Without catalyst; ^c TOF [h⁻¹] = [the number of moles of reactant converted/the number of moles of metal active sites]/time in hours.

To tune the efficacy of the catalyst, substituted and heterocyclic aldehydes are used as substrates and the results are also included in Table 5.2 (entries 1–12). All substituted and

heterocyclic aldehydes exhibit 100% conversion with high turnover frequency except 4-nitro (79%) and 4-bromoaldehydes (52%). It should be mentioned that all the reactions were complete within 20 min at room temperature which demonstrate the superior activity of the catalyst.

To check the chemo-selectivity of (L)Ru(III)@SBA-15 catalyst towards the formation of acetal, equimolar mixture of aldehyde and ketone in one-pot acetalization reaction was carried out (Table 5.3, entries 1–5) and the results reveal that < 5% ketal is formed in reaction mixture compared to acetal (~95%).

Table 5.3: Chemoselective synthesis^a of acetals from aldehydes and ketones.

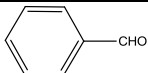
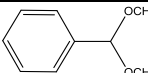
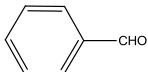
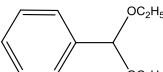
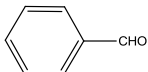
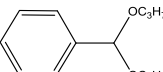
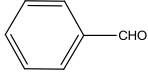
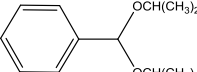
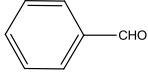
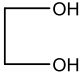
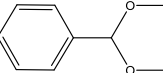
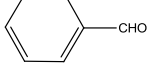
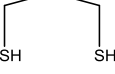
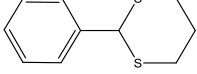
No.	Aldehyde	Ketone	Conv. (%)	Acetal : ketal ratio (%)	TOF ^c (h ⁻¹)
1 ^b			0	00:0	0
2			100	96:4	70.37
3			100	95:5	70.37
4			99	96:4	69.66
5			100	94:6	70.37

^a Reaction conditions: (L)Ru(III)@SBA-15: 10 mg; aldehyde and ketone: 1:1 mmol; MeOH: 250 mmol; Reaction temperature: Room Temperature, Time: 20 mins; ^b Without catalyst; ^c TOF [h⁻¹] = [the number of moles of reactant converted/the number of moles of metal active sites]/time in hours.

The influence of protecting groups in acetalization reaction were performed by using aliphatic and branched alcohols, diols and thiols and its results are mentioned in Table 5.4 (entries 1–6). According to the results of Table 5.4, aliphatic aldehydes (entries 1–3) show > 85% conversion within 1 h compared to branched alcohol (73%, 75 min, entry 4). Diol and thiol protecting

groups (entries 5, 6) masked the carbonyl derivatives of aldehydes with 70% and 75% conversions, respectively.

Table 5.4: Influence of organic protective groups in acetalization^a reactions

No.	Aldehyde	Protective Agents	Acetal	Time	Conv. (%)	TOF ^b (h ⁻¹)
1		CH ₃ OH		20	100	70.37
2		CH ₃ CH ₂ OH		35	85	34.03
3		CH ₃ CH ₂ CH ₂ OH		60	80	18.57
4		(CH ₃) ₂ CHOH		75	73	13.57
5				45	70	21.67
6				35	75	30.07

^a Reaction conditions: (L)Ru(III)@SBA-15: 10 mg; aldehyde: 1 mmol; Protecting groups: 250 mmol; Reaction temperature: Room Temperature; ^bTOF [h⁻¹] = [the number of moles of reactant converted/the number of moles of metal active sites]/time in hours.

The effect of amount of protecting group in acetalization reaction was performed by 25, 50, 100, 150 and 250 mmol of methanol and 250 mmol of methanol was found as optimum for effective protection of aldehydes (Fig. 5.10). To get a clear picture of protection of aldehydes, tentative mechanism was proposed (Scheme 5.3) and explained as; in first step, vacant coordination site of ruthenium is solvated by protecting group like methanol (A) and subsequently, one of the methanol is replaced by aldehyde through the interaction between electropositive ruthenium and carbonyl group. In the second step, attached -OCH₃ groups in Ru migrated to carbonyl carbon in a concerted manner with addition of another methanol group in vacant site (B). The formed hemiacetal (C) converted into acetal through oxocarbenium ion followed by addition of methanol.

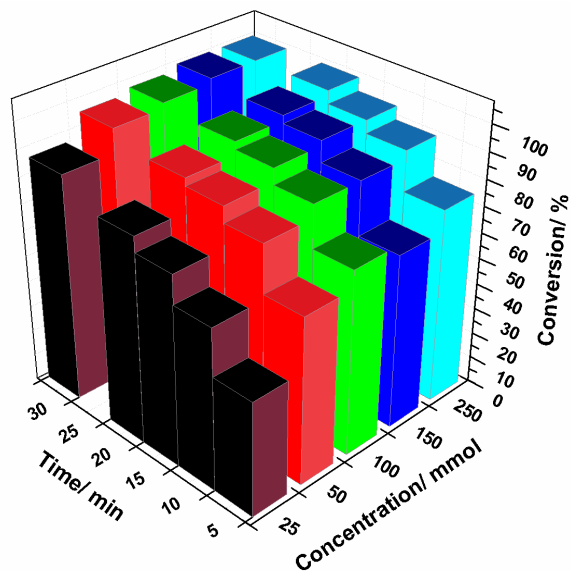
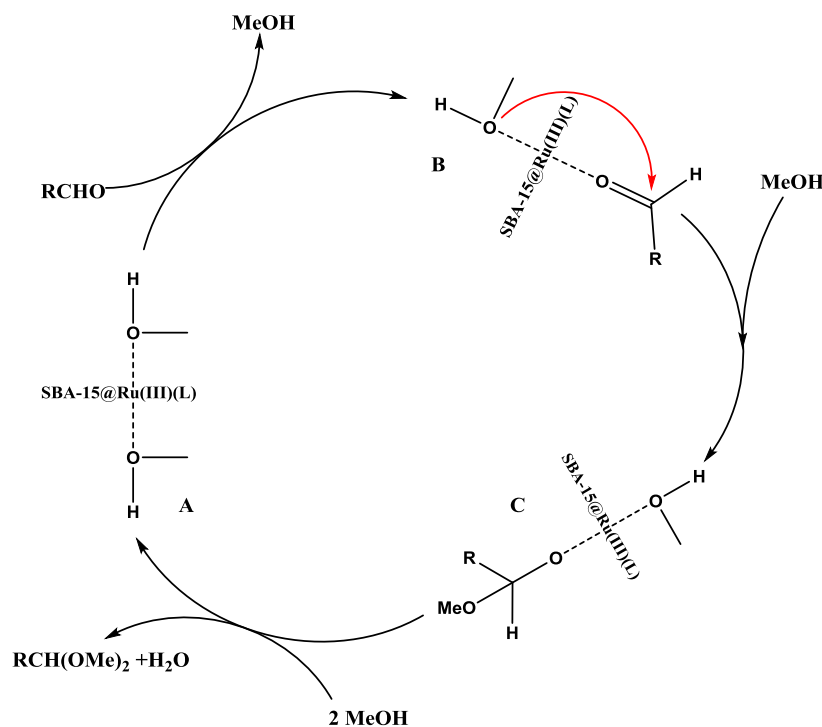


Fig 5.10: The influence of the amount of methanol in acetalization reactions



Scheme 5.3: Tentative mechanism for the acetalization of aldehydes by (L)Ru(III)@SBA-15

Hereogeneity test was performed by Sheldon's hot filtration test (Fig. 5.11A) and recycling studies (Fig.5.11B) with benzaldehyde as model substrate. In Sheldon' test, reaction mixture was filtered through filter paper at approx. 10 min (72% conversion), filtrate again charged and

reaction continued up to 20 min (75%). Moreover, heterogenous nature of (L)Ru(III)@SBA-15 was again demonstrated by recycling studies where catalyst was recycled upto five cycles via. Simple centrifugation method. In Sheldon's hot filtration test and recycling studies, results are point out that (L)Ru(III)@SBA-15 is heterogeneous character with negligible loss of ruthenium content (~1.2 wt%).

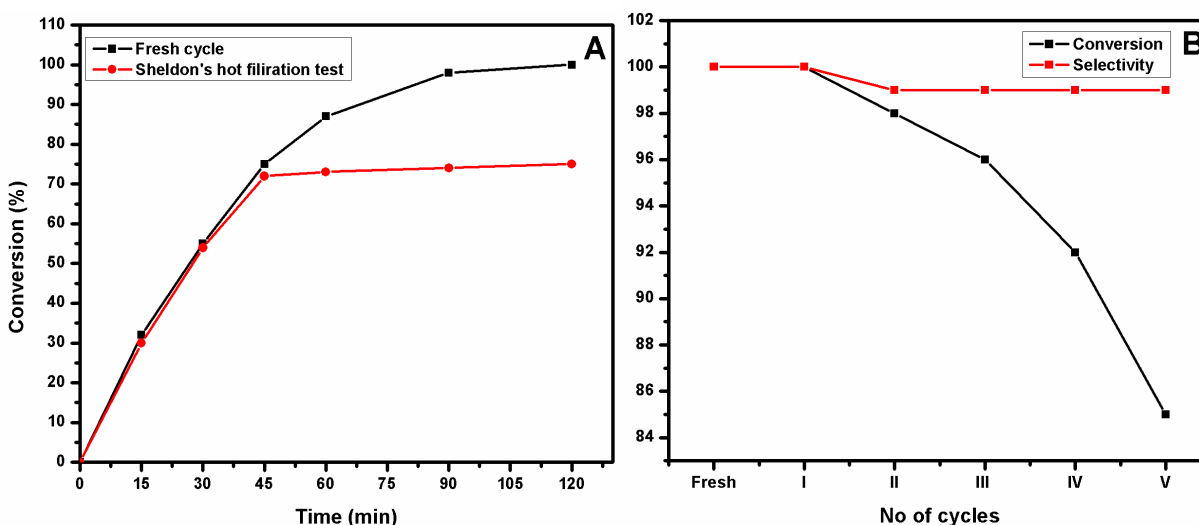


Fig. 5.11: Sheldon's hot filtration test (A) and Recycling studies (B) of (L)Ru(III)@SBA-15

5.4. Conclusions

An efficient Ru(III)-Organofunctionalized SBA-15, (L)Ru(III)@SBA-15, catalyst for acid free and chemo-selective acetalization reaction was synthesized by the grafting of 2,2'-dihydroxy benzophenone ligand over NH_2 @SBA-15 followed by complexation with $\text{RuCl}_3 \cdot 3\text{H}_2\text{O}$. This grafted material can be considered as a competitive and replaceable catalyst to conventional catalysts such as protonic, Lewis and solid acids for the preparation of dimethyl acetals. The catalyst, (L)Ru(III)@SBA-15, was thoroughly characterized by physical, spectroscopic and microscopic techniques. The results of acetalization reaction revealed that (L)Ru(III)@SBA-15 shows high catalytic activity as well as selectivity towards acyclic/cyclic acetals within 20 min with high TOF without the generation of hemiacetals as byproducts. Moreover, the amount of methanol as protecting group, influence of different protecting groups and recycling studies of (L)Ru(III)@SBA-15 in acetalization reaction were performed to attain a clear picture of the

synthesized catalyst. Due to its high potential, this catalyst can be applicable in valorization of glycerol in bio-diesel industry and tandem hydroformylation-acetalization reactions.

5.5. References

1. M. J. Climent, A. Velty, A. Corma, *Green Chem.*, 2002, **4**, 565.
2. J. K. Whitesell, *Chem. Rev.*, 1989, **89**, 158.
3. J. Gora, K. Kula, *J. Synth.*, 1986, **7**, 586.
4. T. P. Kumar, K. R. Reddy, R. S. Reddy, *J. Chem. Res.*, 1994, 394 (S).
5. S. K. De, *Tetrahedron Lett.*, 2004, **45**, 2919.
6. K. Ishihara, Y. Karumi, M. Kubota, H. Yamamoto, *Synlett*, 1996, **35**, 839.
7. D. S. Torok, J. J. Figueroa, *J. Organomet. Chem.*, 1993, **58**, 7274.
8. T. W. Greene, P. G. M. Watts, *Protective Groups in Organic Syntheses*, 2nd ed., Wiley, New York, 1991.
9. A. F. B. Cameron, J. S. Hunt, J. F. Oughton, P. A. Wilkinson, B. M. Wilson, *J. Chem. Soc.*, 1953, 3864.
10. E. Wenkert, T. E. Goodwin, *Synth. Commun.*, 1977, **7**, 409.
11. H. Firouzabadi, N. Iranpoor, B. Karimi, *Synlett*, 1999, 321.
12. R. A. Ugarte, D. Devarajan, R. M. Mushinski, T. W. Hudnall, *Dalton Trans.*, 2016, **45**, 11150.
13. P. Manjunathan, S. P. Maradur, A. B. Halgeri, G. V. Shanbhag, *J. Mol. Catal. A*, 2015, **396**, 47.
14. R. Rodrigues, M. Goncalves, D. Mandelli, P. P. Pescarmona, W. A. Carvalho, *Catal. Sci. Technol.*, 2014, **4**, 2293.
15. Y. Luan, N. Zheng, Y. Qi, J. Yu, G. Wang, *Eur. J. Inorg. Chem.*, 2014, **2014**, 4268.
16. L. Myles, R. G. Gore, N. Gatherhood, S. J. Connon, *Green Chem.*, 2013, **15**, 2740.
17. Y. Luan, N. Zheng, Y. Qi, J. Tang, G. Wang, *Catal. Sci. Technol.*, 2014, **4**, 925.
18. J. Ott, G. M. R. Tombo, B. Schmid, L. M. Venanzi, G. Wang, T. R. Ward, *Tetrahedron Lett.*, 1989, **30**, 6151.
19. Q. Jiang, H. Ruegger, L. M. Venanzi, *Inorg. Chim. Acta*, 1999, **290**, 64.
20. P. Barbaro, C. Bianchini, W. Oberhauser, A. Togni, *J. Mol. Catal. A Chem.*, 1999, **145**, 139.

21. C. Crotti, E. Farnetti, N. Guidolin, *Green Chem.*, 2010, **12**, 2225.
22. R. A. Ugarte, T. W. Hudnall, *Green Chem.*, 2017, **19**, 1990.
23. A. L. Gemal, J. H. Luche, *J. Organomet. Chem.*, 1979, **44**, 4187.
24. B. C. Ranu, R. Jana, S. Samantha, *Adv. Synth. Catal.*, 2004, **346**, 446.
25. S. K. De, R. A. Gibbs, *Tetrahedron Lett.*, 2004, **45**, 8141.
26. J.-Y. Qi, J.-X. Ji, C.-H. Yueng, H.-L. Kwong, A. S. C. Chana, *Tetrahedron Lett.*, 2004, **45**, 7719.
27. D. Zhao, J. Feng, Q. Huo, N. Melosh, G. H. Fredrickson, B. F. Chmelka, G. D. Stucky, *Science*, 1998, **279**, 548.
28. J. Norinder, C. Rodrigues, A. Börner, *J. Mol. Catal. A*, 2014, **391**, 139.
29. C. Rodrigues, F. G. Delolo, J. Norinder, A. Börner, A. L. Bogado, A. A. Batista, *J. Mol. Catal. A*, 2017, **426**, 586.
30. A. Lazar, P. Sharma, A. P. Singh, *Microporous Mesoporous Mater.*, 2013, **170**, 331.
31. A. Lazar, W. R. Thiel, A. P. Singh, *RSC Adv.*, 2014, **4**, 14063.
32. A. Lazar, K. S. Sanjush, A. P. Singh, *Adv. Porous Mater.*, 2016, **4**, 212.
33. A. Lazar, C.P. Vinod, A.P. Singh, *New J. Chem.*, 2016, **40**, 2423.
34. A. Lazar, C. P. Vinod, A. P. Singh, *Microporous Mesoporous Mater.*, 2017, **242**,173.
35. A. Lazar, S. C. George, P. R. Jithesh, C. P. Vinod, A. P. Singh, *Appli. Cata. A*, G. E. N. 2016, **513**,138.

Chapter 6

Summary and Conclusions

6.1. Summary

The current thesis provides an account of, (i) the synthesis of metal-organofunctionalized mesoporous silica heterogeneous catalysts by the anchoring of organofunctionalized groups on SBA-15 followed by the complexation with appropriate metal complexes, (ii) thorough interpretation of synthesized materials by various physical, spectroscopic and microscopic techniques and (iii) evaluation of synthesized materials as heterogeneous catalysts in asymmetric sulfoxidation, epoxidation, hydrogenation, coupling reactions and acetalization reactions of aldehydes.

The current thesis is mainly divided into six chapters and summarized as,

First chapter portrays the importance of mesoporous solids and organofunctionalized mesoporous materials (OMMs) in heterogeneous catalysis along with their up to date literatures. The second part of this chapter mainly focus on significance of physico-chemical characterization techniques which used for the evaluation of an efficient, reusable and catalytic active metal-organofunctionalized SBA-15 heterogeneous catalysts.

Chapter 2 explains the synthesis of reusable, mesoporous, heterogeneous vanadium complex, V(IV)O-Sal-Ind-SBA-15, from (1R,2S)-(+)-Cis-1-amino-2-indanol for enantioselective sulfoxidation reaction. The physico-chemical properties of the functionalized catalyst were analyzed by a series of characterization techniques like XRD, N₂ sorption measurement isotherm, TEM, SEM. TG & DTA, FT-IR, XPS, EPR, DR UV-Visible, ICP-OES and solid & liquid state ¹³C, ²⁹Si and ⁵¹V NMR spectroscopy. Powder X-ray diffraction patterns, TEM and N₂ physisorption analysis confirmed the retention of mesoporous structure after various modifications. Solid-state NMR (¹³C and ²⁹Si CP MAS NMR) and FT-IR analysis proved the integrity of organocatalyst residing inside the pore channels of the mesoporous support. Further, XPS, EPR, ⁵¹V NMR and DR UV-Visible analyses help to find out the oxidation state and coordination environment of vanadium in V(IV)O-Sal-Ind-SBA-15. Catalytic evaluation in asymmetric sulfoxidation reaction of sulfides indicated that V(IV)O-Sal-Ind-SBA-15 exhibited higher catalytic activity, stability, reusability and comparable enantioselectivity than SBA-15, PrNH₂SBA-15 and neat V(IV)O-Sal-Indanol complex. The effects of different catalysts,

temperature, solvents and substrates on sulfoxidation reaction were examined in order to optimize the conversion and enantioselectivity of thioanisoles to sulfoxides.

Chapter 3 describes an efficient and reusable oxidation catalyst 3-[N,N'-bis-3-(salicylidenamino)ethyltriamine]Mo(VI)O₂@SBA-15 which has been synthesized by the anchoring of the 3-[N,N'-bis-3-(salicylidenamino)ethyltriamine] ligand (L or Salpr) on the inner surfaces of organofunctionalized SBA-15 and subsequent complexation with Mo(VI)O₂(acac)₂. The physico-chemical properties of the functionalized catalysts were analyzed by elemental analysis, ICP-OES, XRD, N₂-sorption measurements, TG & DTA, solid state ¹³C, ²⁹Si NMR spectroscopy, FT-IR, Raman spectroscopy, XPS, DR UV-Vis spectroscopy, SEM and TEM. XRD and N₂ sorption analyses helped to find out the morphological and textural properties of the synthesized catalysts and confirmed that an ordered mesoporous channel structure was retained even after the multistep synthetic procedures. TG and DTA results reveal that the thermal stability of (L)Mo(VI)O₂@SBA-15 was maintained up to 200 °C. The organic moieties anchored over the surface of the SBA-15 support were determined by solid state ¹³C NMR and FT-IR spectroscopy. Further, solid state ²⁹Si NMR spectroscopy provides the information about the degree of functionalization of the surface silanol groups with the organic moiety. The electronic environment and the oxidation state of the molybdenum site in (L)Mo(VI)O₂@SBA-15 were monitored by Raman spectroscopy, XPS and DR UV-Vis techniques. Moreover, the morphology and topographic information of the synthesized catalysts were confirmed by SEM and TEM imaging. The synthesized catalysts were evaluated in epoxidation and sulfoxidation reactions, and the results show that (L)Mo(VI)O₂@SBA-15 exhibits high conversion and selectivity towards epoxidation and sulfoxidation reactions in combination with high stability. The anchored solid catalysts can be recycled effectively and reused several times without major loss in activity. In addition, Sheldon's hot filtration test was also carried out.

Chapter 4 is mainly divided into two portions **4A** and **4B** where different palladium based organofunctionalized SBA-15 catalysts for coupling and hydrogenation reactions were included. **Chapter 4A** represents an efficient, simple, phosphine and co-catalyst free C–C coupling reaction carried out and a heterogeneous catalyst is synthesized via a post grafting method. A covalently anchored phosphine free Pd(II) based 2,2'-dihydroxybenzophenone (DHBP) complex over organofunctionalized SBA-15 has been synthesized by the reaction between aminofunctionalized SBA-15 (NH₂SBA-15) and a 2,2'-dihydroxybenzophenone (DHBP) ligand,

and further complexation with Pd(II)(OAc)₂ to get Pd(II)DHBP@SBA-15. The synthesized catalysts were characterized by elemental analysis, XRD, N₂ sorption analyses, TG, DTA, FT-IR, solid state ¹³C and ²⁹Si NMR spectra, XPS, UV-Visible, SEM, EDAX and TEM. The synthesized catalysts were screened in arylation (Heck reactions) and hydrogenation reactions of alkenes, and the results show that Pd(II)DHBP@SBA-15 exhibits high conversion and selectivity towards arylation and hydrogenation reactions of alkenes with high stability. The anchored solid catalysts can be recycled effectively and reused several times without major loss in activity.

Chapter 4B reveals an effective and impressive heterogeneous catalyst, Pd(II)-3-allylsalicylaldiminophenol-SBA-15, dubbed as Pd(II)ASIP@SBA-15, for amination reactions of aryl halides to synthesize secondary amines (2⁰), has been synthesized and characterized. Pd(II)ASIP@SBA-15 has been synthesized by the covalent anchoring of 3-allylsalicylaldehyde over thiofunctionalized SBA-15, then further reaction with 2-aminophenol, followed by metallation process by using Pd(II)(OAc)₂. A specifically designed cheap and easily available organic ligand, 3-allylsalicylaldiminophenol (ASIP), was synthesized from 3-allylsalicylaldehyde and 2-aminophenol. Using this, the synthesis of Pd(II)ASIP@SBA-15 was carried out whereby the ligand providing an active co-ordination or chelating sites for palladium metal. This strategy helped in exposing the Pd(II)ASIP active sites from surface to channels of SBA-15 support during the reactions. The synthesized catalyst were characterized by CHN analysis, PXRD, Nitrogen sorption analyses, TG & DTA, FTIR, ¹³C and ²⁹Si CPMAS NMR spectra, XPS, UV-Visible, SEM, EDAX and TEM. Pd(II)ASIP@SBA-15 catalyst was screened in heterogeneous amination reactions of aryl halides to produce N-aryl derivatives or secondary amines with high catalytic activity as revealed by turn over frequency (TOF) calculations. To explore the heterogeneous nature of catalysts, amination reactions were carried with neat Pd(II)ASIP complex and Pd(II)(OAc)₂ catalysts. The catalyst was recycled several times without much loss of activity and Sheldon hot filtration test has been performed.

Chapter 5 explains a combining effect of electron deficient Ru(III) coordination sites with organofunctionalized SBA-15, (L)Ru(III)@SBA-15, which result in a mild, neutral, water scavenger free and chemo-selective acetalization catalyst for cyclic/acyclic acetals. Vacant coordination sites of ruthenium in (L)Ru(III)@SBA-15 activates protecting groups as well as reactants simultaneously and restricts the reverse acetalization reaction. Synthesized

(L)Ru(III)@SBA-15 catalyst has been thoroughly characterized and act as competitive catalyst compared to conventional acid catalysts. (L)Ru(III)@SBA-15 performs high catalytic activity as well as selectivity within 20 min with high TOF. The catalyst can be recycled and reaction parameters are optimized.

Chapter 6 gives a summary and conclusions of metal based organofunctionalized synthesized catalysts for fine chemical synthesis where synthesis procedures, characterizations and different types of reactions are shortly described.

6.2. Conclusions

Chapter 2: V(IV)O-Organofunctionalized SBA-15 catalyst for efficient asymmetric sulfoxidation reactions

Highly reactive and recyclable heterogeneous catalytic system was developed by immobilizing asymmetric (1R,2S)-(+)-1-[N-(3-tertbutyl-5-chloromethylsalicylidene)amino]-2-indanol (Sal-Indanol) ligand over mesoporous –OH protected amino functionalized SBA-15 with further complexation of V(IV)O(acac)₂ to attain V(IV)O-Sal-Ind-SBA-15. The powder X-ray diffraction, TEM and N₂-adsorption desorption analysis of the catalyst confirmed the structural integrity of the mesoporous hosts and the spectroscopic characterization techniques (FTIR, ¹³C & ²⁹Si MAS-NMR) proved the successful anchoring of the metal complex over the modified mesoporous support. In addition, the oxidation state and coordination environment of vanadium metal in V(IV)O-Sal-Ind-SBA-15 complex were confirmed by XPS, EPR, ⁵¹V NMR and DR UV–Visible techniques. In order to deduce the optimum reaction conditions for asymmetric sulfoxidation reaction, the influence of different temperatures (-10 °C, 0 °C & 20 °C) and solvents (CH₂Cl₂, CH₃COCH₃ and EtOAc) were examined. The results show that CH₂Cl₂ act as an efficient solvent and the temperature at 0 °C provides slightly higher e.e than other temperatures. V(IV)O-Sal-Ind-SBA-15 showed comparative enantioselectivity [30–33% (R)], selectivity (>93%) and slightly higher catalytic conversion of thioanisoles (86–88 %) compared with SBA-15, PrNH₂SBA-15 and neat V(IV)O-Sal-Indanol complex. Moreover, recycling study of V(IV)O-Sal-Ind-SBA-15 shows no major deactivation of the catalyst.

Chapter 3: Mo(VI)O₂-Organofunctionalized SBA-15 catalyst for epoxidation and sulfoxidation reactions

The heterogenization of the (L)Mo(VI)O₂ complex over SBA-15 was achieved by a multistep synthetic procedure, using the 3-[N,N-bis-3(salicylidenamino)ethyltriamine] ligand (L) and Mo(VI)O₂(acac)₂. The physico-chemical properties of the functionalized catalyst were analyzed by a series of characterization techniques like elemental analysis, ICP-OES, XRD, N₂ sorption measurements, TG & DTA, solid state ¹³C, ²⁹Si NMR spectroscopy, FT-IR, Raman spectroscopy, XPS, DRS UV-Vis spectroscopy, SEM and TEM. The integrity and textural properties of mesoporous support and synthesized catalysts were obtained from the XRD and N₂ adsorption–desorption analysis. Thermal stabilities of the complexes were confirmed by thermal analyses like TG and DTA. The organic moieties anchored over the surface of SBA-15 were investigated by solid state ¹³C NMR and FT-IR spectroscopy. The degree of functionalization of surface silanol groups with organic moieties on the mesostructured materials can be monitored by means of ²⁹Si CP MAS NMR spectroscopy. The oxidation state and the chemical environment of molybdenum atoms were determined by Raman spectroscopy, XPS and DRS UV-Vis spectroscopy and the morphology and topographic information of the synthesized catalysts were confirmed by SEM and TEM imaging. (L)Mo(VI)O₂@SBA-15 complex was found to be highly active, selective and recyclable in the epoxidation and sulfoxidation reactions of various cycloolefins and alkyl aryl sulfides, respectively, compared to the neat (L)Mo(VI)O₂ sites and the blank reaction. Further, to confirm the heterogeneity of (L)Mo(VI)O₂@SBA-15 complex, Sheldon's hot filtration test was carried out, and the results show that molybdenum metal does not leach out from the (L)Mo(VI)O₂@SBA-15 complex.

Chapter 4A: Pd(II)-2,2'-Dihydroxybenzophenone(DHBP)-NH₂@SBA-15 catalyst for arylation and hydrogenation of alkenes

An efficient, simple and phosphine free Pd(II)DHBP@SBA-15 catalyst has been synthesized by tethering of the 2,2'-dihydroxybenzophenone (DHBP) ligand over amino-functionalized SBA-15 via the post-grafting method and further metallation with Pd(II)(OAc)₂ resulted in a well-ordered mesostructure with a long range order. The synthesized catalysts were characterized by various characterization techniques like elemental analysis, XRD, N₂ sorption analyses, TG, DTA, FT-

IR, solid state ^{13}C and ^{29}Si NMR spectra, XPS, UV-Visible, SEM, EDAX and TEM. All characterization techniques proved that mesoporous SBA-15 and synthesized catalysts retained their structural integrity, textural properties, organic moieties, oxidation state, morphology and topographic characteristics after heterogenization. The catalytic activity of Pd(II)DHBP@SBA-15 was screened in arylation and hydrogenation reactions of alkenes, and the results show that Pd(II)DHBP@SBA-15 exhibits high conversion and selectivity towards arylation and hydrogenation reactions of alkenes in combination with high stability. The electronic (EWG & EDG effects) and steric effects (bulkier group) of groups on the substrates are also probed and the trend follows those reported in the literature. In addition, aliphatic olefins or less hindered olefins like acrylates gave better conversion and selectivity than aromatic olefins like substituted styrene. Due to these reasons, in the Heck reaction, 4-nitro-1-iodobenzene showed higher reactivity with ethyl acrylate to give the coupling products with 100% conversion and selectivity within 1 h. Moreover, in hydrogenation reactions, all olefins, except conjugated olefins, showed 100% conversion in less than 15 minutes to give alkanes, under mild conditions. The recyclability test was carried out to confirm the stability and the heterogeneous nature of the catalyst and the results concluded that Pd(II)DHBP@SBA-15 is reusable without much loss of activity for several cycles.

Chapter 4B: Pd(II)-3-Allylsalicylaldiminophenol(ASIP)-SH@SBA-15 catalyst for amination reactions of aryl halides

Pd(II)ASIP@SBA-15 catalyst has been synthesized by covalent anchoring of two ligands, namely, 3-allylsalicylaldehyde and 2-aminophenol, respectively, in a step by step manner, on thiofunctionalized SBA-15. This gave favourable coordination sites for metallation of Pd(II)(OAc) $_2$ and flexibility to lengthen the chain of organomoieties from surface to channels in SBA-15. All synthesized materials were characterized by CHN analysis, PXRD, Nitrogen sorption analyses, TG & DTA, FTIR, ^{13}C and ^{29}Si CP MAS NMR spectra, XPS, UV-Visible, SEM, EDAX and TEM and gave a clear indication of mesoporosity, thermal stability, morphology, and organo-functionality of Pd(II)ASIP@SBA-15 materials. Heterogeneous amination reactions of aryl halides were catalyzed by Pd(II)ASIP@SBA-15 catalyst and compared with the neat Pd(II)ASIP complex, Pd(II)(OAc) $_2$ and blank reaction. The results showed that Pd(II)ASIP@SBA-15 exhibited similar conversion compared with neat Pd(II)ASIP

complex and Pd(II)(OAc)₂. Eventually, the recycling studies of Pd(II)ASIP@SBA-15 was carried out for several cycles (fresh + six cycles) which showed good mechanical stability to confirm the heterogeneous nature of Pd(II)ASIP@SBA-15 catalyst.

Chapter 5: Ruthenium-Organofunctionalized SBA-15 catalyst for acetalization of aldehydes and ketones

An efficient Ru(III)-Organofunctionalized SBA-15, (L)Ru(III)@SBA-15, catalyst for acid free and chemo-selective acetalization reaction was synthesized by the grafting of 2,2'-dihydroxy benzophenone ligand over NH₂@SBA-15 followed by complexation with RuCl₃.3H₂O. This grafted material can be considered as a competitive and replaceable catalyst to conventional catalysts such as protonic, Lewis and solid acids for the preparation of dimethyl acetals. The catalyst, (L)Ru(III)@SBA-15, was thoroughly characterized by physical, spectroscopic and microscopic techniques. The results of acetalization reaction revealed that (L)Ru(III)@SBA-15 shows high catalytic activity as well as selectivity towards acyclic/cyclic acetals within 20 min with high TOF without the generation of hemiacetals as byproducts. Moreover, the amount of methanol as protecting group, influence of different protecting groups and recycling studies of (L)Ru(III)@SBA-15 in acetalization reaction were performed to attain a clear picture of the synthesized catalyst. Due to its high potential, this catalyst can be applicable in valorization of glycerol in bio-diesel industry and tandem hydroformylation-acetalization reactions.

Publications
Symposium
Conferences

PUBLICATIONS

- ❖ **Selective oxidation of cyclohexane to cyclohexanone using chromium oxide supported mesoporous MCM-41 nanospheres: Probing the nature of catalytically active chromium sites.**
K. J. Betsy, Chandrani Nayak, Anish Lazar, Athira Krishnan, Dibyendu Bhattacharyya, S. N. Jha and C. P. Vinod*
ChemCatChem, (2018) <https://doi.org/10.1002/cctc.201800309>
- ❖ **Ru(III)-functionalized SBA-15 as highly chemoselective, acid free and sustainable heterogeneous catalyst for acetalization of aldehydes and ketones**
Anish Lazar, K. J. Betsy, C. P. Vinod and A. P. Singh*
Catalysis Communications, 104 (2018) 62-66.
- ❖ **Aqueous phase selective hydrogenation of phenols over RuO₂ nanoparticles supported on MCM-41.**
K. J. Betsy, Anish Lazar and C.P. Vinod
Nano-Structures and Nano-Objects, 13 (2018) 36-43.
- ❖ **A heterogeneous route for transfer hydrogenation reactions of ketones using Ru(II) Cymene complex over modified benzene-organosilica (PMO_B).**
Anish Lazar, S. Silpa, C. P. Vinod and A. P. Singh*
Molecular Catalysis (Formerly, J. Mole. Cat. A) 440 (2017) 66-74.
- ❖ **Exploration of amination reactions on highly extendable active sites of Pd (II)-3-allylsalicylaldiminophenol (ASIP) complex over thiofunctionalized SBA-15.**
Anish Lazar, C. P. Vinod and A. P. Singh*
Microporous and Mesoporous Materials, 242 (2017) 173-181.
- ❖ **A simple, phosphine free, reusable Pd(II)-2,2'-dihydroxybenzophenone-SBA-15 catalyst for arylation and hydrogenation reactions of alkenes.**
Anish Lazar, C. P. Vinod and A. P. Singh*
New Journal of Chemistry, 40(3) (2016) 2423-2432.
- ❖ **Correlating the role of hydrophilic/hydrophobic nature of Rh (I) and Ru (II) supported organosilica/silica catalysts in organotransformation reactions.**
Anish Lazar, S.C. George, P.R. Jithesh, C.P. Vinod and A.P. Singh*
Applied Catalysis A: General 513 (2016) 138-146.
- ❖ **Organofunctionalization of Vanadium (III) Acetylacetonate Complex Over**

Aminofunctionalized SBA-15 for Sulfoxidation Reactions.

Anish Lazar, K. S. Sanjush and A. P. Singh*

Advanced Porous Materials 4 (3) (2016) 212-218.

❖ **Phenylacetylene hydrogenation on Au@Ni bimetallic core-shell nanoparticles synthesized under mild conditions.**

A.B. Vysakh, **Anish Lazar**, V. Yadukiran, A.P. Singh and C.P. Vinod*

Catalysis Science & Technology 6 (3) (2016) 708-712.

❖ **Synthesis of Au@Ni bimetallic core shell nanoparticle and nanochains in soyabean oil and their catalytic hydrogenation reactions**

V.A Bharathan, V. Yadukiran, **Anish Lazar**, A.P. Singh and C. P. Vinod*.

ChemistrySelect 1 (2) (2016) 140-146.

❖ **Synthesis and Characterization of MoO₂(VI)-3-[N,N'-bis-3-(salicylidenamino)ethyl triamine]-SBA-15: Highly stable and reusable catalyst for epoxidation and sulfoxidation.**

Anish Lazar, W. R. Thiel and A. P. Singh*

RSC Advances, 4 (2014) 14063-14073.

❖ **Clay encapsulated Cu(OH)_x promoted homocoupling of arylboronic acids: An efficient and eco-friendly protocol.**

B.A. Dar, S. Singh, N. Pandey, P. Sharma, **Anish Lazar**, A. P. Singh, M. Sharma, R. A. Vishwakarma and B. Singh*.

Applied Catalysis A: General 470 (2014) 232-238.

❖ **Chiral VO^{IV}-Sal-Indanol complex over modified SBA-15: an efficient, reusable enantioselective catalyst for asymmetric sulfoxidation reaction.**

Anish Lazar, P. Sharma and A. P. Singh*

Microporous and Mesoporous Materials, 170 (2013) 331-339.

❖ **Clay entrapped Cu (OH)_x as an efficient heterogeneous catalyst for ipso-hydroxylation of arylboronic acids.**

B. A. Dar, P. Bhatti, **Anish Lazar**, A. P. Singh, P. R. Sharma, M. Sharma and B. Singh*

Applied Catalysis A: General 466 (2013) 60-67.

❖ **Ultrasound promoted efficient and green protocol for the expeditious synthesis of 1, 4 disubstituted 1, 2, 3-triazoles using Cu(II) doped clay as catalyst.**

B. A. Dar, S. Singh, N. Pandey, P. Sharma, **Anish Lazar**, A. P. Singh, M. Sharma, R. A. Vishwakarma and B. Singh*

Applied Clay Science 80 (2013) 351-357.

- ❖ **Mn(III) based binaphthyl Schiff base complex heterogenized over organo-modified SBA-15: Synthesis, characterization and catalytic application.**

P. Sharma, Anish Lazar and A.P. Singh*

Applied Catalysis A: General 439 (2012) 101-110.

- ❖ **Covalently anchored ruthenium–phosphine complex on mesoporous organosilica: Catalytic applications in hydrogenation reactions.**

S. Sisodiya, Anish Lazar, S. Shylesh, L. Wang, W.R. Thiel and A.P. Singh*

Catalysis Communications 25 (2012) 22-27.

- ❖ **Dynamics of Confined Water in Periodic Mesoporous Organosilicates – a Proton Solid State MAS NMR Study.**

Veena V. S, Kavya Illath, Anish Lazar, C. P. Vinod, T. G. Ajithkumar, S. Jayanthi*

(Communicated)

POSTER AND ORAL PRESENTATIONS

- ❖ **An efficient, reusable, enantioselective catalyst V(IV)O-Sal-Indanol@SBA-15 for asymmetric sulfoxidation reactions (Oral)-International Symposium**
Anish Lazar and A. P.Singh*; BITS Pilani, Pilani, India, Octo. 16-18, 2015.
- ❖ **3-[N,N'-bis-3-(salicylidenamino)ethyltriamine]Mo(VI)O₂@SBA-15: Synthesis, Characterization and application in oxidation reactions. (Poster)-CRSI National**
Anish Lazar and A. P.Singh*; CSIR-NCL, Pune, India, Feb. 6-8, 2015.
- ❖ **Chiral V(IV)O-Sal-Indanol complex over SBA-15: An efficient, reusable, enantioselective catalyst for asymmetric sulfoxidation reactions (Oral)-National**
Anish Lazar and A. P.Singh*; CSIR-CSMCRI, Bhavnagar, India, Janu.7-9, 2015
- ❖ **Correlating the role of hydrophilic/hydrophobic nature of Rh (I) and Ru (II) supported organosilica/silica catalysts in hydrogenation reactions (Poster)**
Anish Lazar, C.P.Vinod and A. P.Singh*; CSIR-NCL, Pune. Feb. 25-26, 2015
- ❖ **Chiral V^{IV}O-Sal-Indanol complex over modified SBA-15: An efficient, reusable enantioselective catalyst for asymmetric sulfoxidation reaction (Poster)**
Anish Lazar, Priti Sharma and A.P.Singh*, CSIR-NCL, Pune, Feb. 25-26, 2014.
- ❖ **Mn(III) based binaphthyl Schiff base complex heterogenized over organo-modified SBA-15: Synthesis, Characterization and Catalytic Application (Oral)-National Symposium**
Priti Sharma, **Anish Lazar**, A. P. Singh*; CSIR-IICT, Hyderabad, India, Feb. 10-13, 2013.
- ❖ **Heterogenization of Rh(PPh₃)₃Cl over PMO for hydrogenation of olefins (Poster)-National Symposium**
Anish Lazar, Shoy George C, Priti Sharma, Jithesh P R, A.P. Singh*, IIT-Chennai, Dec 11-13, 2011.
- ❖ **MoO₂(VI)-Salpr-SBA-15: Synthesis, Characterization and Catalytic activity (Poster)**
Anish Lazar, A.P.Singh*, CSIR-NCL, Pune, India, Feb 24-25, 2011.
- ❖ **Study of stable Vanadium-Salen complex covalently anchored on PMO for liquid phase alkane oxidation (Poster)-International Conference**
Sheetal Sisodiya, **Anish Lazar**, K R Kamble, A P Singh*; CUSAT-Kochi, India, Jan. 11-13, 2010.

Curriculum Vitae

Mr. Anish Lazar, son of C. C. Lazar and Mary Lazar, born on 2nd February 1985 in Thrissur district, Kerala-680 602, India, completed his primary education at St. Francis Higher Secondary School, Pavaratty, Kerala, followed by his Bachelor's (2002-2005) and Master's degrees (2005-2007) in Chemistry from St. Thomas College, Thrissur, Kerala (Autonomous), affiliated to Calicut University, Calicut, Kerala. To improve his scientific knowledge, he there worked as Executive Trainee and Research Consultant, respectively, in two R & D centers (2008-2009), namely, KANCOR Ingredient Ltd, Angamaly, Ernakulum, Kerala, India and GE Plastics, JFWTC, Bangalore, India. To get wide openings of basic research in Chemistry, he moved to CSIR-National Chemical Laboratory (CSIR-NCL), Pune-411008, Maharashtra, India in 2009. Therein, he had worked in national and international projects (2009-2014), guided by Dr. Anand Pal Singh, Ex-Chief Scientist and Ex-Chairman/Emeritus Scientist, Catalysis Division, CSIR-NCL, Pune. During this period he worked especially on the synthesis and characterization of efficient heterogeneous catalysts for asymmetric and symmetric reactions, as Project Assistant (PA-II) and Senior Project Fellow (SPF). Meanwhile, he had published more than seven research international publications in peer reviewed journals. After awarding the CSIR-SRF in 2013-2014, he joined for Ph.D program under the supervision of Dr. Anand Pal Singh and Dr. Vinod. C. Prabhakaran, Sr. Scientist, Catalysis Division, CSIR-NCL, Pune. He has exploited his doctoral research program in the area of heterogeneous catalysis, concentrating on the synthesis and characterization of Metal-Organofunctionalized mesoporous silica catalysts for commercial and eco-friendly significant reactions. During his research life at CSIR-NCL, Pune, he has published seventeen research articles (Avg. IF >3.5) in peer reviewed international journals.